JPL Publication 92-3

An Atlas of Monthly Mean Distributions of GEOSAT Sea Surface Height, SSMI Surface Wind Speed, AVHRR/2 Sea Surface Temperature, and ECMWF Surface Wind Components During 1987

D. Halpern
V. Zlotnicki
J. Newman
Jet Propulsion Laboratory

D. Dixon
Colorado College
Colorado Springs, Colorado

O. Brown
University of Miami
Miami, Florida

F. Wentz
Remote Sensing Systems
Santa Rosa, California

January 1992

NASA
National Aeronautics and
Space Administration

Jet Propulsion Laboratory
California Institute of Technology
Pasadena, California

The research described in this publication was carried out, in part, by the Jet Propulsion Laboratory, California Institute of Technology, under a contract with the National Aeronautics and Space Administration.

Reference herein to any specific commercial product, process, or service by trade name, trademark, manufacturer, or otherwise, does not constitute or imply its endorsement by the United States Government or the Jet Propulsion Laboratory, California Institute of Technology.

ACKNOWLEDGEMENTS

Many people contributed to the preparation of the data sets displayed in the atlas, and we thank them for their tremendous support. Brian Beckley (STX), Lee Fu (JPL), Akiko Hayashi (JPL), and Chester Koblinsky (GSFC) helped with the GEOSAT data. James Brown (RSMAS) and Joan Splain (RSMAS) participated in processing the MCSST data set. Paul McClain (NESDIS) kindly sent validation results of the MCSST data product. Elena Lobl (Hughes Aircraft) and Michael Cummings (GE Aerospace) provided photographs of the DMSP and NOAA spacecrafts. We are extremely grateful to NASA (NAGW-273 (OB), RTOP-578-22-26 (DD), RTOP-578-22-29 (DH, JN), NAS8-38075 (FW), RTOP-578-22-25 (VZ), TOPEX Project (VZ)) and ONR (N00014-89-J-1144 (OB)) for their continued support of our research.

CONTENTS

Page

ACKNOWLEDGEMENTS iii

ABSTRACT vi

SATELLITE PHOTOGRAPHS
Plate 1. DMSP Spacecraft vii
Plate 2. GEOSAT Spacecraft viii
Plate 3. NOAA Spacecraft ix

1 INTRODUCTION 1

2 DATA PROCESSING 1

2.1 GEOSAT Sea Surface Height 1
2.1.1 Altimeter Measurement 2
2.1.2 Orbit Height 2
2.1.3 Environmental Corrections 2
2.1.4 Corrected Sea Surface Height 4
2.1.5 Alongtrack Sea Surface Height Residual 4
2.1.6 1/3° x 1/3° Gridded Monthly Data Set 4
2.1.7 Sea Surface Height Accuracy 5

2.2 SSMI Wind Speed 5
2.2.1 Microwave Radiometer Measurement 5
2.2.2 Environmental Corrections 11
2.2.3 1/3° x 1/3° Gridded Monthly Data Set 11
2.2.4 Wind Speed Accuracy 16

2.3 AVHRR/2 Sea Surface Temperature 16
2.3.1 Infrared Radiometer Measurement 16
2.3.2 Environmental Corrections 17
2.3.3 1/3° x 1/3° Gridded 28-Day Data Set 17
2.3.4 Sea Surface Temperature Accuracy 21

2.4 ECMWF Surface Wind Components 21

3 DATA PRESENTATION 21

4 REFERENCES 22

APPENDIX A: Atlas of Monthly Mean Distributions 25
A1 Monthly Mean GEOSAT Sea Surface Height Variation 26
A2 Monthly GEOSAT Sampling Distribution 33
A3 Monthly Mean SSMI Surface Wind Speed 40
A4 Monthly SSMI Sampling Distribution 44
A5 Monthly Standard Deviation of SSMI Surface Wind Speed 48
A6 Annual Mean and Sampling Distribution of AVHRR/2 Sea Surface Temperature 52
A7 28-Day Mean AVHRR/2 Sea Surface Temperature 54

A8 28-Day AVHRR/2 Sampling Distribution 61
A9 Annual Mean ECMWF Surface Wind Components 68
A10 Monthly Mean ECMWF Surface Wind Components..... 70
A11 Monthly Standard Deviation of ECMWF Surface Wind Components..... 83
A12 Annual Mean ECMWF Surface Wind Speed..... 96
A13 Monthly Mean ECMWF Surface Wind Speed..... 98
A14 Monthly Standard Deviation of ECMWF Surface Wind Speed..... 105

ABSTRACT

The following monthly mean global distributions for 1987 are presented with a common color scale and geographical map: sea surface height variation estimated from the U.S. Navy geodetic satellite GEOSAT; 10-m height wind speed estimated from the special sensor microwave imager (SSMI) on a U.S. Air Force Defense Meteorological Satellite Program (DMSP) spacecraft; sea surface temperature estimated from the advanced very high resolution radiometer (AVHRR/2) on a U.S. National Oceanic and Atmospheric Administration (NOAA) spacecraft; and the Cartesian components of the 10-m height wind vector computed by the European Center for Medium-Range Weather Forecasting (ECMWF). Charts of monthly mean value, sampling distribution, and standard deviation value are displayed. Annual mean distributions are displayed.

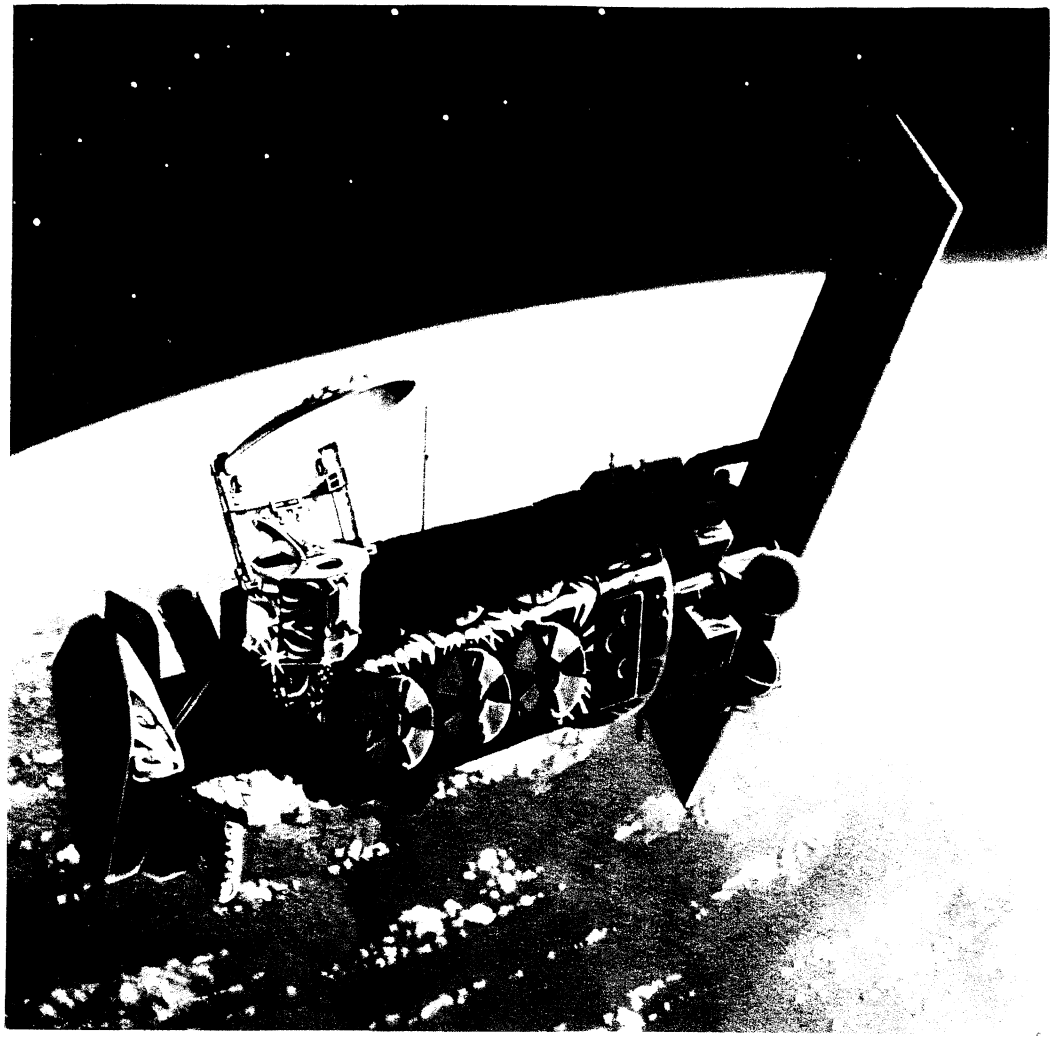

Plate 1. Defense Meteorological Satellite Program (DMSP) satellite with special sensor microwave imager (SSMI) located at the upper left. (Courtesy of Hughes Aircraft Company, Los Angeles.)

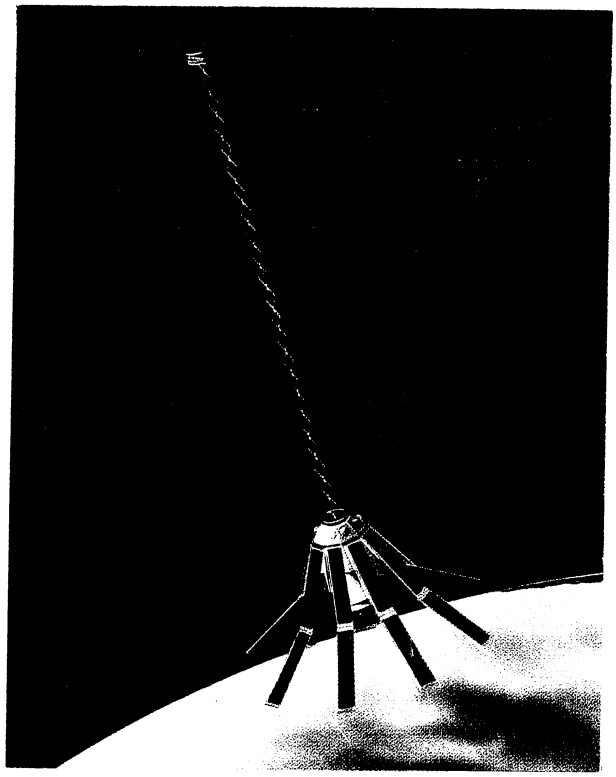

Plate 2. GEOSAT radar altimeter spacecraft. (Reproduced from Frain *et al.*, 1987.)

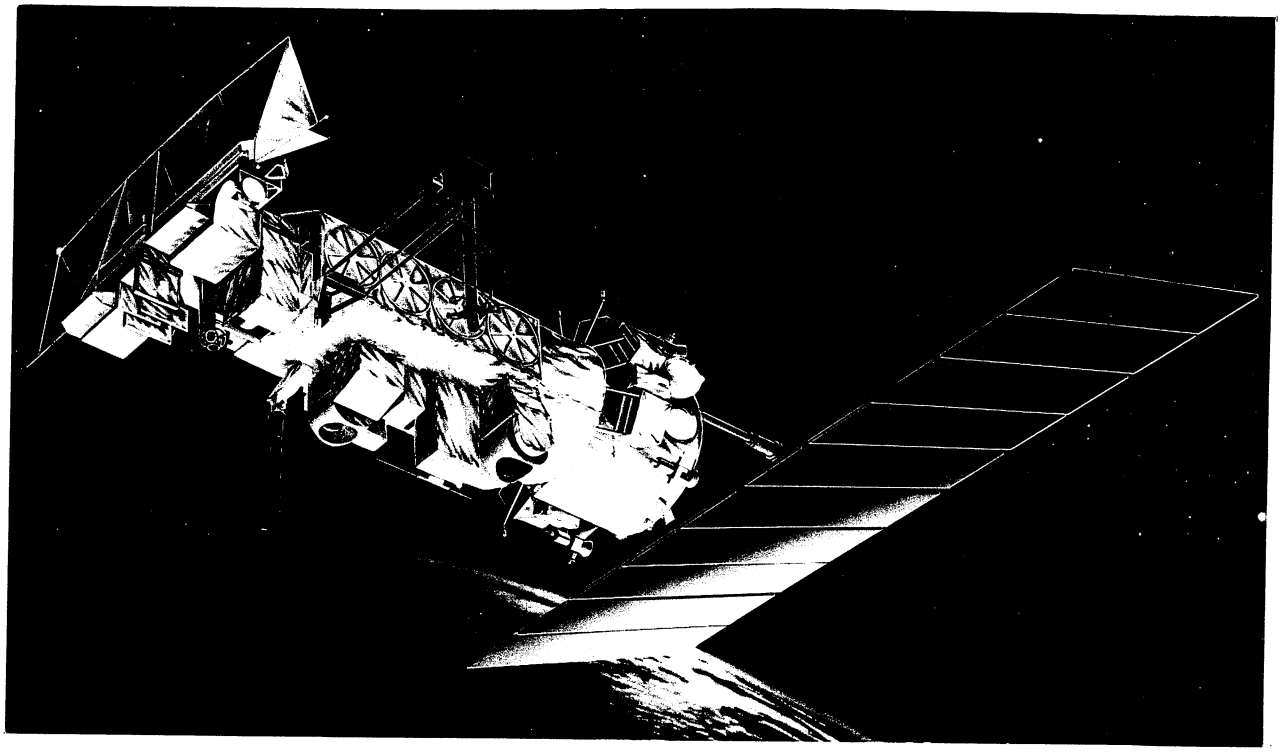

Plate 3. NOAA-9 or TIROS-I spacecraft. (Courtesy of GE Aerospace, Princeton.)

1 INTRODUCTION

This is the second volume of a series of annual summaries (Halpern *et al.*, 1991) of monthly mean global distributions of surface oceanographic variables.

Progress in climate research depends on the availability of a variety of geophysical data sets to describe the boundary conditions and forcing functions of the climate system. The importance of long-period global data sets is highlighted in the U.S. National Aeronautics and Space Administration (NASA) Earth Observing System and the U.S. Committee on Earth and Environmental Sciences Global Change Research Program. The unique perspective from space provides the opportunity for observations well suited for the global ocean, which is an essential component of the climatic system and which remains severely undersampled.

Stommel and Fieux (1978), in their guide to oceanographic atlases, stated that "the oceanographic atlas is one of the main tools of the oceanographer". Because of the scarcity of oceanographic data, very few atlases cover the world ocean, and none provide monthly mean distributions for a particular year. Several years of monthly mean data are necessary to analyze the seasonal cycle and interannual variations.

Since about ten years ago, substantial advances in remote and *in situ* techniques to record temperature, sea level, horizontal current, and surface wind have helped define annual cycles and interannual variations. Innovative ideas of how the ocean and atmosphere are coupled together occurred in parallel with new instrumentation. Three examples are El Niño Southern Oscillation (Philander, 1989), the ocean-atmosphere flux of carbon (Oeschger, 1988), and the relationship between global sea surface temperature and precipitation over Africa (Palmer, 1986). Monthly mean distributions of geophysical variables, which cover the globe or a large-scale region like an ocean basin, are becoming *de rigueur*.

Although both satellite- and ground-based recording systems provide essential information for global climate studies, satellite-borne instrumentation yields unprecedented spatial and temporal coverage of the global ocean. This report contains monthly mean distributions of satellite measurements of surface wind speed, sea surface temperature, and sea surface height variation during 1987. The first report (Halpern *et al.*, 1991) of the series displayed data for 1988 because it was the first occasion when an entire annual cycle of simultaneous satellite observations of these variables was recorded. The second report (this volume) of the atlas series contains data for 1987.

The report displays observations from three different satellites, each operated by a different agency. Very little averaging or interpolation of the data was made in order to retain the sampling characteristics of each data set. The report also displays surface wind vector components, which were computed by a numerical forecast-analysis system.

Data presented in Appendices A1, A3, and A7 are available on magnetic tape from the Physical Oceanography Distributed Active Archive Center, M/S 300-323, Jet Propulsion Laboratory, 4800 Oak Grove Drive, Pasadena, CA 91109.

2 DATA PROCESSING

2.1 GEOSAT Sea Surface Height

On 1 October 1986 the U.S. Navy's *geo*detic *sat*ellite (GEOSAT), which was launched on 12 March 1985, was maneuvered into an exact repeat orbit for oceanographic studies, now known as the Exact Repeat Mission (ERM). Each GEOSAT ERM orbit repeats within 1 km every 17.0505 days. The ground track separation at the equator is about 164 km. Global ERM data exists from 8 November 1986 until September 1989 when both tape recorders on GEOSAT ceased to operate; however, global data coverage was very poor after March 1989.

The GEOSAT sea surface height data set used in this report was prepared by V. Zlotnicki and is based on the Zlotnicki *et al.* (1990) data product, which is a resampled, edited and condensed version of the Cheney *et al.* (1987) geophysical data record (GDR).

The technique is complex to convert a radar altimeter's travel time measurement between the

satellite and the sea surface into a meaningful estimate of the elevation of the sea surface relative to a reference surface, which becomes the oceanographic signal of interest. Numerous algorithms are involved (Cheney *et al.*, 1987; Chelton, 1988). No universal set of algorithms exists and the exact model functions and magnitudes are issues of current investigations.

2.1.1 Altimeter Measurement

Electronic noise of the GEOSAT altimeter is about 3 cm root-mean-square (rms). This is about one-half the noise of the SEASAT altimeter and about 10% of the GEOS-3 altimeter (Sailor and LeSchack, 1987).

The Cheney *et al.* (1987) GDR contained 10 altimeter height measurements per s and a 1-s averaged altimeter height value obtained by an iterative linear fit with outlier rejections. The 1-s averaged altimeter height measurement is here called H_{alt}. A H_{alt} value was deleted when the standard deviation of the 0.1-s altimeter heights was greater than 15 cm (2% rejected), or when it was not within 30 cm of the second degree polynomial fitted to the data 4 s before and after the time of H_{alt} (0.1% rejected), or when the location was on land (7.5% rejected) (Zlotnicki *et al.*, 1990). H_{alt}, which depends upon sea state, is representative of circular areas with diameters between 3 and 12 km. H_{alt} forms the basic data set for subsequent data processing.

2.1.2 Orbit Height

The satellite orbit height above the reference ellipsoid, H_{orbit}, in the Cheney *et al.* (1987) GDR had been supplied by the U.S. Navy Astronautics Group (NAG). The NAG orbit was based on the Goddard Space Flight Center's (GSFC's) Goddard Earth Model 10 (GEM-10) of the gravity field and on Doppler tracking observations of GEOSAT's position by the U.S. Navy's Operational Network (OPNET), which consisted of three sites within the continental U.S. and one site in Hawaii. The NAG radial orbit error was about 2.2 m rms worldwide (Zlotnicki *et al.*, 1990), but 4.5 m systematic differences occurred at high latitudes with the 1984 world geodetic system reference frame (Shum *et al.*, 1990).

In this report we used the GEM-T2 H_{orbit}, which was computed by GSFC's Space Geodesy Branch. It combined the Marsh *et al.* (1989) GEM-T2 satellite-only gravitational model with Doppler tracking measurements of GEOSAT's position by the Defense Mapping Agency's (DMA's) 48-station Transit Network (TRANET). The preliminary radial orbit error of GEM-T2 H_{orbit} for GEOSAT is about 35 cm rms (Haines *et al.*, 1990).

2.1.3 Environmental Corrections

GEOSAT's altitude was approximately 800 km and the round-trip travel time of the radar altimeter electromagnetic pulse between the sea surface and the satellite is affected by atmospheric and ionospheric conditions. Also, ocean surface waves complicate the interpretation of the returned radar pulse. In addition, the sea surface height relative to the reference ellipsoid,

$$SSH = H_{orbit} - H_{alt},$$

is influenced by vertical displacements caused by earth tides, ocean tides, and the static response of the sea surface to atmospheric pressure load (*i. e.*, the inverse barometer effect). Atmospheric and ionospheric effects on travel time produce an apparent lowering of the sea surface height.

The largest environmental corrections affecting the altimeter pulse are the travel-time delays or path lengthening caused by air molecules within the troposphere (*i. e.*, dry troposphere correction, H_{dry}) and by water vapor within the troposphere (*i. e.*, wet troposphere correction, H_{wet}). The global average of H_{dry} is about 225 cm (Chelton, 1988); H_{wet} is about 15 cm (Monaldo, 1990). Of all environmental corrections, H_{wet} is the most troublesome because the magnitude changes by about 10 - 15 cm over spatial scales which closely match mesoscale oceanographic phenomena (Emery *et al.*, 1990).

For H_{dry}, we used the Cheney *et al.* (1987) GDR values, $H_{dry\text{-}FNOC}$, which were computed from the surface atmospheric pressure, p_o. The p_o was a product of the U.S. Navy's Fleet

Numerical Oceanography Center (FNOC) 12-hour, 2.5°-latitude x 2.5°-longitude global atmosphere general circulation model. A 4.4 hPa (or 4.4 mbar) uncertainty in p_o produces an error in H_{dry} of about 1.0 cm (Chelton, 1988).

During 1 January - 6 July 1987, we used the Cheney *et al.* (1987) values of H_{wet} (called $H_{wet\text{-}FNOC}$), which were estimated from surface air temperature and surface water vapor pressure derived from the FNOC 2.5° x 2.5°-gridded atmospheric general circulation model at 12-hour intervals. The $H_{wet\text{-}FNOC}$ underestimated equatorial water vapor in zones of atmospheric convergence (Zlotnicki and Liu, in preparation).

During 7 July - 31 December 1987, H_{wet} (called $H_{wet\text{-}SSMI}$) was estimated from vertically integrated water vapor measurements recorded globally at 25-km resolution with the special sensor microwave imager (SSMI) on board a polar-orbiting Defense Meteorological Satellite Program (DMSP) spacecraft. The 1394-km wide swath of SSMI yielded global coverage in 3.5 days. The SSMI water vapor data set used herein was processed by Wentz (1989a), and the accuracy is about 3.0 kg m^{-2}. $H_{wet\text{-}SSMI}$ in cm was equal to the SSMI water vapor measurements in kg m^{-2} multiplied by 6.55×10^{-3} m^3 kg^{-1} (Wentz, 1988). A global estimate of the uncertainty of $H_{wet\text{-}SSMI}$ is about 2.0 cm.

$H_{wet\text{-}SSMI}$ is considered an improvement over the $H_{wet\text{-}FNOC}$ used by Cheney *et al.* (1987) and Zlotnicki *et al.* (1990). $H_{wet\text{-}SSMI}$ was computed from total water vapor measured throughout the atmosphere, unlike $H_{wet\text{-}FNOC}$ which used only the water vapor at the surface. The 25-km resolution of $H_{wet\text{-}SSMI}$ was one-tenth the spatial scale of $H_{wet\text{-}FNOC}$ and, consequently, provided more realistic estimates of H_{wet} in narrow regions of large atmospheric moisture, such as the Intertropical Convergence Zone. However, $H_{wet\text{-}SSMI}$ will continue to underestimate the true H_{wet} in narrow areas of high moisture. Research on alternate methods to estimate integrated water vapor is an active subject (Lybanon and Crout, 1987; Emery *et al.*, 1990).

Free electrons in the ionosphere reduce the speed of the altimeter signal compared to the speed of light in a vacuum; the range correction caused by refraction from ionospheric electrons is denoted H_{ion}. The report uses H_{ion} values provided by Cheney *et al.* (1987) on the GDR, which were computed from Klobuchar's semiempirical ionospheric model (Musman *et al.*, 1990). H_{ion} has annual and interannual fluctuations over large latitudinal distances. During January - March 1987 the solar flux was small, which produced day-time ionospheric corrections of 1 - 2 cm (Cheney *et al.*, 1988). The rising solar flux yielded a 7-cm ionospheric correction at the end of the year (Cheney *et al.*, 1988).

Ocean waves complicate the interpretation of the measurement of the 2-way travel time of the radar altimeter pulse. Sea state bias has three components which, to a first approximation, are proportional to local wave height. First, the corrugated sea surface degrades the returned pulse waveform so the uncertainty in travel time produced by the onboard tracker's discrete digitization interval is about 0.7 cm (Chelton *et al.*, 1989); this correction is called $H_{tracker}$. Second, because an ocean wave signature is generally skewed with a flat trough and peaked crest, the returned power of the radar pulse is biased towards wave troughs. This error is called electromagnetic (em) bias, H_{em}, and is expressed as a percentage of significant wave height for Gaussian distributed heights. For this report, H_{em} = 1% of GEOSAT measurements of significant wave height, which are listed on the Cheney *et al.* (1987) GDR. The uncertainty of H_{em} could be 2 - 3 times greater than the magnitude of H_{em} used herein (Chelton *et al.*, 1989; Walsh *et al.*, 1989; Zlotnicki *et al.*, 1989), and caution is advised in interpretation of sea surface height where ocean wave heights change by a large amount. No additional correction to H_{em} was made for wave age (Fu and Glazman, 1991). A third source of error caused by ocean waves is related to the non-Gaussian nature of the skewed sea surface height distribution, $H_{skewness}$. Estimates of $H_{skewness}$ are very uncertain and range from 20 - 100% of H_{em} (Chelton *et al.*, 1989). For the report, $H_{skewness}$ = 0.

Tide corrections used in this report were provided on the GDR by Cheney *et al.* (1987). The solid-earth tide height, $H_{solid\ tide}$, was determined from the tide generating potential and its gradient over a 30-s interval along the groundtrack (Cartwright and Tayler, 1971). The ocean tide height at the sea surface, $H_{ocean\ tide}$, was based on Schwiderski's (1980) 1°-latitude x 1°-longitude global gridded model of 11 tidal constituents.

The inverted barometer correction, $H_{barom\ pressure}$, produced by atmospheric pressure was not included in the Cheney *et al.* (1987) GDR. For this report, we used the Zlotnicki *et al.* (1990) values of $H_{barom\ pressure}$, which is defined by

$$H_{barom\ pressure} = -9.948\ (H_{dry\text{-}FNOC}/(-2.277)(1+(0.0026 \cdot \mathrm{Cos}(2 \cdot \mathrm{latitude})))-1013.3).$$

$H_{dry\text{-}FNOC}$ values were contained in the Cheney *et al.* (1987) GDR.

2.1.4 Corrected Sea Surface Height

The environmentally corrected GEOSAT sea surface height relative to the reference ellipsoid is defined by

$$SSH_{corrected} = H_{orbit} - H_{alt} - H_{solid\ tide} - H_{ocean\ tide} - H_{barom\ pressure} - H_{dry} - H_{wet} - H_{ion} - H_{em}$$

Table 1 summarizes the evolution of the corrections applied to the GEOSAT altimeter data.

2.1.5 Alongtrack Sea Surface Height Residual

Along each groundtrack, the $SSH_{corrected}$ values were resampled at fixed latitudes at about every 7 km using a cubic spline. No interpolation was made over a data gap larger than 3 s (≈ 21 km). During each ERM year, the groundtrack was repeated approximately 22 times. For each series of 22 repeats of the groundtracks, the repeated groundtrack with the most resampled $SSH_{corrected}$ values was defined as a reference groundtrack. $SSH_{corrected}$ differences or residuals, called SSH', were computed between the reference groundtrack and all other groundtracks within the series. This deleted a 25 m rms uncertainty caused by the geoid (Zlotnicki, 1991). The orbit error was further reduced from 35 cm rms (§2.1.2) to less than 5 cm rms by fitting a once per revolution (≈ 101 minutes) sine wave to resampled SSH'. The resampled, edited, environmentally corrected, GEOSAT residual sea surface heights are called SSH".

2.1.6 1/3° x 1/3° Gridded Monthly Data Set

A 2-year (6 November 1986 - 5 November 1988) arithmetic mean SSH" value, <SSH">, was computed at each location where 17 or more SSH" values existed. At sites where the 2-year mean SSH" value was not computed because of insufficient data, SSH" values were deleted from further data processing. Sea surface heights relative to the 2-year mean, η = SSH" - <SSH">, were then computed for 1987. All η values with positions within nonoverlapping 1/3° x 1/3° squares were arithmetically averaged in 30.5-day intervals to form the basic monthly data set for this report. The origin of our global 1/3° x 1/3° grid is 90°N and 0° longitude.

Table 1

Heritage of GEOSAT sea surface height, $SSH_{corrected}$, described in this report.

Parameter	Cheney *et al.* (1987)	Zlotnicki *et al.* (1990)	This report
H_{orbit}	NAG/OPNET	NAG/OPNET	GEM-T2/TRANET
H_{alt}	outliers	§ 2.1.1 (this report)	§ 2.1.1
$H_{solid\ tide}$	Cartwright/Tayler	Cartwright/Tayler	Cartwright/Tayler
$H_{ocean\ tide}$	Schwiderski	Schwiderski	Schwiderski
$H_{barom\ pressure}$	none	FNOC p_o	FNOC p_o
H_{dry}	FNOC	FNOC	FNOC
H_{wet} (Jan-Jul)	FNOC	FNOC	FNOC
H_{wet} (Jul-Dec)	FNOC	FNOC	SSMI
H_{ion}	Klobucher	Klobucher	Klobucher
H_{em}	none	none	1% SWH
$H_{skewness}$	none	none	none

The total number of 1/3° x 1/3° monthly-averaged η values was almost the same each month (Figure 1A). Each 1/3° x 1/3° value of η represented the arithmetic mean of several η values. The total number of individual η values involved in the creation of each monthly averaged distribution decreased from January to December 1987 and continued to decrease during 1988 (Figure 1B).

The GEOSAT orbital pattern is repeated every 3.0045 days, and at the equator the pattern of ascending orbits is shifted 1.475° towards the west (Zlotnicki *et al.*, 1990). At 17.0505-day intervals, the groundtrack is repeated. Figures 2A - 2C display the sea surface height variations at 3-, 6- and 9-day intervals.

The data loss near the northern hemisphere continents is caused primarily by off-nadir spacecraft attitude angles greater than 1.1°. This situation is particularly severe when the GEOSAT spacecraft passes from land to water because the altimeter is unable to "lock on" to the return radar pulse (Cheney *et al.*, 1988).

2.1.7 Sea Surface Height Accuracy

The accuracy of satellite altimeter estimates of sea surface height depends very much on the data processing procedures (Cheney and Miller, 1990). The data contained in this report should be subjected to continuous ground-truth studies (Wyrtki and Mitchum, 1990).

V. Zlotnicki compared GEOSAT alongtrack data with the Wyrtki *et al.* (1988) tide gauge data from the Indian and Pacific Oceans. The η values were averaged over a 100-km groundtrack nearest to a tide gauge; this time series is called $\eta_{100\,km}$. The *in situ* 1-hour sampled sea level time series was low-passed filtered so that 50 and 95% of the amplitude squared were deleted at 2.5 and 1.7 days, respectively. Each low-passed filtered tide gauge time series was resampled at 17.05 days so that the times were coincident with the $\eta_{100\,km}$ data set; the resampled *in situ* time series are called SL. Comparison of $\eta_{100\,km}$ and SL time series at during 1987 - 1988 indicated an rms difference of 12.8 cm and the median correlation between the two time series was 0.43.

V. Zlotnicki noted that the global distribution of the phase of the annual cycle of η contained a spurious fluctuation, which was associated with an approximate 5- to 10-cm amplitude and 900-km zonal wavelength. The strength of the erroneous feature varied with the geographic pattern of the groundtracks and is believed to be caused by aliasing the semidiurnal ocean tide associated with a particular satellite sampling scheme (Cartwright and Ray, 1990; Jacobs *et al.*, 1991). The 1988 atlas (Halpern *et al.*, 1991) and this report do not contain a correction for this error.

2.2 SSMI Wind Speed

The special sensor microwave imager (SSMI) is a 7-channel, 4-frequency, linearly polarized, passive microwave radiometer flown on the U.S. Air Force's Defense Meteorological Satellite Program (DMSP) F8 spacecraft in a circular sun-synchronous near-polar orbit at an altitude of approximately 860 km and an orbit period of 102.0 min. The orbit has an ascending (south-to-north) equatorial crossing at 0613 local time. The SSMI was launched on 7 July 1987 and is the first of a series of about ten; the second SSMI was launched on a DMSP satellite in December 1990. The nearly 1400-km swath of SSMI produces complete coverage between 87°36'S to 87°36'N every 3 days. Each of the 7 separate passive radiometers measures naturally occurring microwave emissions from land, water and ice surfaces and from the intervening atmosphere. The SSMI receives both vertical and horizontal linearly polarized radiation at 19.3, 37.0 and 85.5 GHz and vertical only at 22.2 GHz.

2.2.1 Microwave Radiometer Measurement

The emitted microwave radiometer at the ocean surface is affected by roughness of the sea surface, which is correlated with the near-surface wind speed. Wentz (1989b) prepared the SSMI surface wind speed data product used in this report. Attenuation of 37-GHz radiation propagating from the sea surface to the satellite is very small, except when an appreciable amount of rain in the

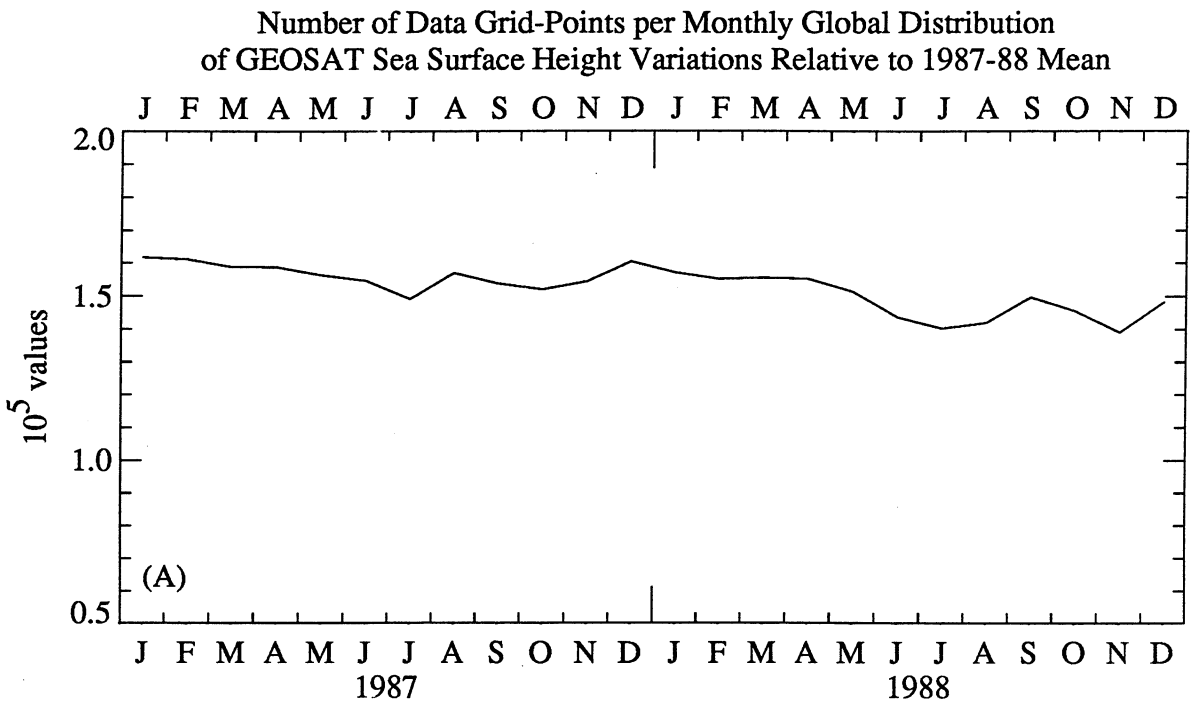

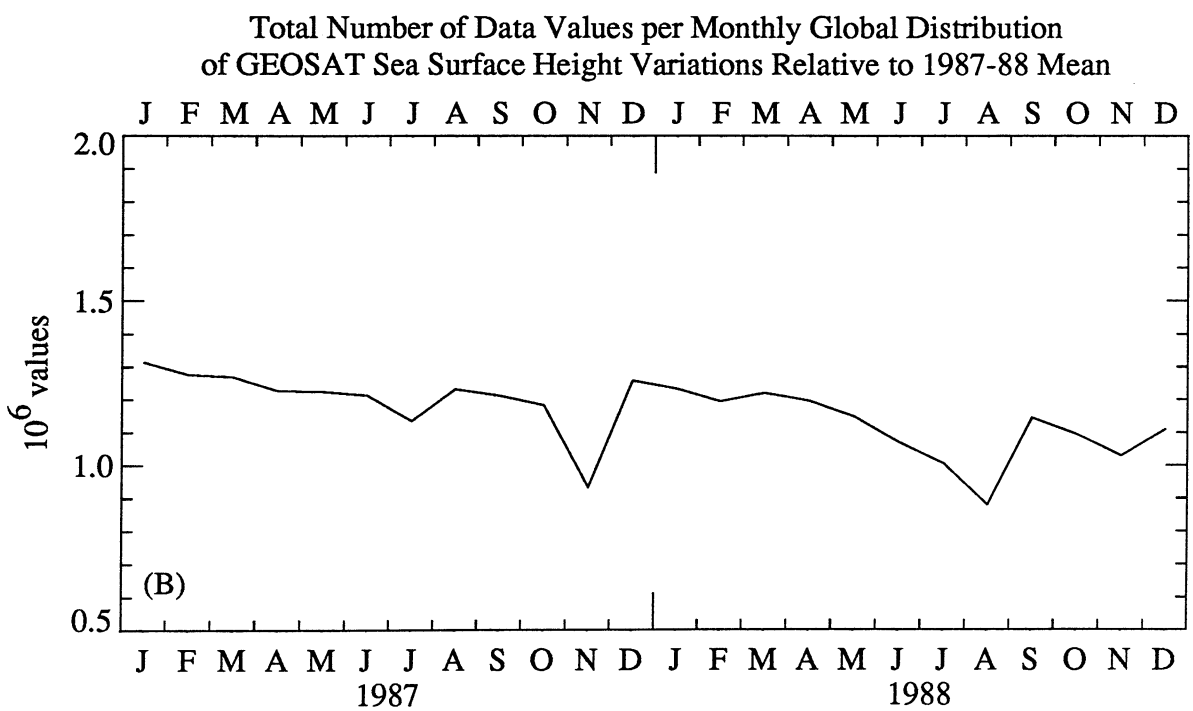

Figure 1. Time series of monthly totals of (A) number of pixels or picture elements and (B) number of sea surface height variations relative to 2-year mean.

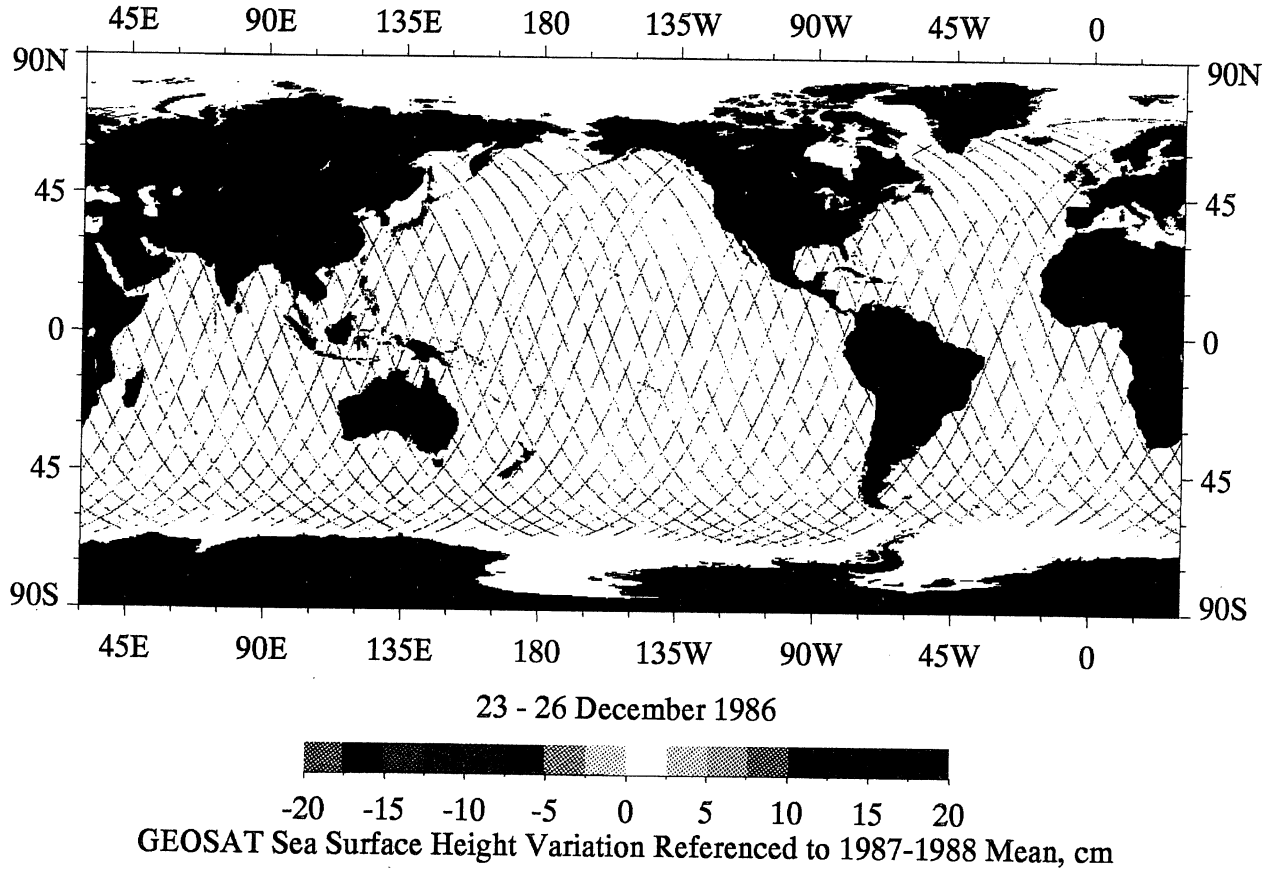

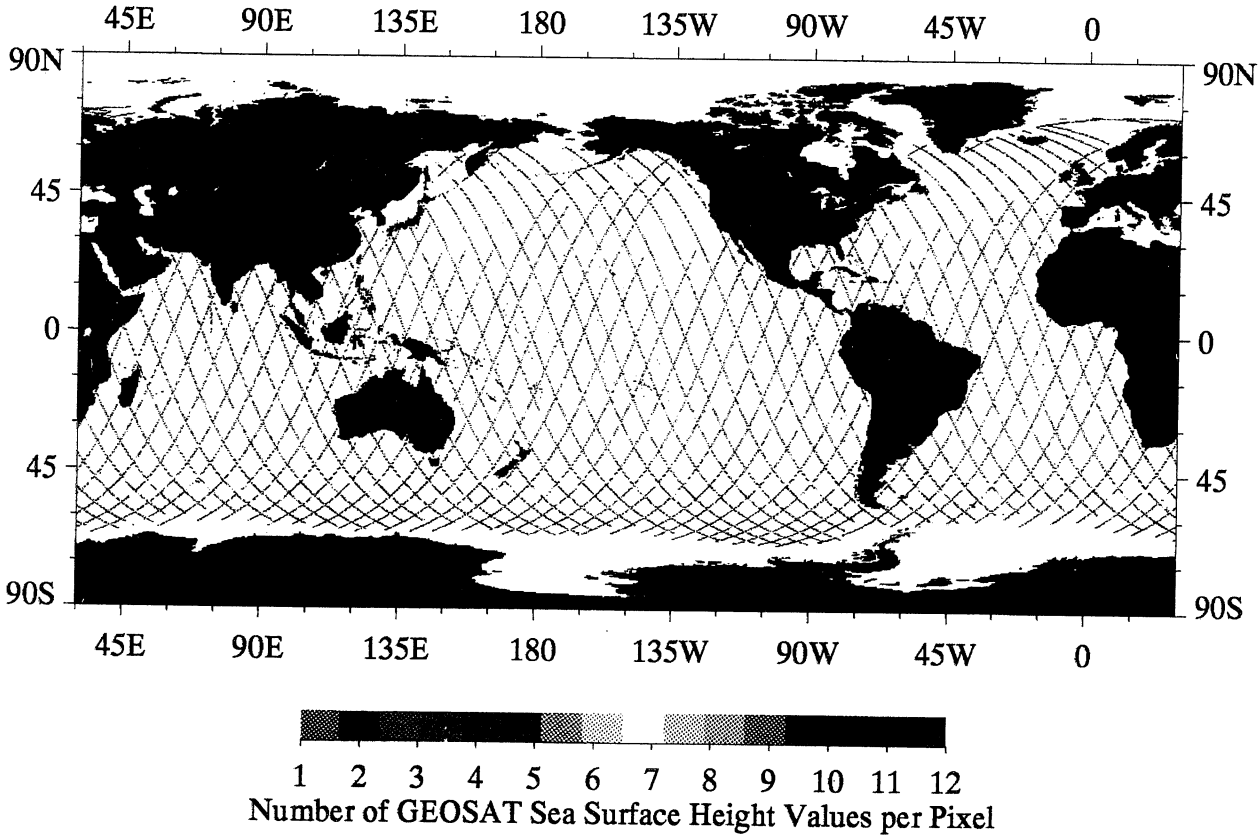

Figure 2A. Distributions of sea surface height variations relative to 2-year mean and pixel coverage during 23 - 26 December 1986.

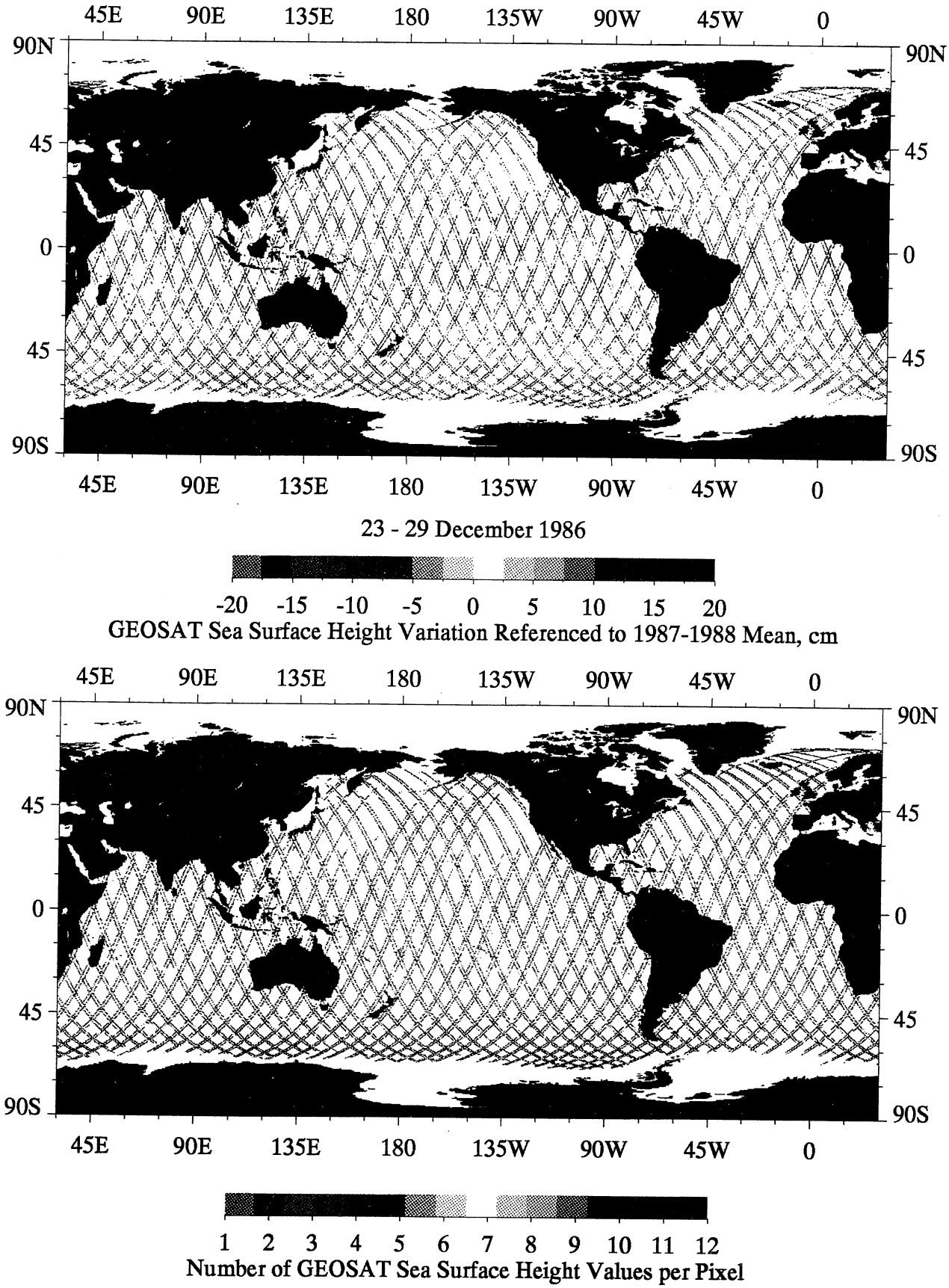

Figure 2B. Distributions of sea surface height variations relative to 2-year mean and pixel coverage during 23 - 29 December 1986.

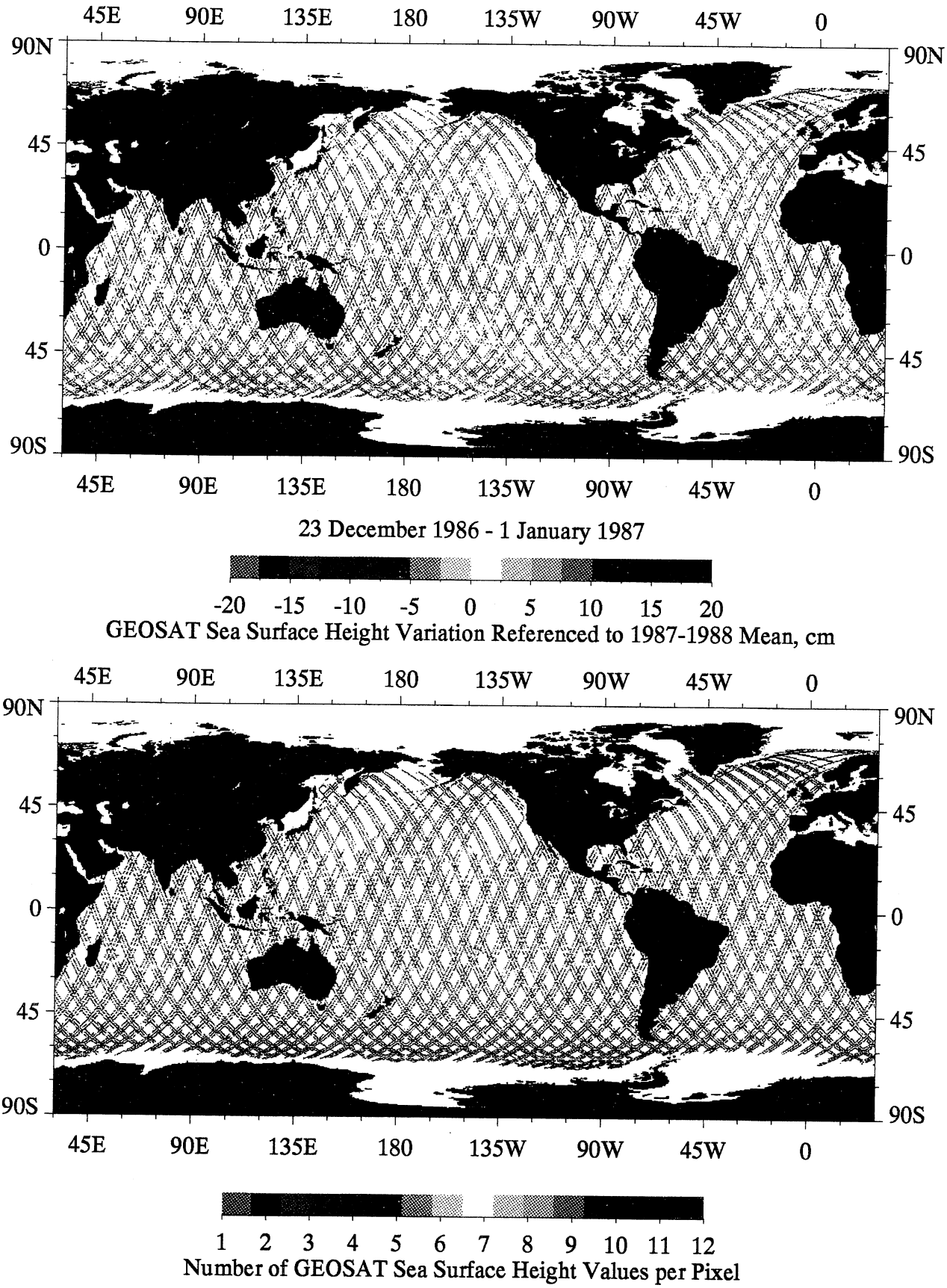

Figure 2C. Distributions of sea surface height variations relative to 2-year mean and pixel coverage during 23 December 1986 - 1 January 1987.

atmosphere scatters the 37-GHz radiation. The Wentz (1989b) algorithm relates wind speed at 19.5-m height (w, m s^{-1}) to the 37-GHz brightness temperatures, which are computed from the SSMI 37-GHz horizontal and vertical polarized radiance measurements, and to the radiative transfer and absorption between the sea surface and SSMI. The horizontal and vertical polarized (denoted by superscript "h" and "v" for horizontal and vertical, respectively) 37-GHz brightness temperatures (T_B^h, T_B^v) are defined by (Wentz, 1983)

$$T_B^h = T_{Bu} + \tau(E^h T_s + (1-E^h)\,(1+\omega^h w)\,(T_{Bd} + \tau T_{B\text{-}cold})) \qquad (1a)$$

$$T_B^v = T_{Bu} + \tau(E^v T_s + (1-E^v)\,(1+\omega^v w)\,(T_{Bd} + \tau T_{B\text{-}cold})), \qquad (1b)$$

where T_{Bu} is the upwelling brightness temperature (°K) caused by atmospheric emission and absorption, T_{Bd} is the downwelling brightness temperature (°K) produced by atmospheric emission and absorption, (E^h, E^v) are the emissivities of the sea surface for 37-GHz electromagnetic radiation, (ω^h, ω^v) are coefficients (Table 2) describing the intensities of electromagnetic radiation scattering at the sea surface, τ is atmospheric transmittance along the viewing path between the sea surface and SSMI, $T_{B\text{-}cold}$ is the 37-GHz cold brightness temperature of cosmic background radiation and equals 2.8 °K, and T_s is the sea surface temperature (°K).

The upward and downward atmospheric brightness temperatures for a non-scattering atmosphere are (Wentz, 1991)

$$T_{Bu} = (1 - \tau)\,(T_a - 14.6)$$
$$T_{Bd} = (1 - \tau)\,(T_a - 13.0),$$

where T_a is the surface air temperature (°K). Let the air temperature at the sea surface equal the sea surface temperature, *i. e.*, $T_a = T_s$, and let T_s be specified by Reynolds' (1982) climatological-mean monthly, 1°-latitude x 1°-longitude sea surface temperature analysis.

Sea surface emissivities (E^h, E^v) are given by

$$(E^h, E^v) = (E_o^h, E_o^h) + (\Delta E_o^h, \Delta E_o^h) + (b^h, b^v)[w\,(\theta - 49)],$$

where (E_o^h, E_o^v) are emissivities for a specular or perfectly flat sea surface, (ΔE_o^h, ΔE_o^v) account for changes in emissivities because of occurrences of surface roughness and foam, (b^h, b^v)[w (θ - 49)] account for changes in incidence angle θ of the SSMI radiometer, and (b^h, b^v) are wind-induced emissivity coefficients. Table 2 contains values of (b^h, b^v). Microwave radiation at frequencies above 10 GHz is only weakly sensitive to salinity changes (Maul, 1985), and the specular emissivity for an ocean surface of constant salinity of 35 PSU is (Wentz, 1991)

$$E_o^h = (s_o^h + s_1^h t + s_2^h t^2 + s_3^h t^3 + s_4^h u + s_5^h tu + s_6^h u^2 + s_7^h t^2 u)/T_s$$
$$E_o^v = (s_o^v + s_1^v t + s_2^v t^2 + s_3^v t^3 + s_4^v u + s_5^v tu + s_6^v u^2 + s_7^v t^2 u)/T_s$$

and

$$t = T_s - 273.16$$
$$u = \theta - 51.$$

Table 2 contains values of (s_i^h, s_i^v), where i = 0 to 7. The incidence angle is computed from the geometry of the DMSP/SSMI orbit. Wind-forced variations of emissivities are given by (Wentz *et al.*, 1986)

$$(\Delta E_o^h, \Delta E_o^v) = (m_1^h, m_1^v)\,w, \qquad \text{for } w \le 7 \text{ m s}^{-1},$$
$$(\Delta E_o^h, \Delta E_o^v) = (m_1^h, m_1^v)\,w + c^{-1}\,[(m_2^h, m_2^v) - (m_1^h, m_1^v)]\,(w - 7)^2, \qquad \text{for } 7 < w < 17 \text{ m s}^{-1},$$
$$(\Delta E_o^h, \Delta E_o^v) = (m_2^h, m_2^v)\,w - d\,[(m_2^h, m_2^v) - (m_1^h, m_1^v)], \qquad \text{for } w \ge 17 \text{ m s}^{-1}.$$

The constants c (= 20 m s^{-1}) and d (= 12 m s^{-1}) provide continuity between the segments of (ΔE_o^h, ΔE_o^v). The coefficients (m_1^h, m_1^v) and (m_2^h, m_2^v) are listed in Table 2.

The two unknowns, w and τ, in equations (1a) and (1b) are determined by Newton's iteration method. "First-guess" values for w and τ are 8 m s^{-1} and 0.8, respectively, which represent typical values over the ocean. Convergence is defined when the difference between successive iterations of w becomes less than 0.05 m s^{-1}. Convergence is usually found after 3 to 5 iterations. If convergence is not reached after 10 iterations, then the measured brightness temperatures (T_B^h, T_B^v) are considered erroneous or caused by heavy rain.

SSMI wind speeds referenced to 10-m height, which are equal to 94.3% of w (Wentz, 1989b), are used in the report.

Table 2

Parameters used by Wentz (1989b) to calculate SSMI wind speed from 37-GHz horizontal and vertical polarized radiance measurements.

Symbol	Parameter	Unit	V-polarization	H-polarization
b	Wind-induced emissivity coefficient	$s\ m^{-1}\ degree^{-1}$	-1.193×10^{-4}	1.052×10^{-4}
m_1	Wind-induced emissivity coefficient	$s\ m^{-1}$	0.70×10^{-3}	4.10×10^{-3}
m_2	Wind-induced emissivity coefficient	$s\ m^{-1}$	2.50×10^{-3}	7.30×10^{-3}
ω	Surface scattering coefficient	$s\ m^{-1}$	3.52×10^{-3}	8.55×10^{-3}
s_1	Specular emissivity coefficient	none	-5.637×10^{-1}	-6.171×10^{-1}
s_2	Specular emissivity coefficient	$°K^{-1}$	1.481×10^{-2}	1.437×10^{-2}
s_3	Specular emissivity coefficient	$°K^{-2}$	-2.96×10^{-5}	-7.07×10^{-5}
s_4	Specular emissivity coefficient	$°K\ degree^{-1}$	2.123	-1.701
s_5	Specular emissivity coefficient	$degree^{-1}$	1.17×10^{-2}	0.55×10^{-2}
s_6	Specular emissivity coefficient	$°K\ degree^{-2}$	4.1×10^{-2}	-1.9×10^{-2}
s_7	Specular emissivity coefficient	$°K^{-1}\ degree^{-1}$	-0.71×10^{-4}	-1.27×10^{-4}

2.2.2 Environmental Corrections

Environmental conditions reduce the amount of emitted radiation measured at the satellite. At 37 GHz, microwave emission from the ocean surface is masked by the emission and attenuation characteristics of rain. If the integrated liquid water content throughout the atmosphere is greater than 0.25 kg m^{-2}, then the Wentz (1989b) algorithm is considered invalid because there would be too much radiative scattering from water droplets. Brightness temperatures measured within about 100 km of land, which is defined with a geographical data base, are not used to estimate surface wind speed because the emissivity of land is very different than water. For the same reason, surface wind speed within 200 km of the climatological-mean monthly position of the ice edge was not used in the report.

2.2.3 1/3° x 1/3° Gridded Monthly Data Set

The Wentz (1989b) GDR contains wind speed values in nonoverlapping areas of 25 km x 25 km, which are arrayed across the 1394-km SSMI swath width. Geographical coordinates are provided at the center of each 25-km x 25-km region. SSMI wind speeds within nonoverlapping 1/3° x 1/3° squares were arithmetically averaged to form the basic data set for the report. The origin of the global 1/3° x 1/3° grid is 90°N and 0° longitude.

The December 1987 data set ended on 4 December because of a 40-day off-period to avoid possible damage of the SSMI by increased heating of the bearing and power transfer assembly (Hollinger *et al.*, 1990). During the winters of 1988 and 1989, the DMSP spacecraft solar arrays were repositioned so that the SSMI was not turned off.

Most of the 1/3° x 1/3° areas contained at least 50 wind speed values per month, or about 1 - 2 values per day. For each month, the standard deviation of daily-averaged SSMI surface wind speeds was computed for 1/3° x 1/3° areas containing 10 or more daily values per month.

The total number of 1/3° x 1/3° monthly-averaged SSMI wind speeds was constant during July to November 1987, and less than the amount during 1988 (Figure 3A). Each 1/3° x 1/3° SSMI wind speed represented the arithmetic mean of several values. The total number of individual SSMI values was low in July 1987 and January 1988 (Figure 3B) because of the instrument was not operated the entire months.

Coverage of SSMI wind speeds over the global ocean is nearly complete every 3 days (Figures 4A - 4C).

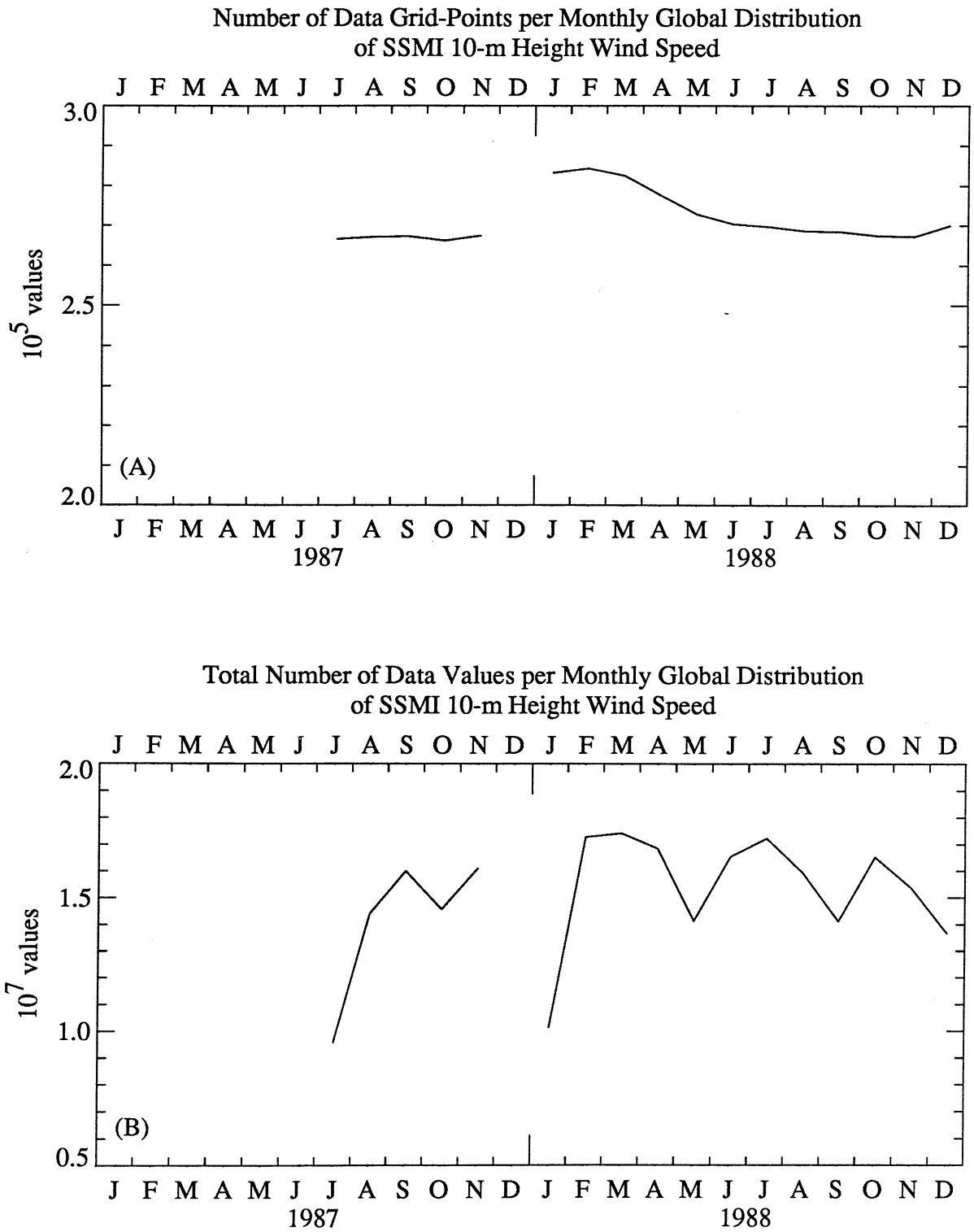

Figure 3. Time series of monthly totals of (A) number of pixels or picture elements and (B) number of 10-m height wind speeds.

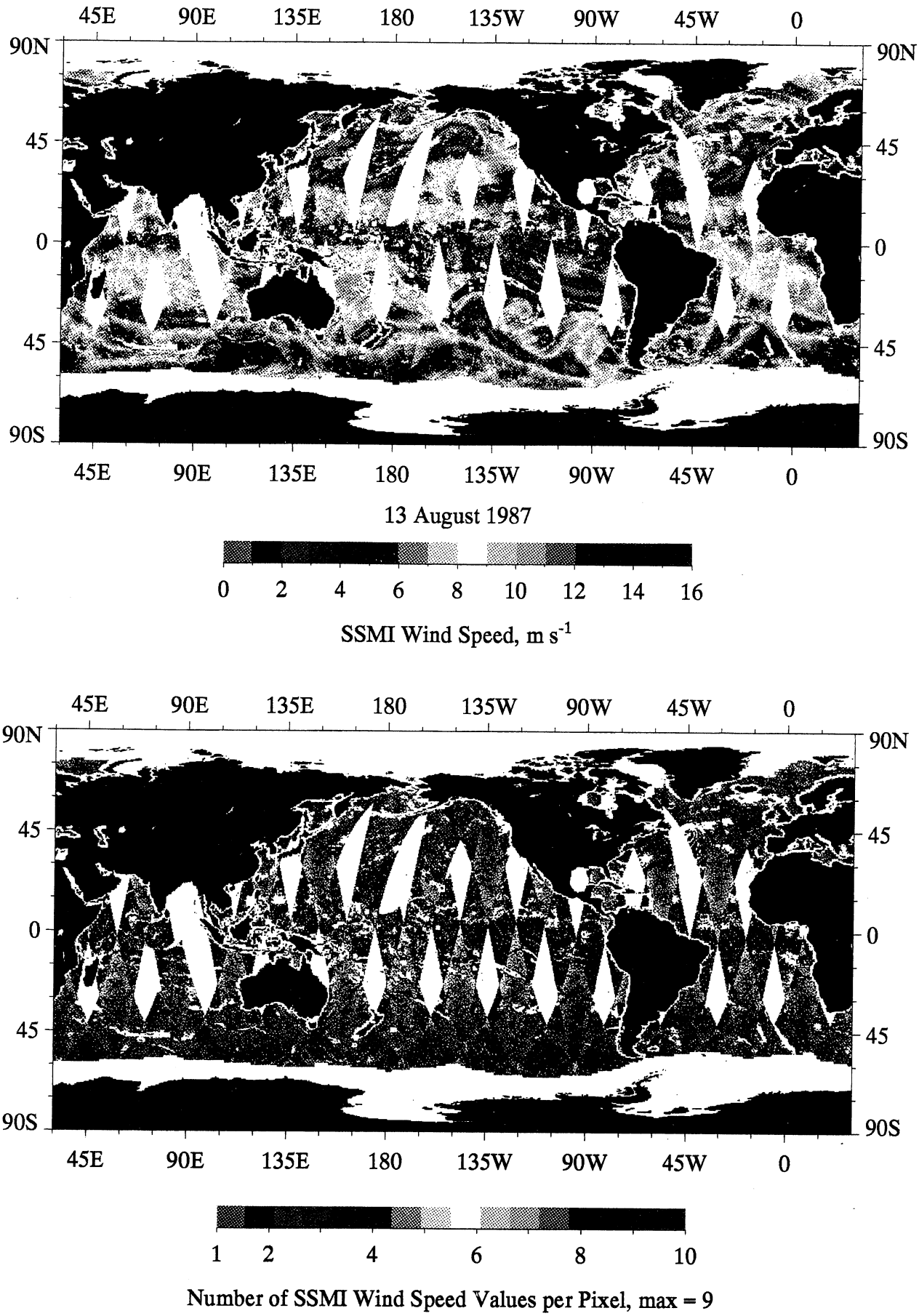

Figure 4A. Distributions of 10-m height wind speed and pixel coverage on a single day, 13 August 1987.

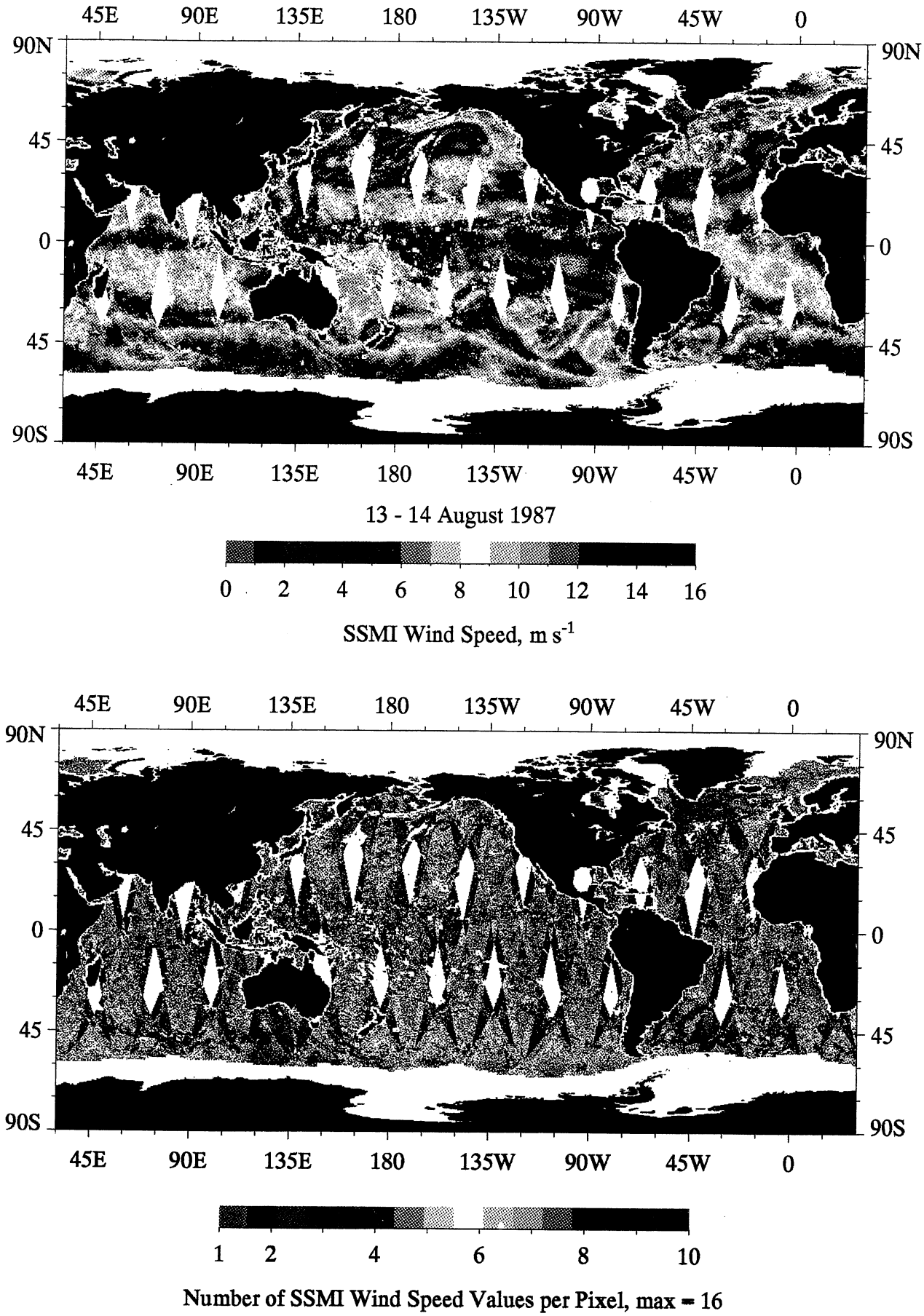

Figure 4B. Distributions of 10-m height wind speed and pixel coverage on two successive days, 13 and 14 August 1987.

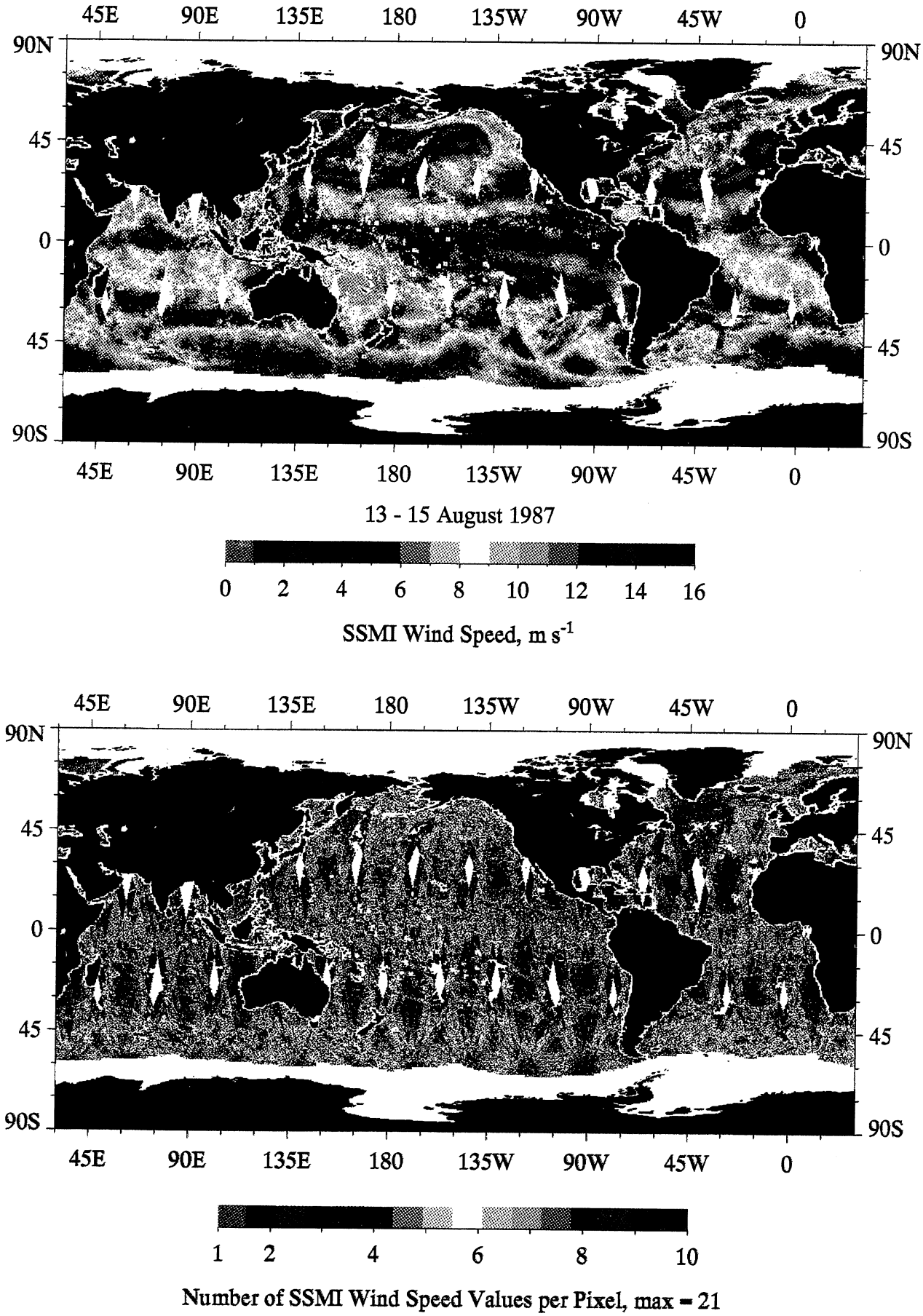

Figure 4C. Distributions of 10-m height wind speed and pixel coverage on three successive days, 13 - 15 August 1987.

2.2.4 Wind Speed Accuracy

The SSMI accuracy specification for wind speed retrievals under rain-free conditions is ± 2 m s^{-1} rms over the range 3 - 25 m s^{-1}. Wentz (1991) compared SSMI wind speeds with a National Oceanic and Atmospheric Administration (NOAA) National Data Buoy Center moored buoy wind data set prepared by Goodberlet *et al.* (1990), and found differences of zero bias and 1.6 m s^{-1} rms. Model functions different than Wentz' (1989b) physically-based algorithm exist. The Environmental Research and Technology (ERT) algorithm for SSMI surface wind speed did not meet the accuracy specification (Goodberlet *et al.*, 1990). Bates' (1991) statistical algorithm with brightness temperatures from five SSMI channels had a 1.1 m s^{-1} bias and a 1.8 m s^{-1} rms difference with moored buoy wind measurements at four sites from 5° to 5°N along 165°E.

2.3 AVHRR/2 Sea Surface Temperature

The NOAA satellite platforms (called NOAA-j where j is an integer) are in sun-synchronous orbits at altitudes of 833 or 870 km with ascending equatorial crossings at 0730 or 1400 local time. Since the 1981 launch of NOAA-7, odd-numbered NOAA satellites have a five-channel advanced very high resolution radiometer called AVHRR/2. Even-numbered satellites have a four-channel advanced very high resolution radiometer called AVHRR. NOAA-9 was operational in 1987.

The AVHRR/2 scan rate is 360 swaths per min with a total field of view of ± 55.4° from nadir and with an effective ground resolution of 1.1 km at nadir in five co-registered bands. Two spectral channels are in the visible range (0.58 - 0.68 and 0.725 - 1.1 μm) and three in the infrared range (3.55 - 3.93 (*i. e.*, 3.7) μm, 10.3 - 11.3 (*i. e.*, 11) μm, 11.5 - 12.5 (*i. e.*, 12) μm).

2.3.1 Infrared Radiometer Measurement

Infrared radiation received by a satellite radiometer is determined primarily by the sea surface emissivity and temperature and by atmospheric transmittance. Infrared radiation emitted from the ocean surface at wavelengths of about 3.5 - 4.0 μm propagates through a dry atmosphere with little attenuation, while under similar conditions the radiation in the 10 - 12 μm window can have approximately 10 - 15% attenuation (Maul, 1985). Only about 30% of the emitted radiation at 10 - 12 μm is transmitted through a wet atmosphere with 5.5-cm precipitable water. The oceanic emissivity in both spectral bands is approximately constant and close to unity for small zenith angles or nadir viewing. Emissivity changes with zenith angle, but the change from near-unity is small for zenith angles less than 40° (Bramson, 1968). The NOAA AVHRR/2 algorithms assume unit emissivity for all bands and angles. Thus the amount of radiation emitted at the surface can be assumed to be proportional to the sea surface temperature.

Atmospheric absorption of emitted radiation at the AVHRR/2 infrared wavelengths is primarily by water vapor, which occurs in the lower levels of the atmosphere so that the atmosphere is perceived to be optically thin. The transmission of emitted radiation through the atmosphere differs for each AVHRR/2 wavelength so that the difference of satellite-measured radiances at two or more wavelengths is independent of atmospheric absorber concentration. For small cumulative amounts of water vapor in the atmosphere, a linear combination of AVHRR/2 infrared radiation measurements recorded at the satellite yields an estimate of sea surface temperature, which is known as multi-channel sea surface temperature (MCSST) (Maul, 1985).

The report contains day-time MCSST data produced operationally by NOAA's National Environmental Satellite and Data Information Service (NESDIS). The procedure is described by McClain *et al.* (1985). Two MCSST algorithms were used in 1987. From 1 January - 15 July the day-time MCSST algorithm is (P. McClain, personal communication, 1991)

$$MCSST = 3.6446T_{11} - 2.6616T_{12} - 267.96,$$

where MCSST is the sea surface temperature in °C, and T_{11} and T_{12} are the brightness temperatures in °K computed from radiance measurements at 11 μm (AVHRR/2 channel 4) and 12

μm (AVHRR/2 channel 5), respectively. From 16 July - 31 December the day-time MCSST algorithm is (P. McClain, personal communication, 1991)

$$MCSST = 3.4317T_{11} - 2.5062T_{12} - 251.24.$$

2.3.2 Environmental Corrections

Major sources of error are water vapor absorption in the lower atmosphere and aerosol absorption. Radiance measurements from only cloud-free areas are processed by NOAA into MCSSTs. Very conservative cloud tests, which involve various combinations of the visible and infrared AVHRR/2 data, detect clouds so that cloud-free MCSSTs are computed (McClain *et al.*, 1985); on a typical day, less than 2% of the maximum possible number of MCSSTs are retained.

2.3.3 1/3° x 1/3° Gridded 28-Day Data Set

The 1.1-km AVHRR/2 observations are available only within areas containing a downlink ground station to receive high-resolution data transmission. Global AVHRR/2 measurements have an effective ground resolution of 4 km. A computer on board the NOAA spacecraft generates an average radiance for each channel from four 1.1-km elements within each nonoverlapping group of five consecutive 1.1-km measurements along a scan. The day-time MCSSTs archived on NESDIS global retrieval tapes represent the average sea surface temperatures within 8 km x 8 km areas, which would occur at 25-km intervals in a cloud-free environment. The 8-km x 8-km MCSSTs are mapped at the University of Miami's Rosenstiel School of Marine and Atmospheric Sciences (RSMAS) onto a cylindrical equi-rectangular grid of 2048 (longitude) x 1024 (latitude) space-elements (Olson *et al.*, 1988). At the equator the dimension of each space-element is approximately 18 km x 18 km, and geographical coordinates are assigned to the center of the element. The origin of the grid is 90°N, 180°W. RSMAS produces MCSSTs averaged over 7 days. For this report, four consecutive 7-day values are arithmetically averaged to form 28-day mean MCSST values. On three occasions (1 January - 4 February, 4 June - 8 July, 1 October - 4 November) when one of the weekly average MCSST distribution was missing, four 7-day values were averaged to produce a 35-day mean MCSST distribution. A 1024 x 512 grid was created by computing the arithmetic mean of four 18-km x 18-km MCSSTs adjacent to each other in a 2-

Table 3

Monthly mean bias and root-mean-square (rms) difference between day-time MCSST and drifting buoy sea surface temperature (DRIBU SST) global matchups during 1987.
Bias = DRIBU SST - MCSST.
(Courtesy of P. McClain, NOAA NESDIS)

Month	Number of Matchups	Bias ℃	RMS Difference ℃
Jan	197	0.05	0.69
Feb	341	0.02	0.76
Mar	329	-0.06	0.76
Apr	352	-0.26	0.75
May	294	-0.22	0.78
Jun	218	-0.08	0.72
Jul	168	-0.12	0.82
Aug	210	-0.21	0.73
Sep	172	-0.15	0.61
Oct	199	0.25	0.81
Nov	165	0.16	0.65
Dec	168	0.21	0.66

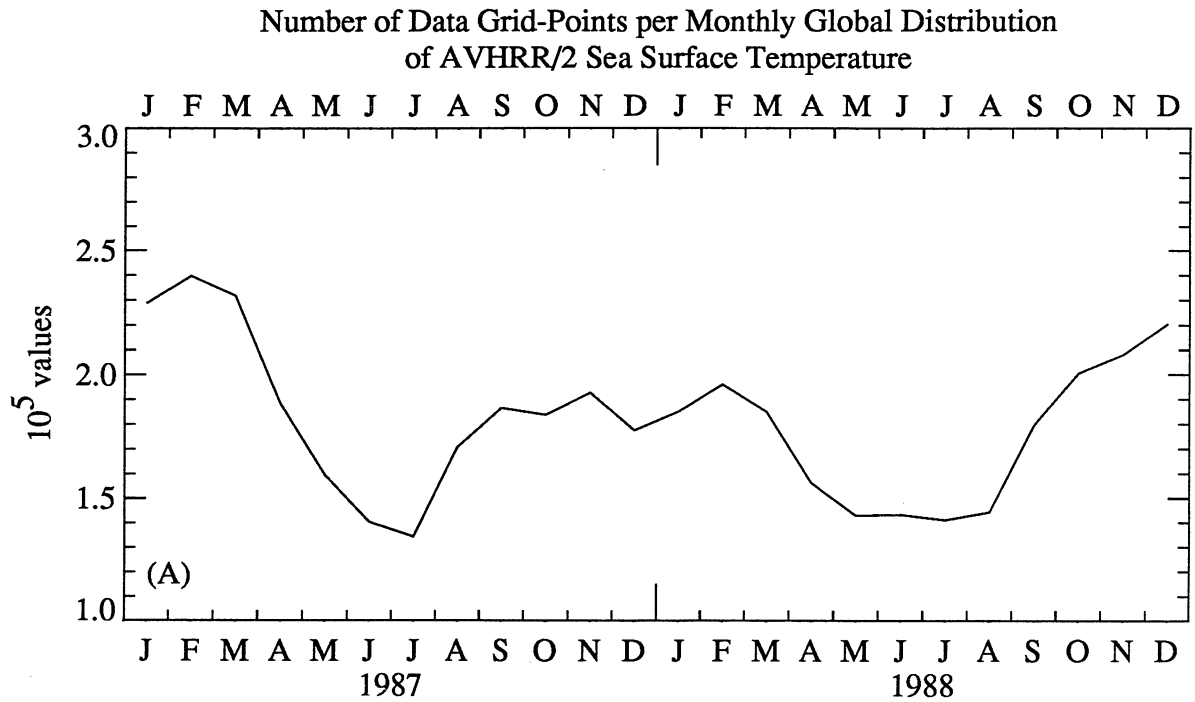

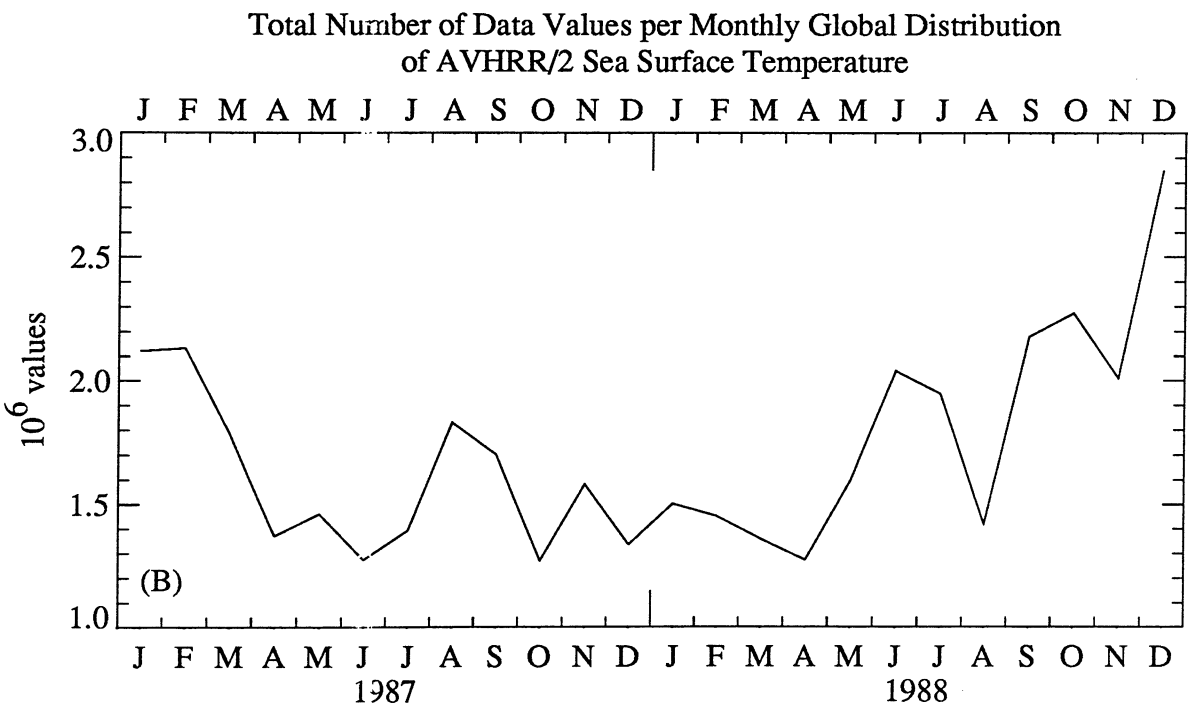

Figure 5. Time series of monthly totals of (A) number of pixels or picture elements and (B) number of sea surface temperatures.

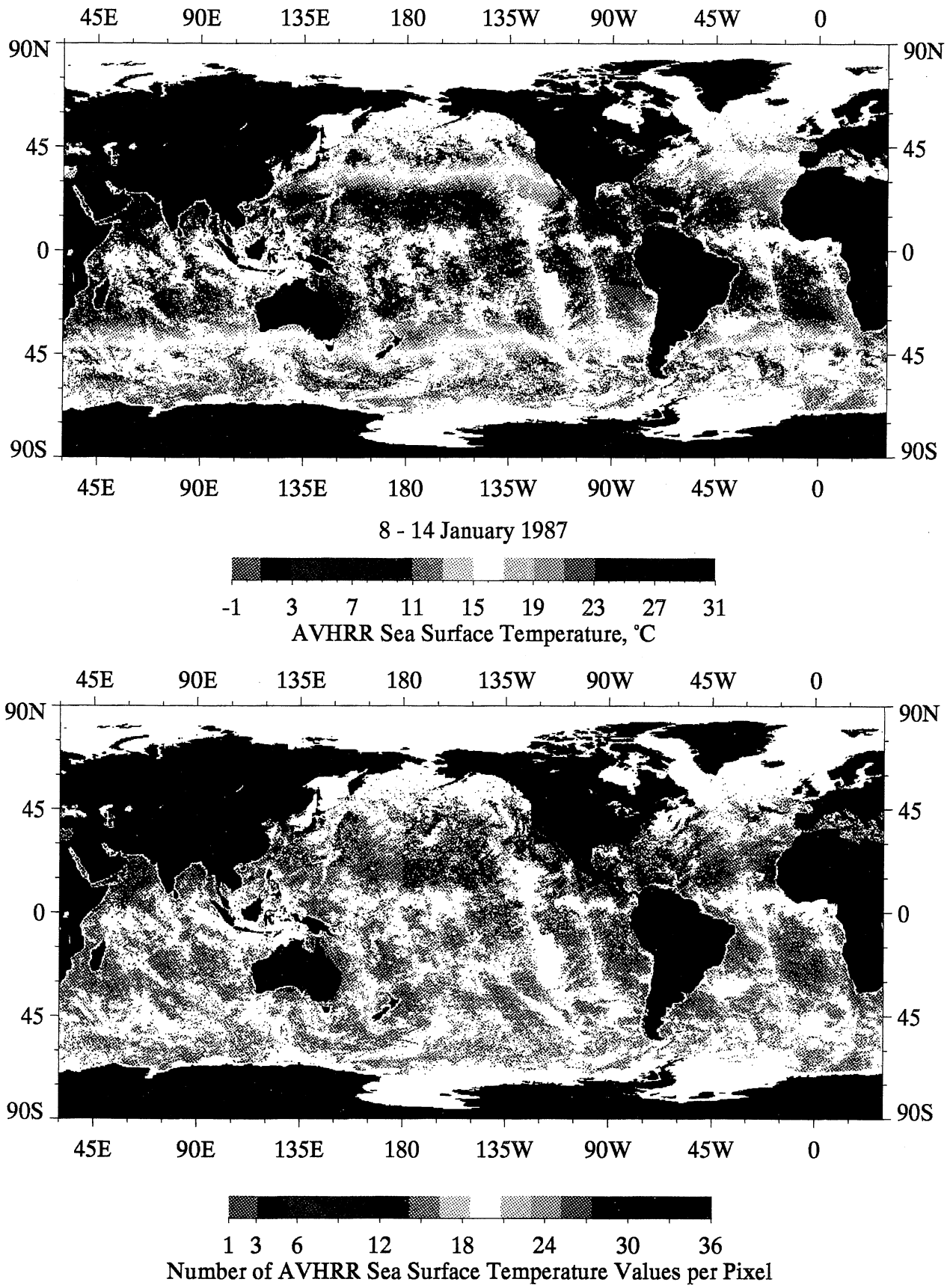

Figure 6A. Distributions of sea surface temperature and pixel coverage during a single 7-day interval, 8 - 14 January 1987.

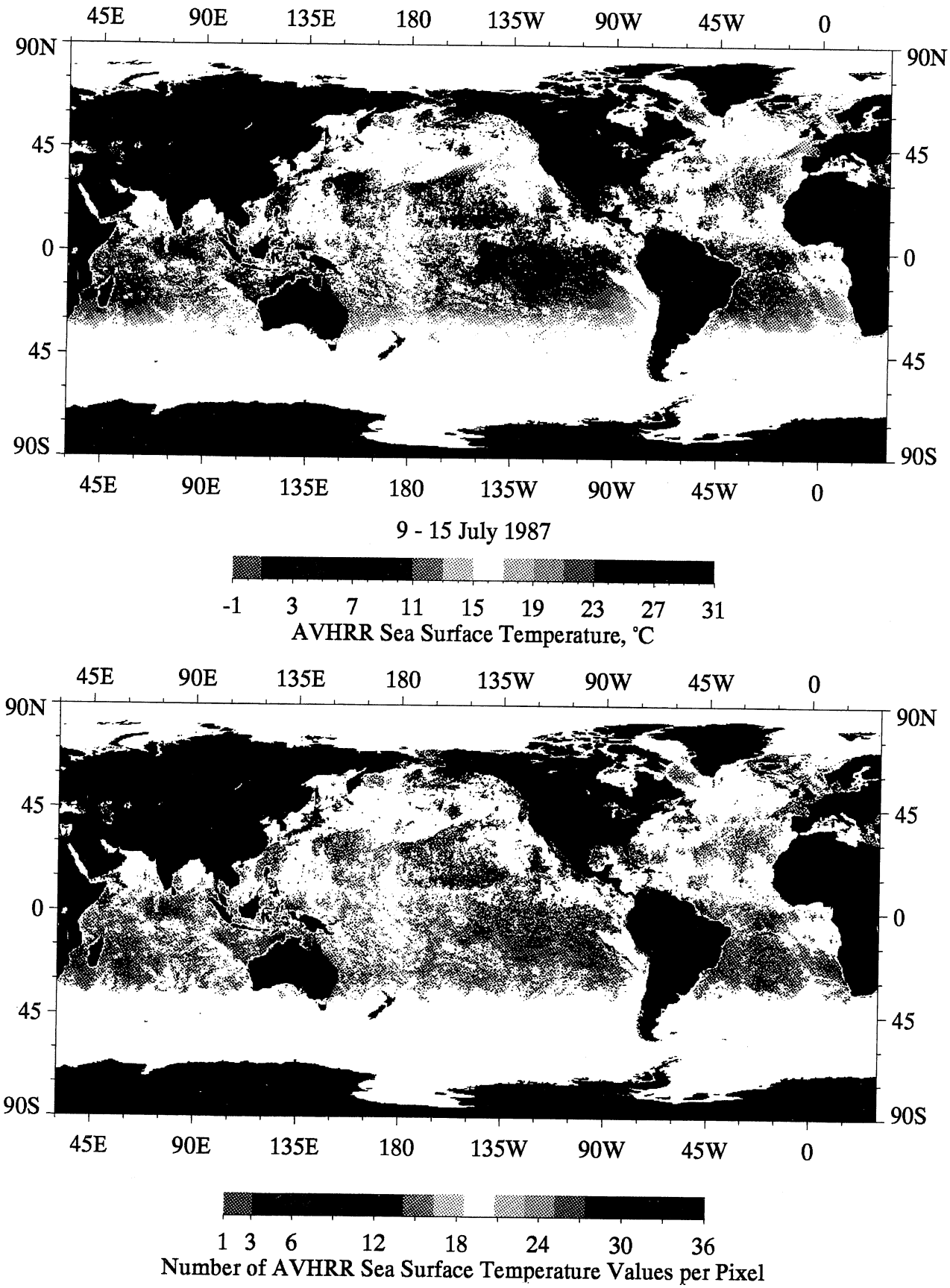

Figure 6B. Distributions of sea surface temperature and pixel coverage during a single 7-day interval, 9 - 15 July 1987.

dimensional array. The average MCSSTs of 4-element groups, which were independent of each other, represent an approximate 1/3° x 1/3° gridded MCSST data set.

The total number of 1/3° x 1/3° monthly-averaged MCSST values was smallest during June, July, and August, which coincided with intense cloud cover over huge oceanic areas of the middle latitudes of the southern hemisphere, and was highest during December, January, and February (Figure 5A). The range between maxima and minima was more than 25% of the annual mean.

The RSMAS MCSST data set contains the number of 8 km x 8 km values averaged to yield the 2048 x 1024 grid. The total number of 8 km x 8 km values per month (Figure 5B) was low throughout most of 1987 and 1988 compared to the beginning of 1987 and the latter part of 1988.

Distributions of MCSST and areal coverage for two typical 7-day intervals, one in January 1987 and the other in July 1987, are shown in Figures 6A and 6B.

2.3.4 Sea Surface Temperature Accuracy

The coefficients used in the NOAA MCSST algorithm change only as the operational satellite is replaced and on rare occasions when the continuous validation procedure indicates a need for a change. NOAA continuously monitors the performance of the MCSST data product with satellite-tracked drifting buoy sea surface temperature measurements, which are recorded within 25 km and 4 h of the location of the MCSST. During 1987, the MCSST was 0.03°C less than the *in situ* data and the rms difference was 0.7°C for an average of 234 matchups per month throughout the global ocean (Table 3).

2.4 ECMWF Surface Wind Components

Month-to-month variations of upper ocean circulation are primarily caused by spatial and temporal changes in the surface wind vector: both east-west (u; positive eastward) and north-south (v; positive northward) wind components are important. To augment the SSMI scalar surface wind speed data (§2.2), the report contains the Cartesian components of the surface wind field computed by the European Center for Medium-Range Weather Forecasting (ECMWF). The ECMWF forecast-analysis system, like all operational atmospheric general circulation models, is complex and continually being improved. During 1987, three important changes (one in April, July, and December) were made to the ECMWF analysis-forecast system (Hoskins *et al.*, 1989); the effect of these changes upon the surface wind vector is not known.

ECMWF analyses, instead of other model-generated results, are used because Trenberth and Olson (1988) considered them to be the best operational global analyses available for general use. Kalnay *et al.* (1990) showed that ECMWF northern hemisphere daily 1000- and 500-hPa rms height errors of the 1-, 3-, and 5-day forecasts during August 1989 were smaller than National Meteorological Center (NMC) results.

The area of each element of the ECMWF 144 x 73 grid was approximately 2.5° x 2.5°. ECMWF forecast-analyses of surface wind components at 10-m height were issued twice a day, at 0000 and 1200 GMT. Wind speed, s, was computed at 12-h intervals: $s = (u^2 + v^2)^{1/2}$.

3 DATA PRESENTATION

All data are presented in the form of color-coded maps. To ease interpretation of features among different parameters, a common color code is used: blues represent low values, reds are high values, yellow and green are in the middle range, white means no data, and black represents land. Data are linearly scaled for color and an incremental color scale represents a contour interval. A single geographical scale is used for all maps. The land mask, which was prepared by O. Brown from the U.S. Central Intelligence Agency (CIA) World Data Base II, is the same throughout this report.

The color maps were generated on a Sun™-4 computer using IDL®, which prepared the PostScript® files. Each PostScript® file was transferred to an Apple Macintosh™ IIci and printed with PostScript® Dumper on a Tektronix™ Phaser CP Color Printer. All data values are retained in the PostScript® image files. The GEOSAT and SSMI images contain 1080 x 540 pixels (picture elements) and the AVHRR images contain 1024 x 512 pixels. All images are plotted on a 5.75-in x 2.875-in map. The PostScript® interpreter linearly transforms the size of each pixel within the user image file into a source-image coordinate system, which is compatible with the 300 dot-per-in. resolution of the Tektronix™, to achieve the maximum rendition of the image within the specified dimensions (Adobe Systems, 1985).

Data presented in Appendices A1, A3, and A7 are available on magnetic tape from the Physical Oceanography Distributed Active Archive Center, M/S 300-323, Jet Propulsion Laboratory, 4800 Oak Grove Drive, Pasadena, CA 91109.

4 REFERENCES

Adobe Systems, Inc. (1985) *PostScript® Language Reference Manual.* Addison-Wesley, 321 pp.

Bates, J.J. (1991) High frequency variability of SSMI-derived wind speed and moisture during an intraseasonal oscillation. *Journal of Geophysical Research, 96*, 3411-3424.

Bramson, M.A. (1968) *Infrared Radiation: A Handbook for Applications.* Plenum Press, New York, 623 pp.

Cartwright, D.E., and R.J. Tayler (1971) New computations of the tide generating potential. *Geophysical Journal of the Royal Society, 23*, 45-74.

Cartwright, D.E., and R.D. Ray (1990) Oceanic tides from GEOSAT altimetry. *Journal of Geophysical Research, 95*, 3069-3090.

Chelton, D.B. (1988) WOCE/NASA altimeter algorithm workshop. U.S. WOCE Technical Report No. 2, U.S. Planning Office for WOCE, Texas A&M University, College Station, 70 pp.

Chelton, D.B., E.J. Walsh and J.L. MacArthur (1989) Pulse compression and sea level tracking in satellite altimetry. *Journal of Atmospheric and Oceanic Technology, 6*, 407-438.

Cheney, R.E., and L.L. Miller (1990) Recovery of the sea level signal in the western tropical Pacific from GEOSAT altimetry. *Journal of Geophysical Research, 95*, 2977-2984.

Cheney, R.E., B.C. Douglas, R.W. Agreen, L.L. Miller, D.L. Porter and N.S. Doyle (1987) GEOSAT altimeter geophysical data record user handbook. NOAA Technical Memorandum NOS-NGS-46, National Oceanic and Atmospheric Administration, U.S. Department of Commerce, Washington, 32 pp.

Cheney, R.E., B.C. Douglas, R.W. Agreen, L. Miller and N. Doyle (1988) The NOAA GEOSAT geophysical data records: Summary of the first year of the Exact Repeat Mission. NOAA Technical Memorandum NOS-NGS-48, National Oceanic and Atmospheric Administration, U.S. Department of Commerce, Washington, 20 pp.

Emery, W.J., G.H. Born, D.G. Baldwin and C.L. Norris (1990) Satellite-derived water vapor corrections for GEOSAT altimetry. *Journal of Geophysical Research, 95*, 2953-2964.

Frain, W.E., M.H. Barbagallo and R.J. Harvey (1987) The design and operation of GEOSAT. *Johns Hopkins APL Technical Digest, 8*, 184-189.

Fu, L.-L., and R. Glazman (1991) The effect of the degree of wave development on the sea-state bias in radar altimetry measurements. *Journal of Geophysical Research, 96*, 829-834.

Goodberlet, M.A., C.T. Swift and J.C. Wilkerson (1990) Ocean surface wind speed measurements of the special sensor microwave imager (SSMI). *IEEE Transactions on Geoscience and Remote Sensing, 28*, 823-828.

Haines, B.J., G.H. Born, G.W. Rosborough, J.G. Marsh and R.G. Williamson (1990) Precise orbit computation for the GEOSAT Exact Repeat Mission. *Journal of Geophysical Research, 95*, 2871-2885.

Halpern, D., V. Zlotnicki, J. Newman, O. Brown and F. Wentz (1991) An atlas of monthly mean

distributions of GEOSAT sea surface height, SSMI surface wind speed, AVHRR/2 sea surface temperature, and ECMWF surface wind components during 1988. JPL Publication 91-8, Jet Propulsion Laboratory, Pasadena, 110 pp.

Hollinger, J.P., J.L. Pierce and G.A. Poe (1990) SSMI instrument evaluation. *IEEE Transactions on Geoscience and Remote Sensing*, *28*, 781-790.

Hoskins, B.J, H.H. Hsu, I.N. James, M. Masutani, P.D. Sardeshmukh and G..H. White (1989) Diagnostics of the global atmospheric general circulation based on ECMWF analyses 1979-1989. WCRP-27, WMO/TD-No. 326, World Climate Research Program, World Meteorological Organization, Geneva, 217 pp.

Jacobs, G.A., G.H. Born and M. Parke (1991) Construction of the global annual cycle from GEOSAT altimeter data with an estimation of the M2 tidal alias error. *EOS, Supplement to October 29, 1991*, 258. (Abstract)

Kalnay, E., M. Kanamitsu and W.E. Baker (1990) Global numerical weather prediction at the National Meteorological Center. *Bulletin of the American Meteorological Society*, *71*, 1410-1428.

Lybanon, M., and R.L. Crout (1987) The NORDA GEOSAT ocean applications program. *Johns Hopkins APL Technical Digest*, *8*, 212-218.

Marsh, J.G., F.J. Lerch *et al.* (1989) The GEM-T2 gravitational model. NASA Technical Memorandum 100746, Goddard Space Flight Center, Greenbelt, Maryland, 91 pp.

Maul, G.A. (1985) *Introduction to Satellite Oceanography*. Matinus Nijhoff, Dordrecht, 606 pp.

McClain, E.P., W.G. Pichel and C.C. Walton (1985) Comparative performance of AVHRR-based multichannel sea surface temperatures. *Journal of Geophysical Research*, *90*, 11587-11601.

Monaldo, F. (1990) Path length variations caused by atmospheric water vapor and their effects on the measurement of mesoscale ocean circulation features by a radar altimeter. *Journal of Geophysical Research*, *95*, 2923-2932.

Musman, S., A. Drew and B. Douglas (1990) Ionospheric effects on GEOSAT altimeter observations. *Journal of Geophysical Research*, *95*, 2965-2967.

Oeschger, H. (1988) The ocean system - ocean/climate and ocean/CO_2 interactions. In: *Scales and Global Change*, edited by T. Rosswall, R.G. Woodmansee and P.G. Risser, John Wiley & Sons, New York, 319-352.

Olson, D.B., G.P. Podesta, R.H. Evans and O.B. Brown (1988) Temporal variations in the separation of Brazil and Malvinas Currents. *Deep-Sea Research*, *35*, 1971-1990.

Palmer, T.N. (1986) Influence of the Atlantic, Pacific and Indian Oceans on sahel rainfall. *Nature*, *322*, 251-253.

Philander, S.G.H. (1989) *El Niño, La Niña, and the Southern Oscillation*. Academic Press, San Diego, 293 pp.

Reynolds, R.W. (1982) A monthly averaged climatology of sea surface temperature. NOAA Technical Report NWS 31, National Oceanic and Atmospheric Administration, Silver Springs, Maryland, 35 pp.

Sailor, R.V., and A.R. LeSchack (1987) Preliminary determination of the GEOSAT radar altimeter noise spectrum. *Johns Hopkins APL Technical Digest*, *8*, 182-183.

Schwiderski, E.W. (1980) On charting global tides. *Reviews of Geophysics and Space Physics*, *18*, 243-268.

Shum, C.K., D.N. Yuan, J.C. Ries, J.C. Smith, B.E. Shutz and B.D. Tapley (1990) Precision orbit determination for the GEOSAT exact repeat mission. *Journal of Geophysical Research*, *95*, 2887-2898.

Stommel, H., and M. Fieux (1978) *Oceanographic Atlases*. Woods Hole Press, Woods Hole, Massachusetts, 6 pp + 97 charts.

Trenberth, K.E., and J.G. Olson (1988) ECMWF global analysis 1979-1986: Circulation statistics and data evaluation. NCAR Technical Note NCAR/TN-300+STR, National Center for Atmospheric Research, Boulder, 94 pp.

Walsh, E.J., F.C. Jackson, E.A. Uliana and R.N. Swift (1989) Observations on electromagnetic bias in radar altimeter sea surface measurements. *Journal of Geophysical Research*, *94*, 14575-14584.

Wentz, F. (1983) A model function for ocean microwave brightness temperatures. *Journal of Geophysical Research, 88*, 1892-1908.

Wentz, F.J. (1988) Water vapor path length correction for altimeters. In: Appendix to U.S. WOCE Technical Report No. 2, edited by D.B. Chelton, U.S. Planning Office for WOCE, Texas A&M University, College Station, 5 pp.

Wentz, F.J. (1989a) User's manual for the collocated GEOSAT SSMI tape. RSS Technical Report 100190, Remote Sensing Systems, Santa Rosa, California, 3 pp.

Wentz, F.J. (1989b) User's manual: SSMI geophysical tapes. RSS Technical Report 060989, Remote Sensing Systems, Santa Rosa, California, 16 pp.

Wentz, F. (1991) Measurement of oceanic wind vector using satellite microwave radiometers. Submitted to *Journal of Geophysical Research.*

Wentz, F.J., L.A. Mattox and S. Peteherych (1986) New algorithms for microwave measurements of ocean winds: Applications to SEASAT and the special sensor microwave imager. *Journal of Geophysical Research, 91*, 2289-2307.

Wyrtki, K., and G. Mitchum (1990) Interannual differences of GEOSAT altimeter heights and sea level: The importance of a datum. *Journal of Geophysical Research, 95*, 2969-2975.

Wyrtki, K., P. Caldwell, K. Constantine, B.J. Kilonsky, G.T. Mitchum, B. Miyamoto, T. Murphy and S. Nakahara (1988) The Pacific island sea level network. JIMAR 88-137, University of Hawaii, Honolulu, 71 pp.

Zlotnicki, V. (1991) Sea level differences across the Gulf Stream and Kuroshio Extension. *Journal of Physical Oceanography, 21*, 599-609.

Zlotnicki, V., L.-L. Fu and W. Patzert (1989) Seasonal variability in global sea level observed with GEOSAT altimetry. *Journal of Geophysical Research, 94*, 17959-17969.

Zlotnicki, V., A. Hayashi and L.-L. Fu (1990) The JPL-Oceans-8902 version of GEOSAT altimetry data. JPL Internal Document D-6939, Jet Propulsion Laboratory, Pasadena, 17 pp + 60 charts.

Appendix A

Atlas of Monthly Mean Distributions

A1

Monthly Mean GEOSAT Sea Surface Height Variation

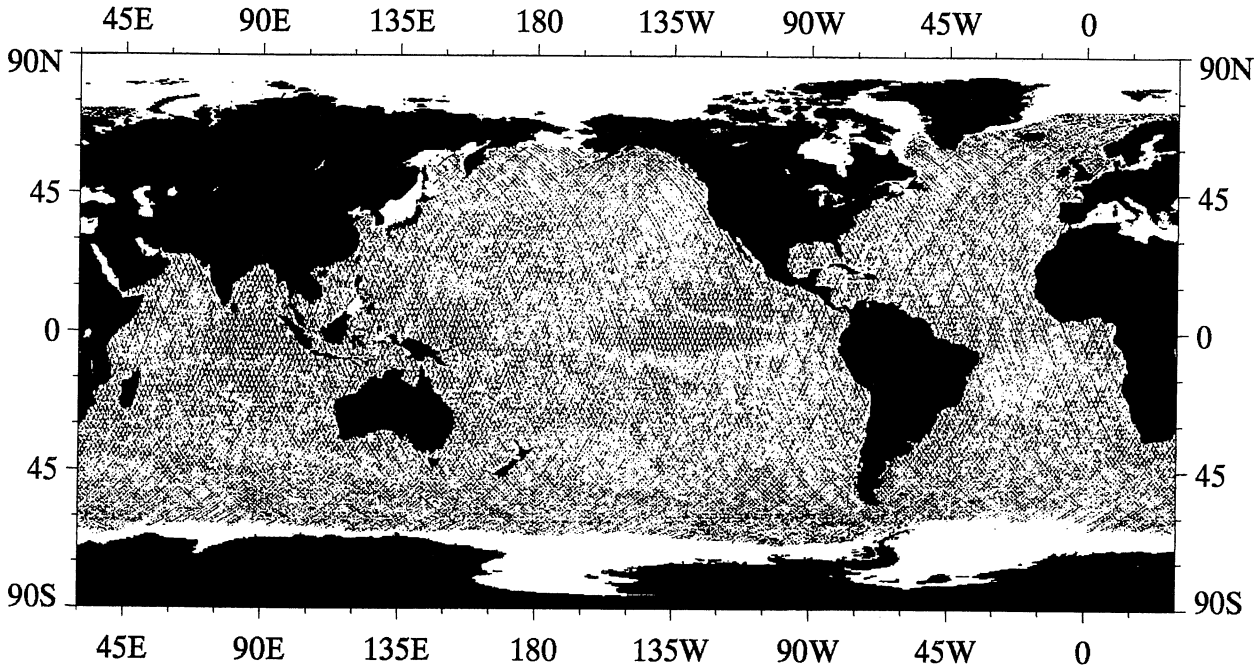

January 1987

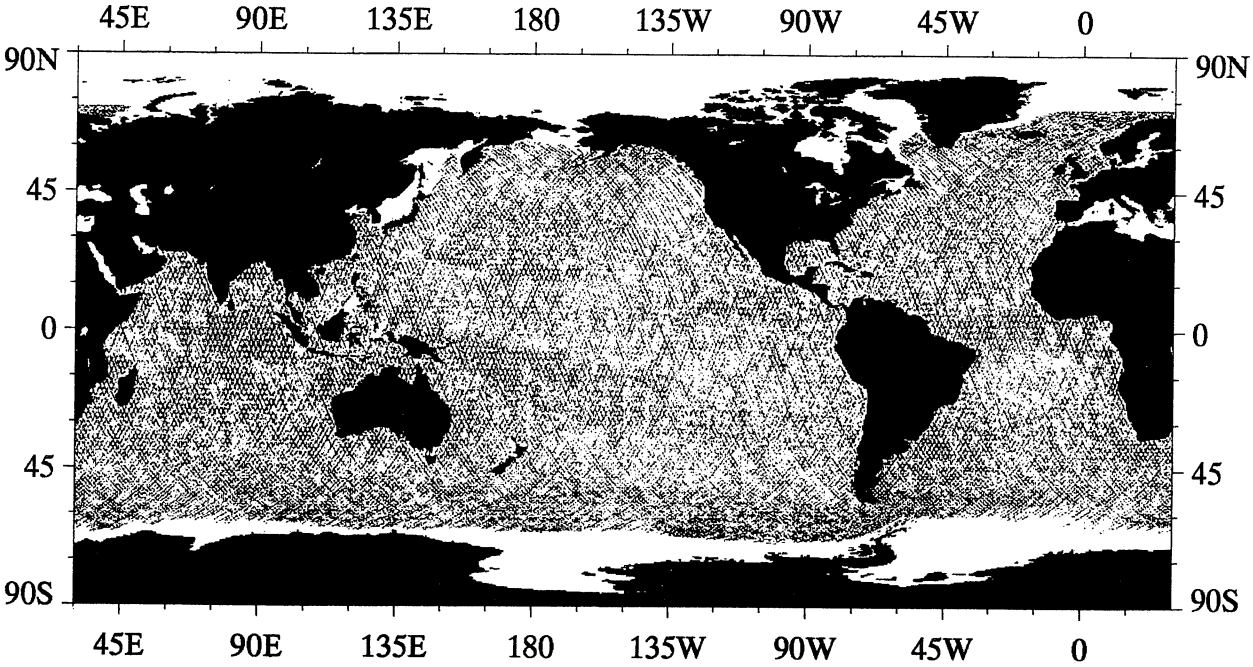

February 1987

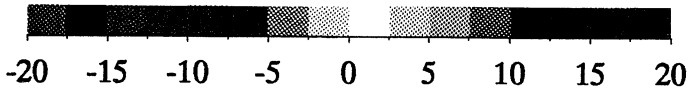

GEOSAT Sea Surface Height Variation Referenced to a 2-Year Mean, cm

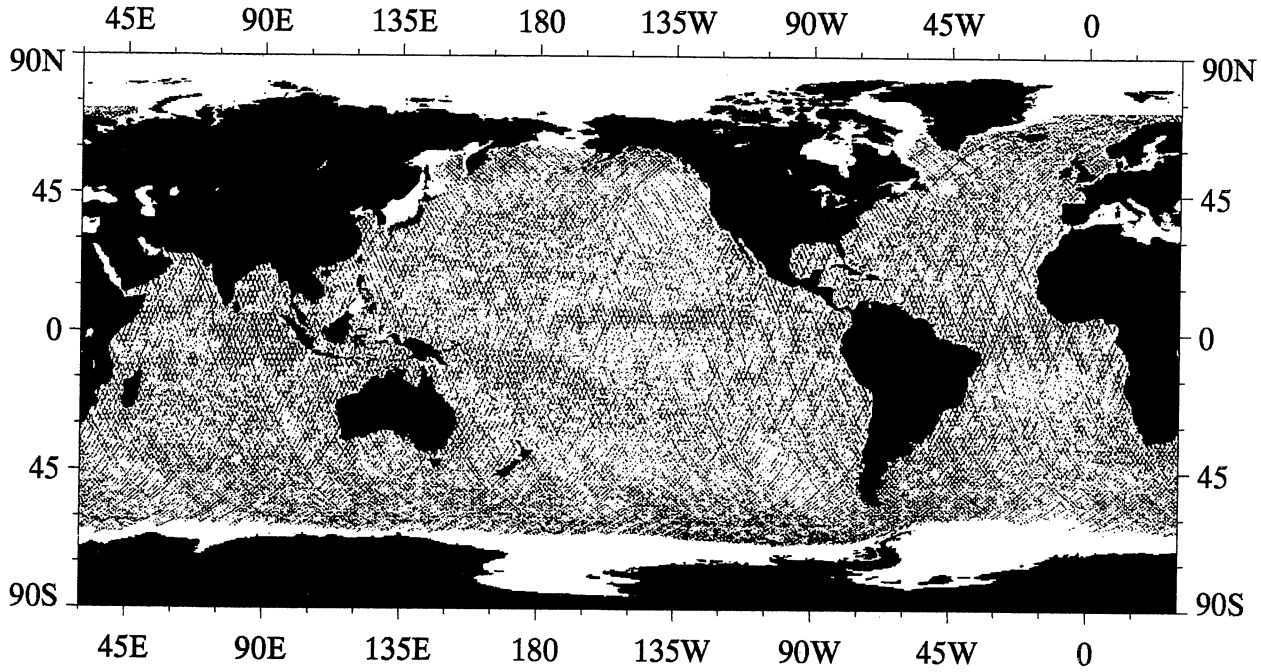

March 1987

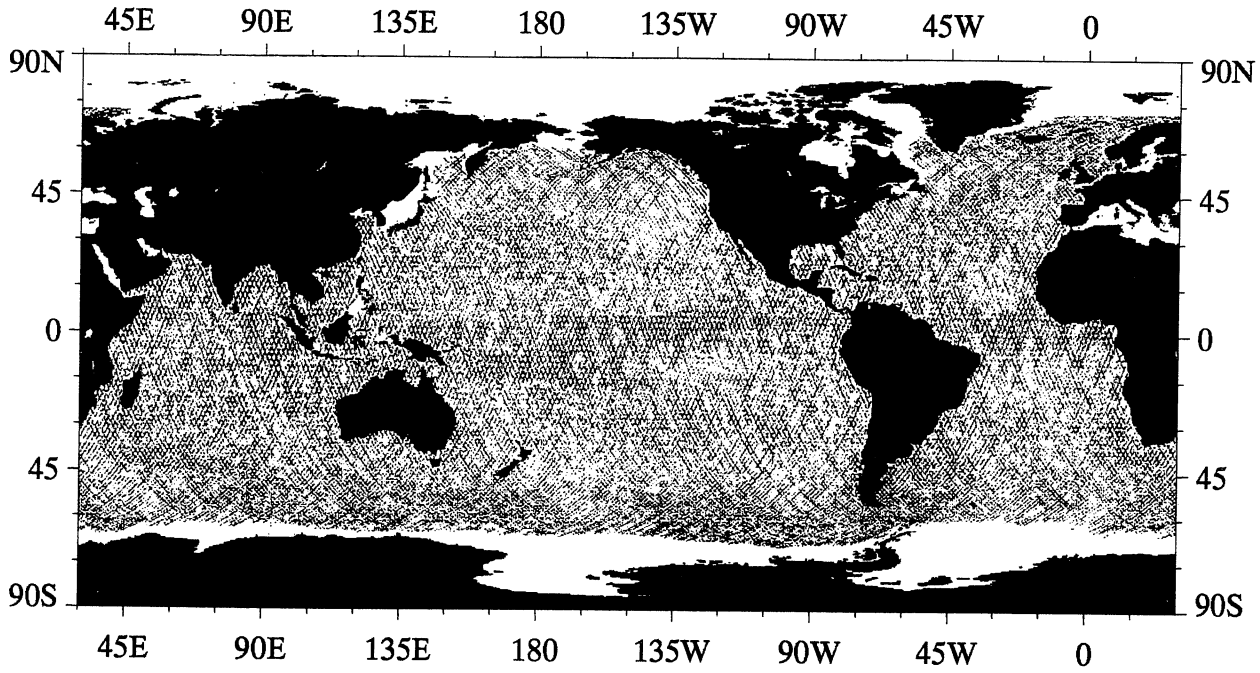

April 1987

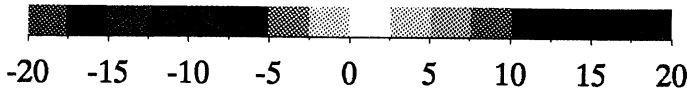

GEOSAT Sea Surface Height Variation Referenced to a 2-Year Mean, cm

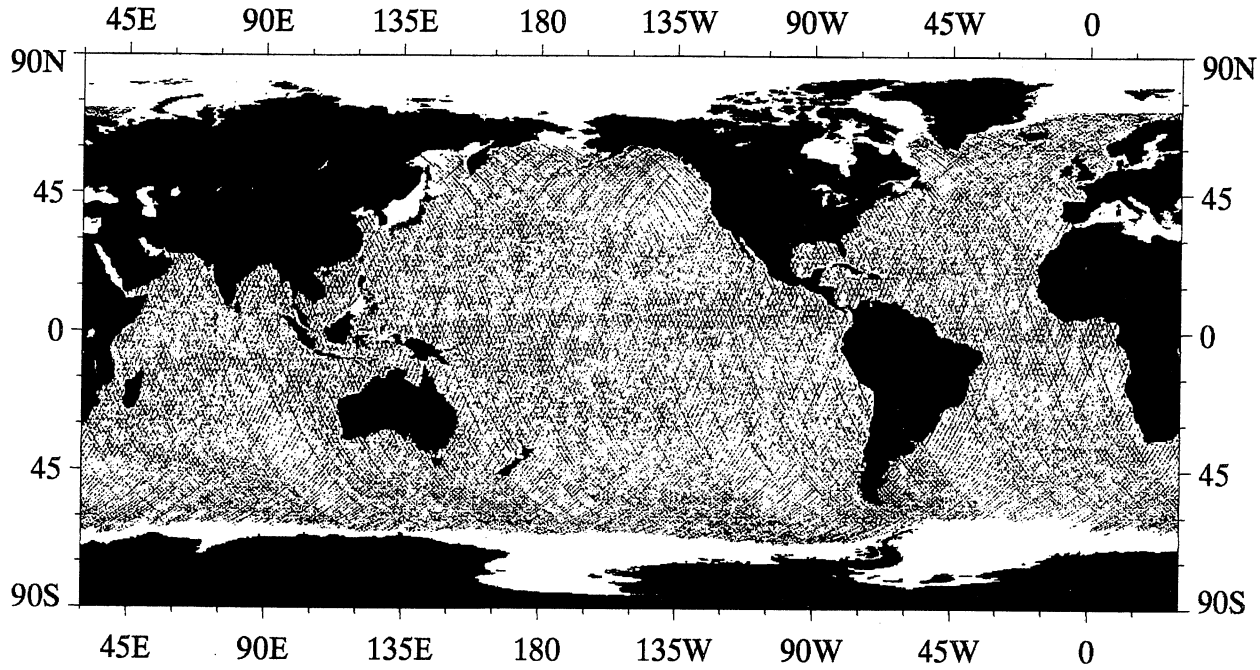

May 1987

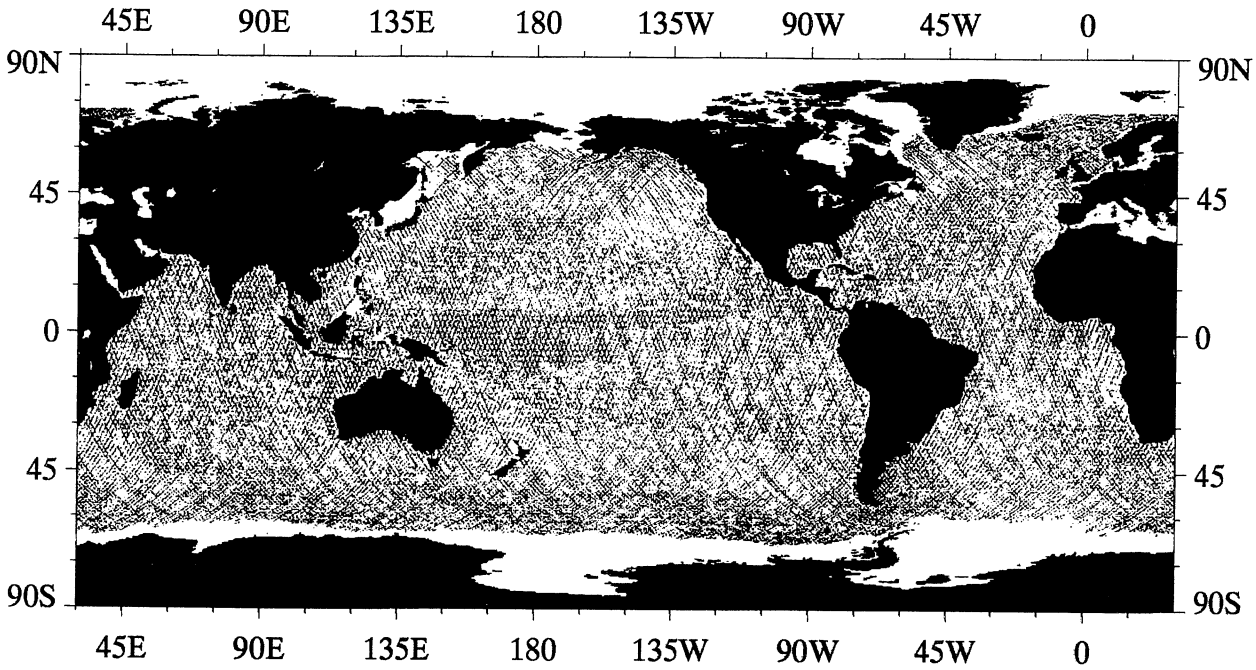

June 1987

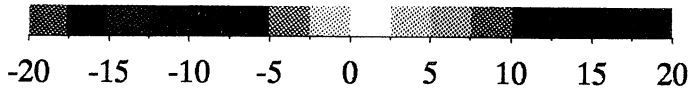

GEOSAT Sea Surface Height Variation Referenced to a 2-Year Mean, cm

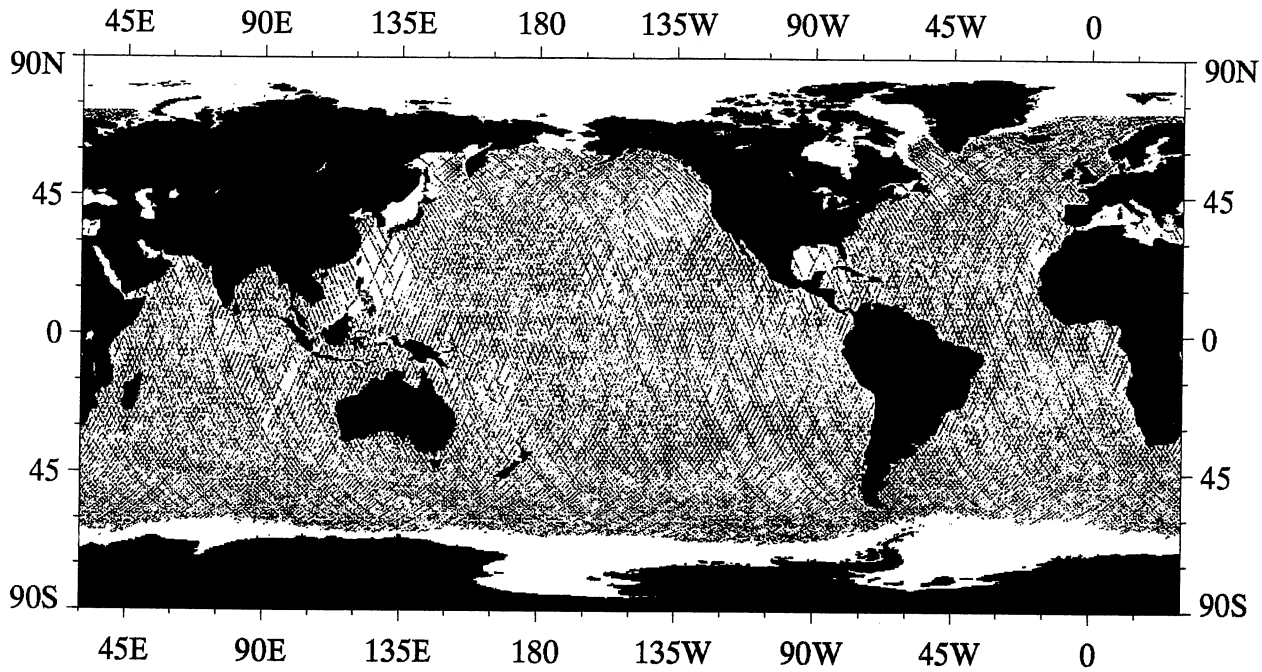

July 1987

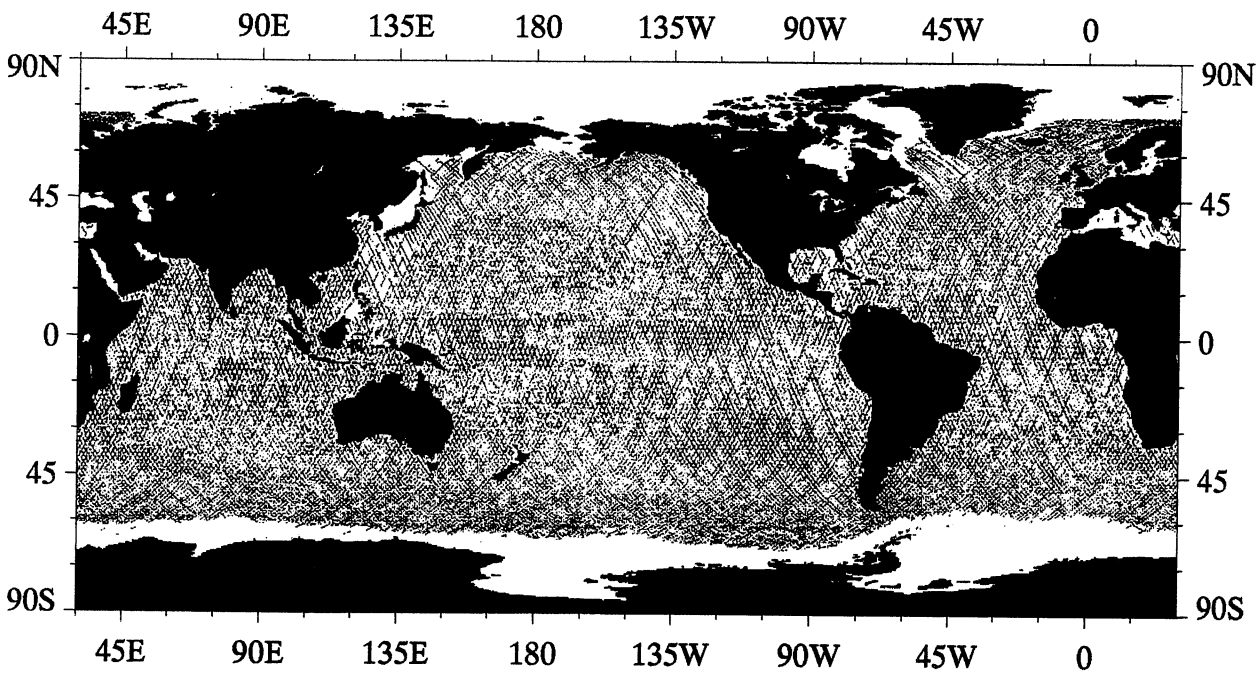

August 1987

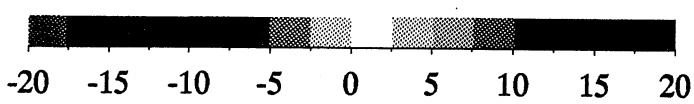

GEOSAT Sea Surface Height Variation Referenced to a 2-Year Mean, cm

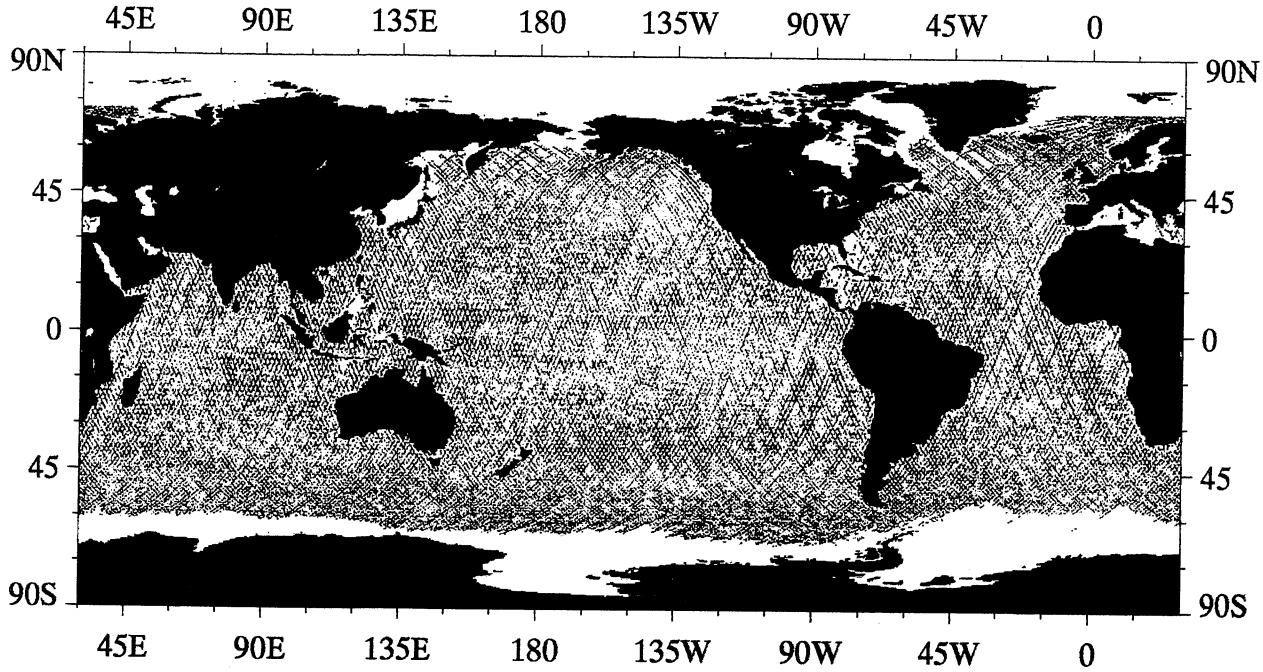

September 1987

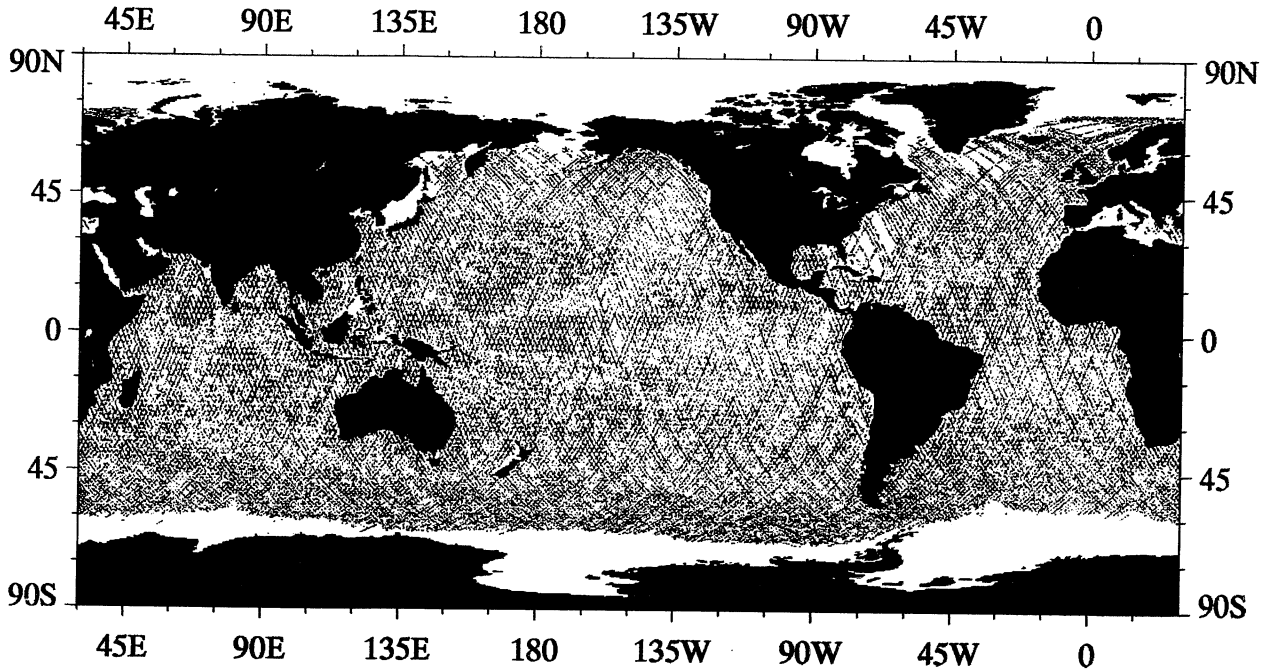

October 1987

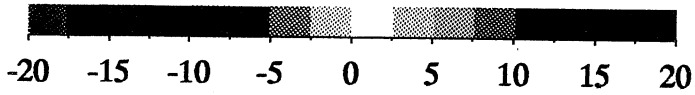

GEOSAT Sea Surface Height Variation Referenced to a 2-Year Mean, cm

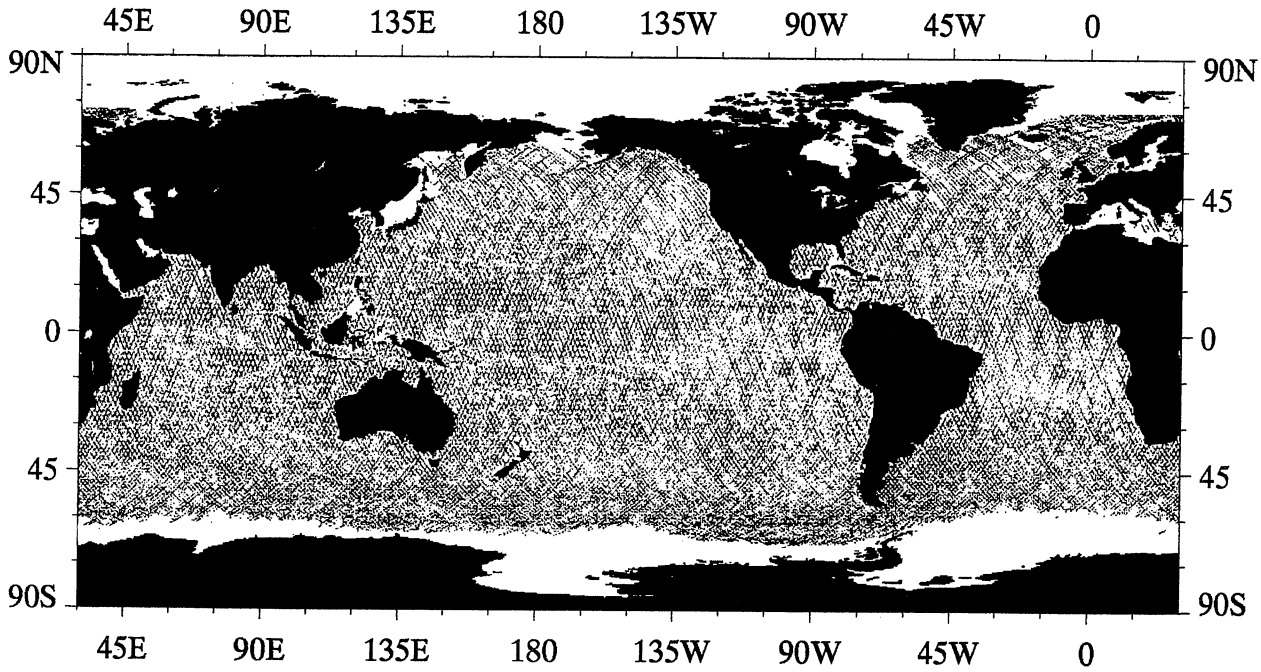

November 1987

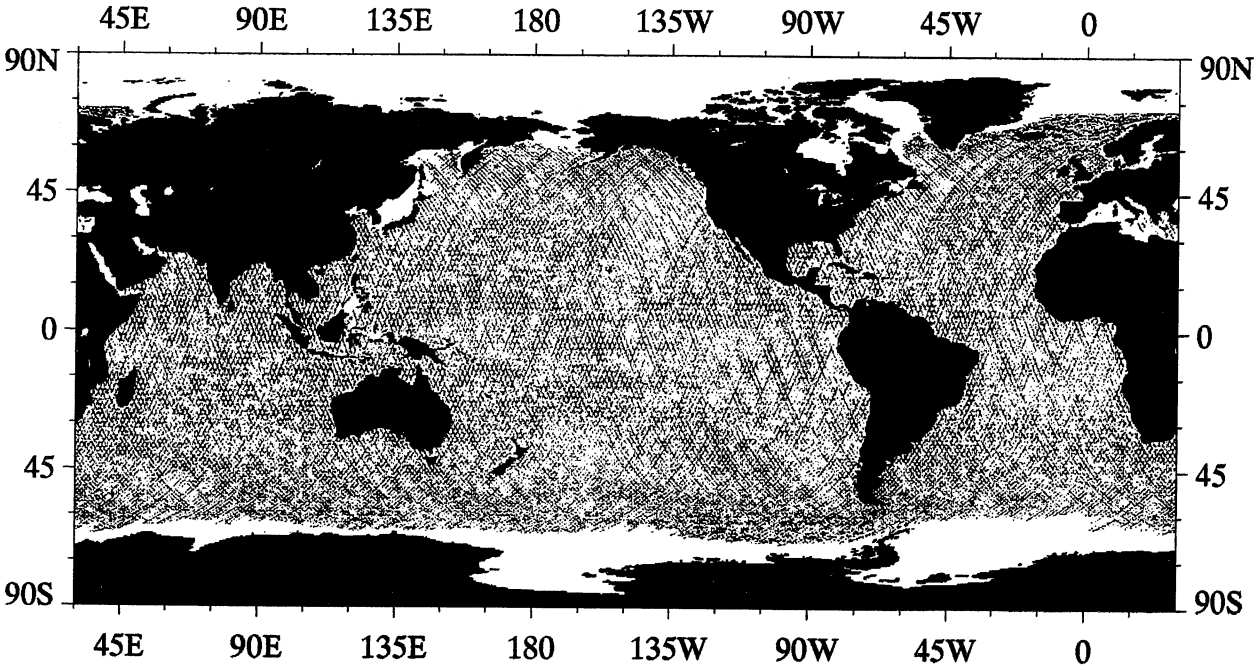

December 1987

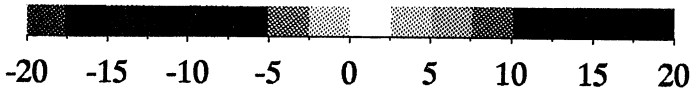

GEOSAT Sea Surface Height Variation Referenced to a 2-Year Mean, cm

A2

Monthly GEOSAT Sampling Distribution

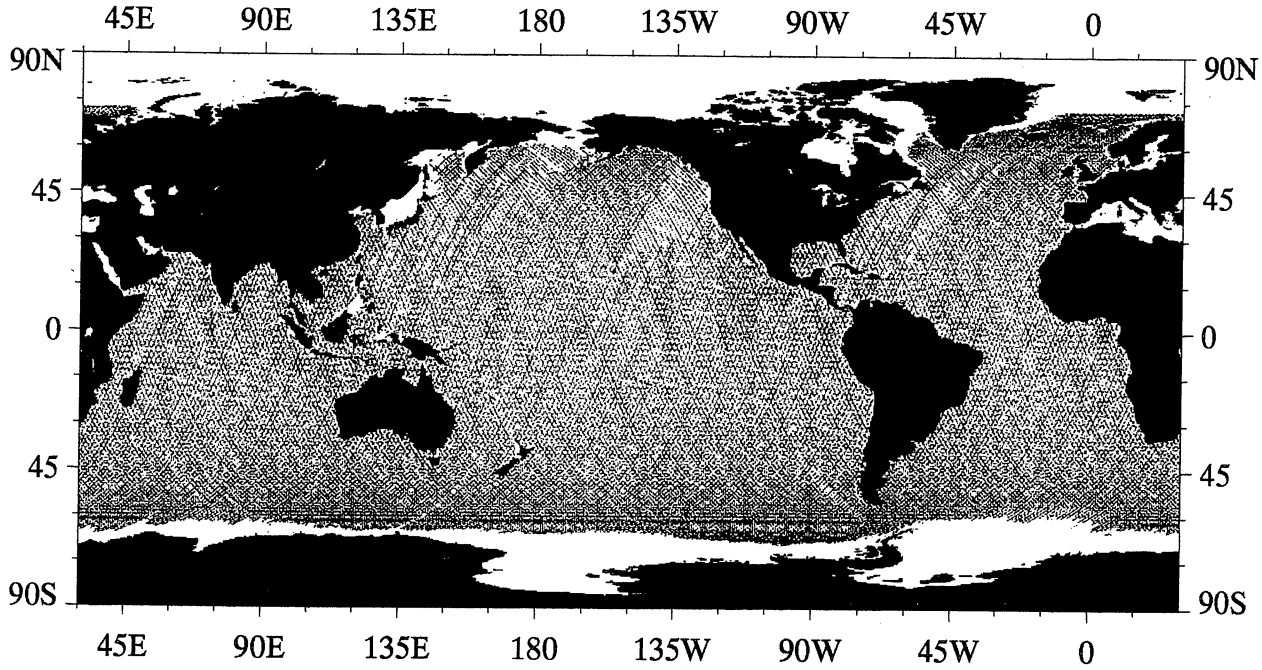

January 1987, max = 35

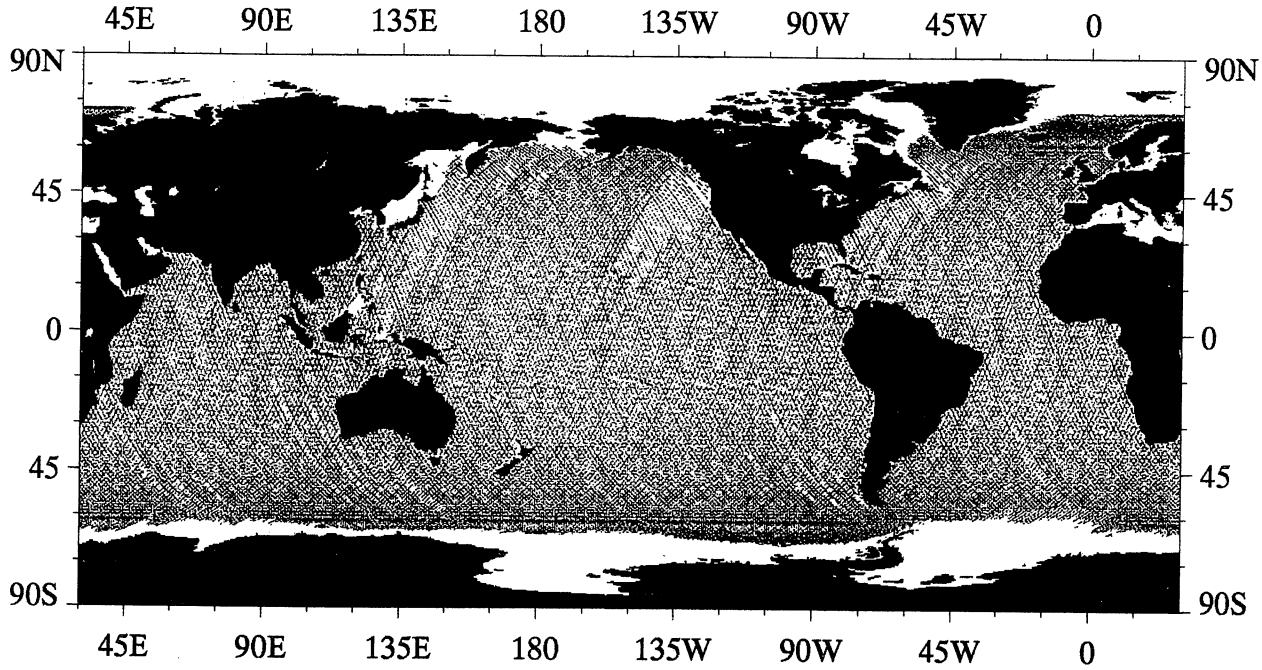

February 1987, max = 36

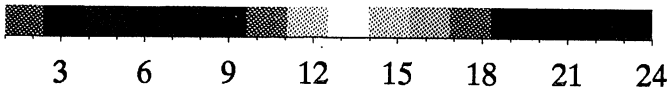

Number of GEOSAT Sea Surface Height Values per Pixel

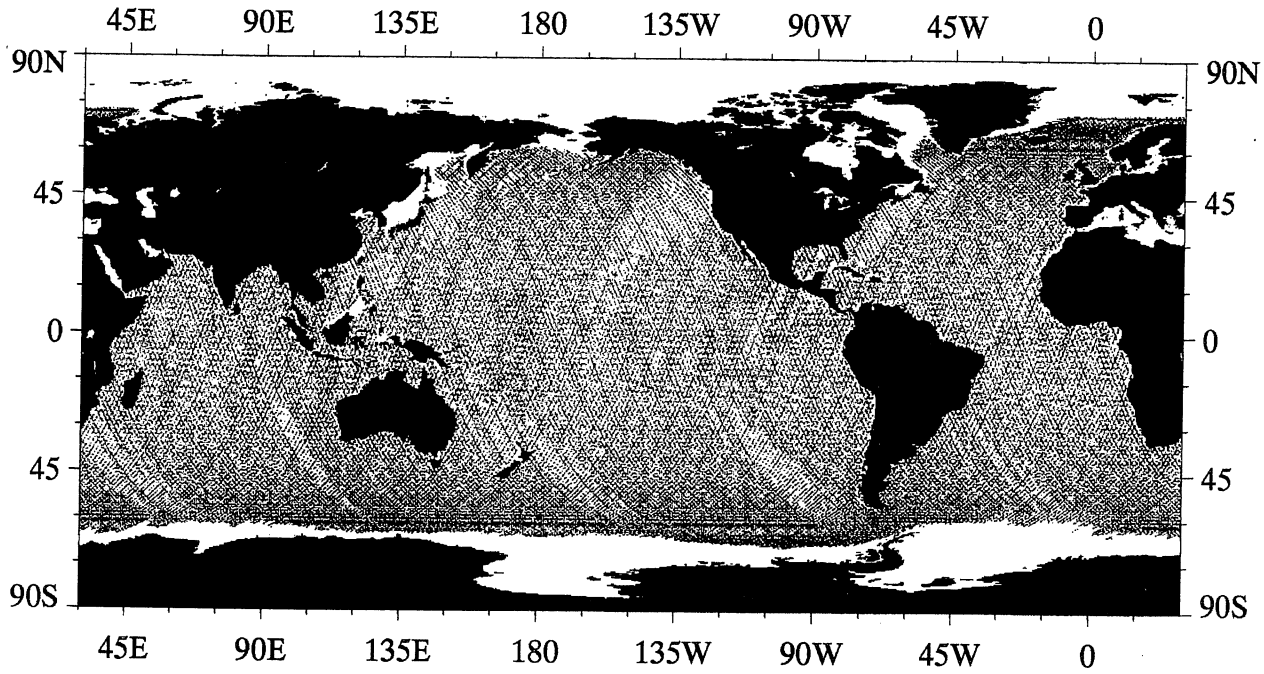

March 1987, max = 39

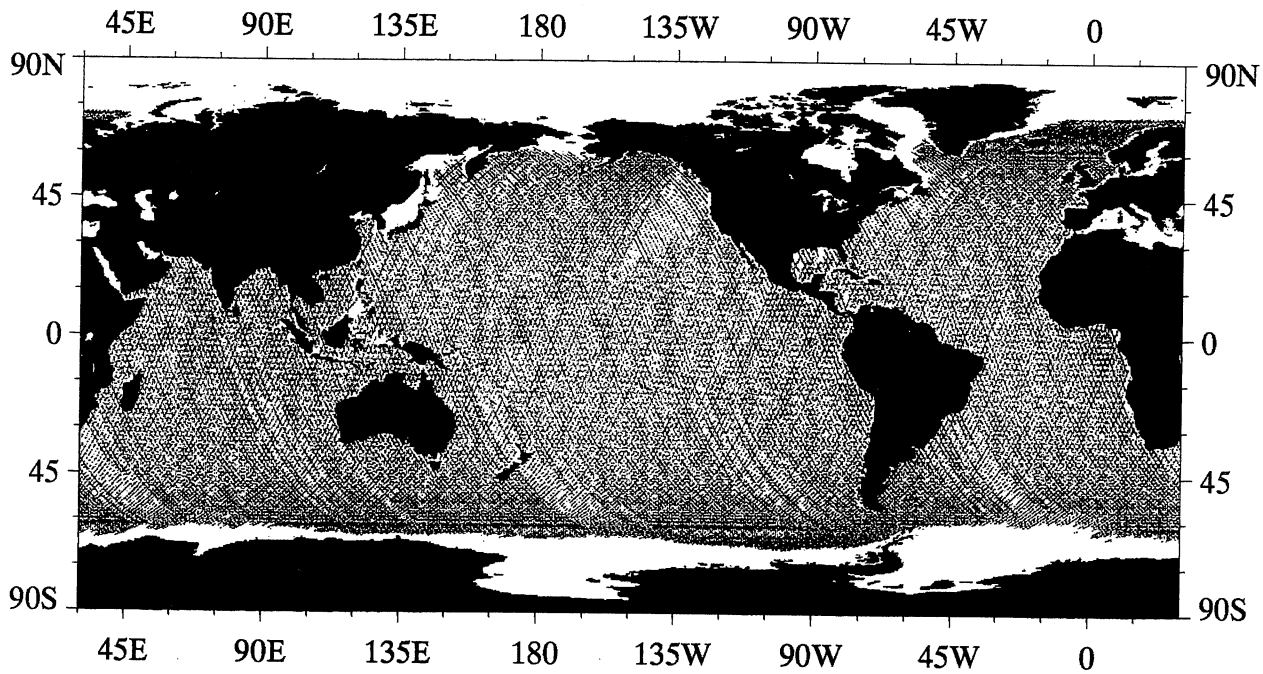

April 1987, max = 37

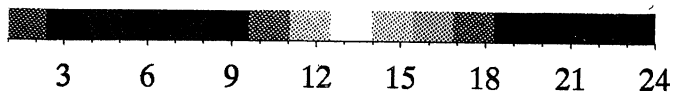

Number of GEOSAT Sea Surface Height Values per Pixel

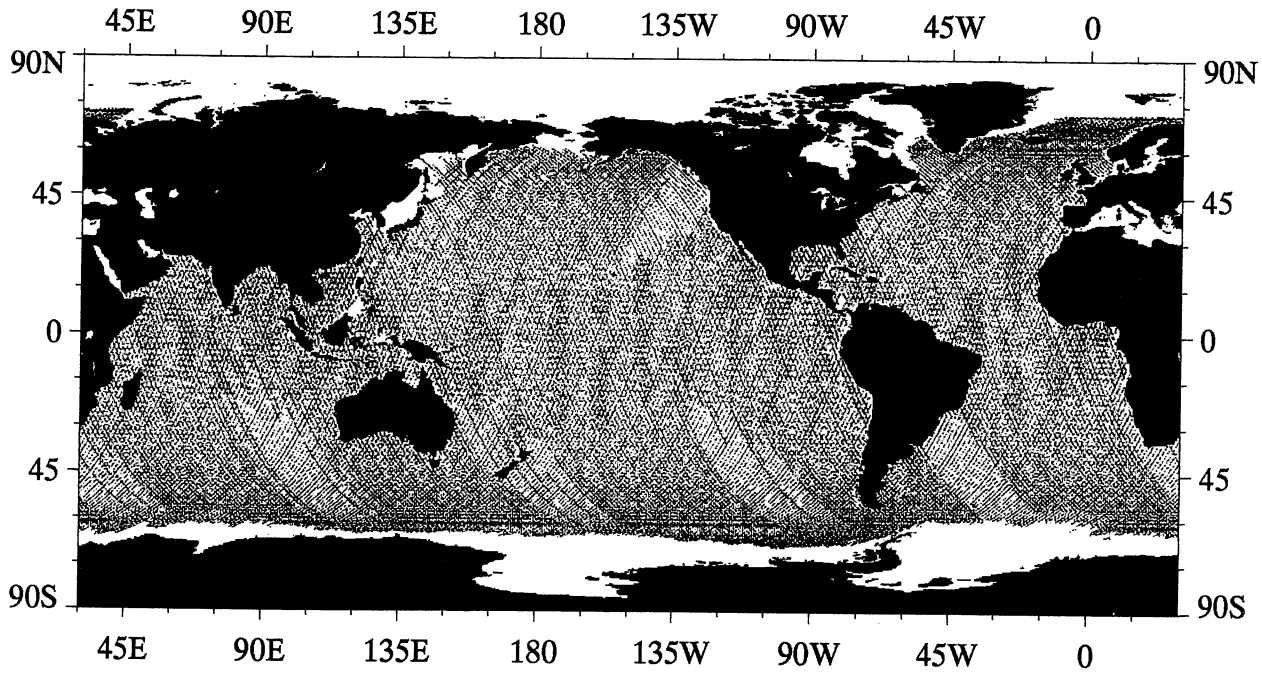

May 1987, max = 37

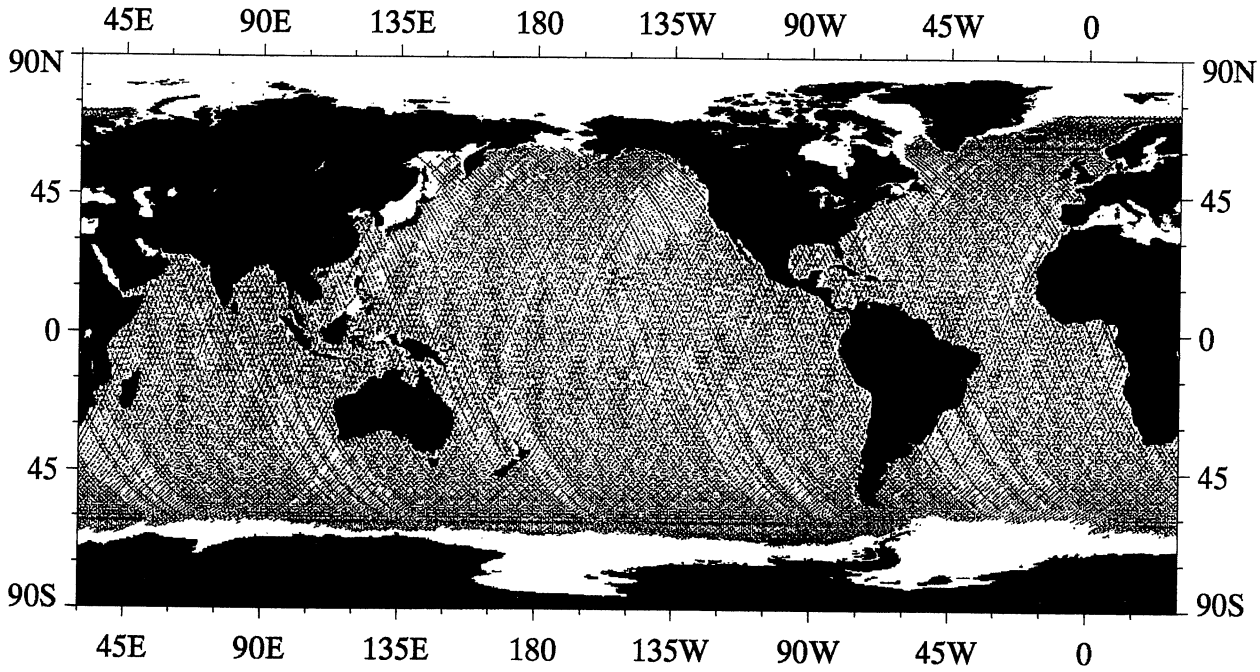

June 1987, max = 39

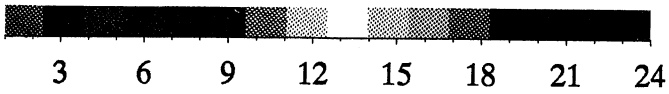

Number of GEOSAT Sea Surface Height Values per Pixel

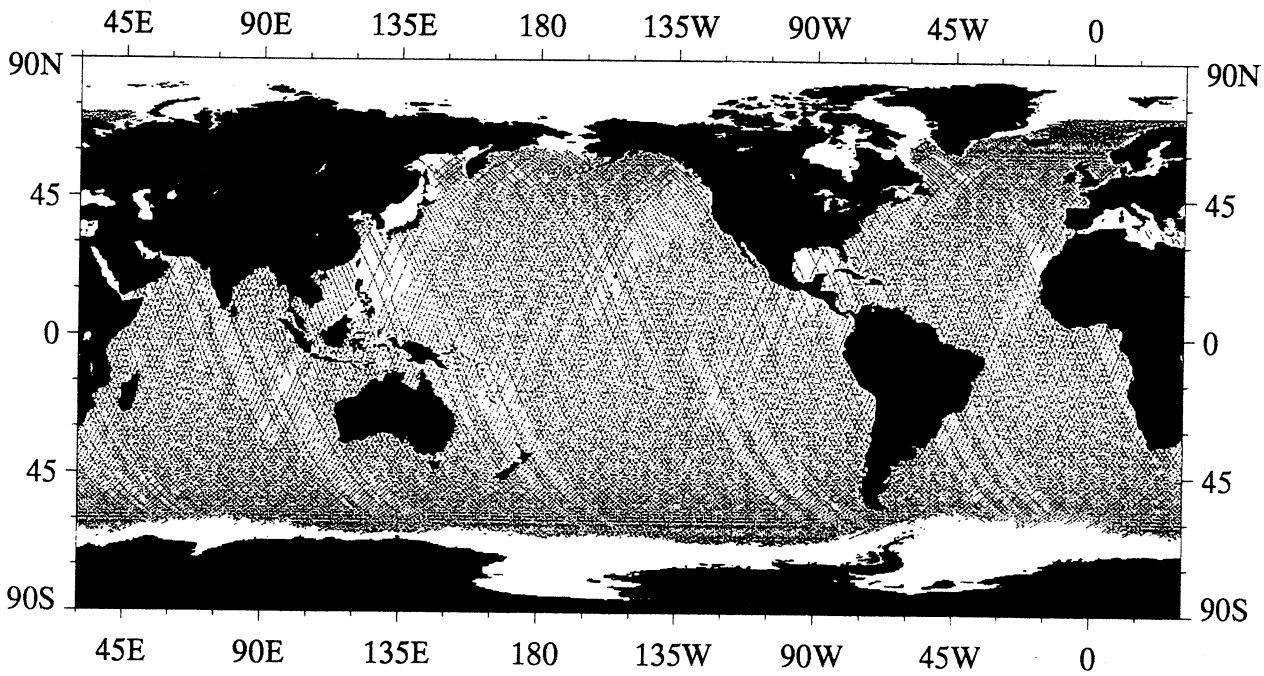

July 1987, max = 34

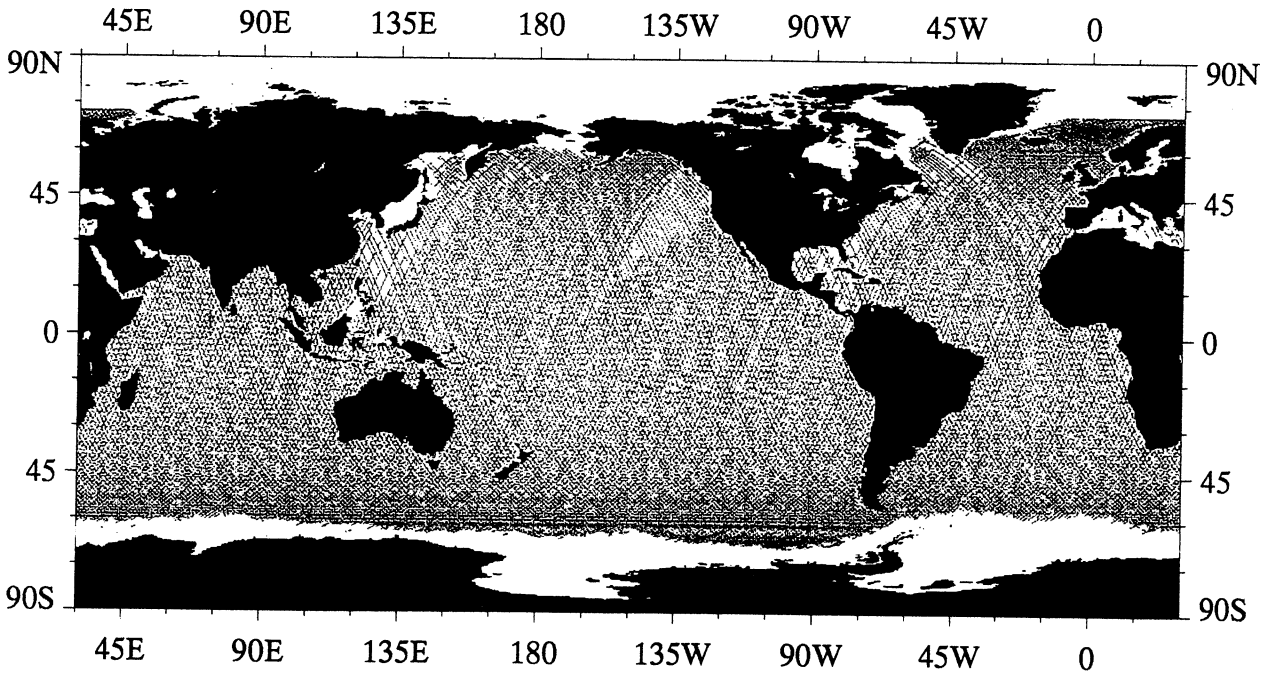

August 1987, max = 32

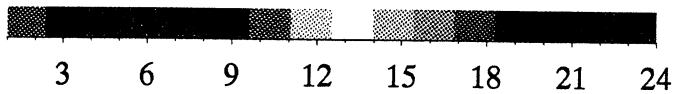

Number of GEOSAT Sea Surface Height Values per Pixel

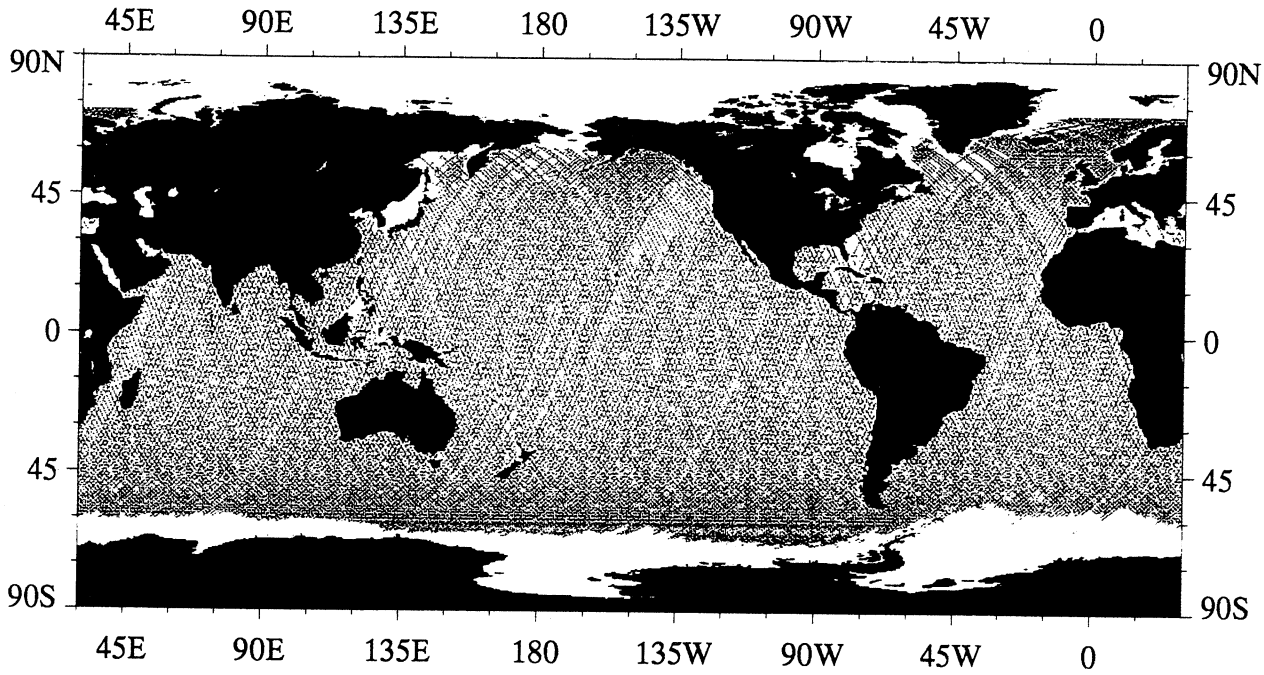

September 1987, max = 25

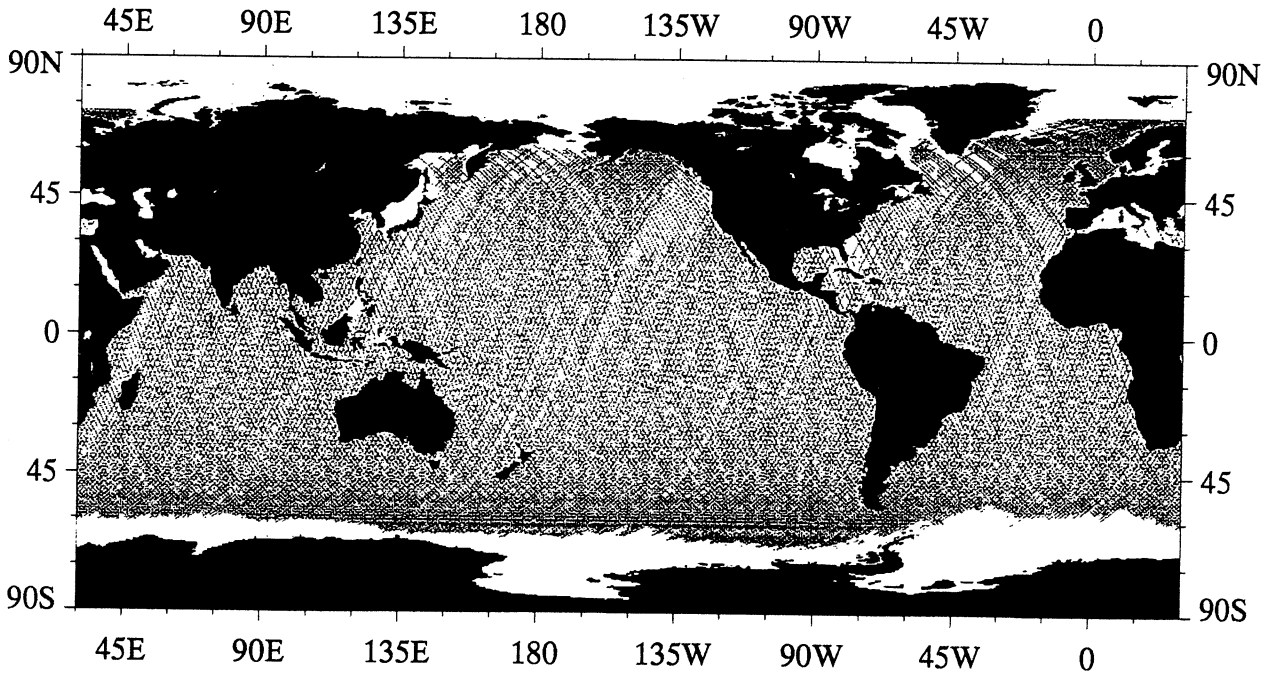

October 1987, max = 28

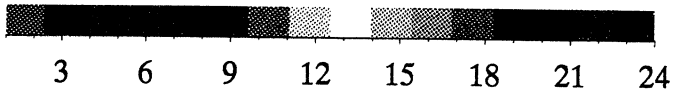

Number of GEOSAT Sea Surface Height Values per Pixel

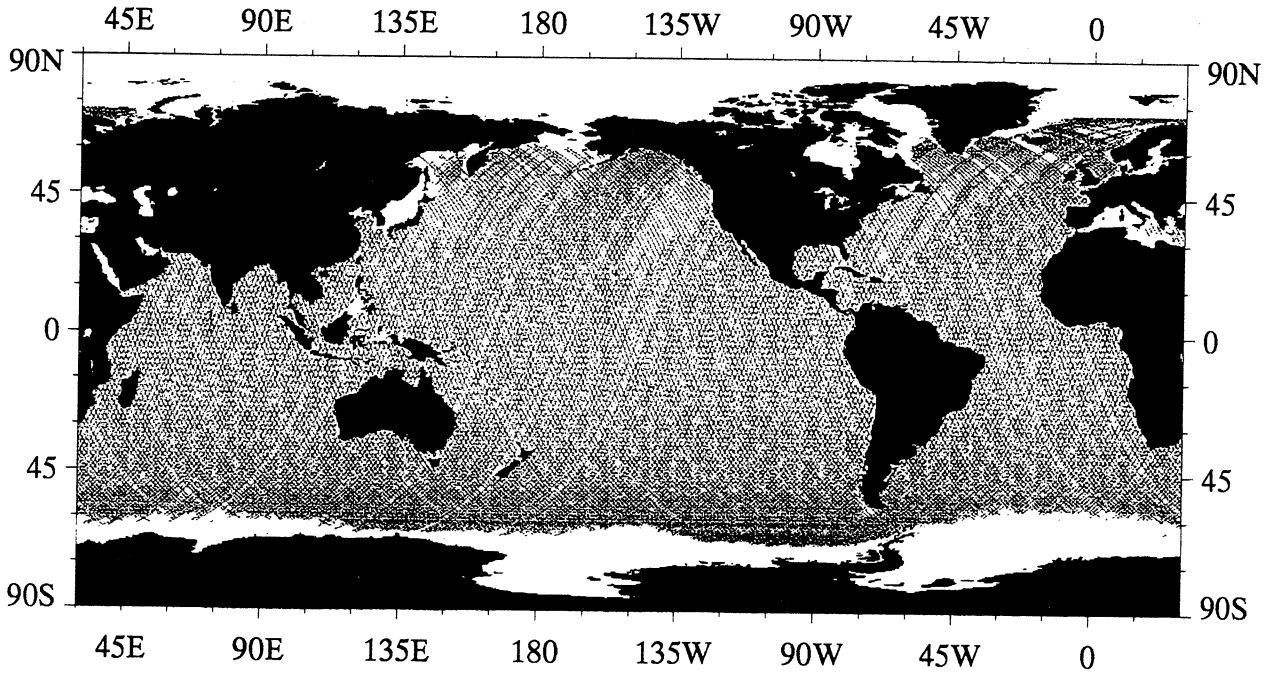

November 1987, max = 24

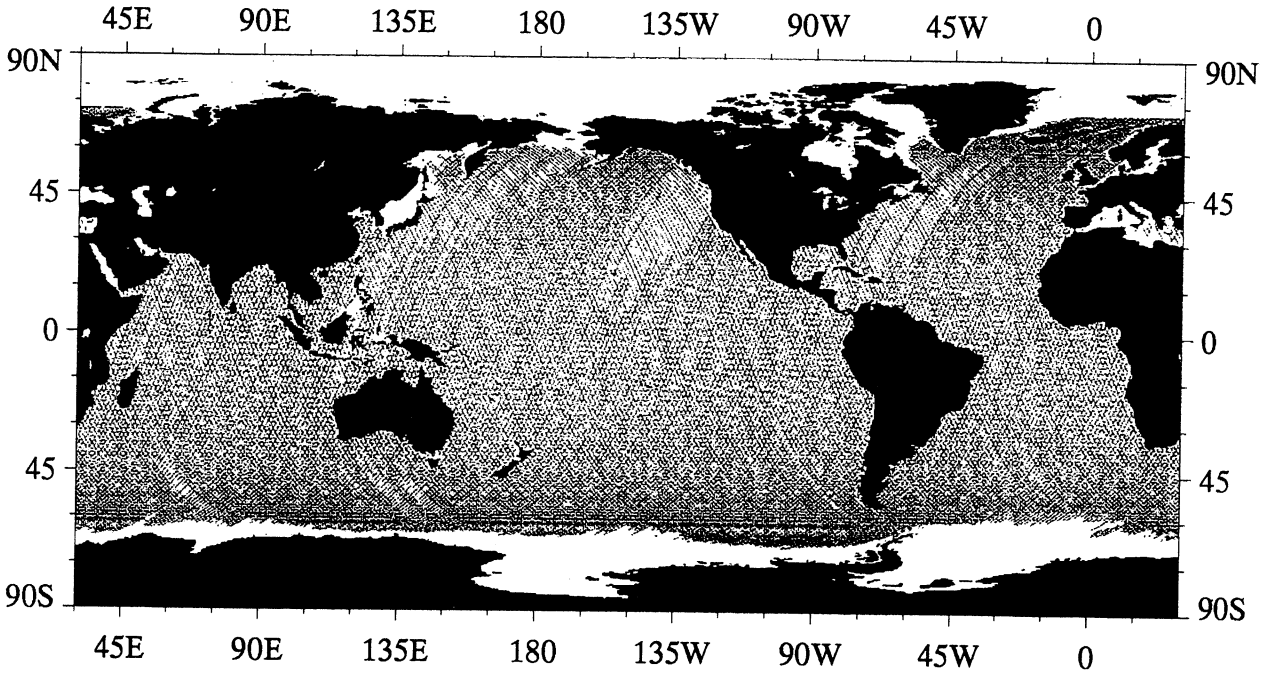

December 1987, max = 34

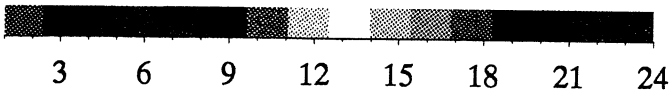

Number of GEOSAT Sea Surface Height Values per Pixel

A3

Monthly Mean SSMI Surface Wind Speed

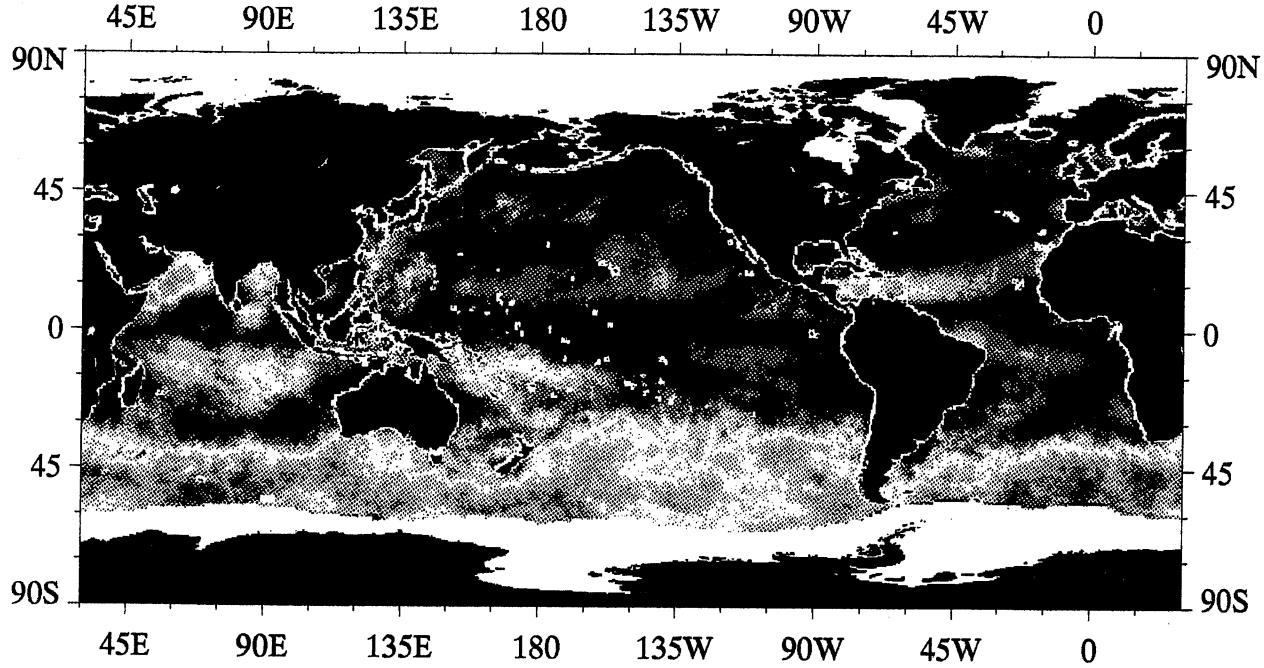

9 - 31 July 1987

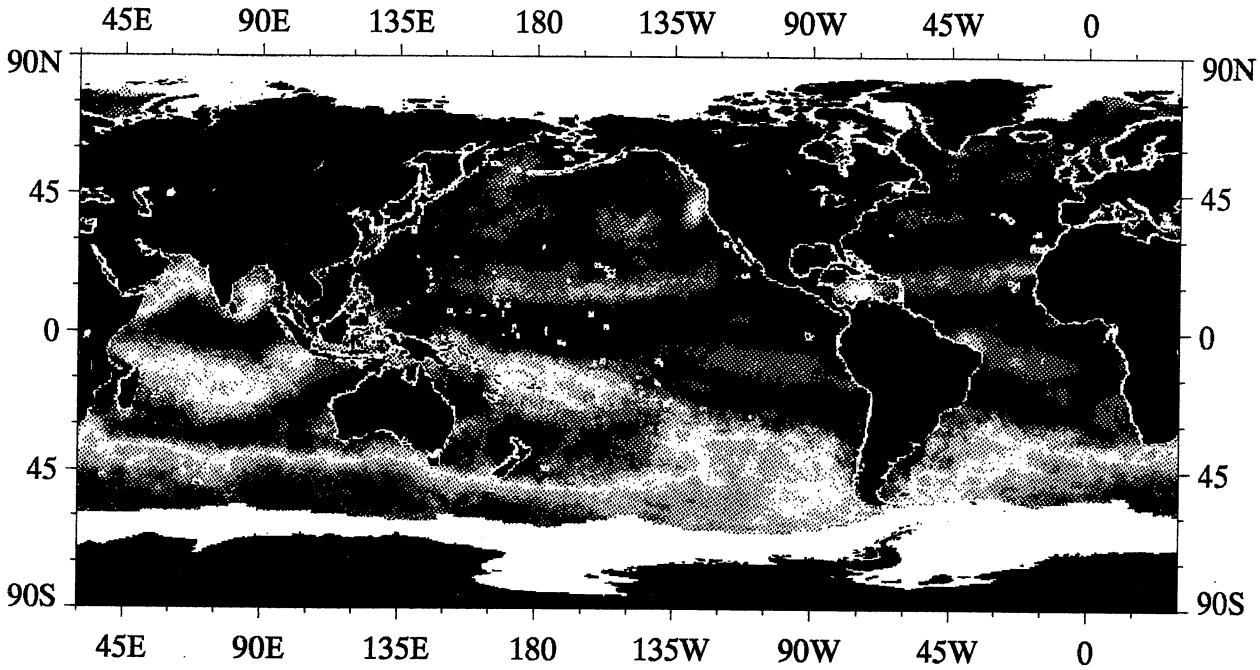

August 1987

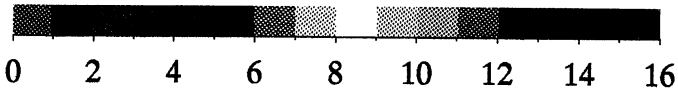

SSMI Wind Speed Referenced to 10 m, m s^{-1}

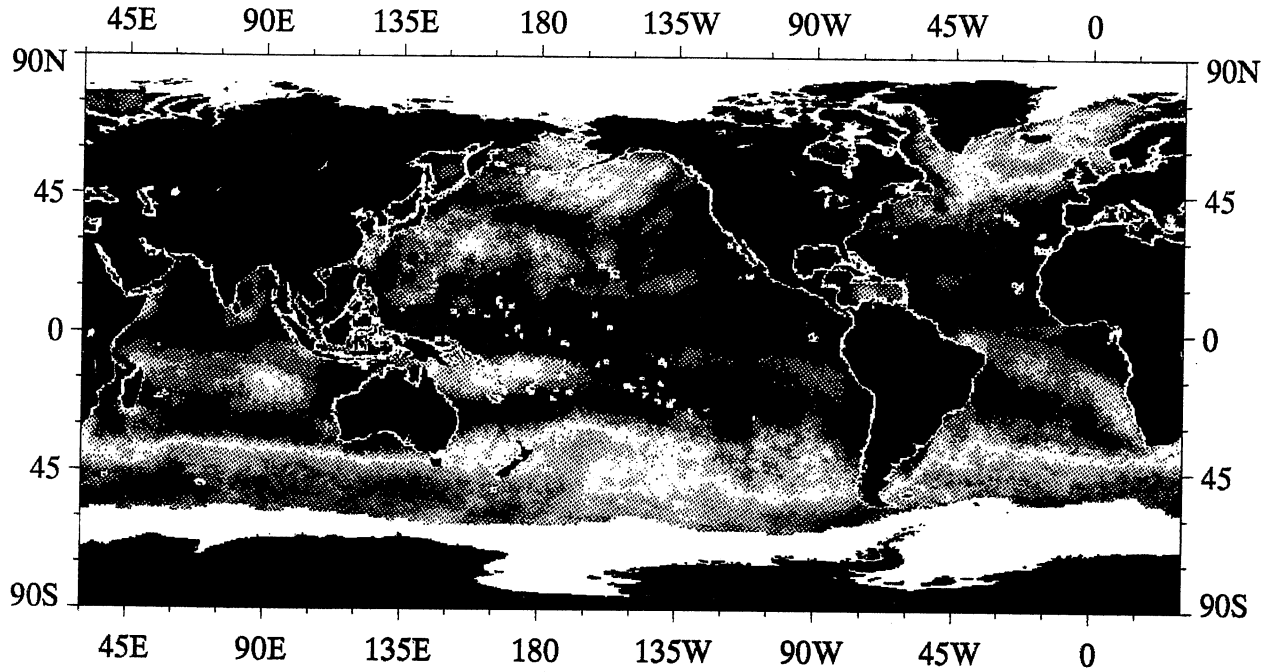

September 1987

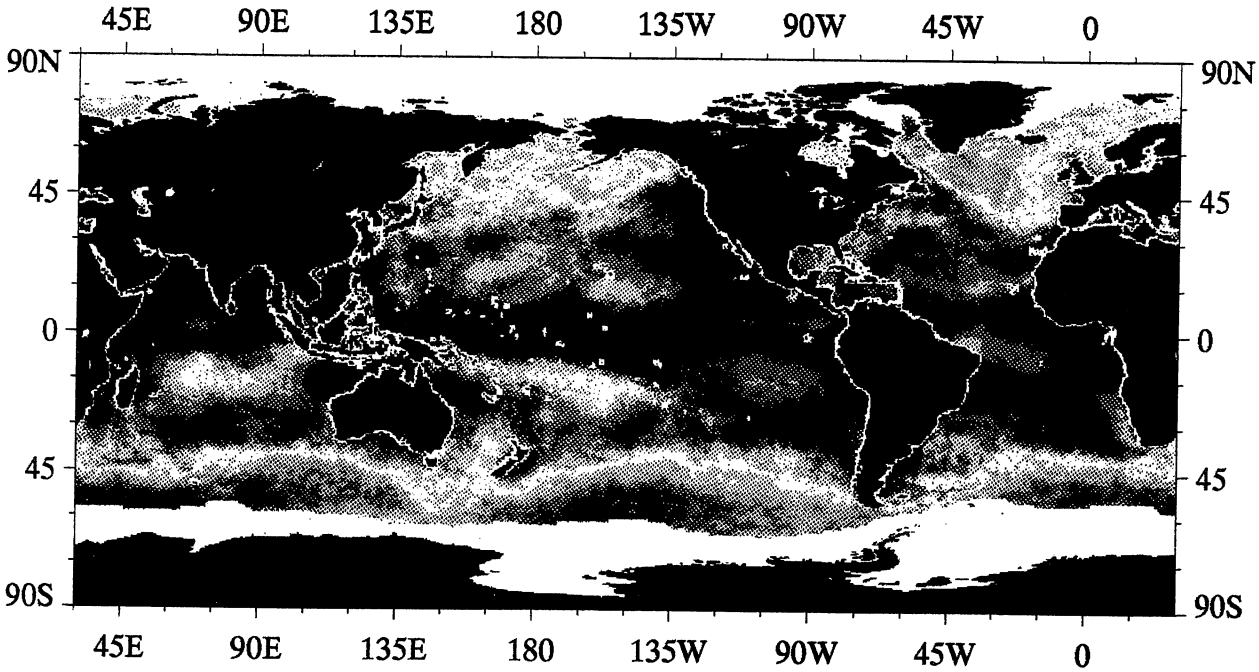

October 1987

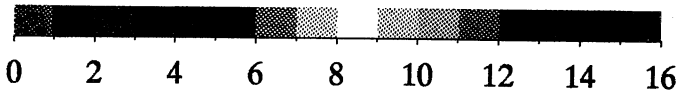

SSMI Wind Speed Referenced to 10 m, m s^{-1}

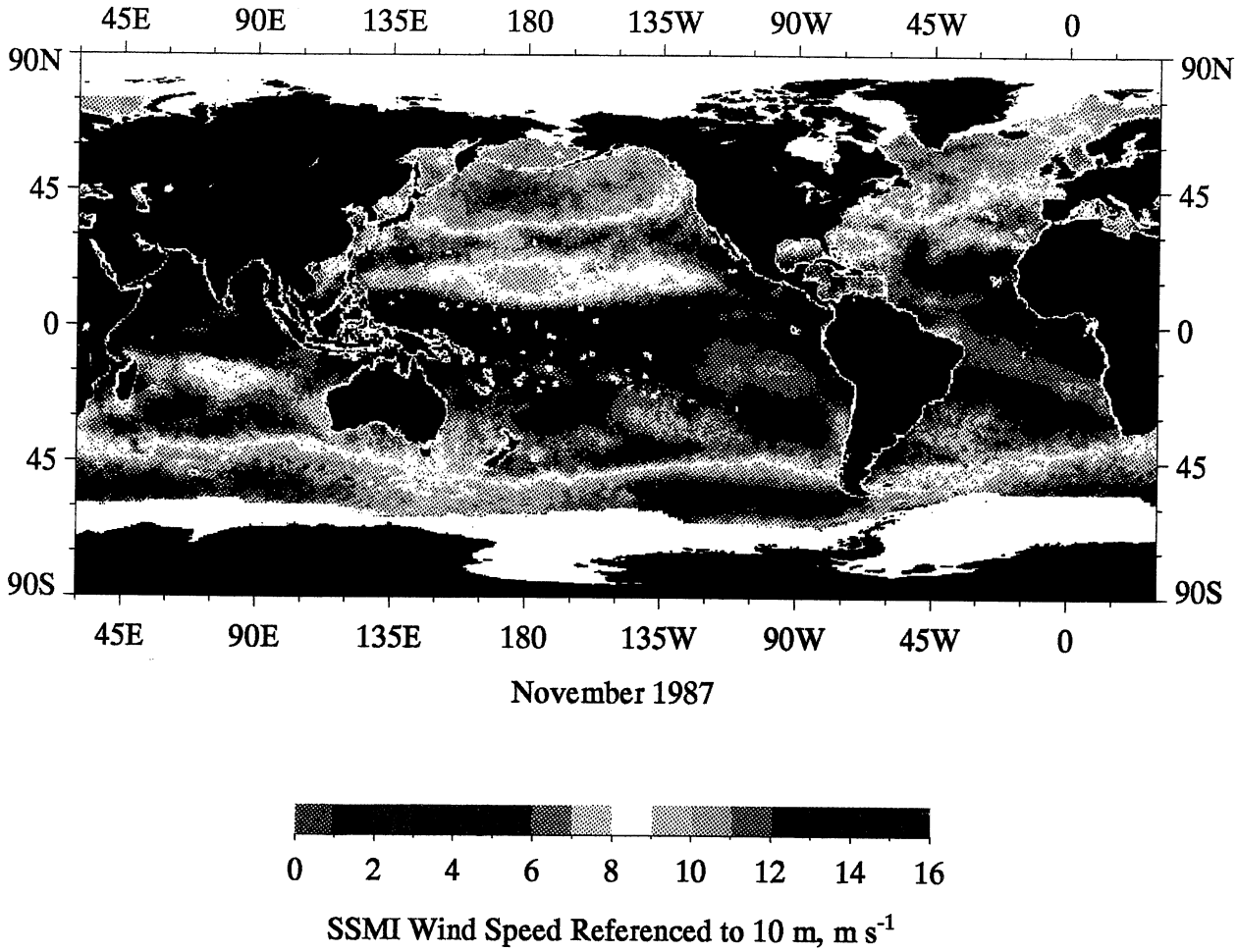
45E
90E
135E
180
135W
90W
45W
0
90N
45
0
45
90S
November 1987
0
2
4
6
8
10
12
14
16
SSMI Wind Speed Referenced to 10 m, m s-1

A4

Monthly SSMI Sampling Distribution

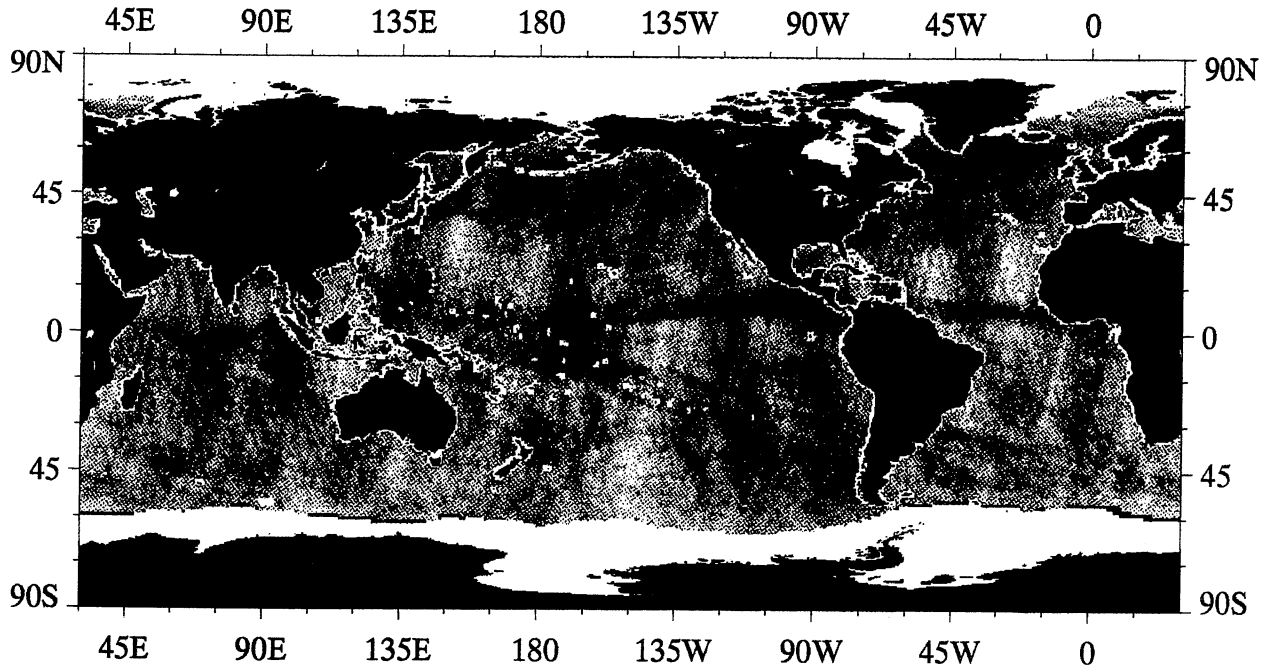

9 - 31 July 1987, max = 68

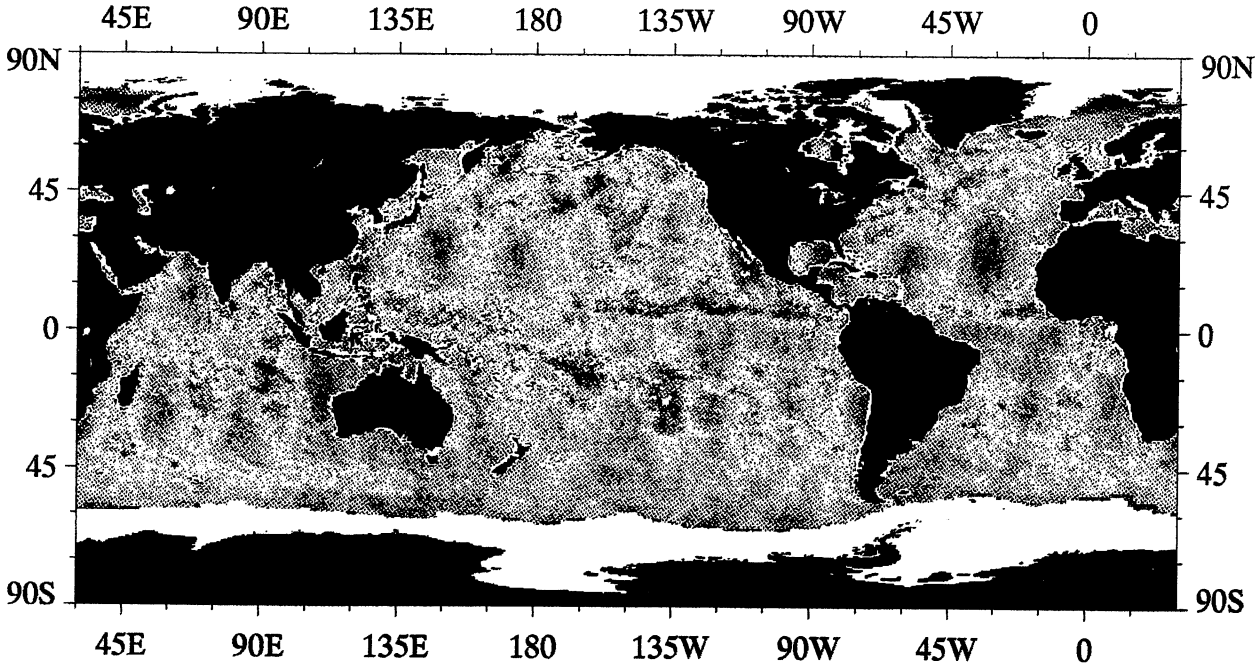

August 1987, max = 118

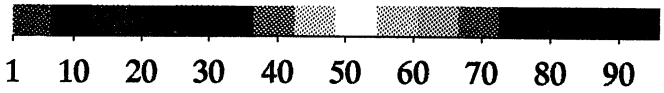

Number of SSMI Wind Speed Values per Pixel

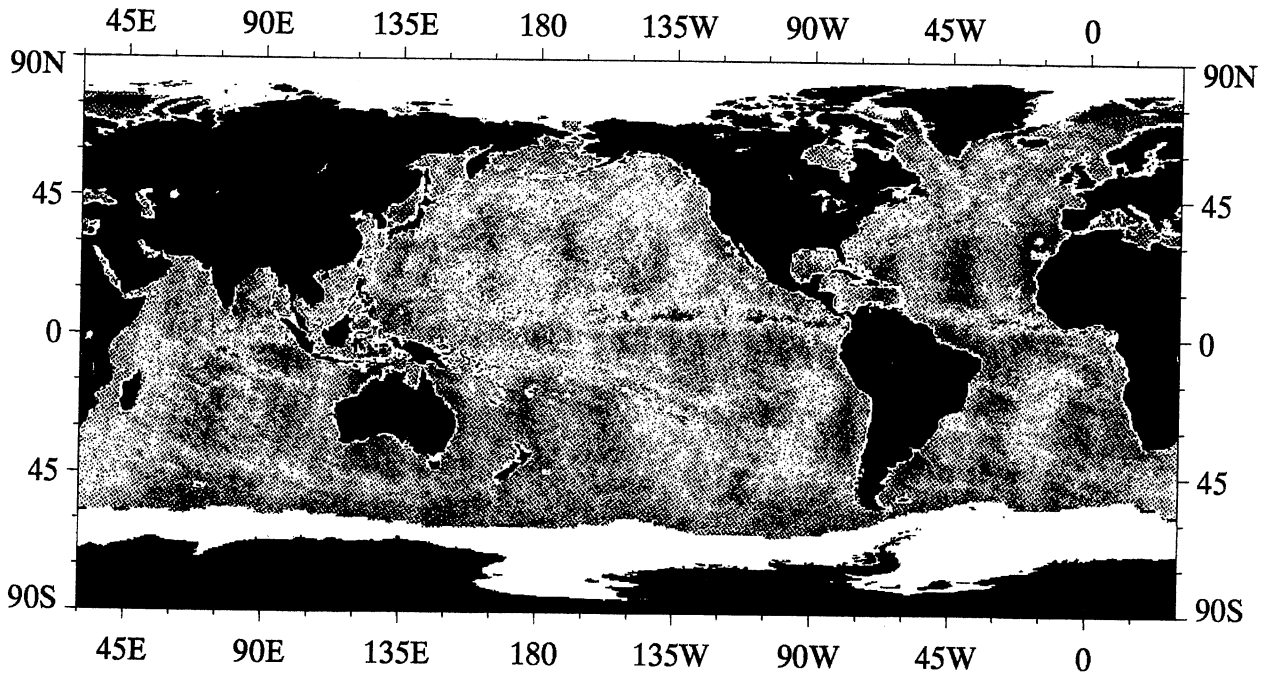

September 1987, max = 132

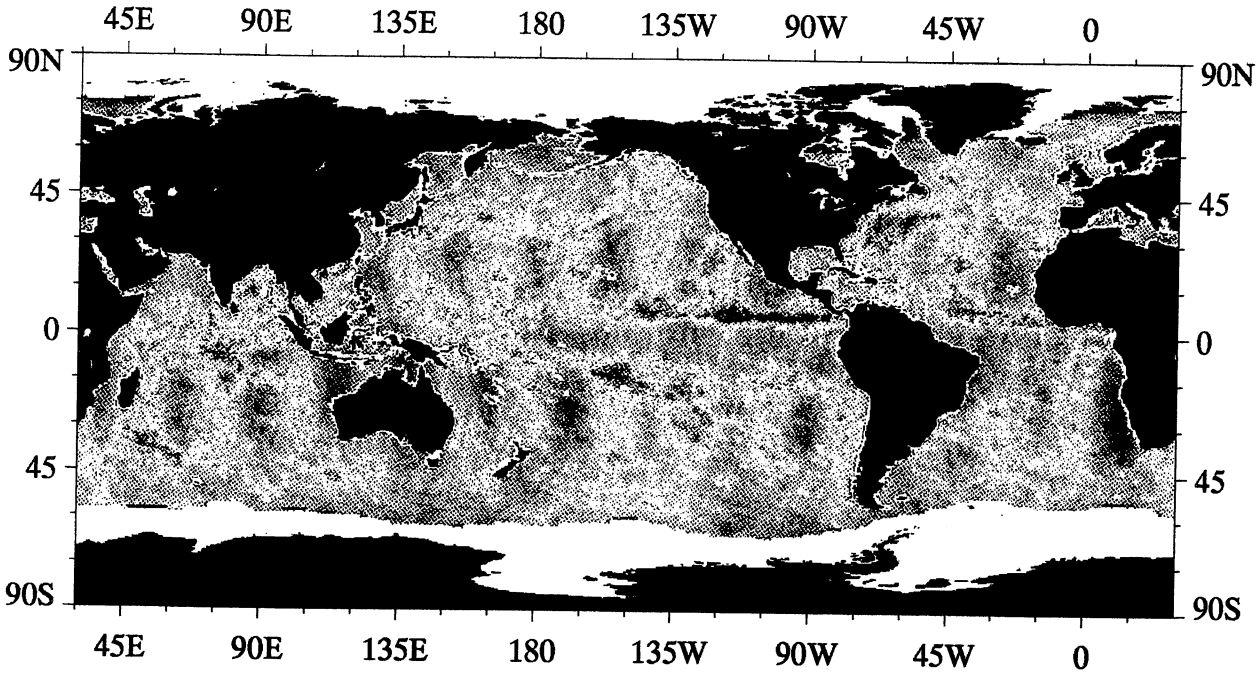

October 1987, max = 107

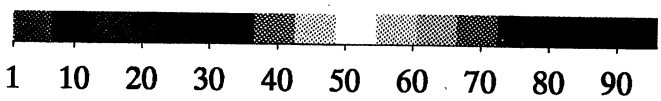

Number of SSMI Wind Speed Values per Pixel

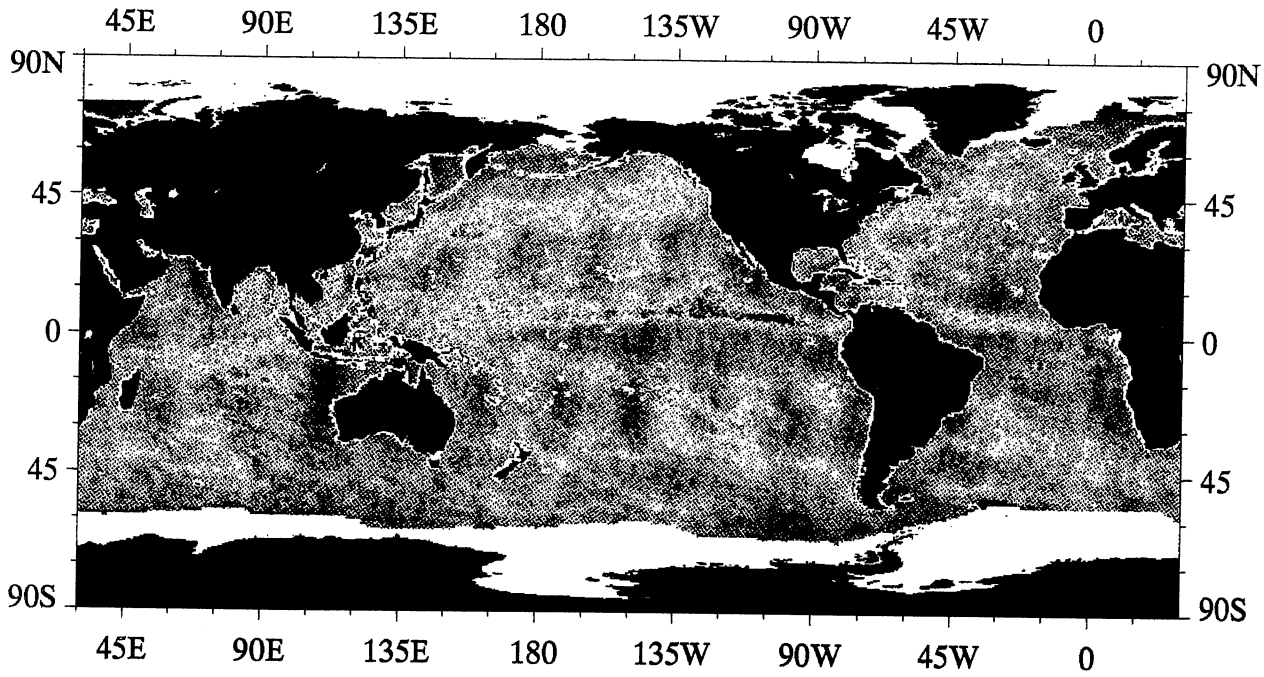

November 1987, max = 142

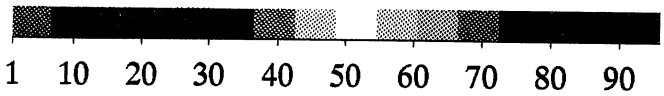

Number of SSMI Wind Speed Values per Pixel

A5

Monthly Standard Deviation of SSMI Surface Wind Speed

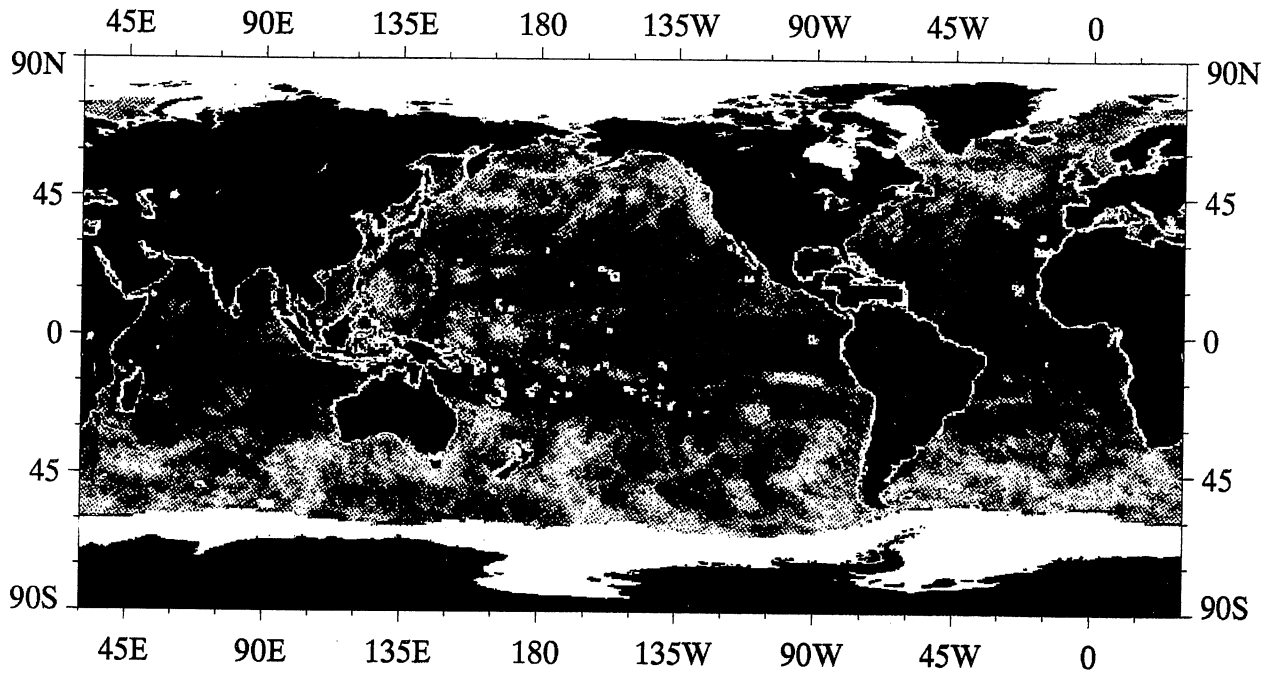

9 - 31 July 1987

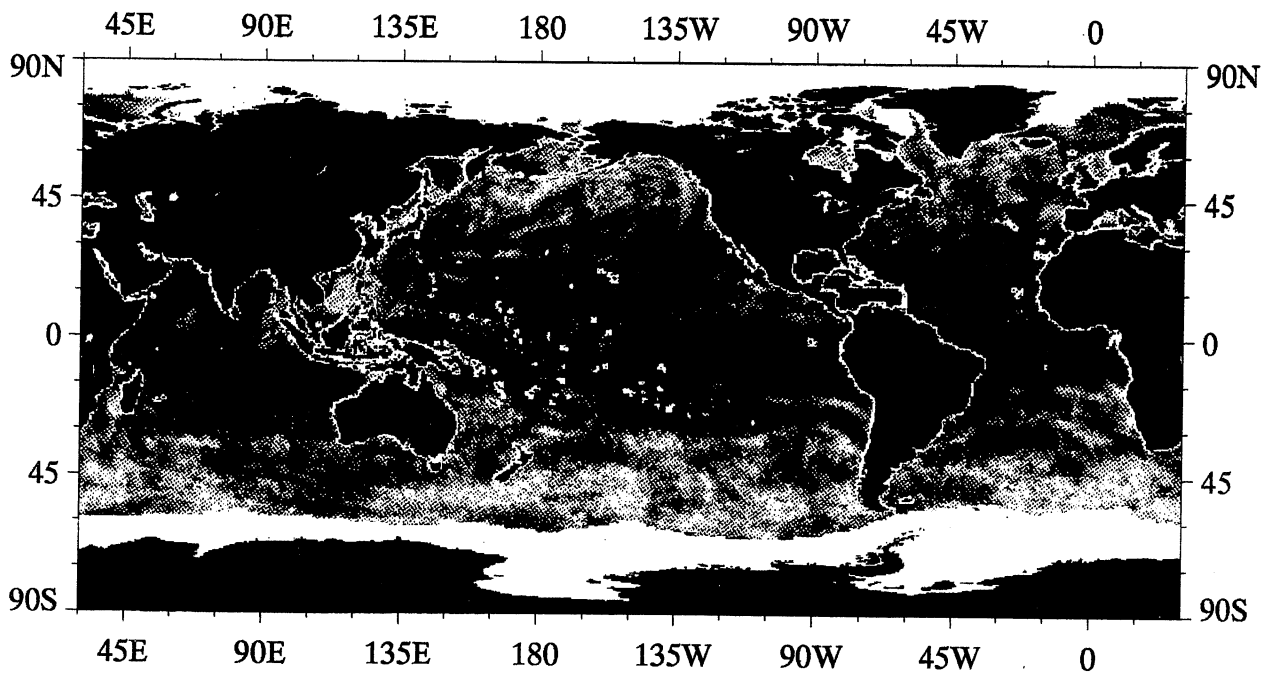

August 1987

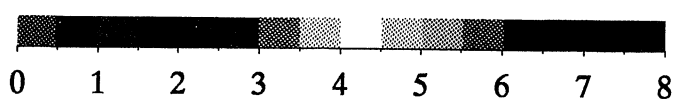

Standard Deviation of SSMI 10 m Wind Speed, m s^{-1}

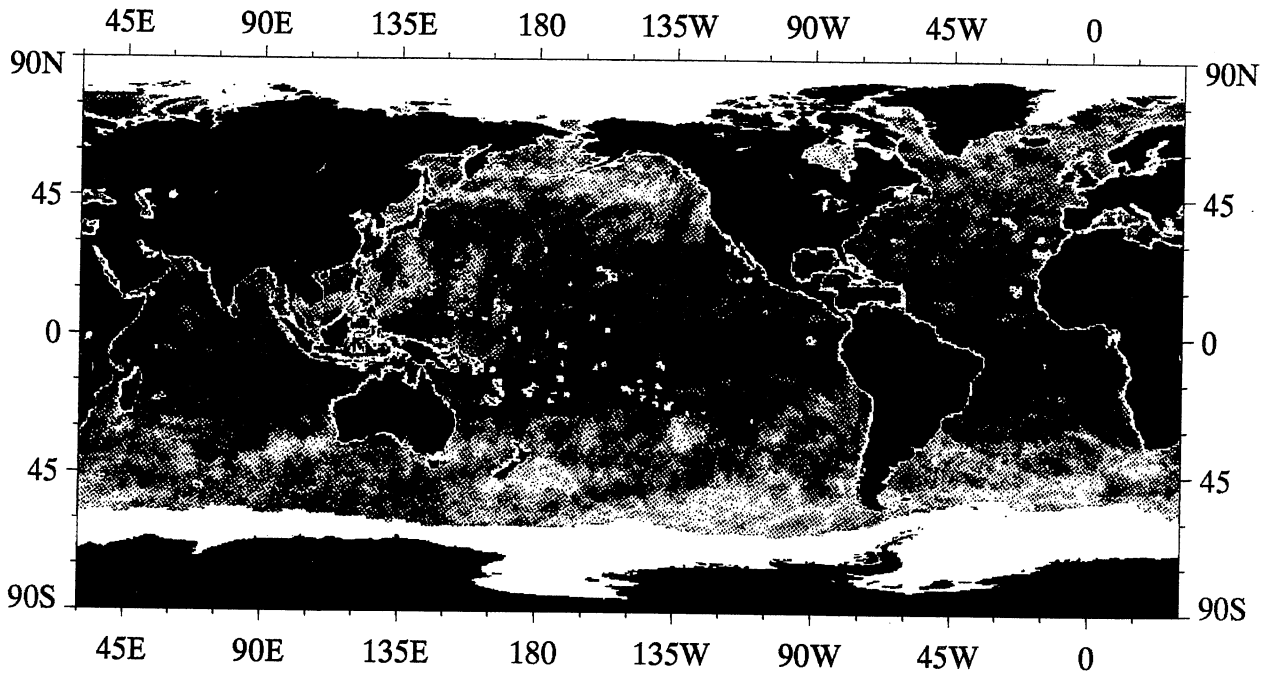

September 1987

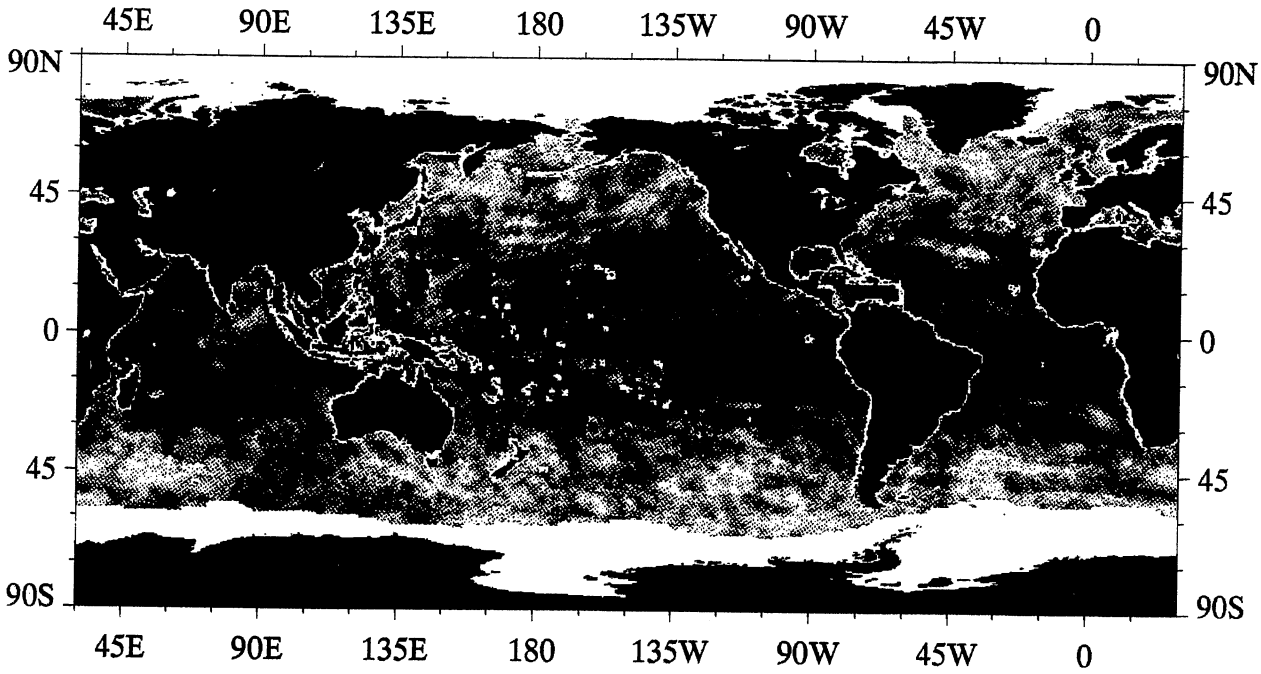

October 1987

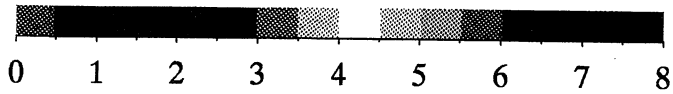

Standard Deviation of SSMI 10 m Wind Speed, m s^{-1}

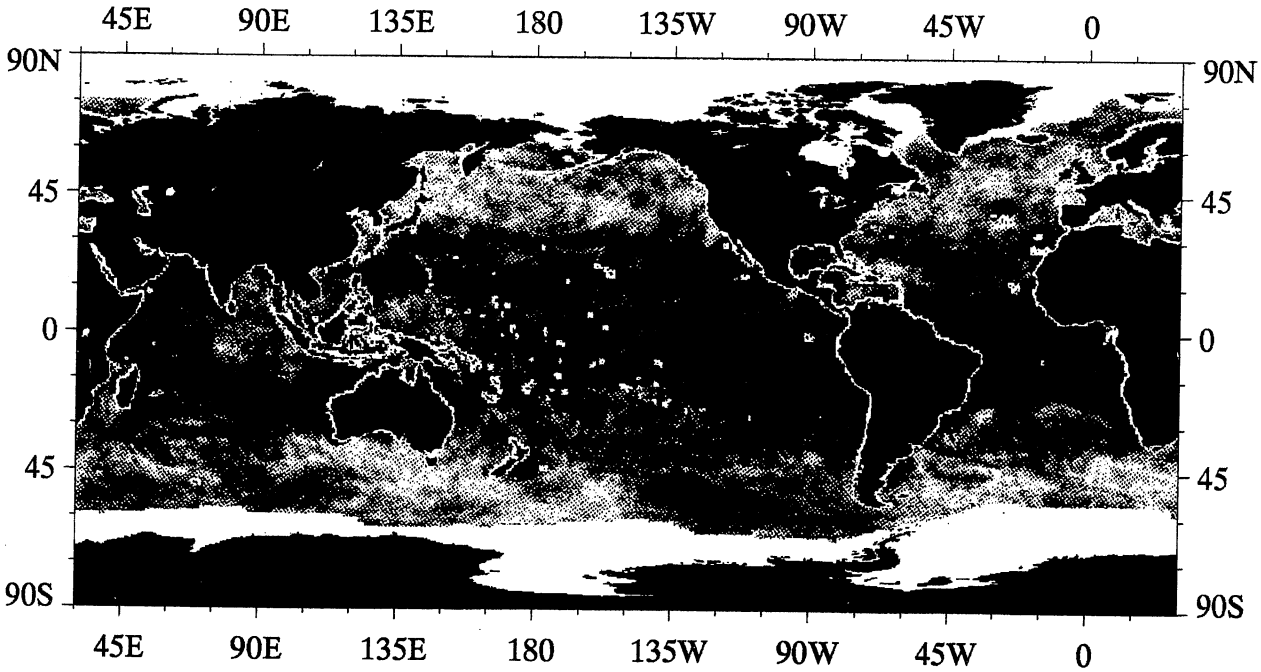

November 1987

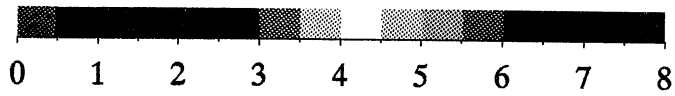

Standard Deviation of SSMI 10 m Wind Speed, m s^{-1}

A6

Annual Mean and Sampling Distribution of AVHRR/2 Sea Surface Temperature

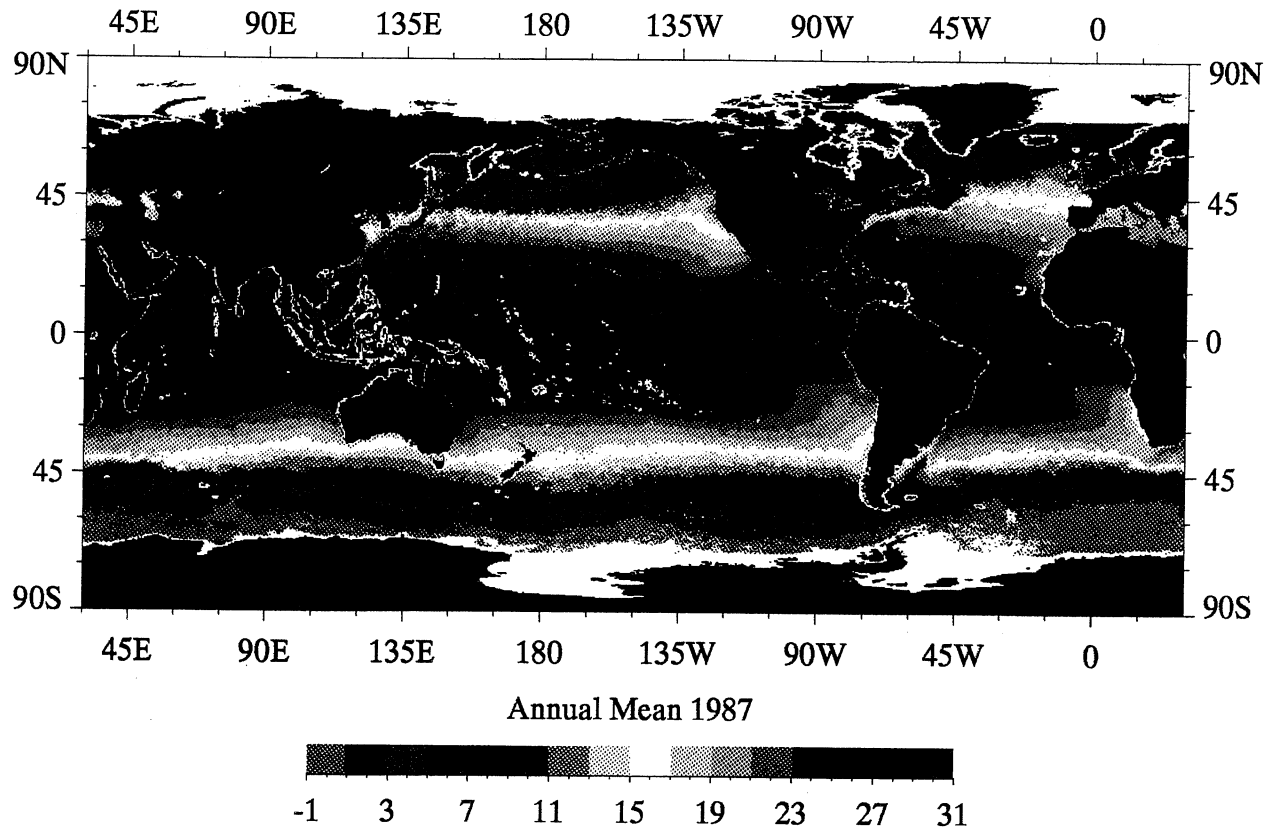

AVHRR Sea Surface Temperature, °C

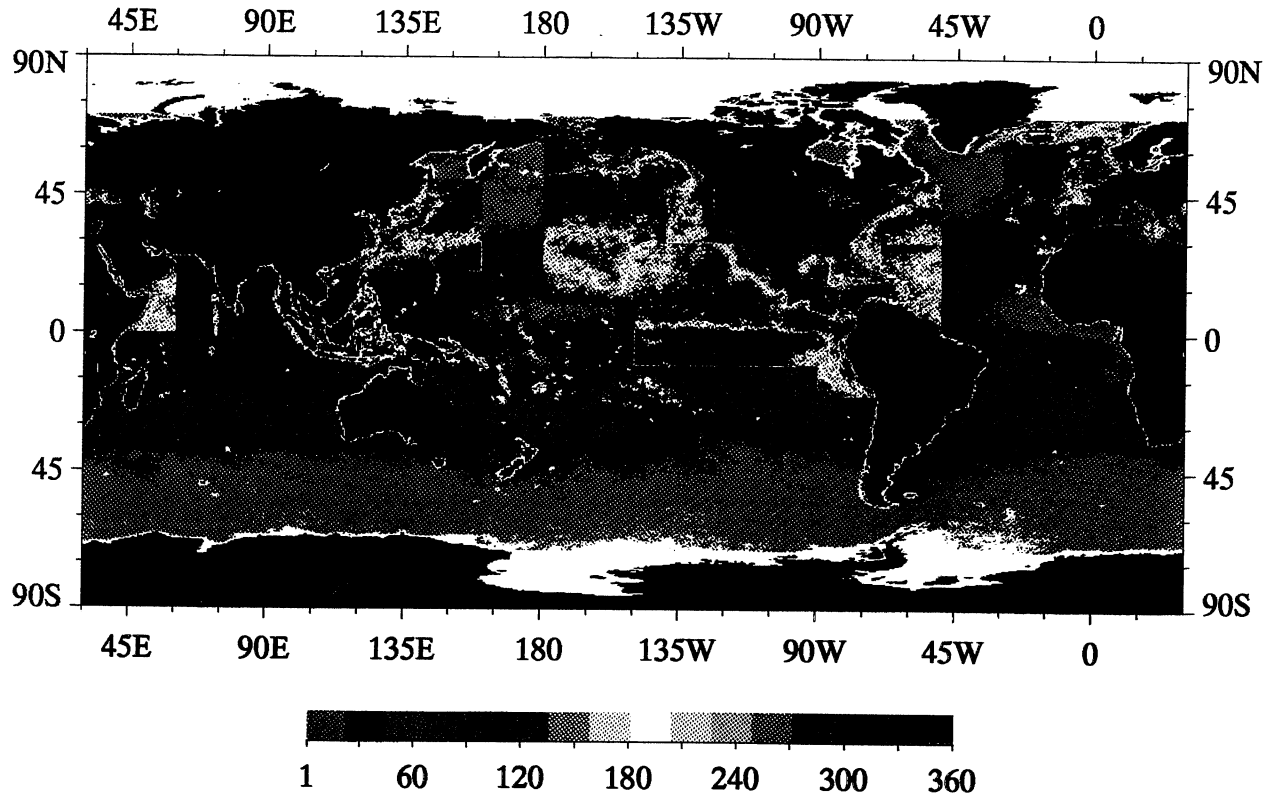

Number of Sea Surface Temperature Values per Pixel During 1987, max = 1627

A7

28-Day Mean AVHRR/2 Sea Surface Temperature

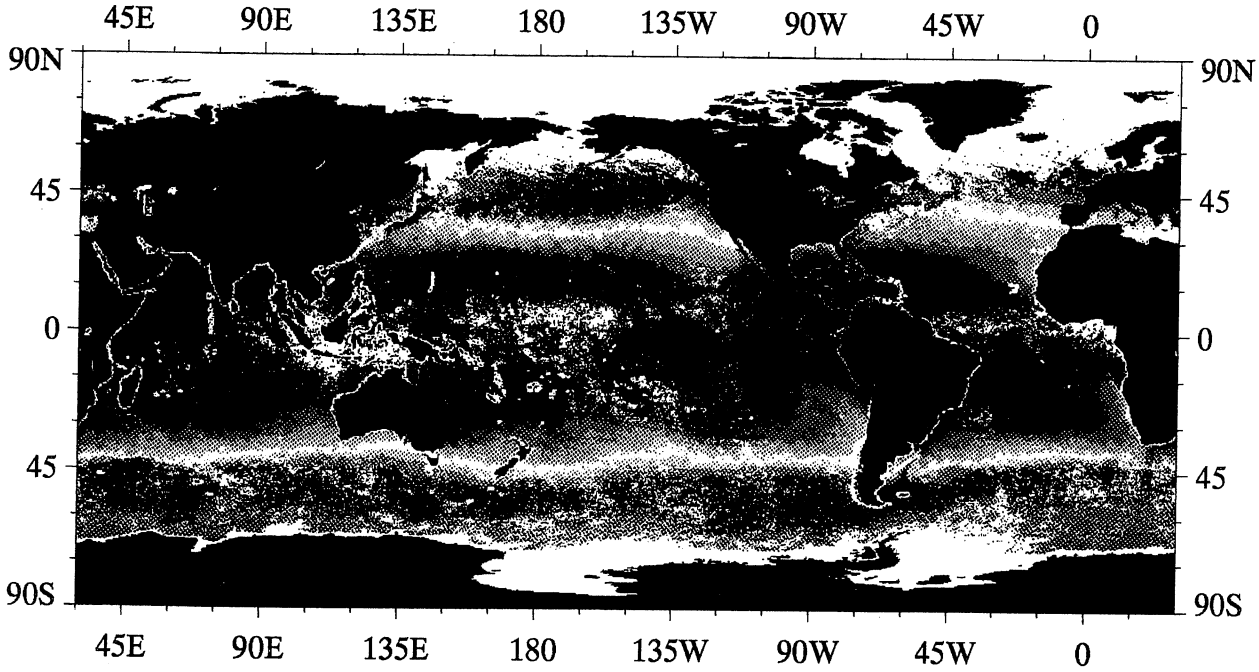

1 January to 4 February 1987

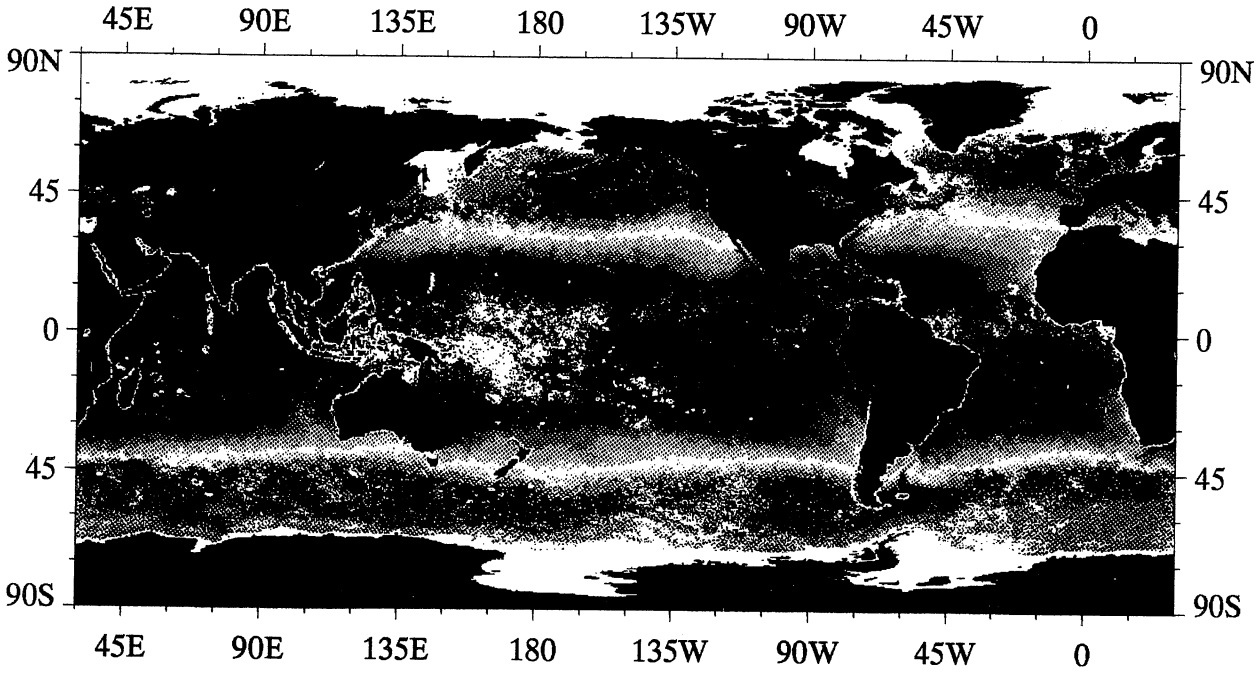

5 February to 4 March 1987

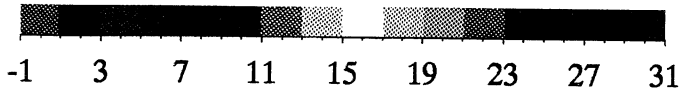

AVHRR Sea Surface Temperature, °C

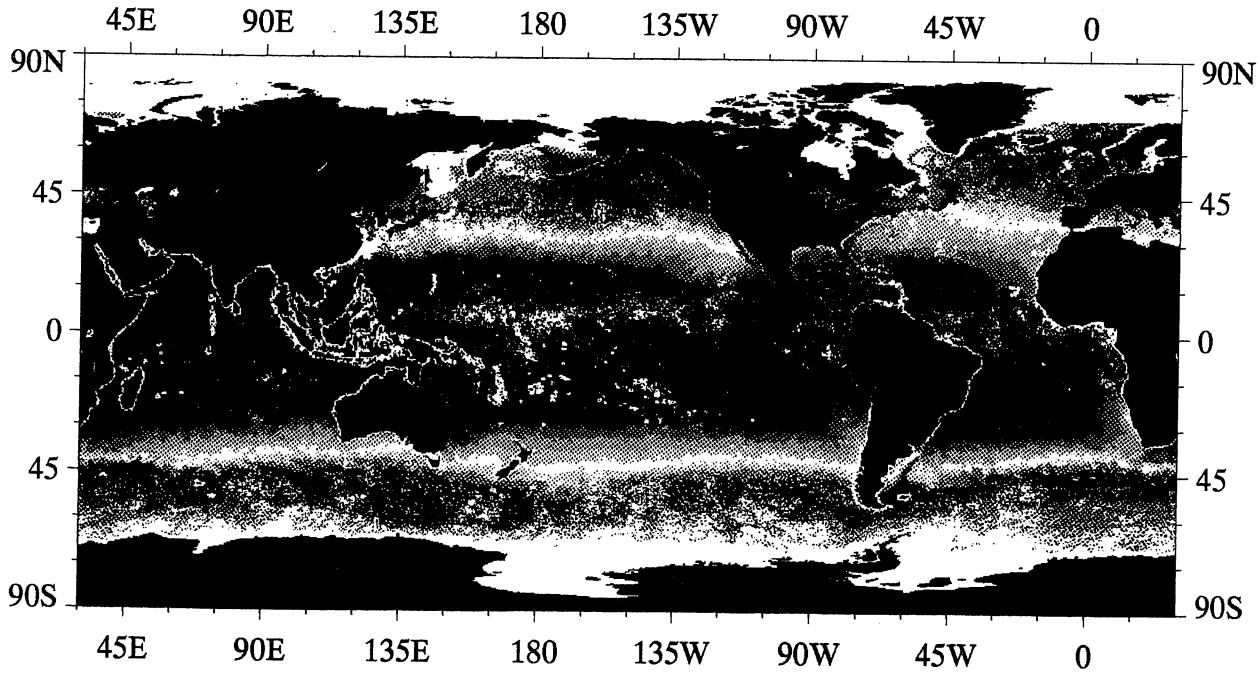

5 March to 1 April 1987

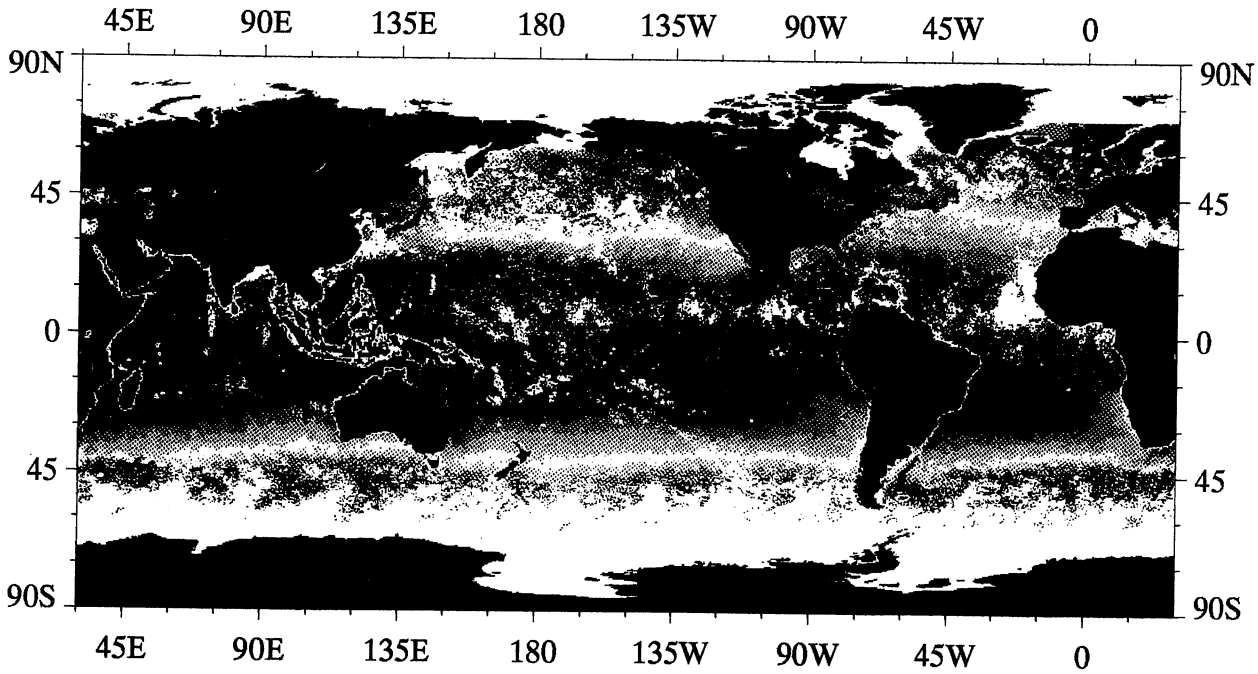

2 April to 29 April 1987

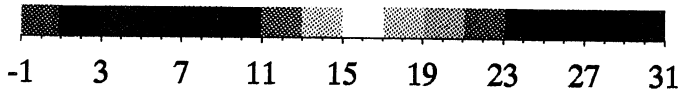

AVHRR Sea Surface Temperature, °C

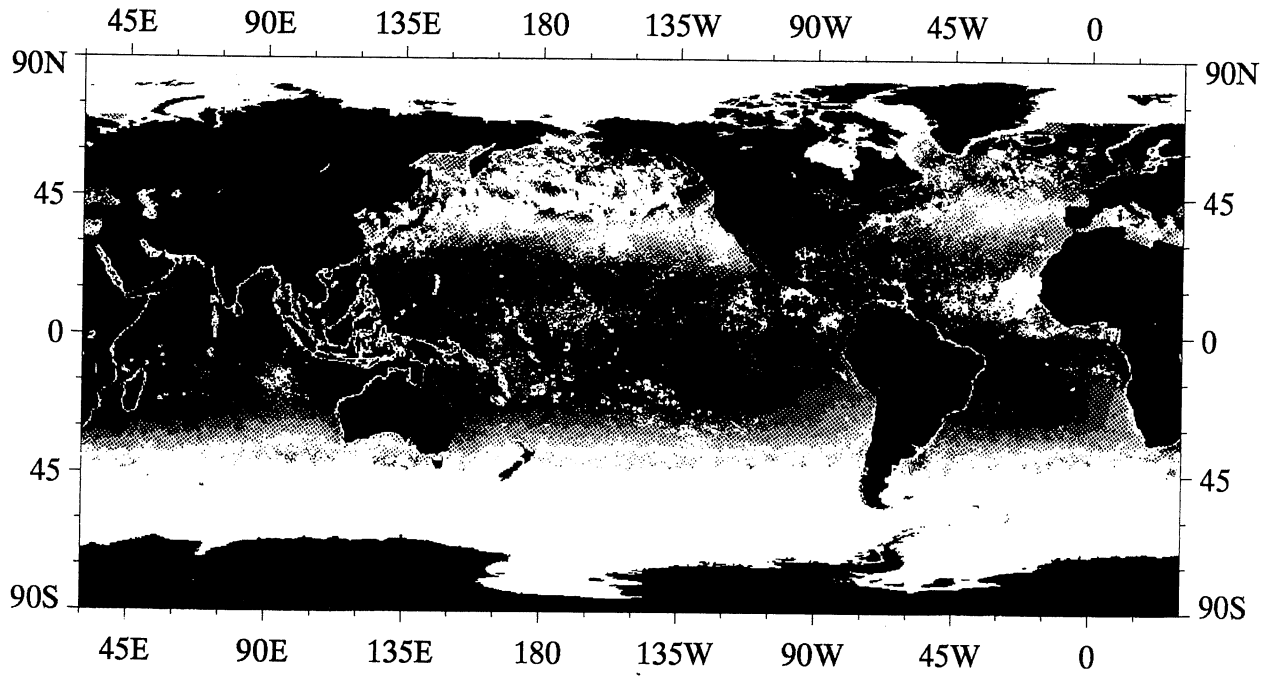

7 May to 3 June 1987

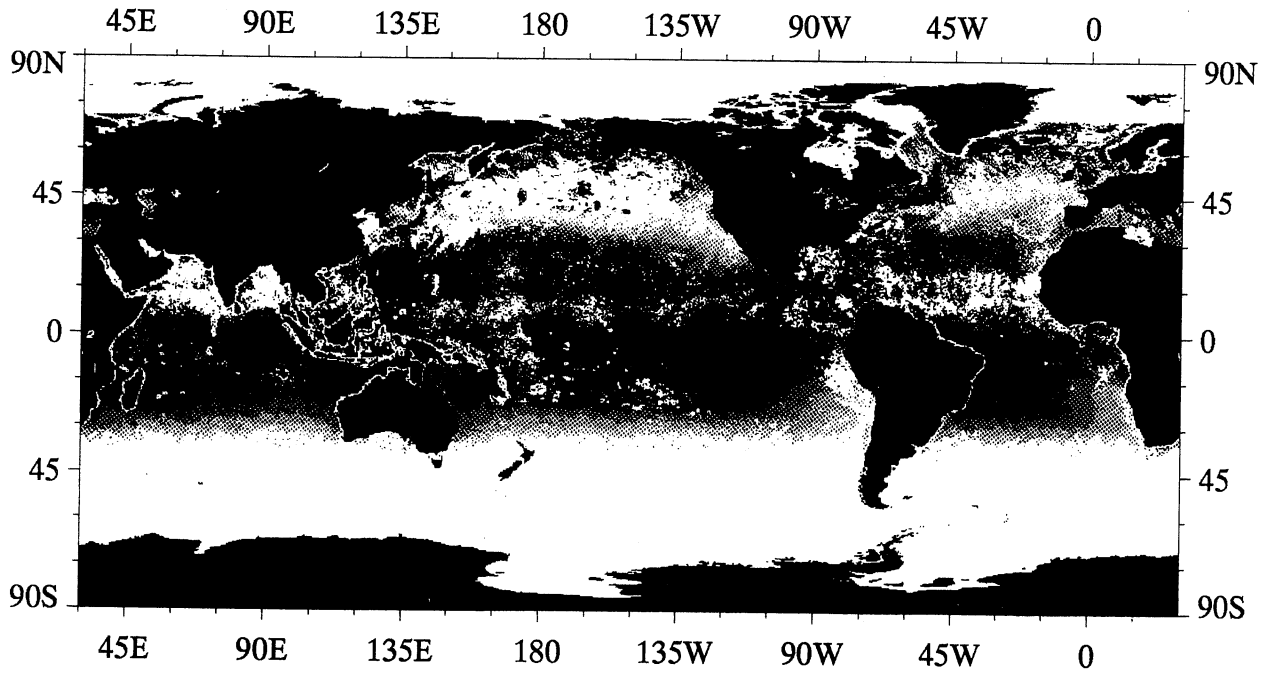

4 June to 8 July 1987

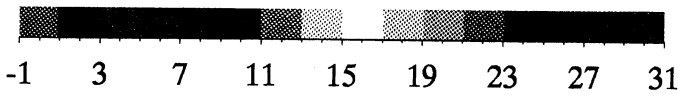

AVHRR Sea Surface Temperature, °C

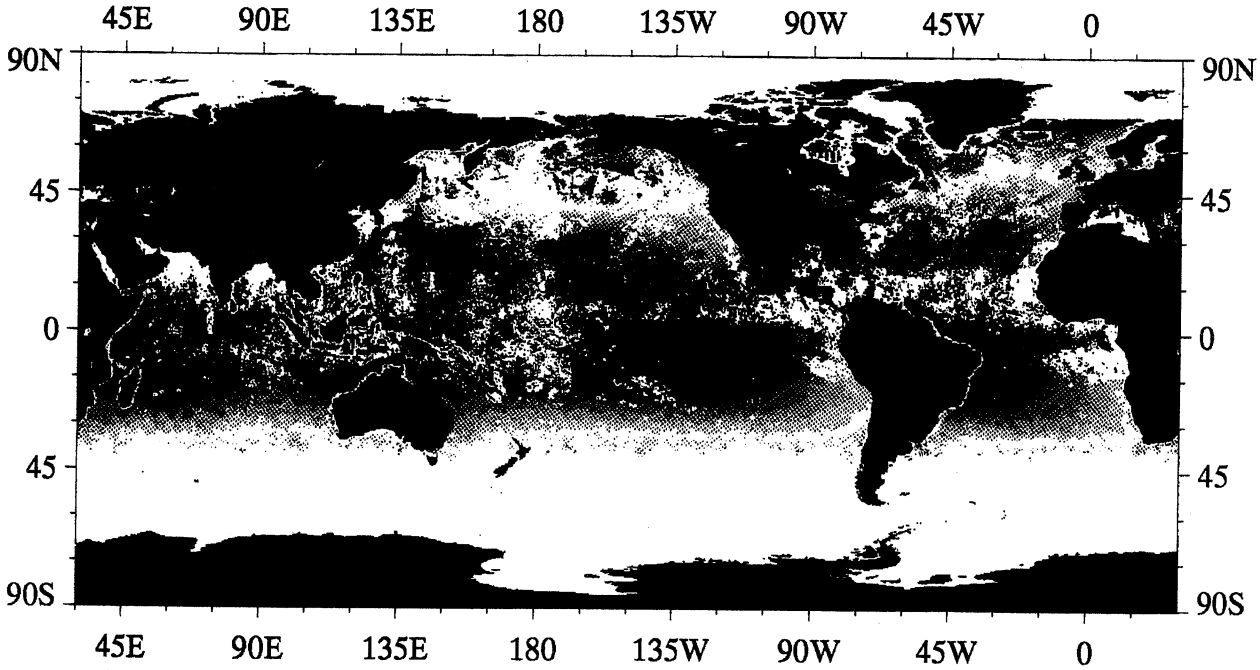

9 July to 5 August 1987

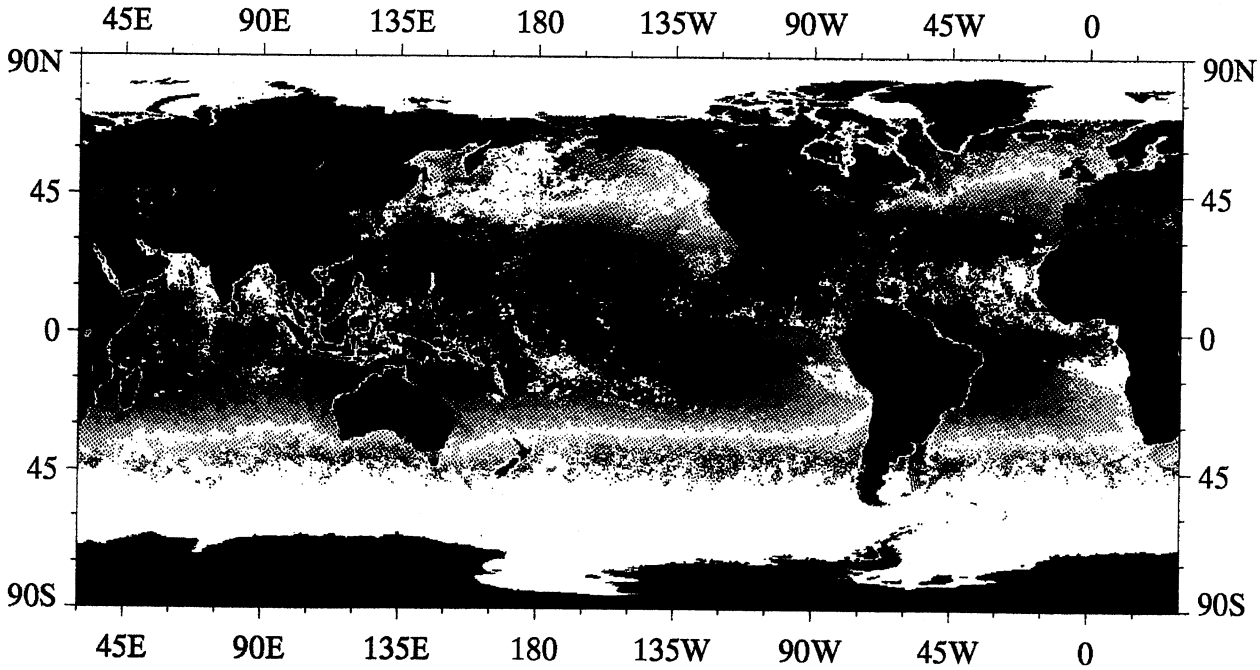

6 August to 2 September 1987

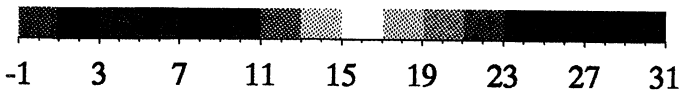

AVHRR Sea Surface Temperature, °C

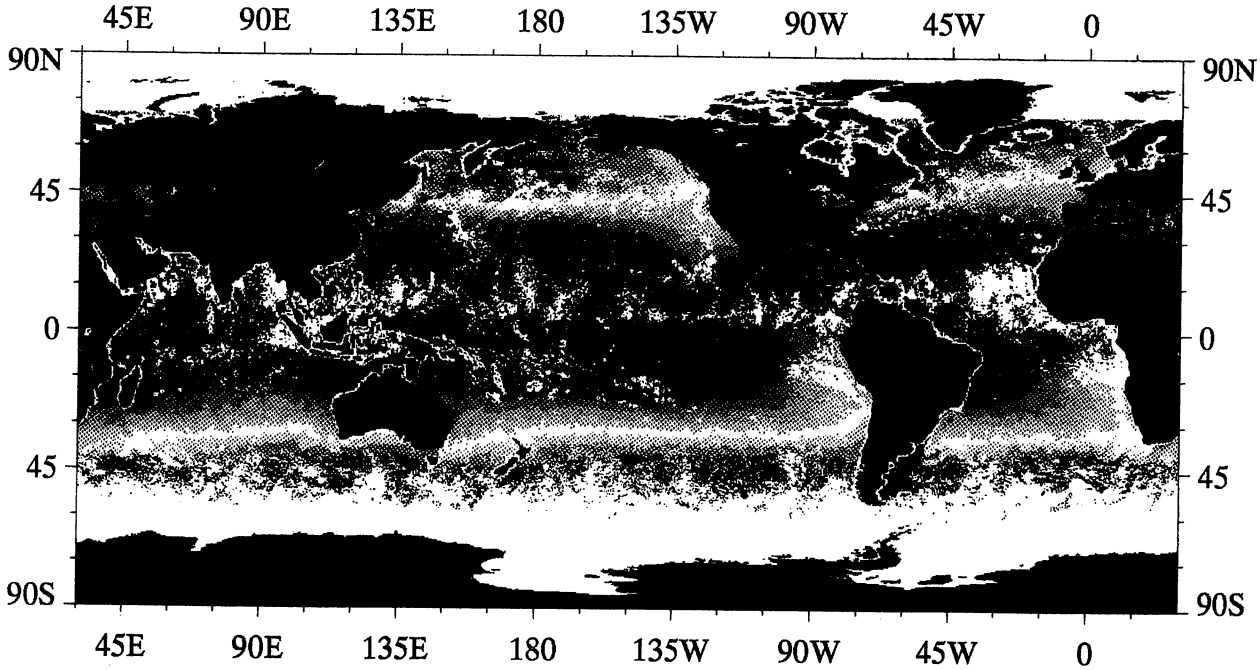

3 September to 30 September 1987

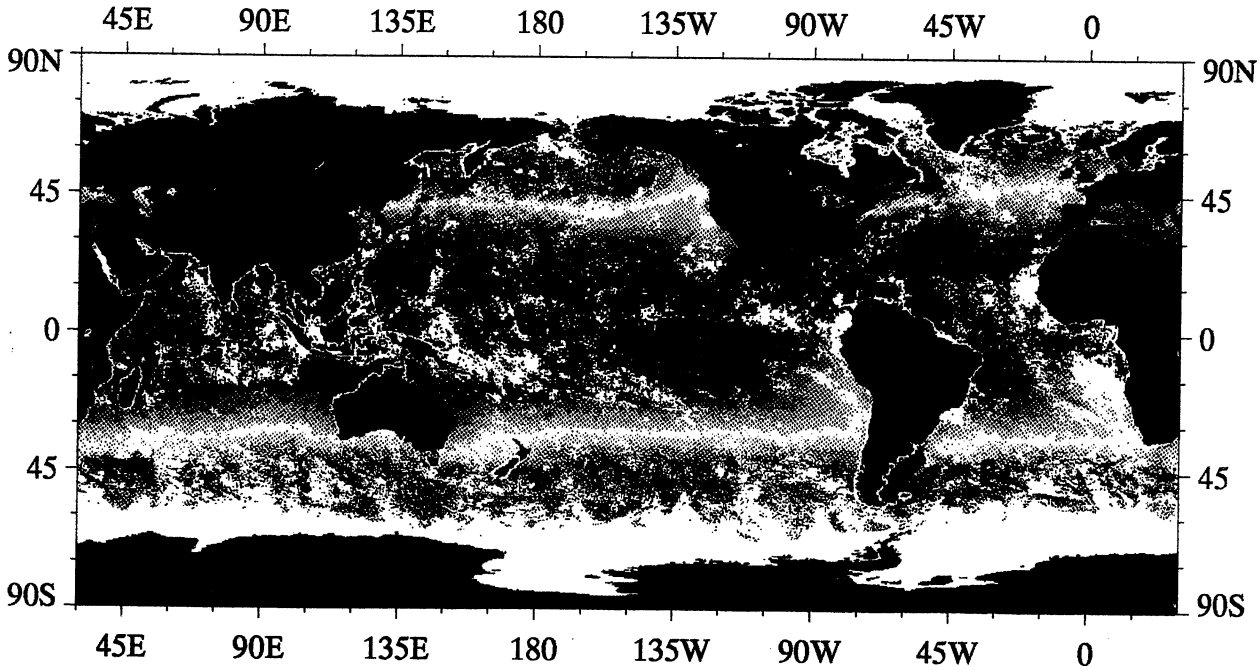

1 October to 4 November 1987

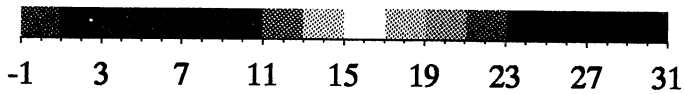

AVHRR Sea Surface Temperature, °C

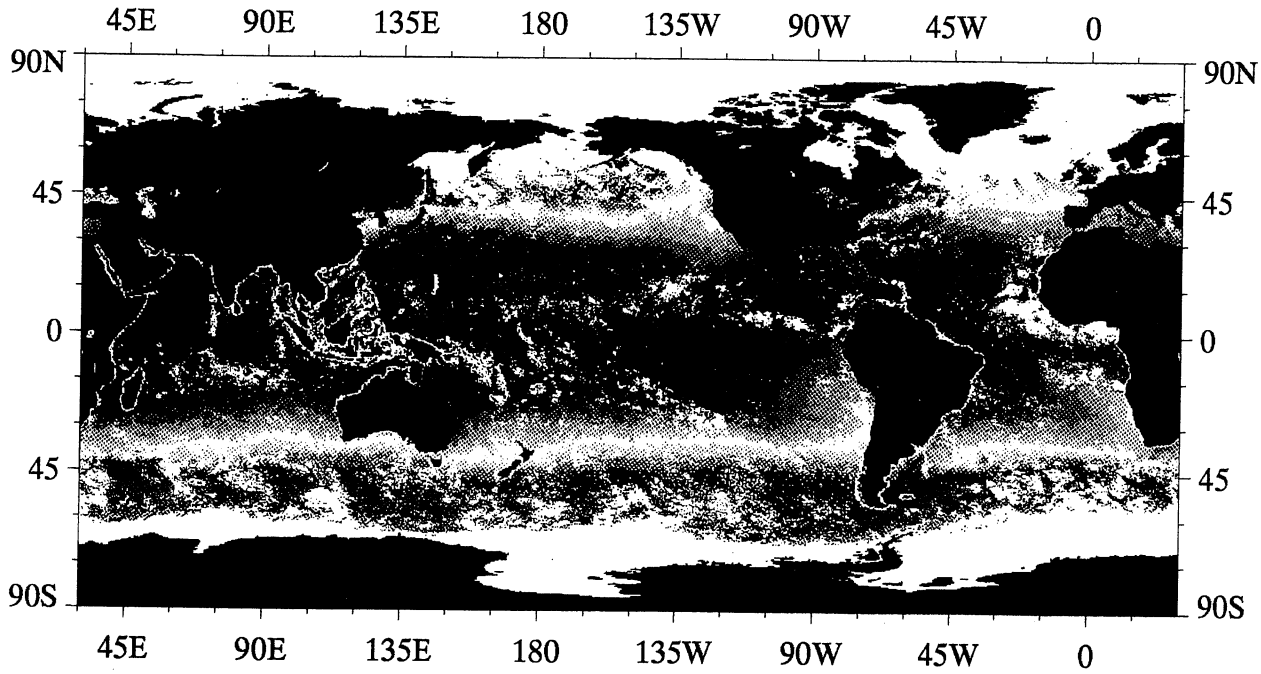

5 November to 2 December 1987

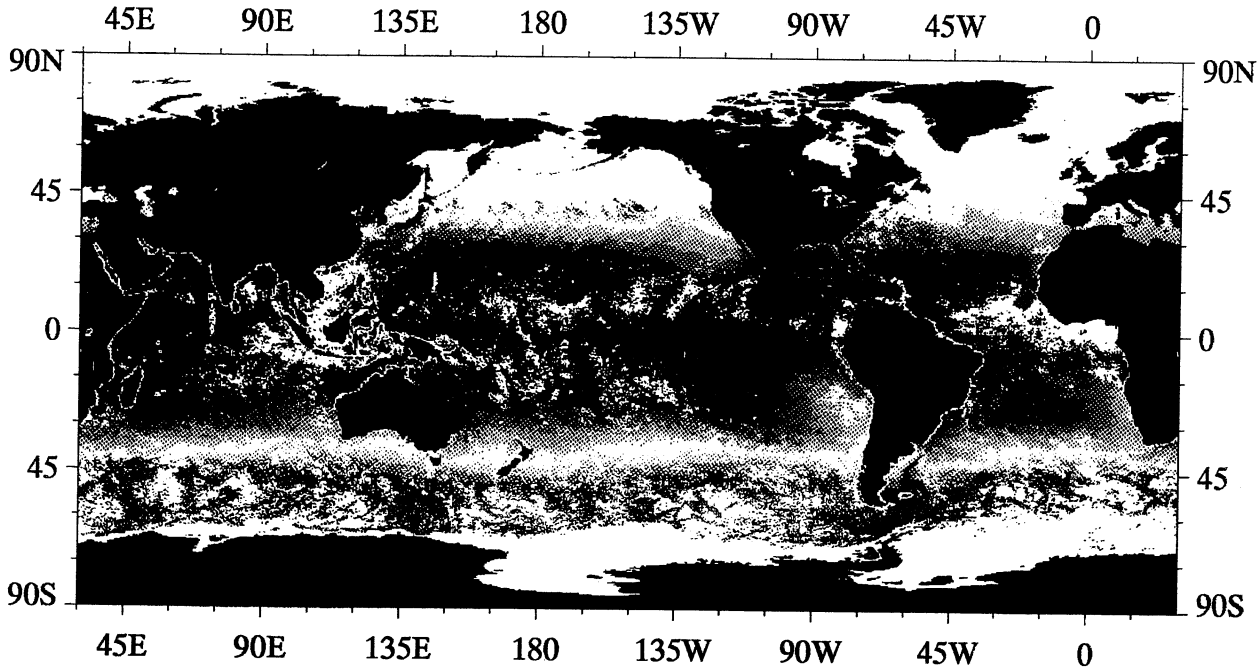

3 December to 30 December 1987

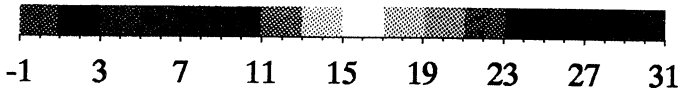

AVHRR Sea Surface Temperature, °C

A8

28-Day AVHRR/2 Sampling Distribution

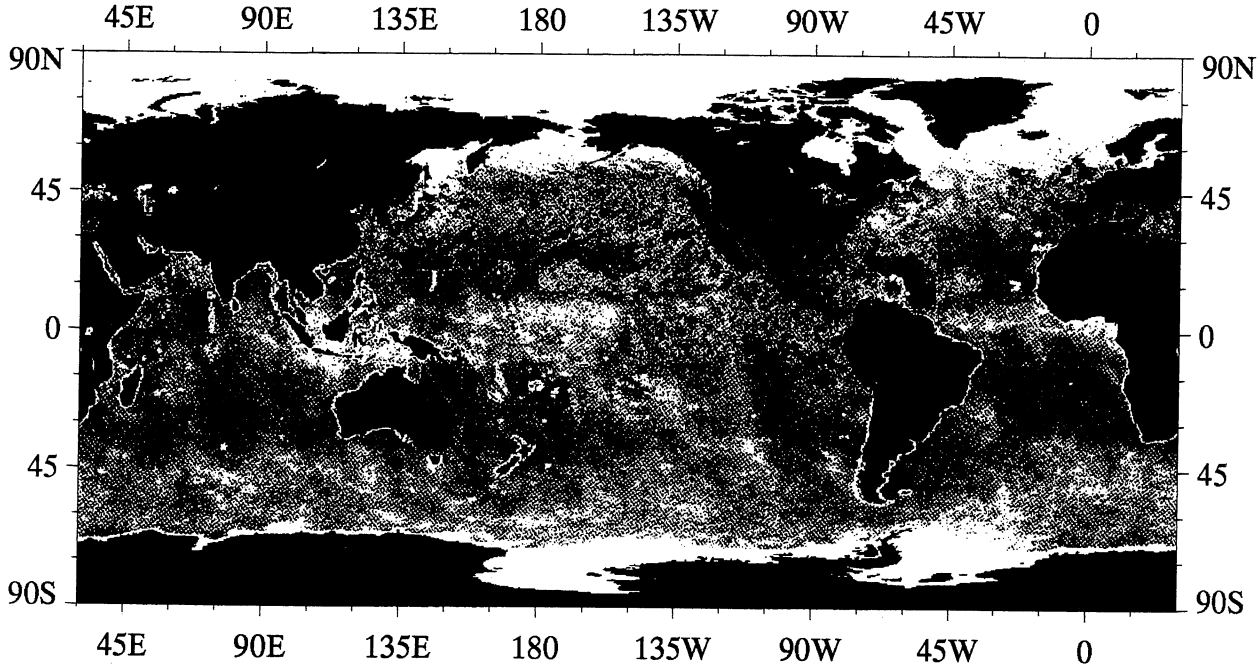

1 January to 4 February 1987, max = 332

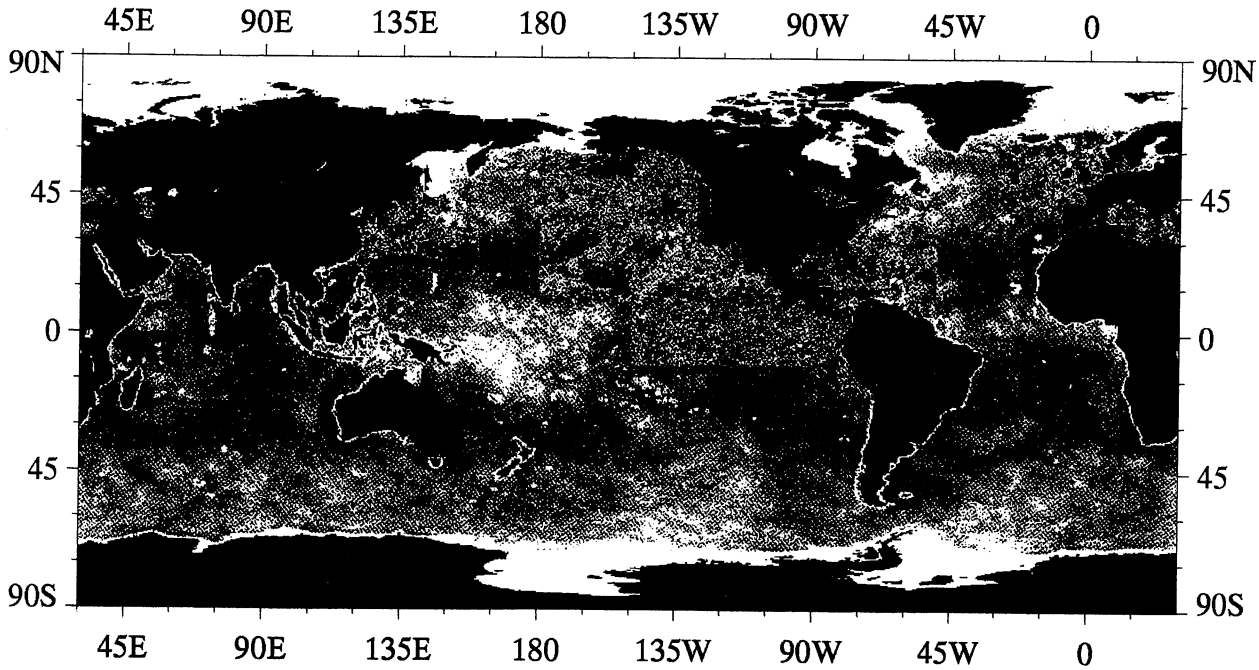

5 February to 4 March 1987, max = 174

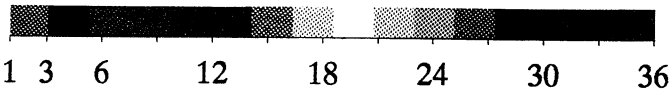

Number of AVHRR Sea Surface Temperature Values per Pixel

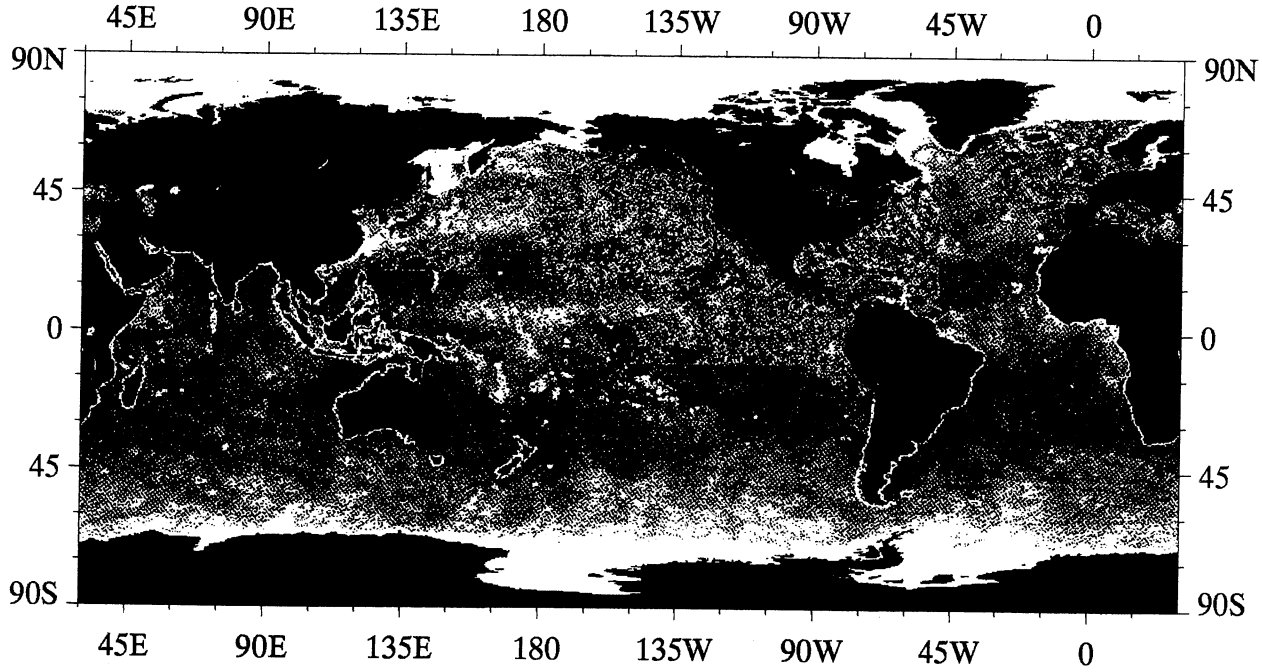

5 March to 1 April 1987, max = 153

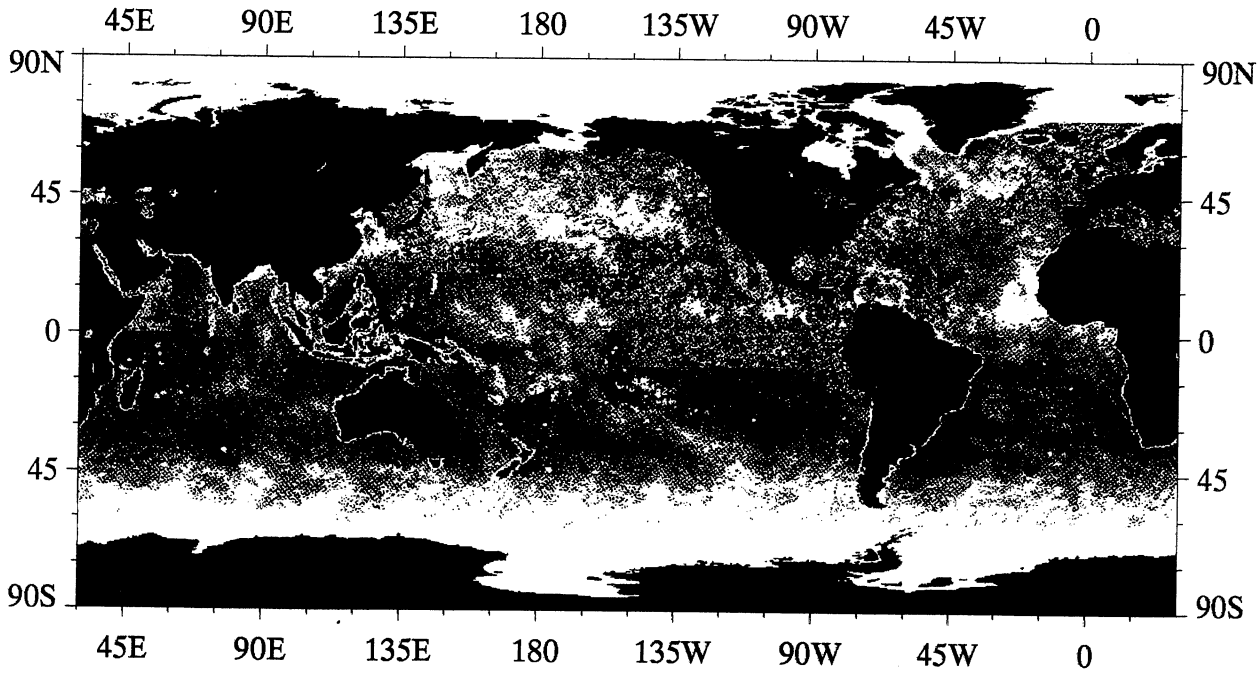

2 April to 29 April 1987, max = 162

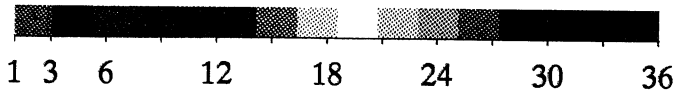

Number of AVHRR Sea Surface Temperature Values per Pixel

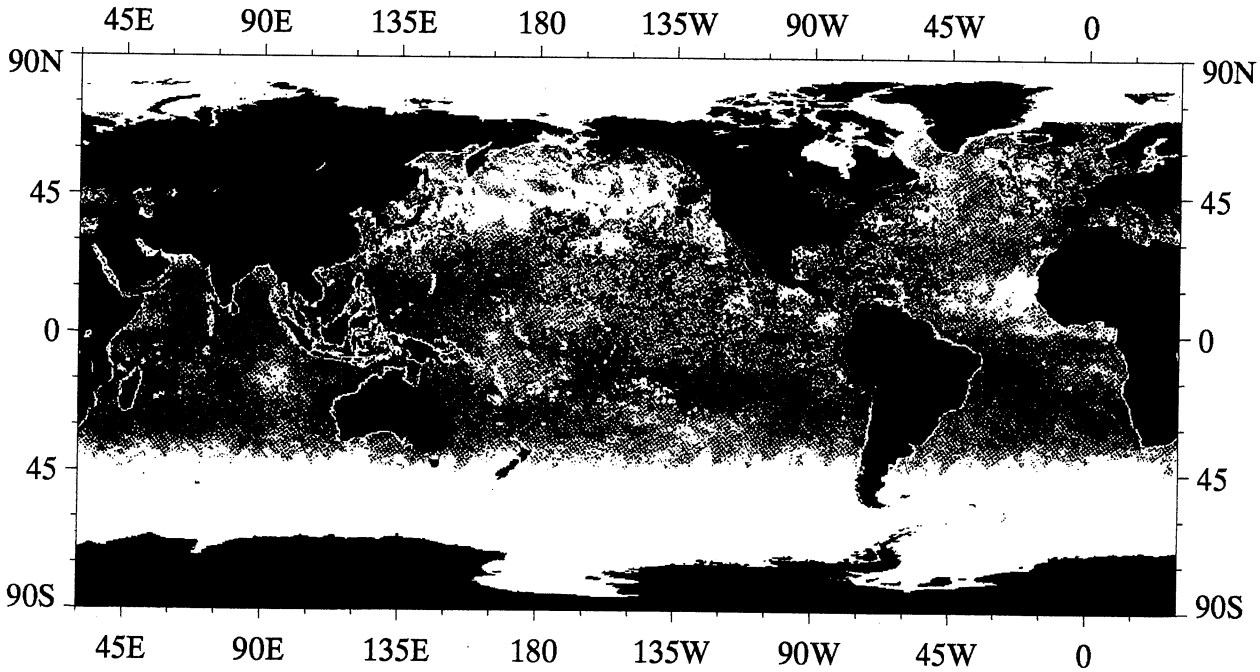

7 May to 3 June 1987, max = 152

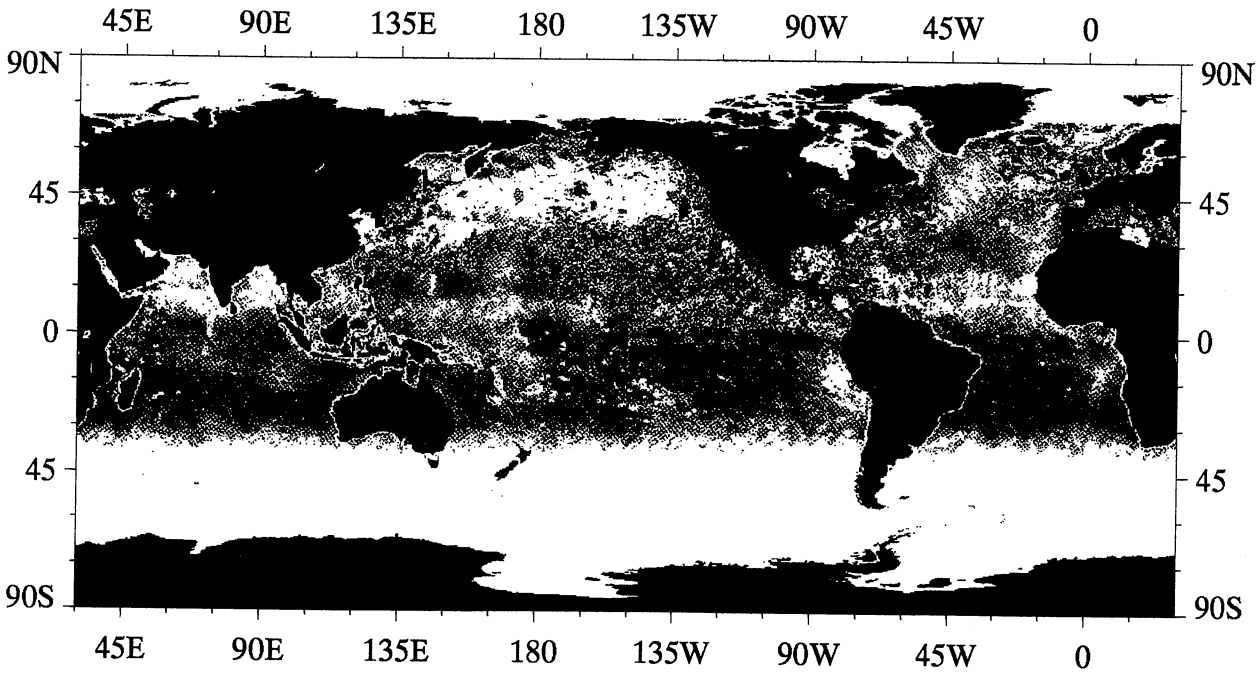

4 June to 8 July 1987, max = 177

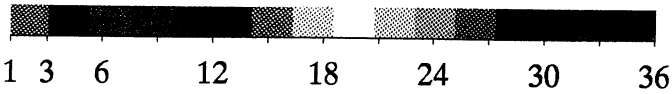

Number of AVHRR Sea Surface Temperature Values per Pixel

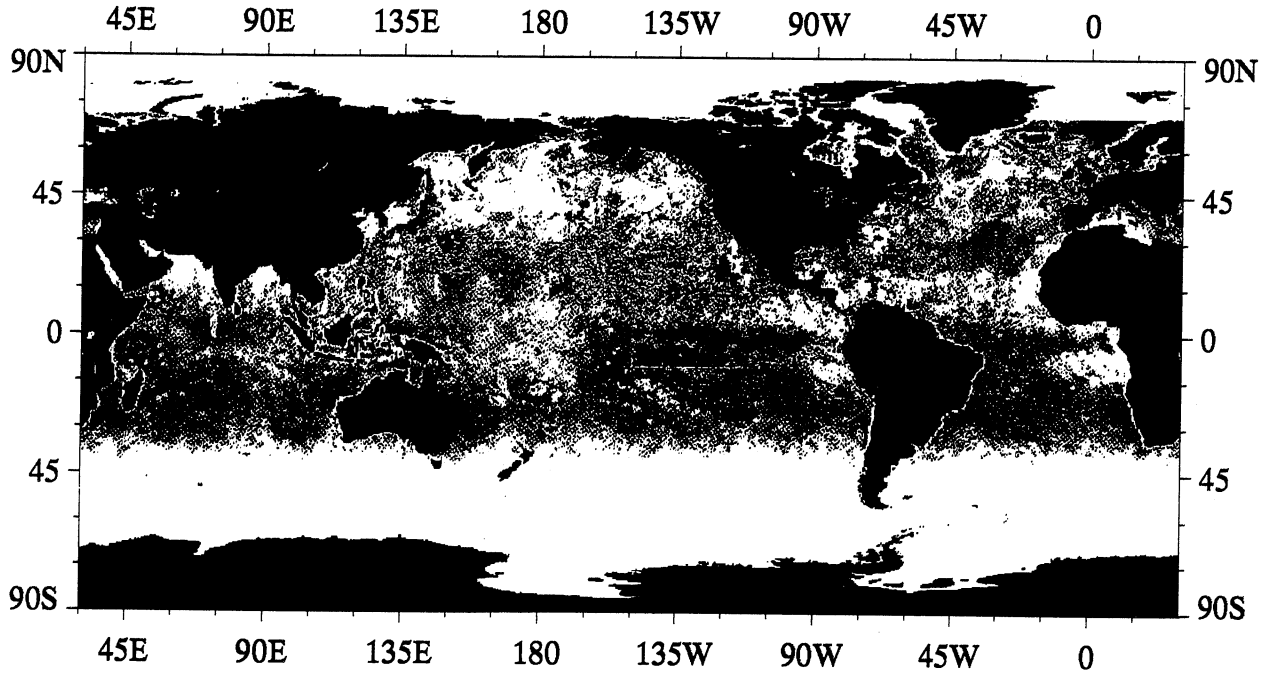

9 July to 5 August 1987, max = 258

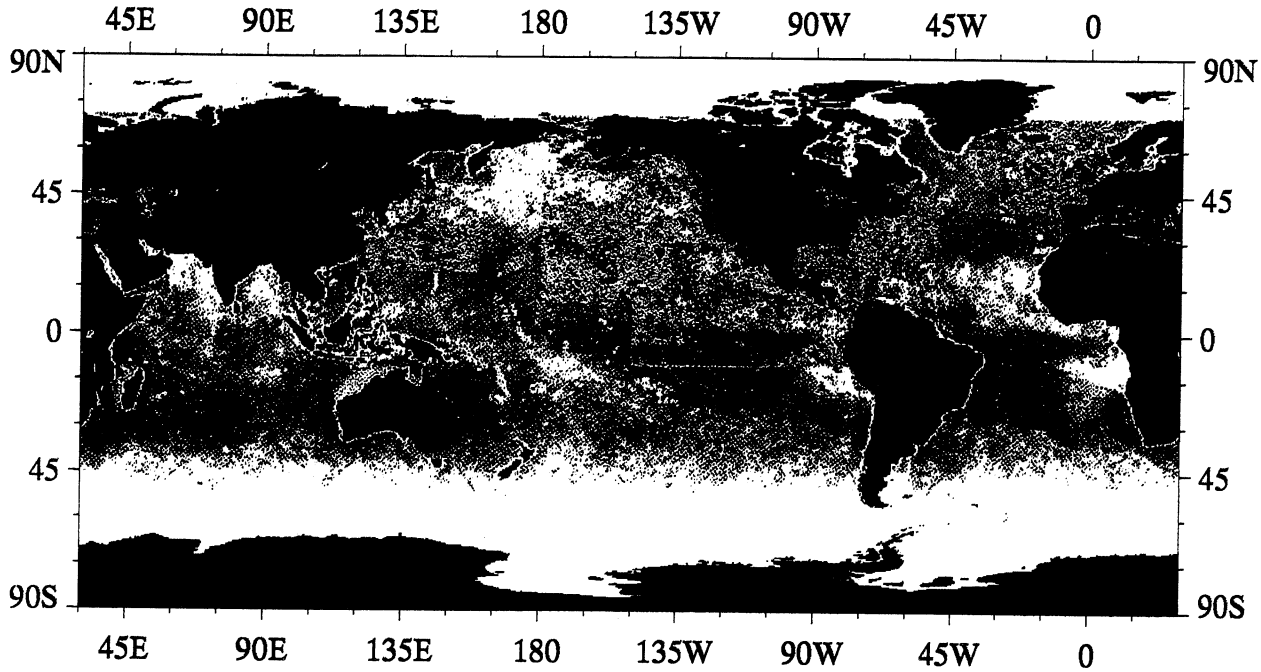

6 August to 2 September 1987, max = 191

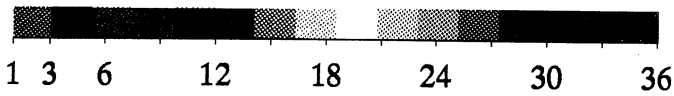

Number of AVHRR Sea Surface Temperature Values per Pixel

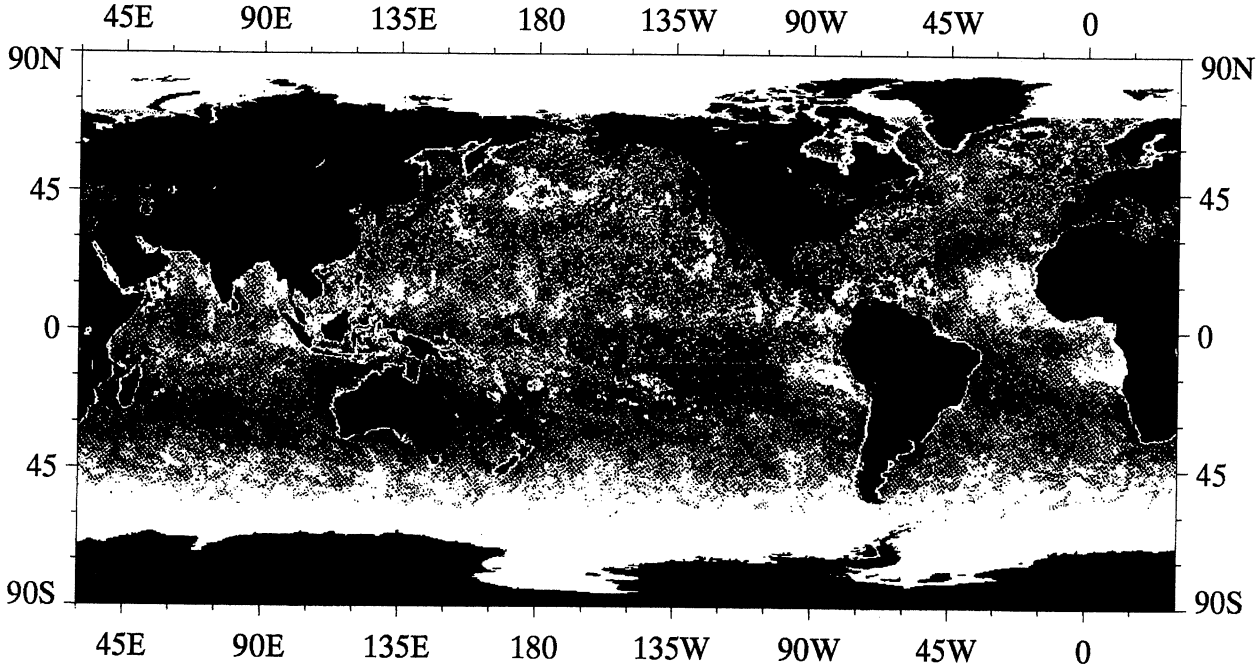

3 September to 30 September 1987, max = 220

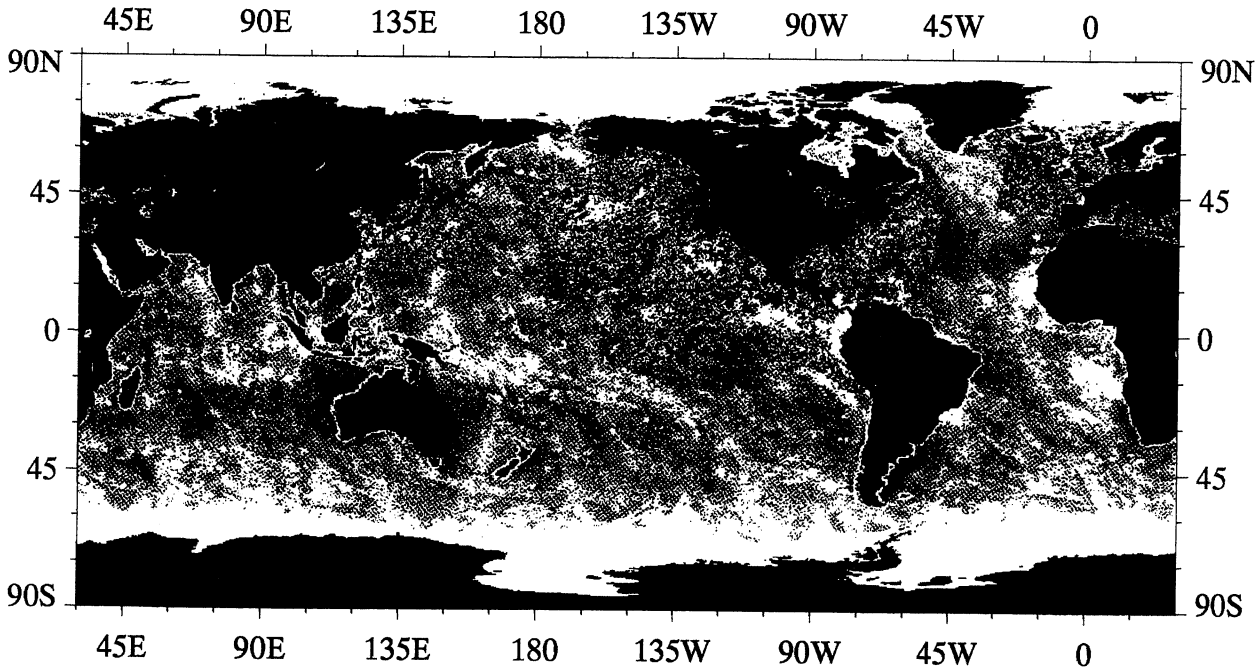

1 October to 4 November 1987, max = 192

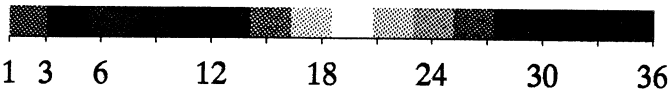

Number of AVHRR Sea Surface Temperature Values per Pixel

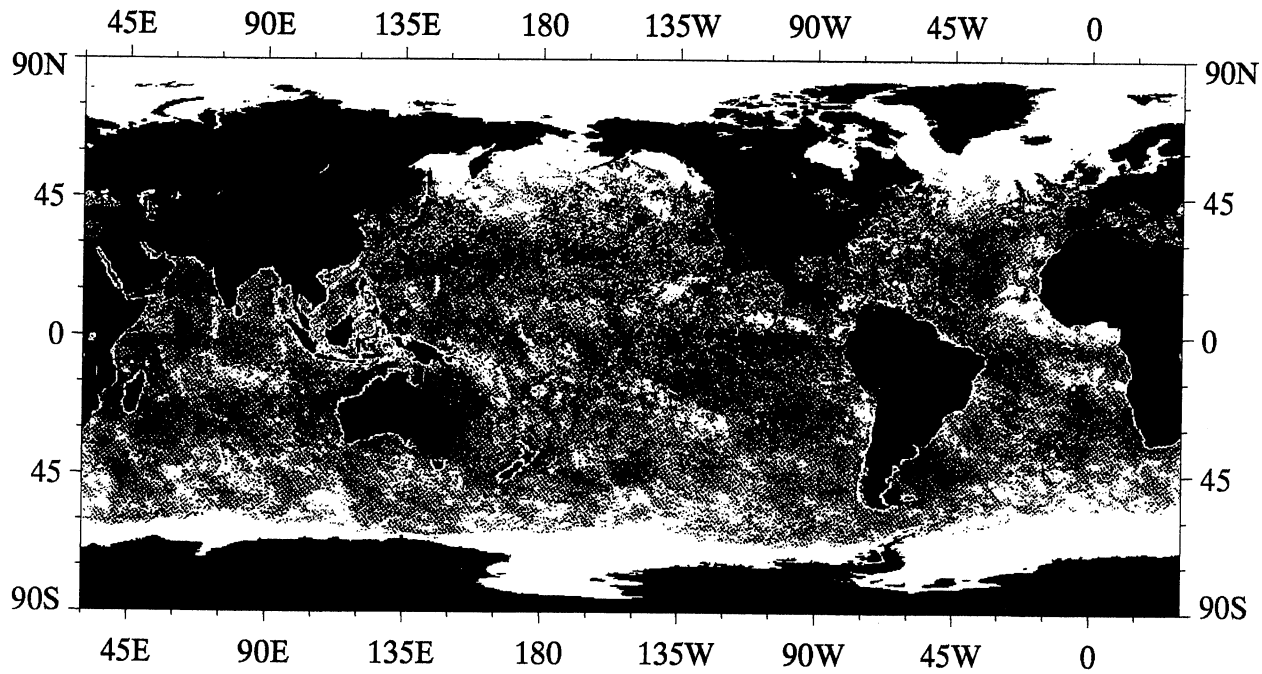

5 November to 2 December 1987, max = 188

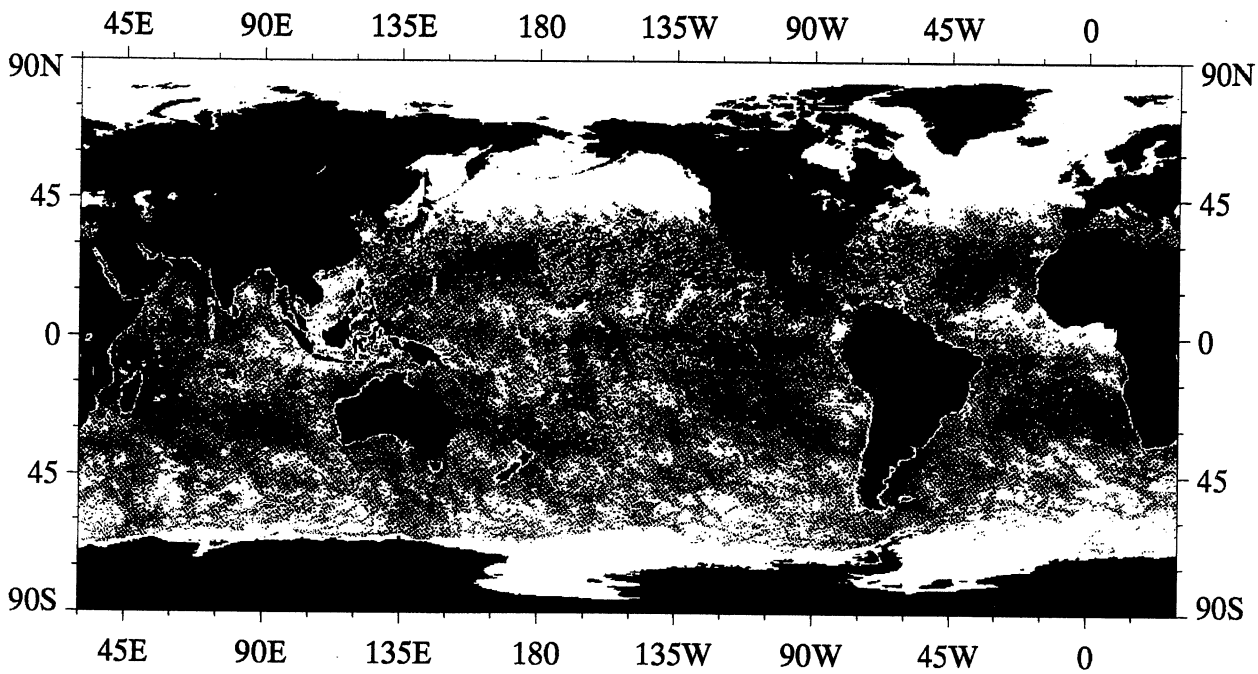

3 December to 30 December 1987, max = 168

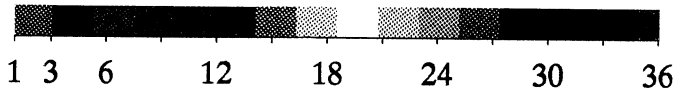

Number of AVHRR Sea Surface Temperature Values per Pixel

A9

Annual Mean ECMWF Surface Wind Components

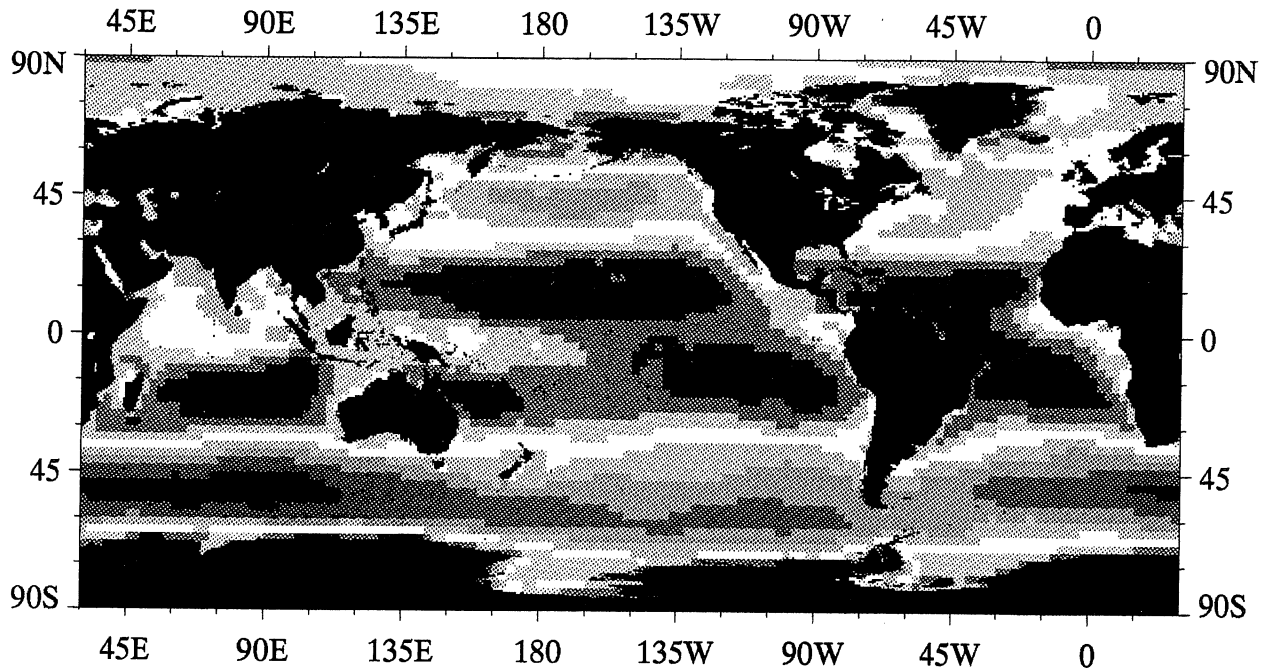

Zonal Wind Speed, Annual Mean 1987

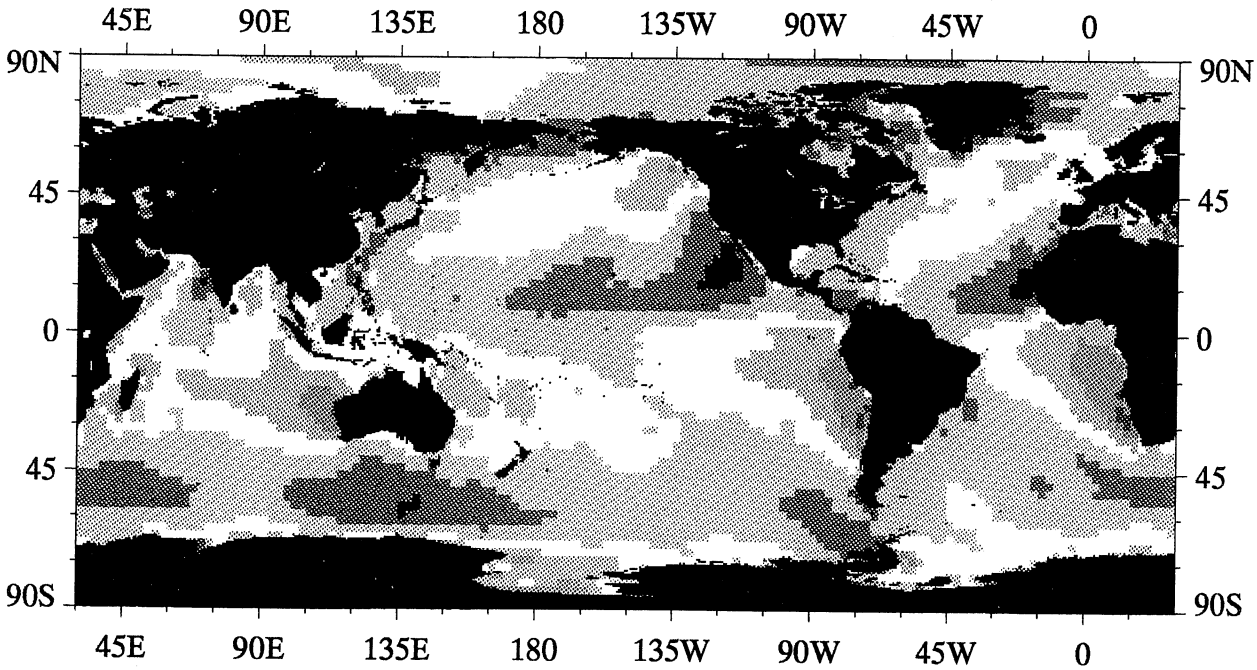

Meridional Wind Speed, Annual Mean 1987

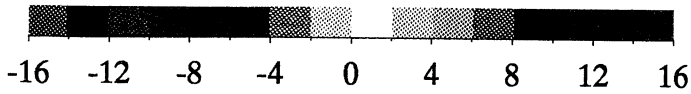

ECMWF 10 m Wind Speed, m s^{-1}

A10

Monthly Mean ECMWF Surface Wind Components

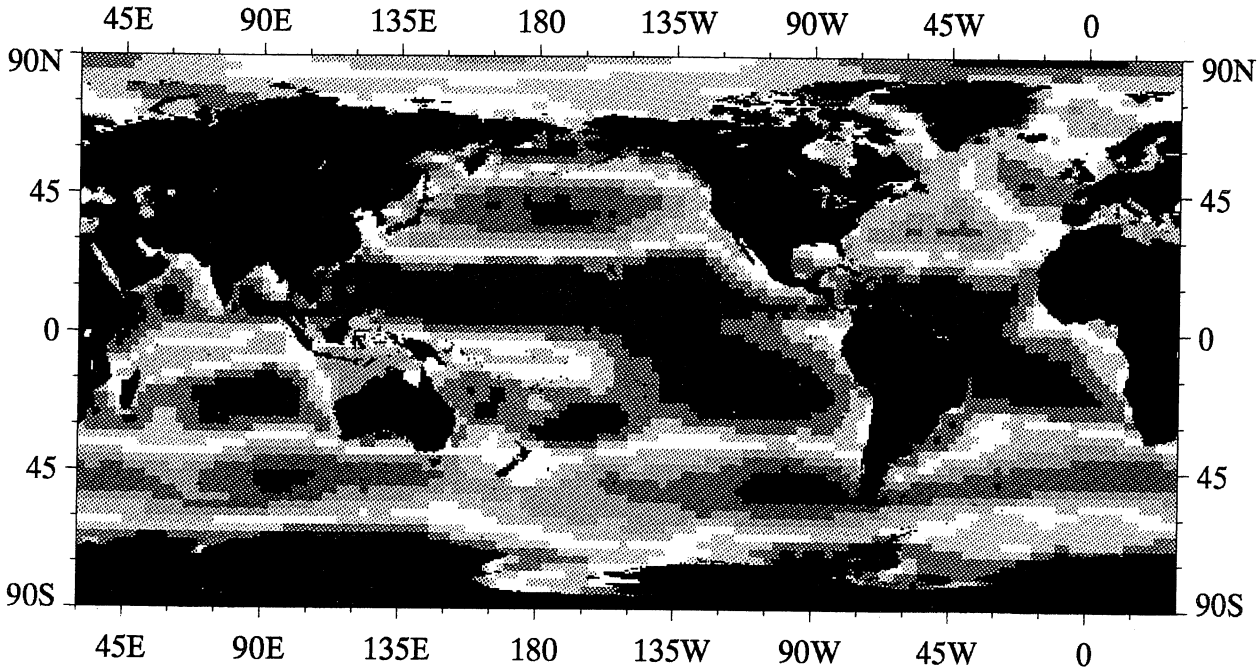

Zonal Wind Speed, January 1987

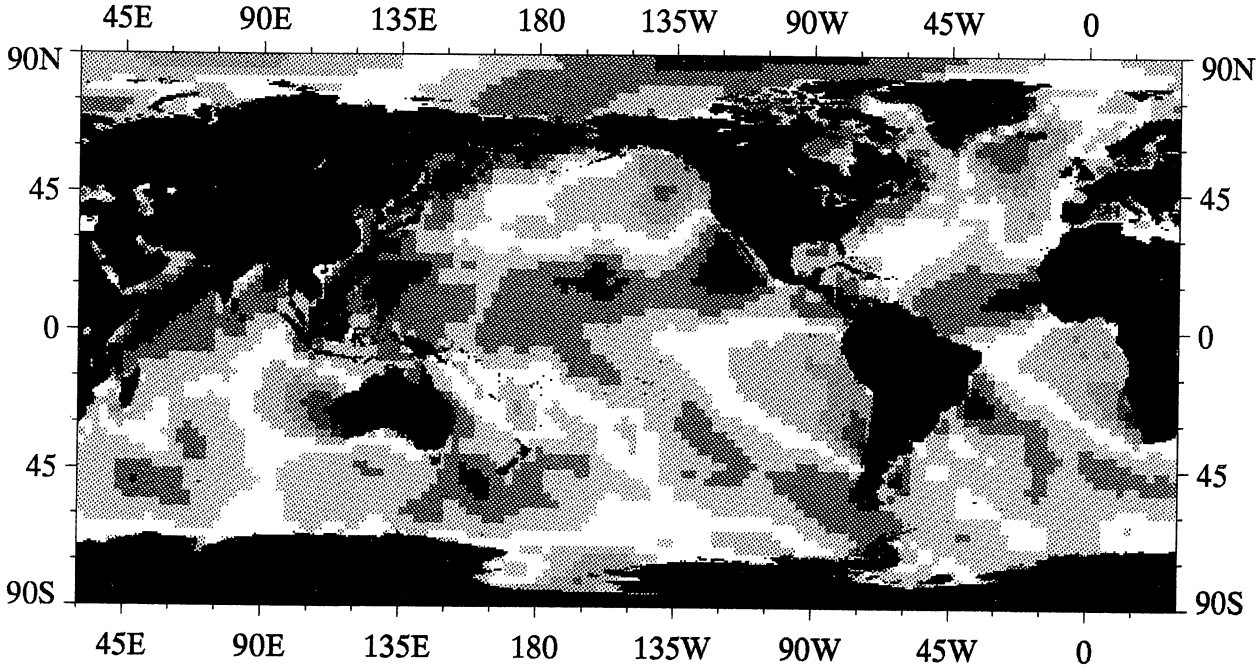

Meridional Wind Speed, January 1987

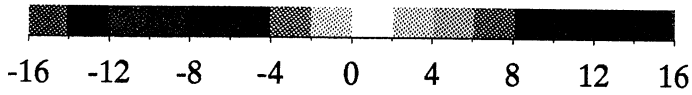

ECMWF 10 m Wind Speed, m s^{-1}

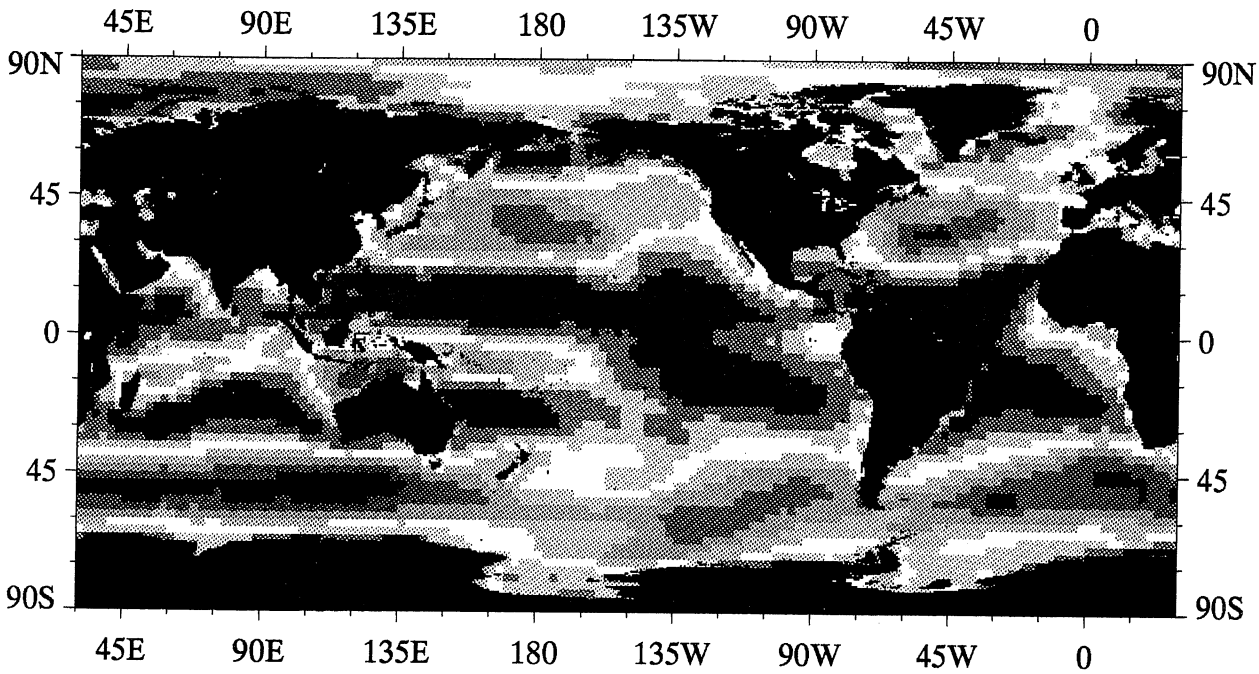

Zonal Wind Speed, February 1987

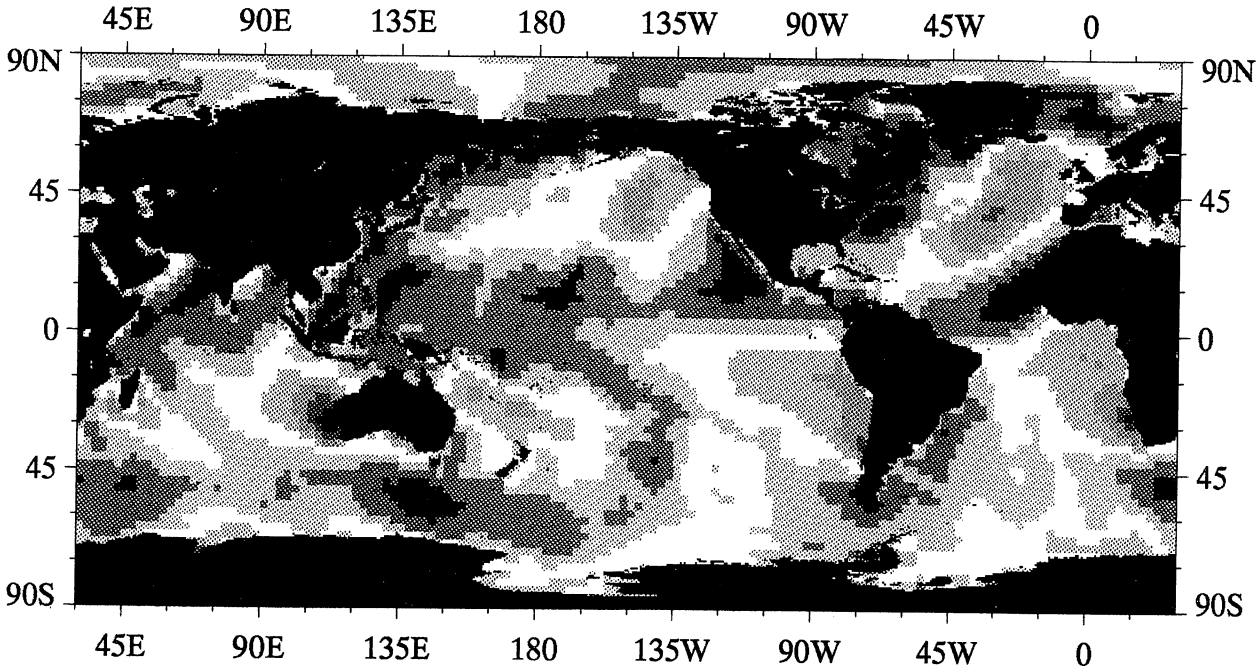

Meridional Wind Speed, February 1987

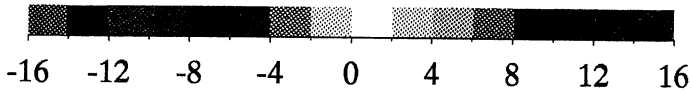

ECMWF 10 m Wind Speed, m s^{-1}

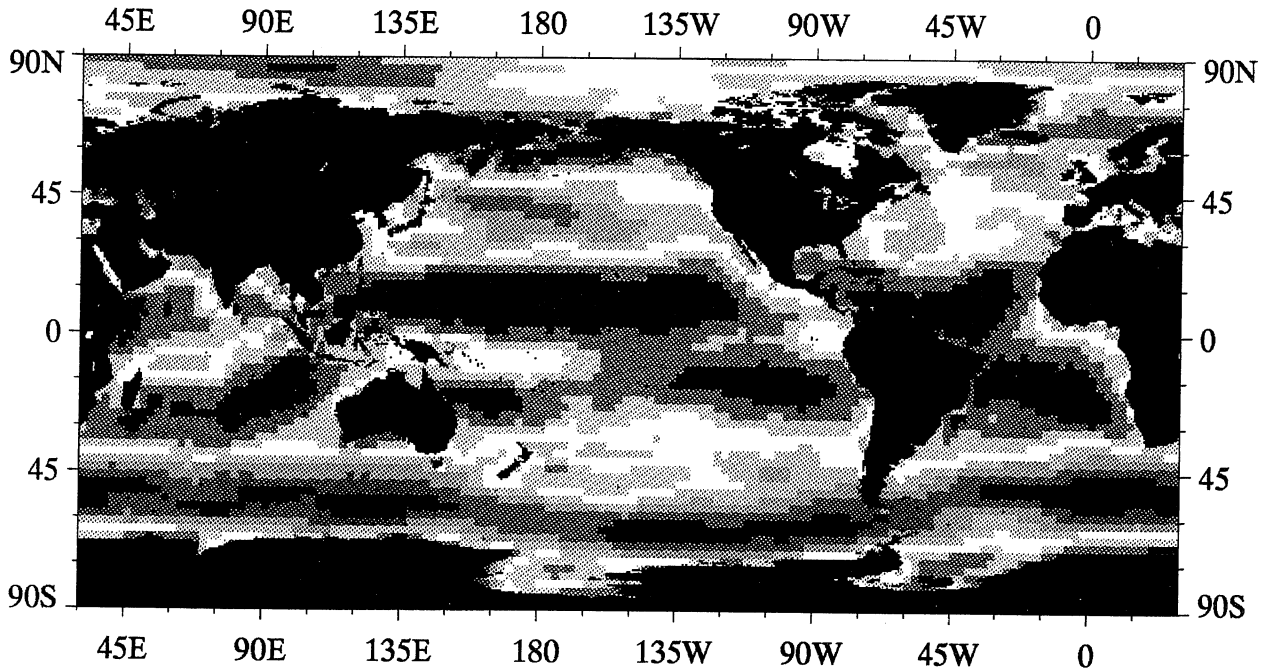

Zonal Wind Speed, March 1987

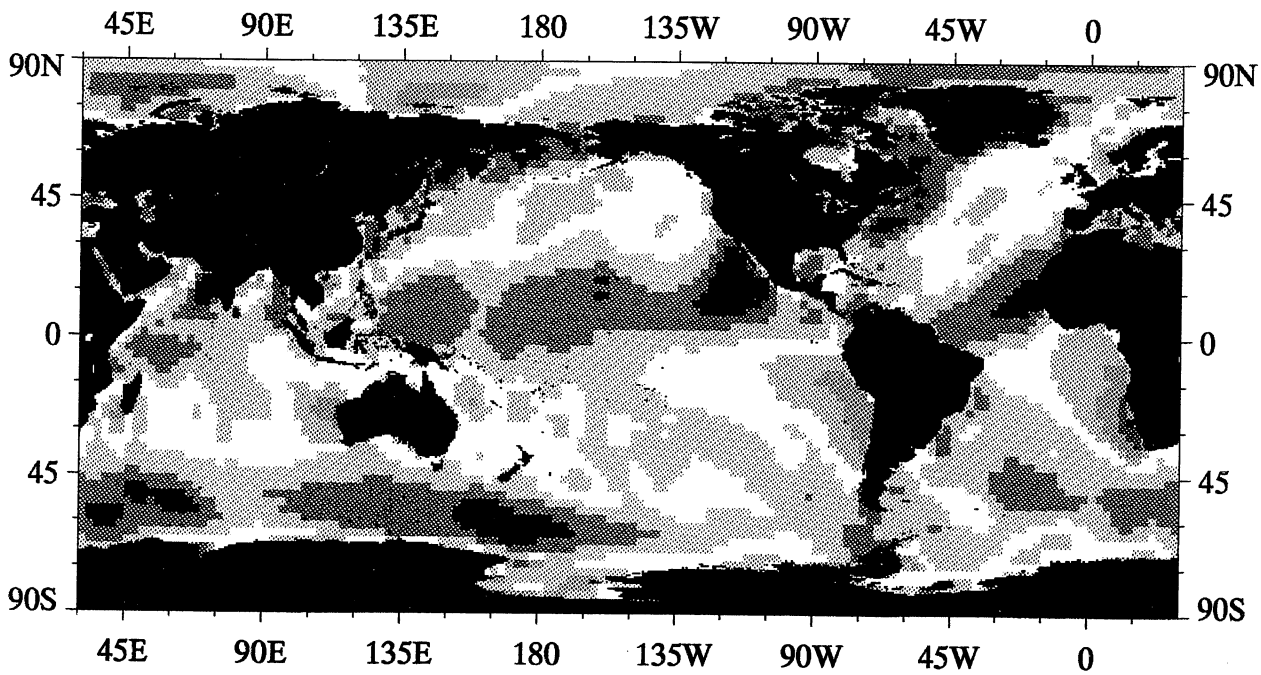

Meridional Wind Speed, March 1987

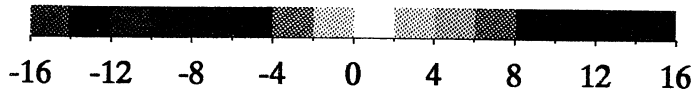

ECMWF 10 m Wind Speed, m s^{-1}

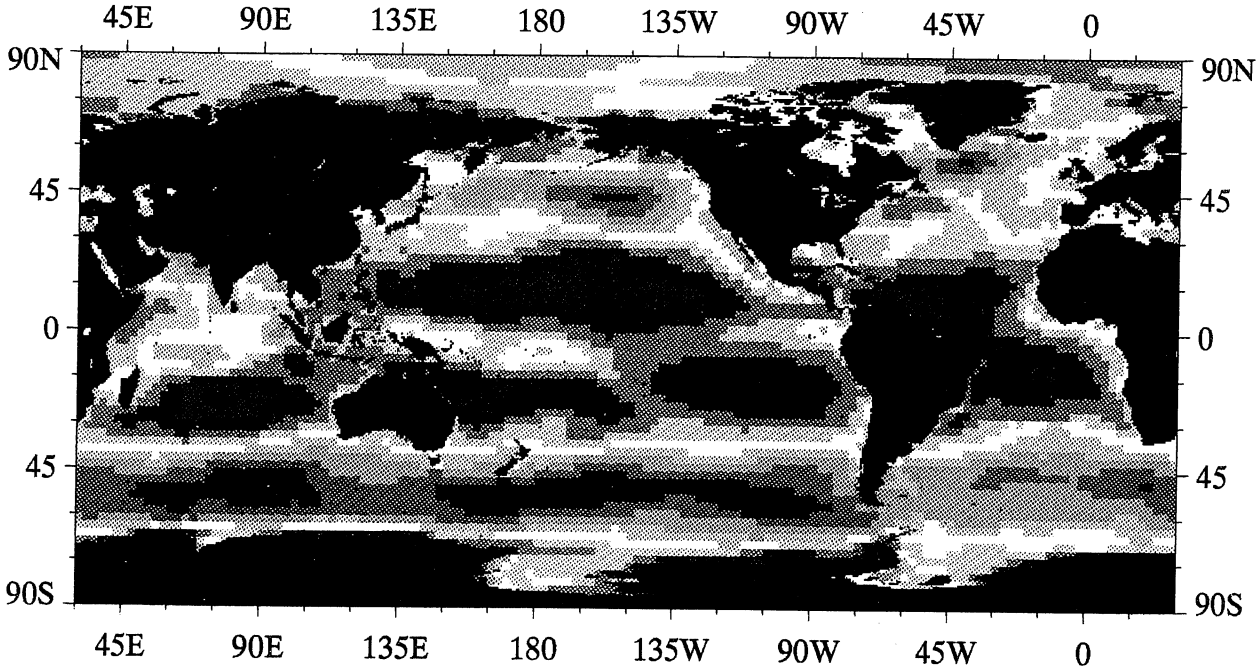

Zonal Wind Speed, April 1987

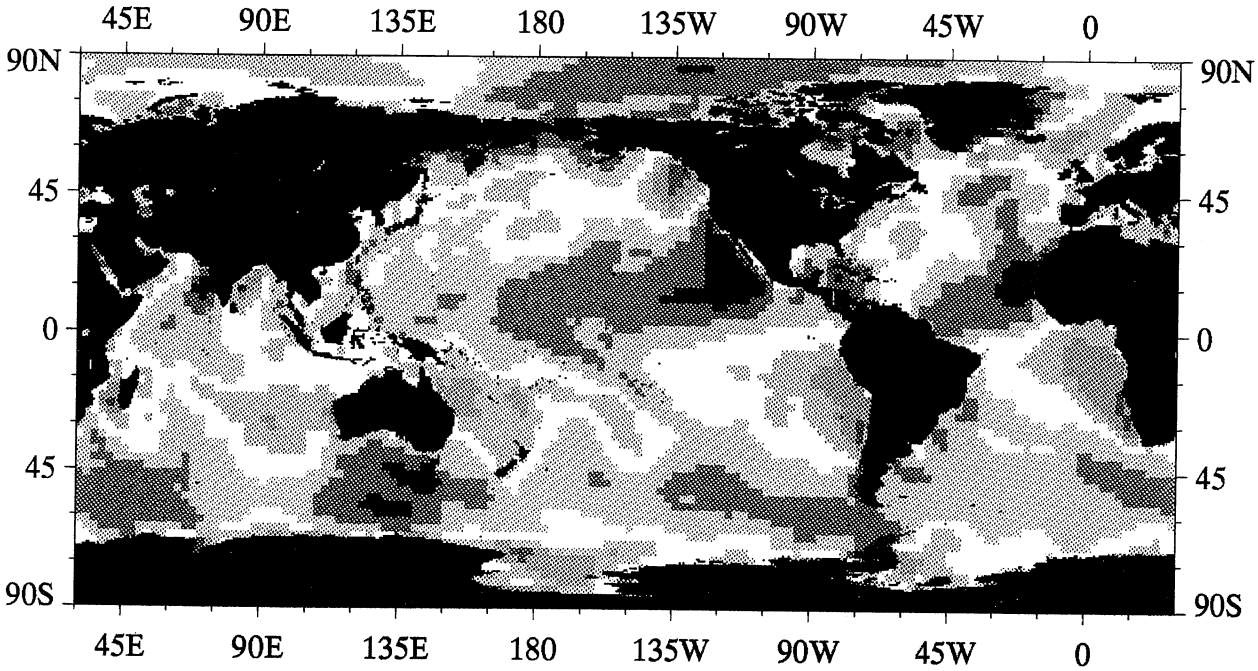

Meridional Wind Speed, April 1987

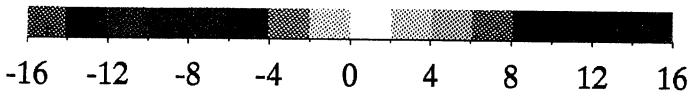

ECMWF 10 m Wind Speed, m s^{-1}

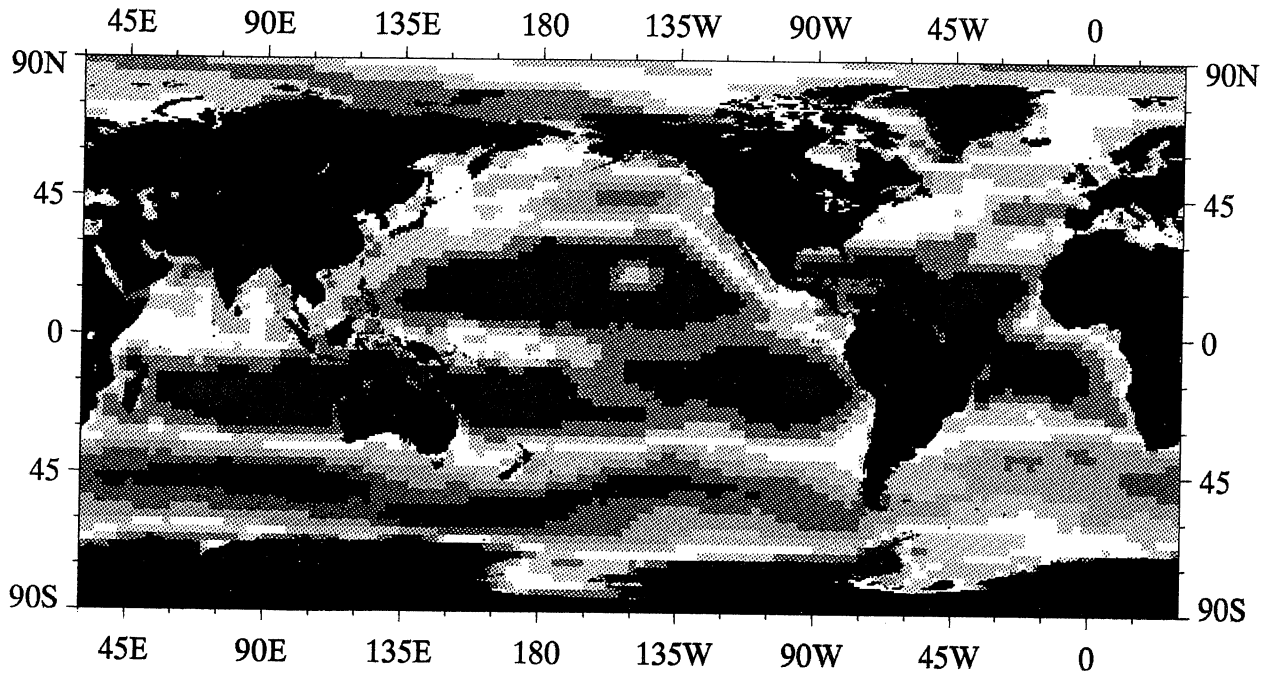

Zonal Wind Speed, May 1987

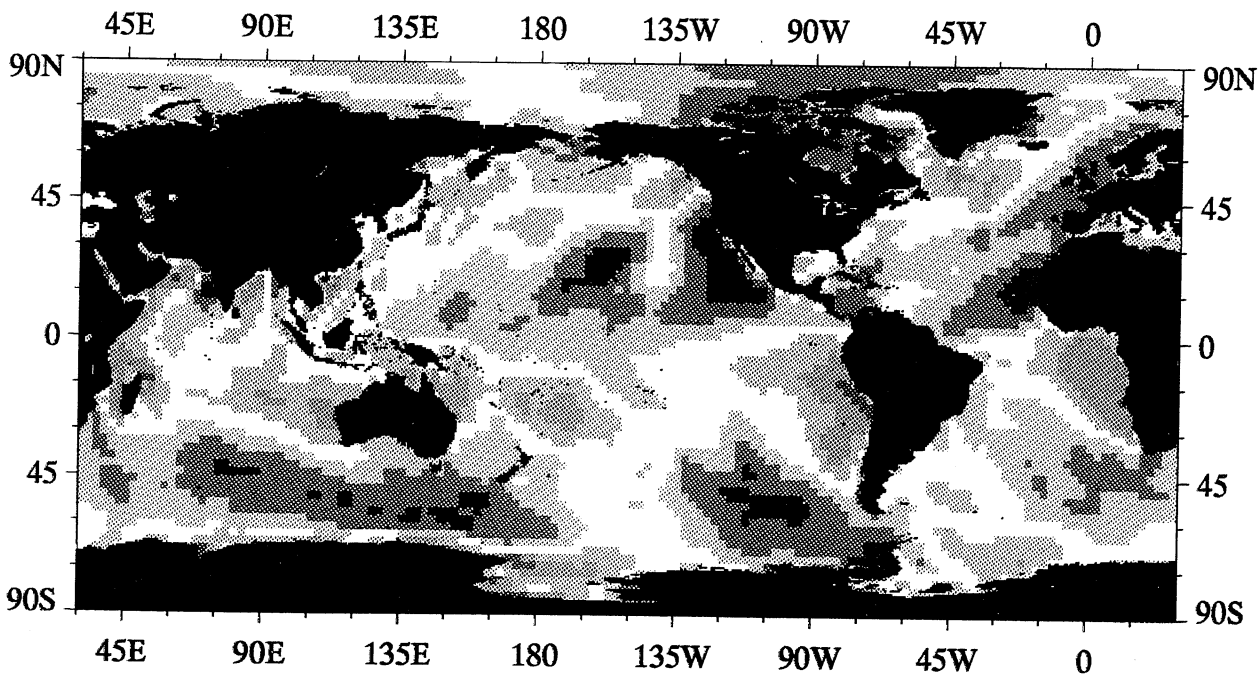

Meridional Wind Speed, May 1987

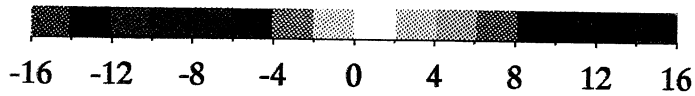

ECMWF 10 m Wind Speed, m s^{-1}

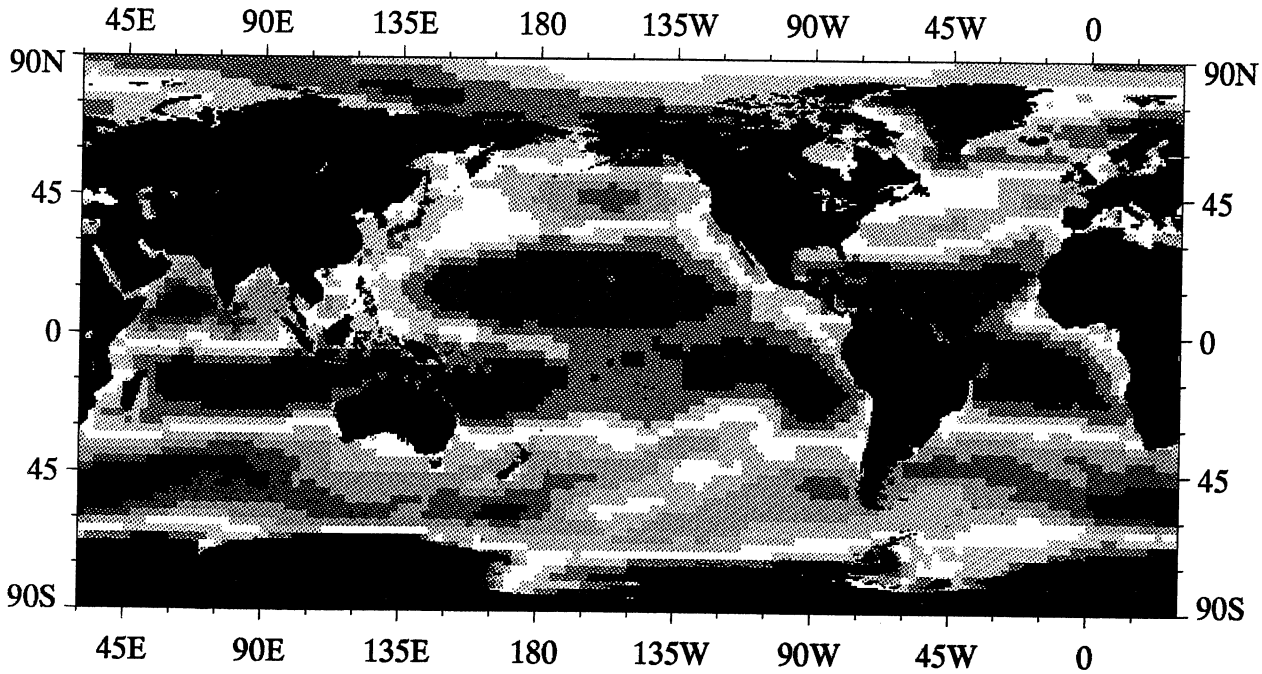

Zonal Wind Speed, June 1987

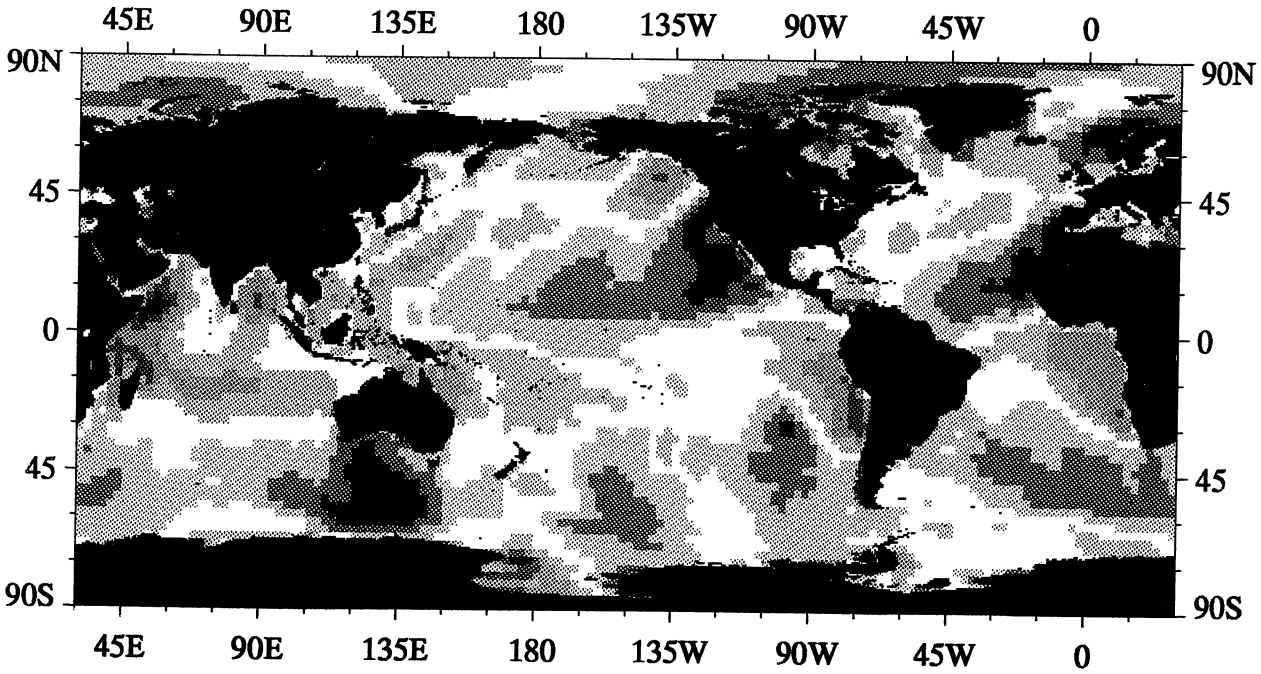

Meridional Wind Speed, June 1987

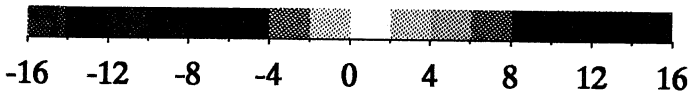

ECMWF 10 m Wind Speed, m s^{-1}

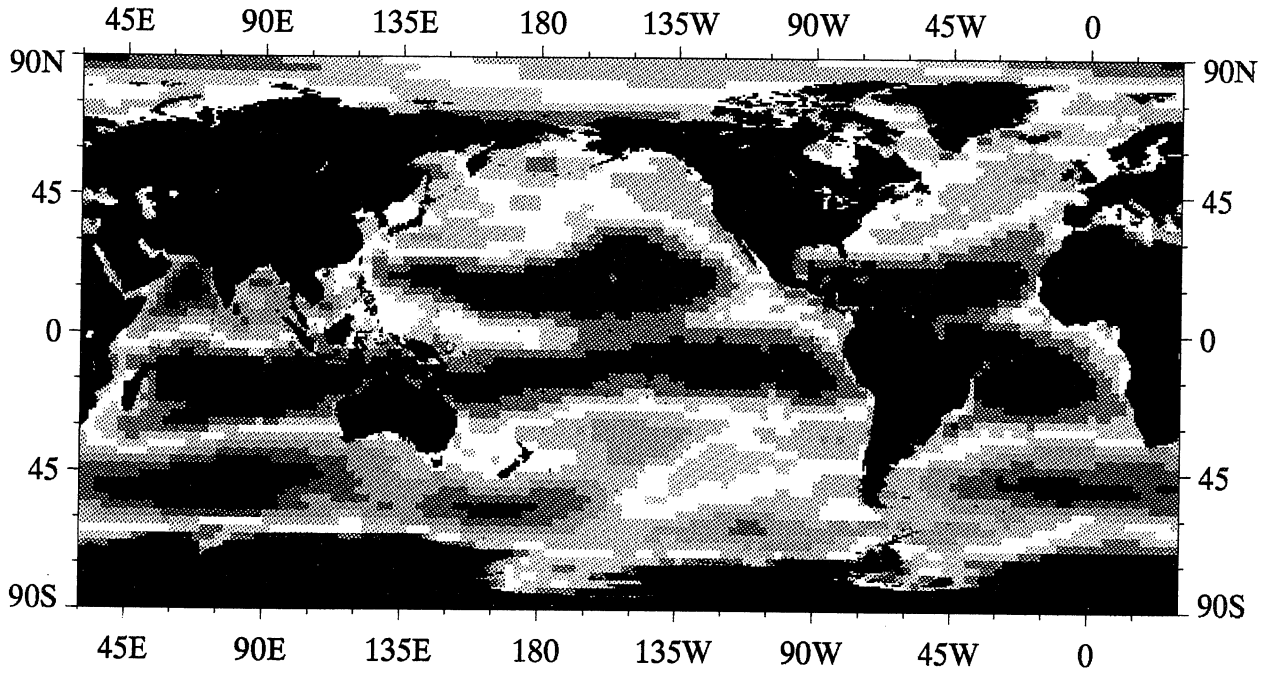

Zonal Wind Speed, July 1987

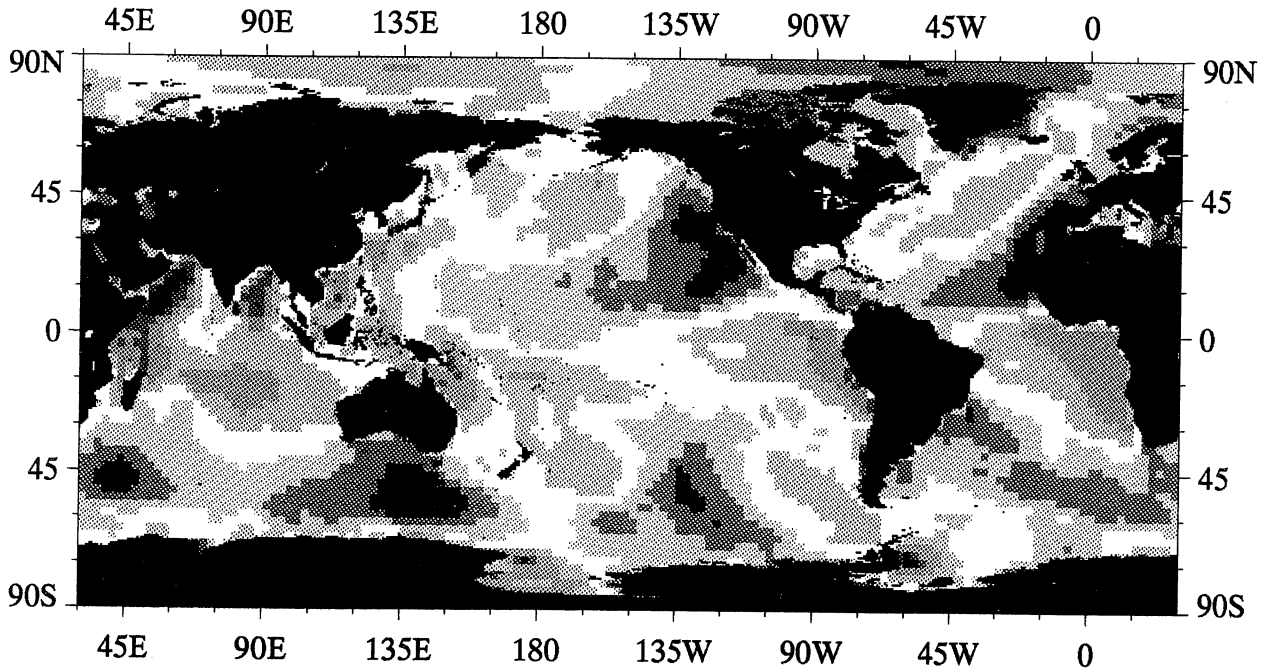

Meridional Wind Speed, July 1987

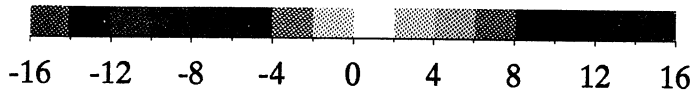

ECMWF 10 m Wind Speed, m s^{-1}

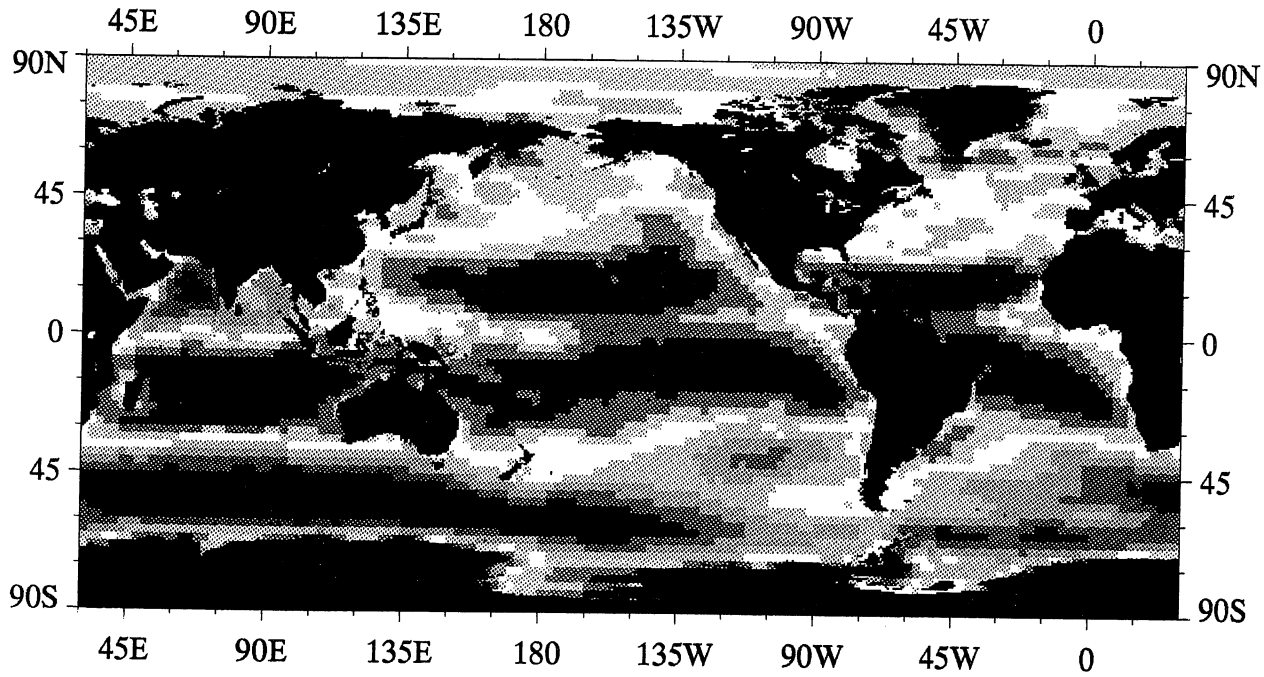

Zonal Wind Speed, August 1987

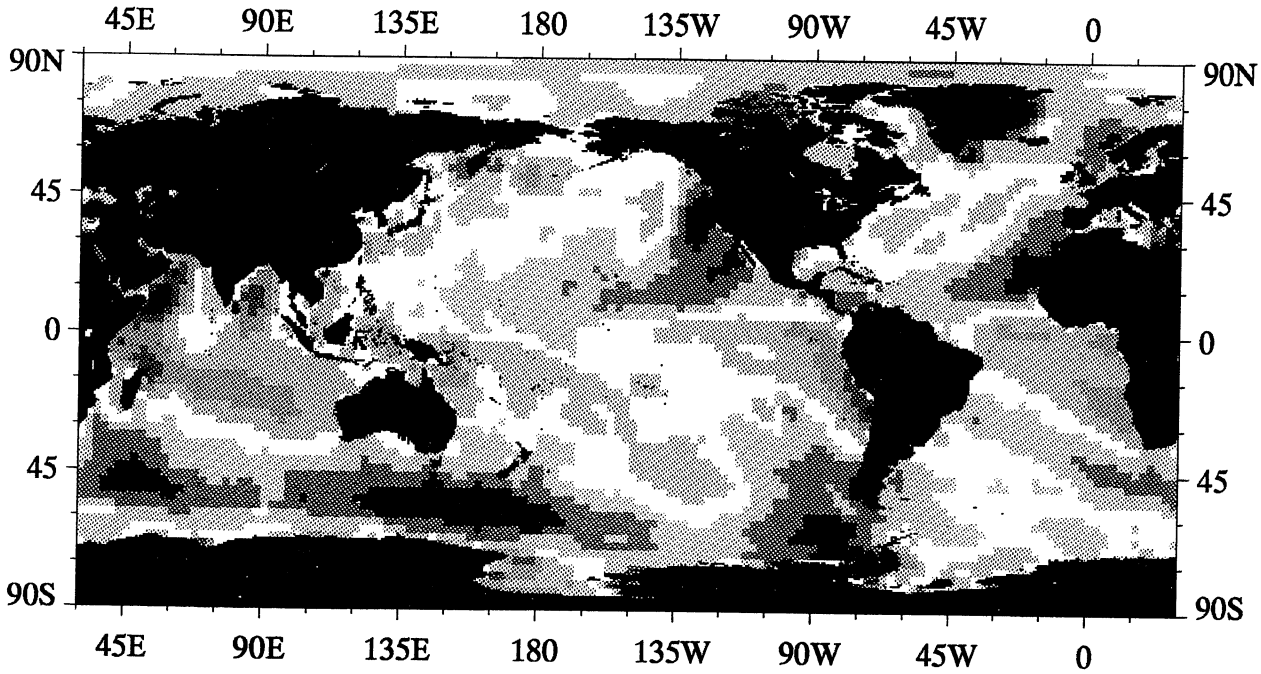

Meridional Wind Speed, August 1987

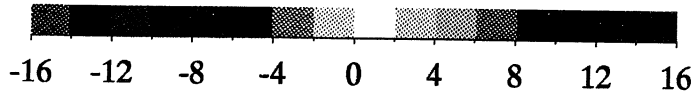

ECMWF 10 m Wind Speed, m s^{-1}

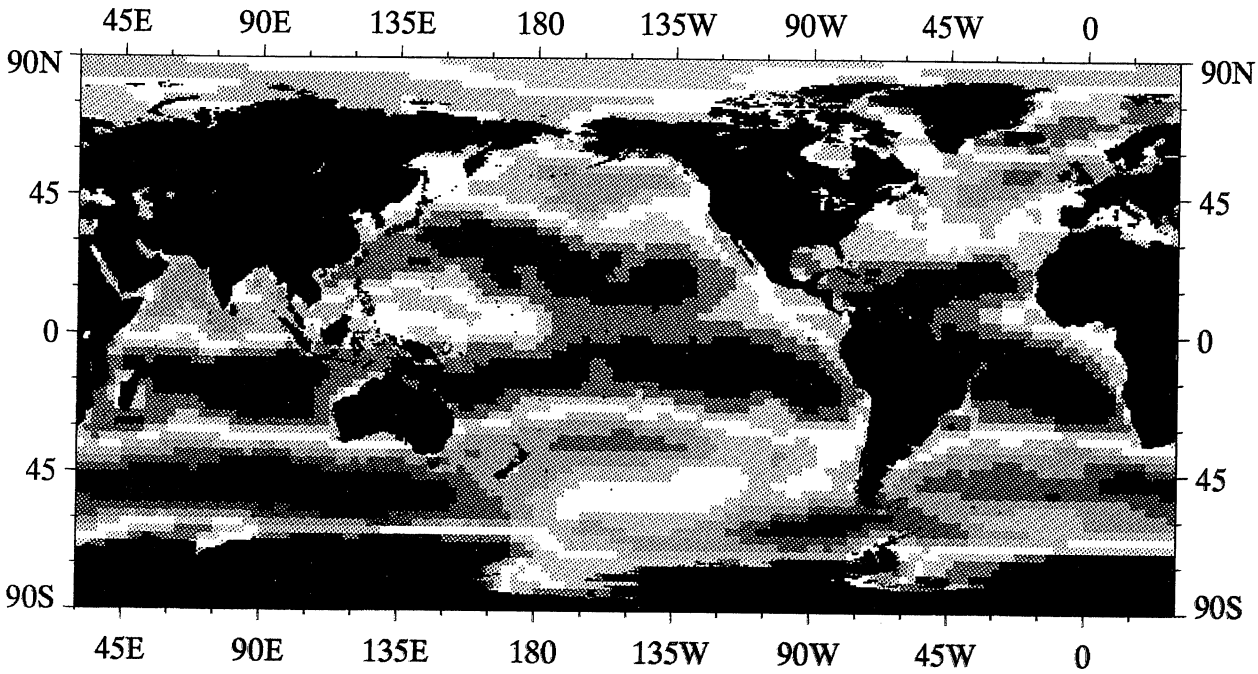

Zonal Wind Speed, September 1987

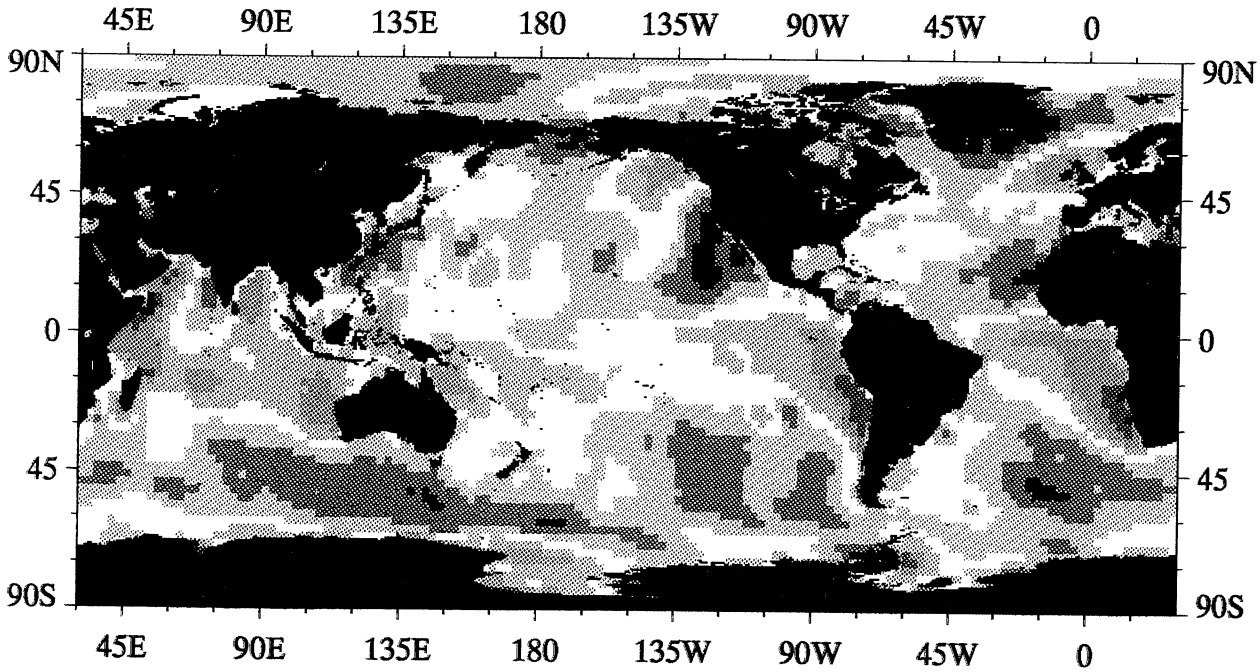

Meridional Wind Speed, September 1987

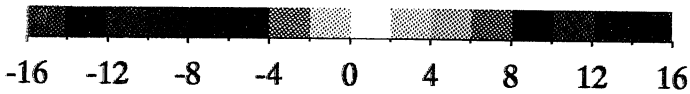

ECMWF 10 m Wind Speed, m s^{-1}

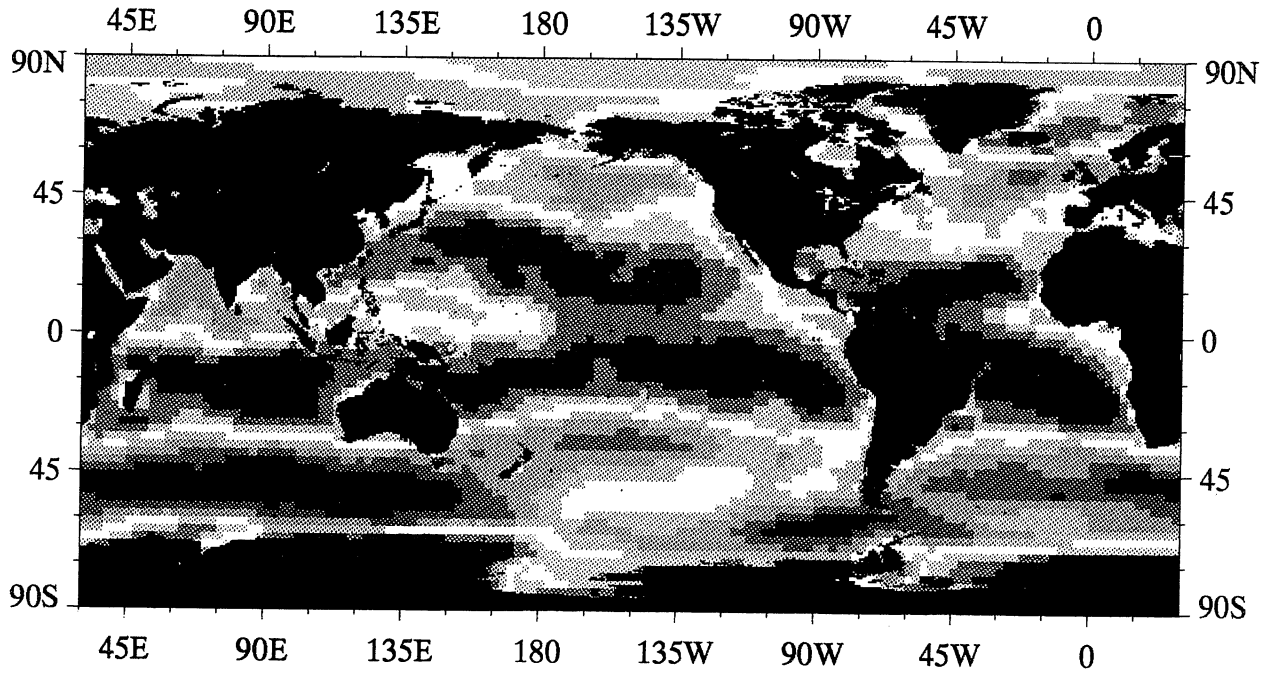

Zonal Wind Speed, October 1987

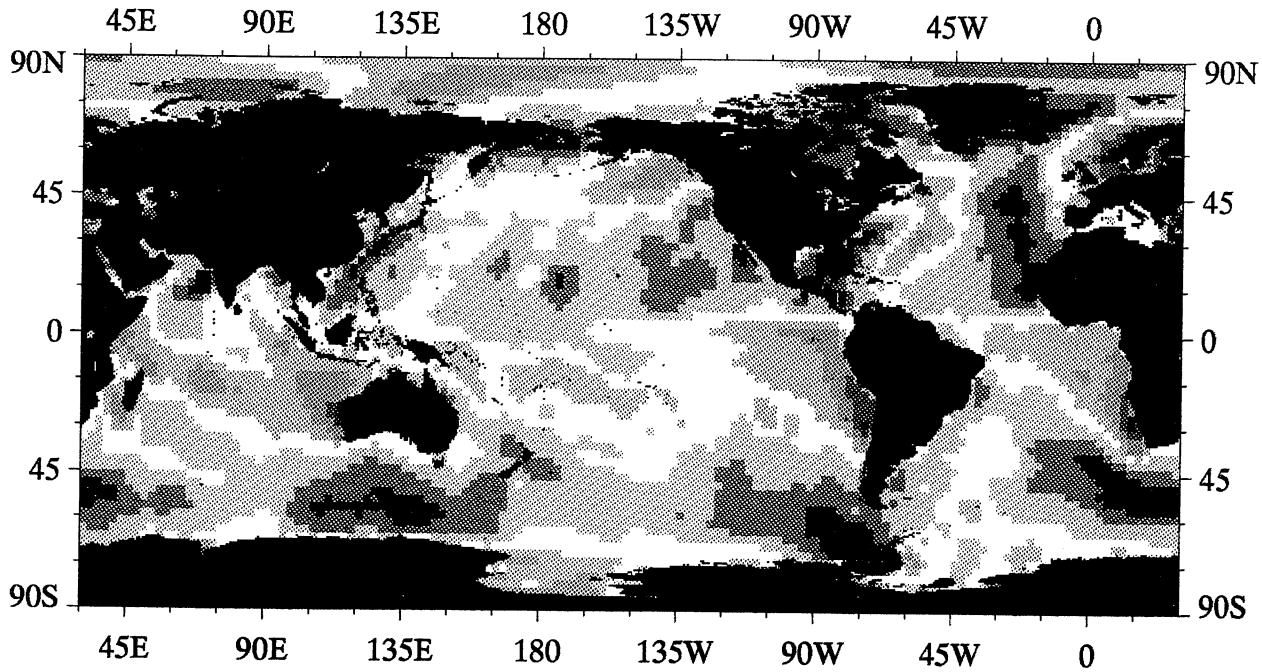

Meridional Wind Speed, October 1987

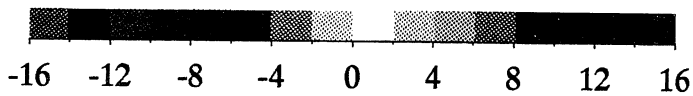

ECMWF 10 m Wind Speed, m s^{-1}

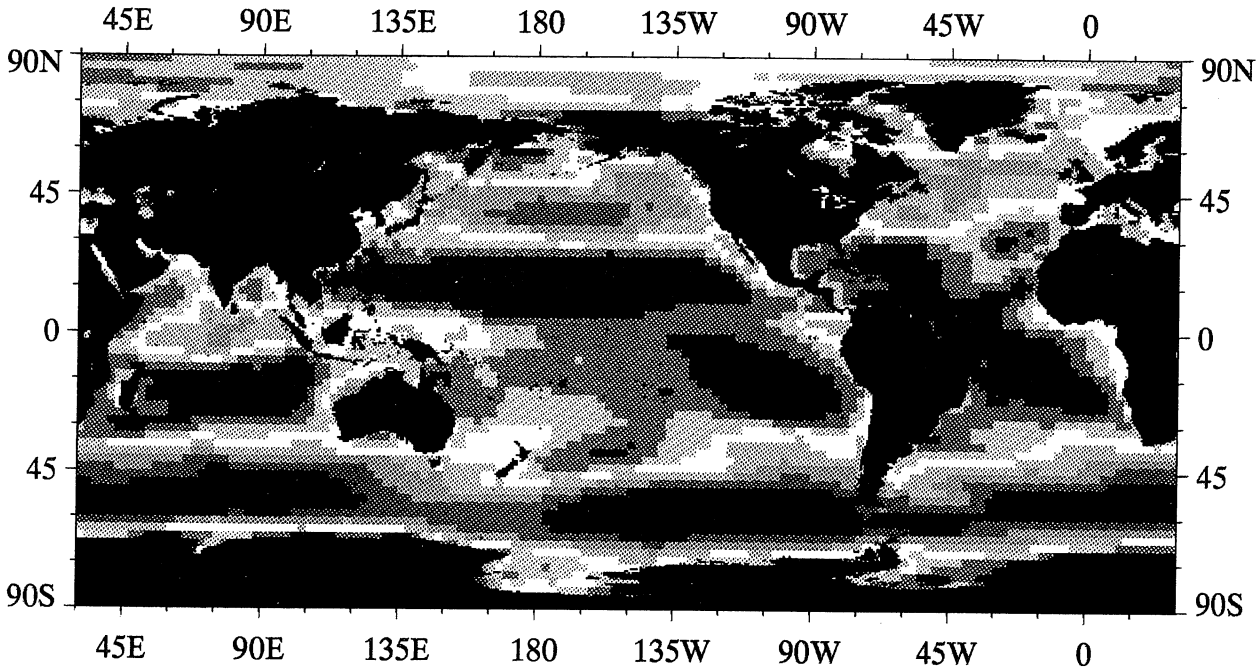

Zonal Wind Speed, November 1987

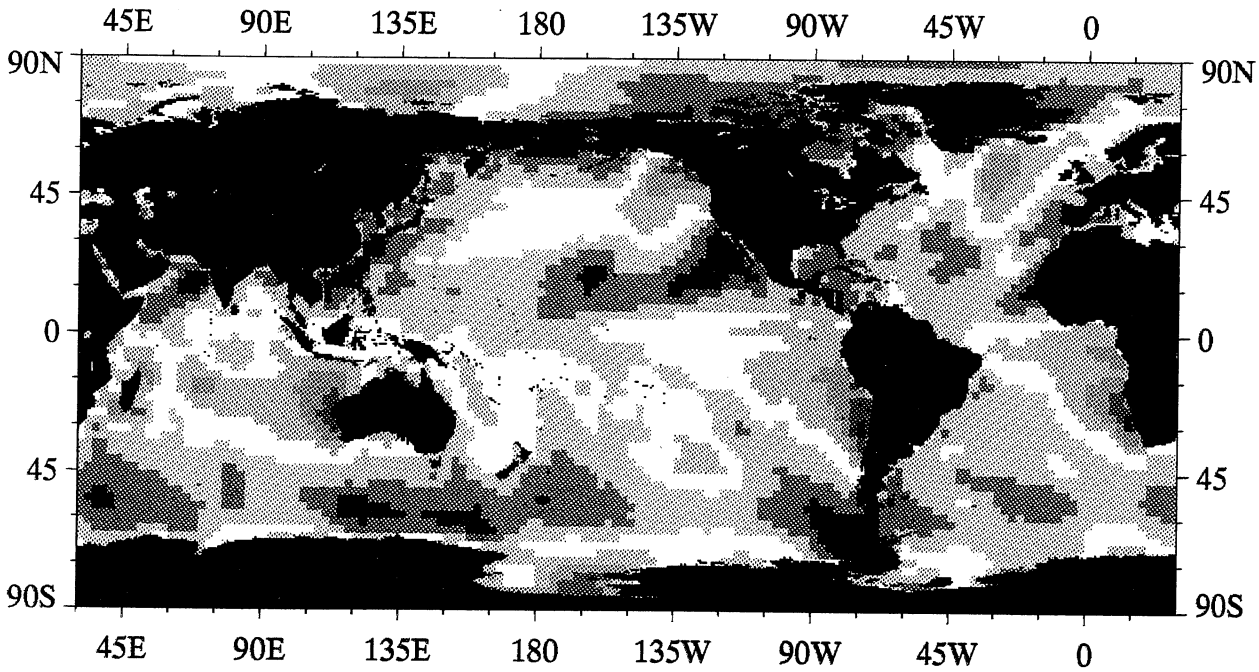

Meridional Wind Speed, November 1987

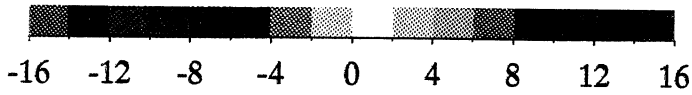

ECMWF 10 m Wind Speed, m s^{-1}

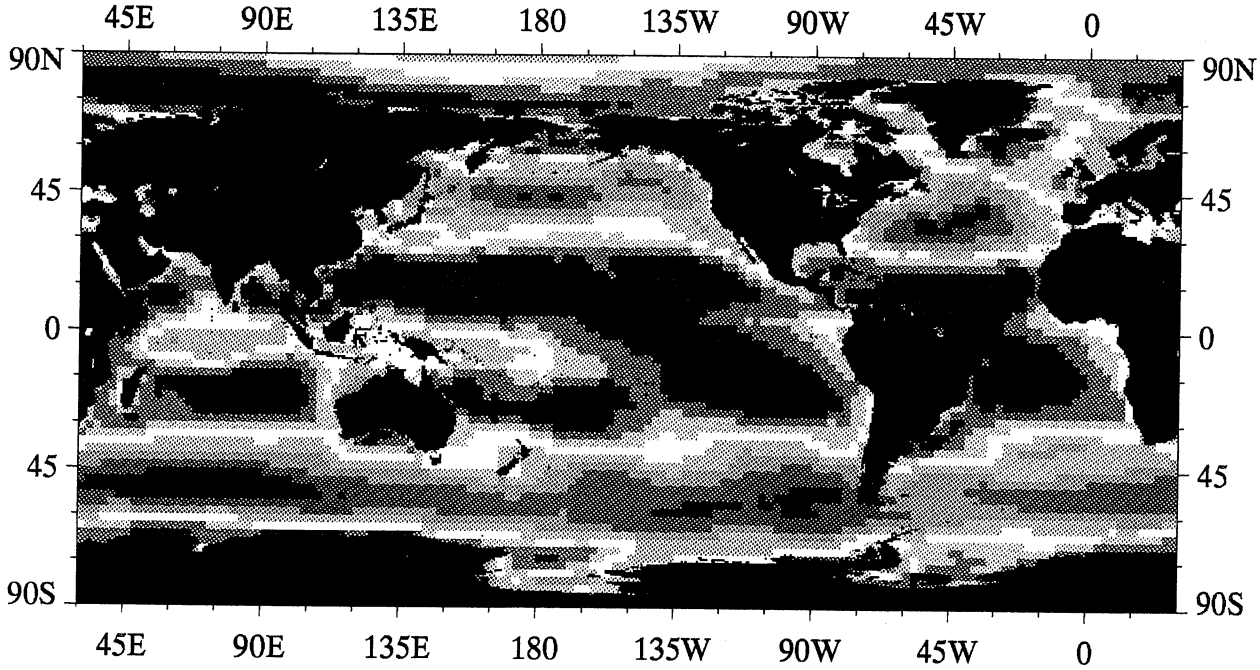

Zonal Wind Speed, December 1987

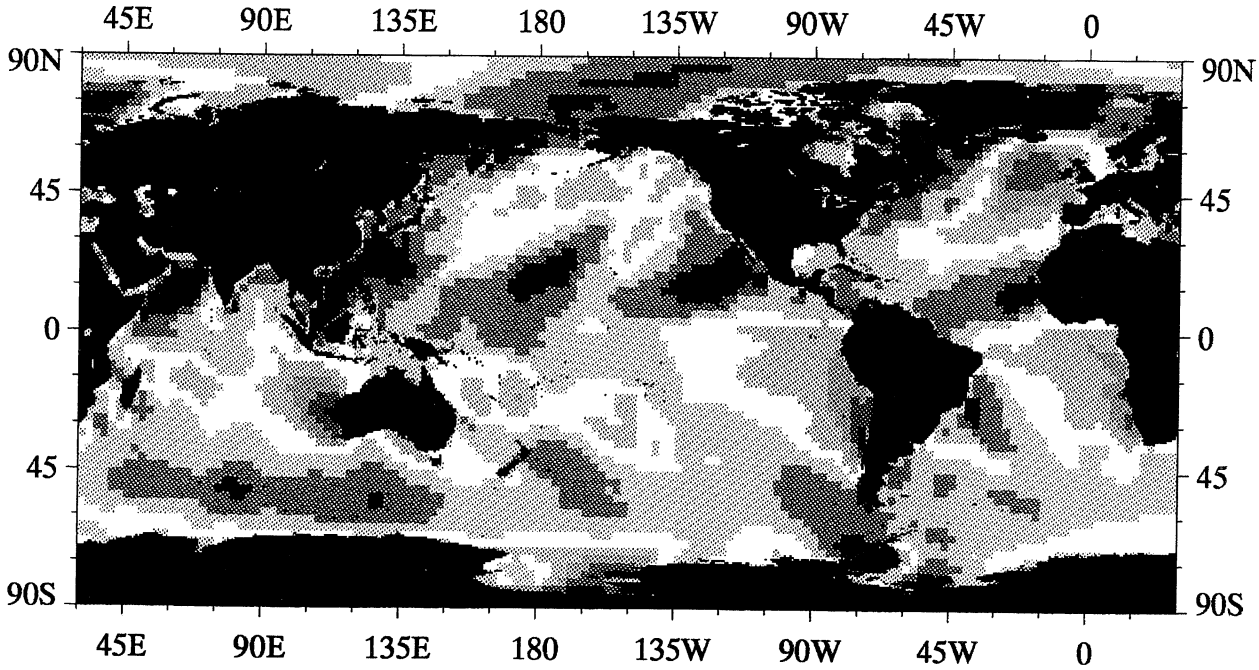

Meridional Wind Speed, December 1987

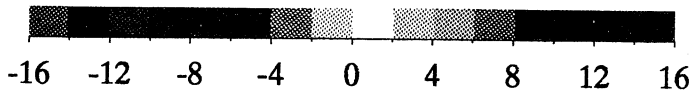

ECMWF 10 m Wind Speed, m s^{-1}

A11

Monthly Standard Deviation of ECMWF Surface Wind Components

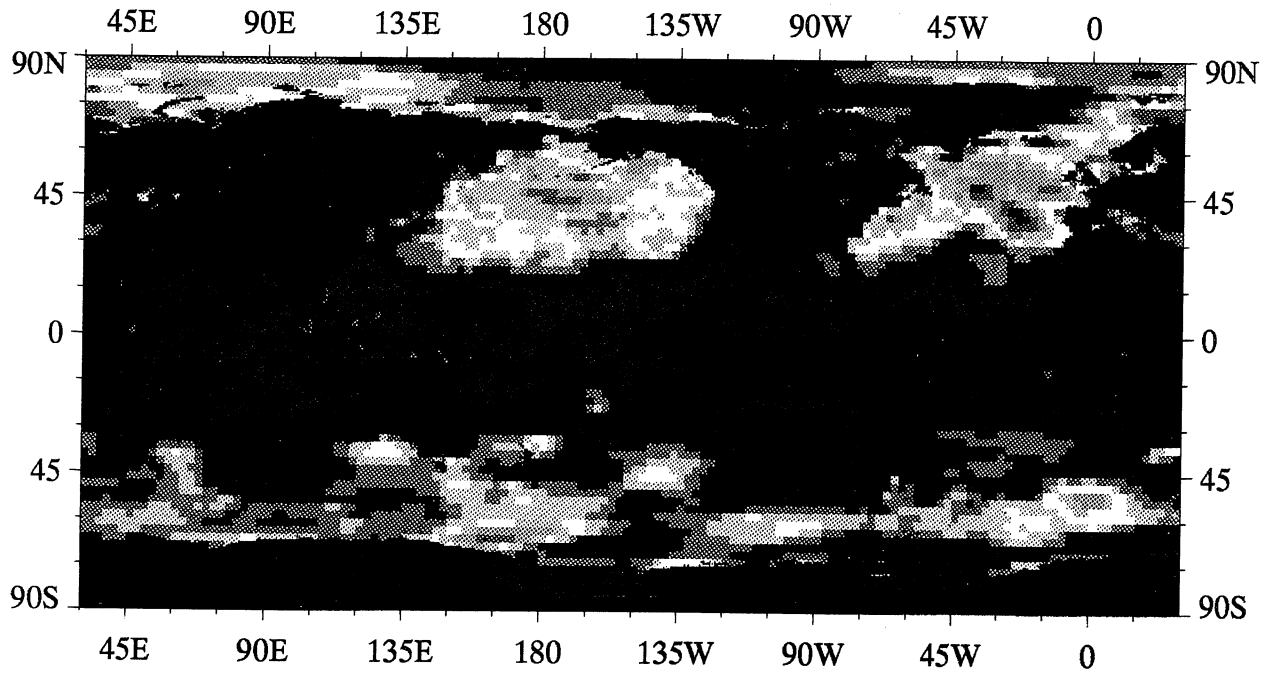

Zonal Wind Speed, January 1987

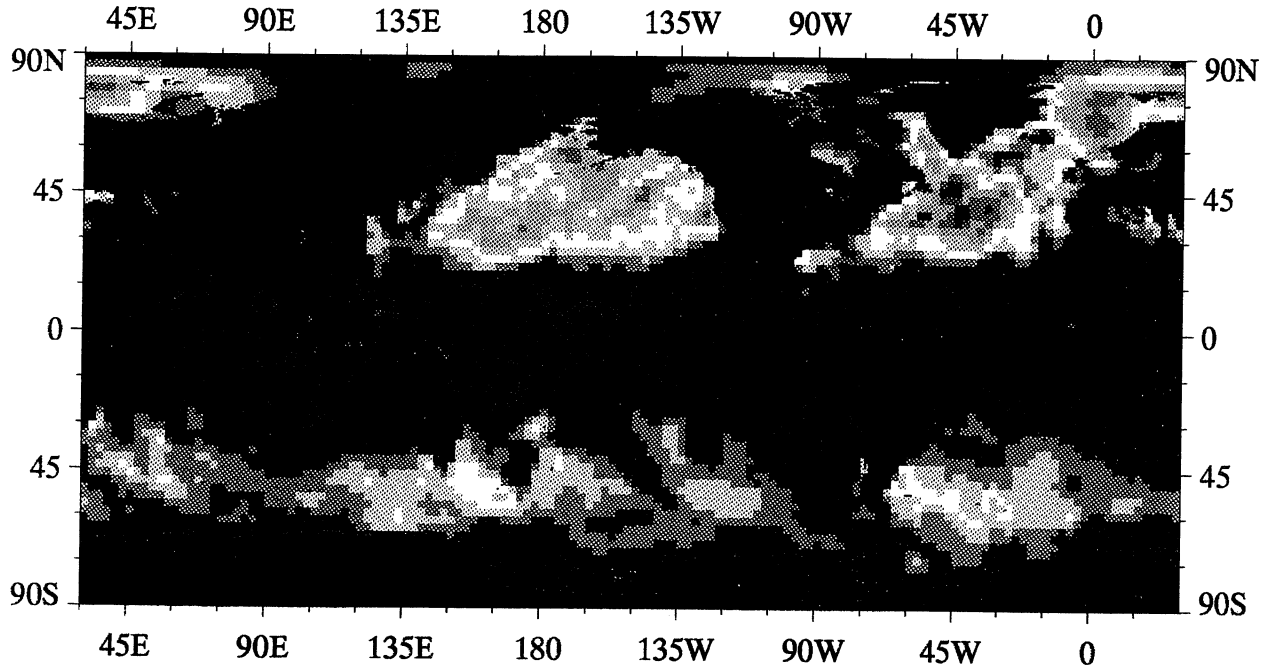

Meridional Wind Speed, January 1987

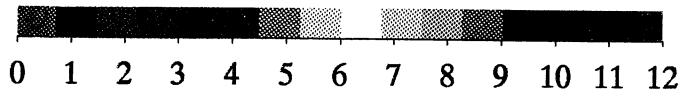

Standard Deviation of ECMWF 10 m Wind Speed, m s^{-1}

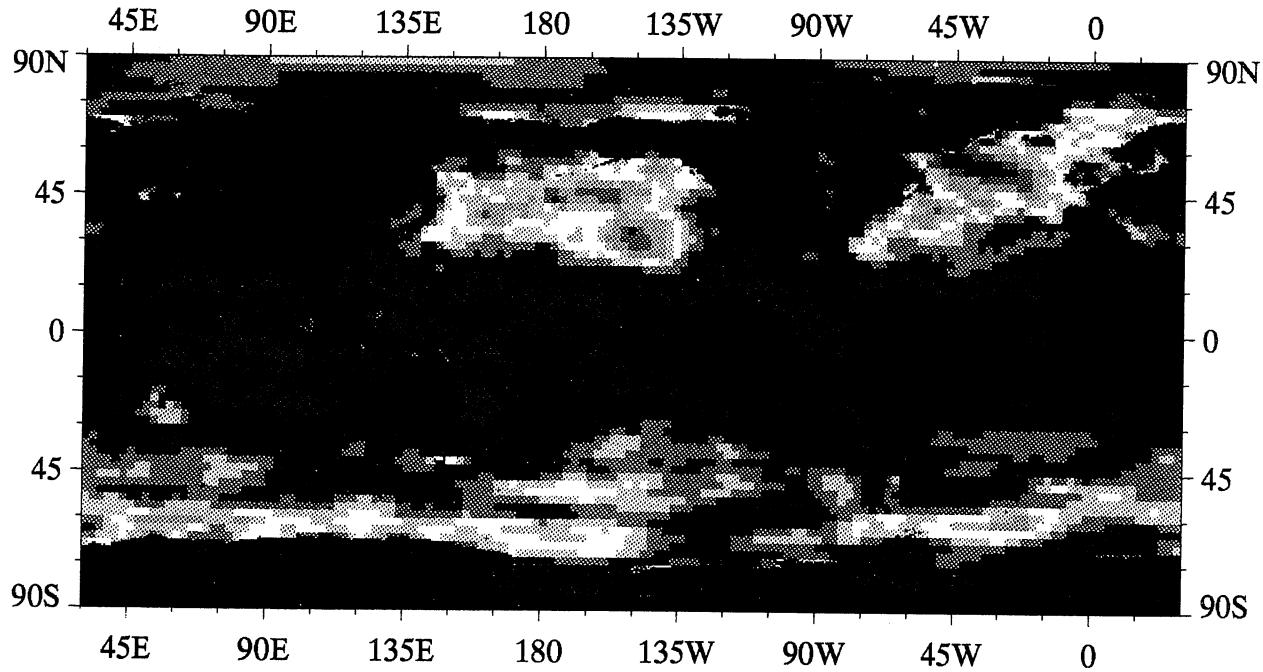

Zonal Wind Speed, February 1987

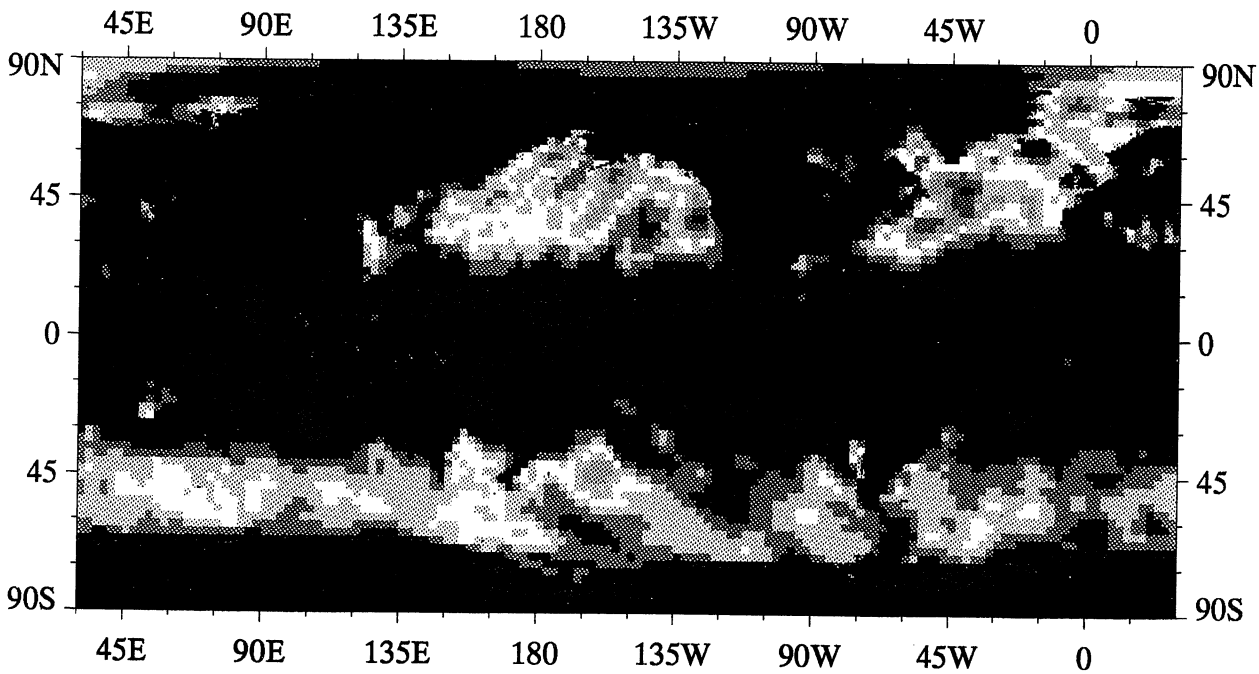

Meridional Wind Speed, February 1987

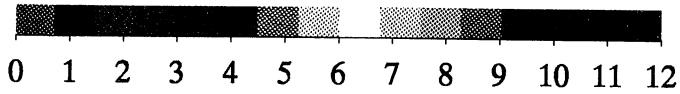

Standard Deviation of ECMWF 10 m Wind Speed, m s^{-1}

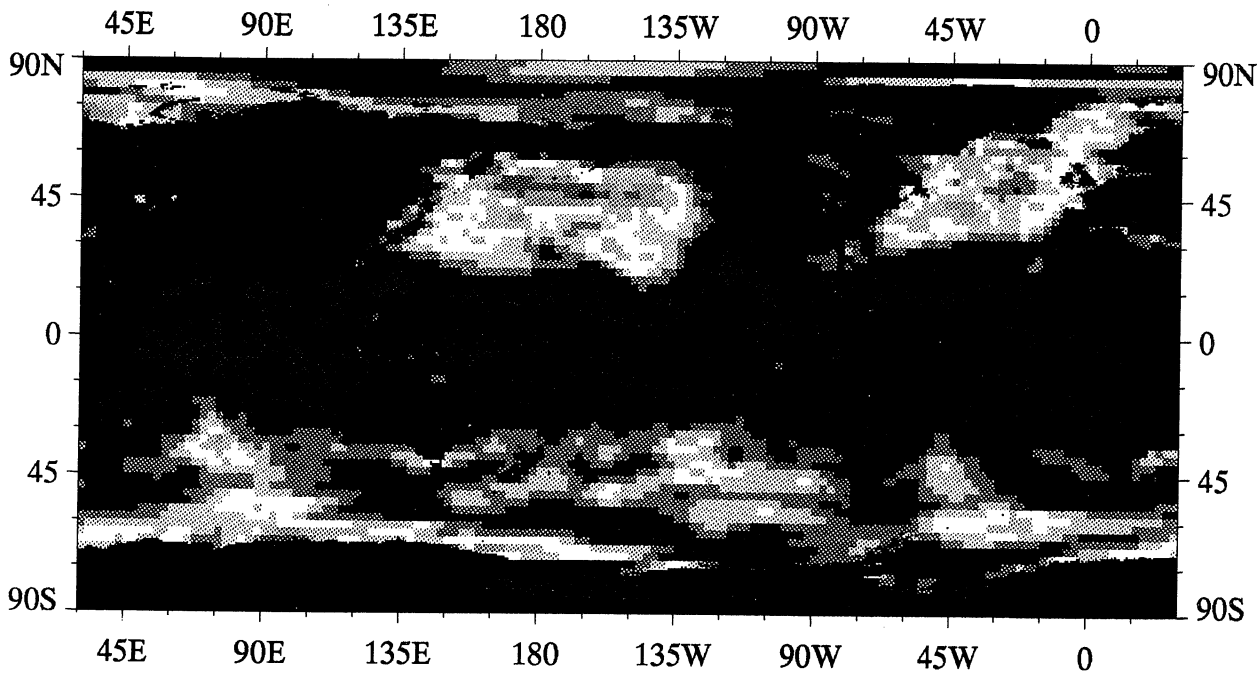

Zonal Wind Speed, March 1987

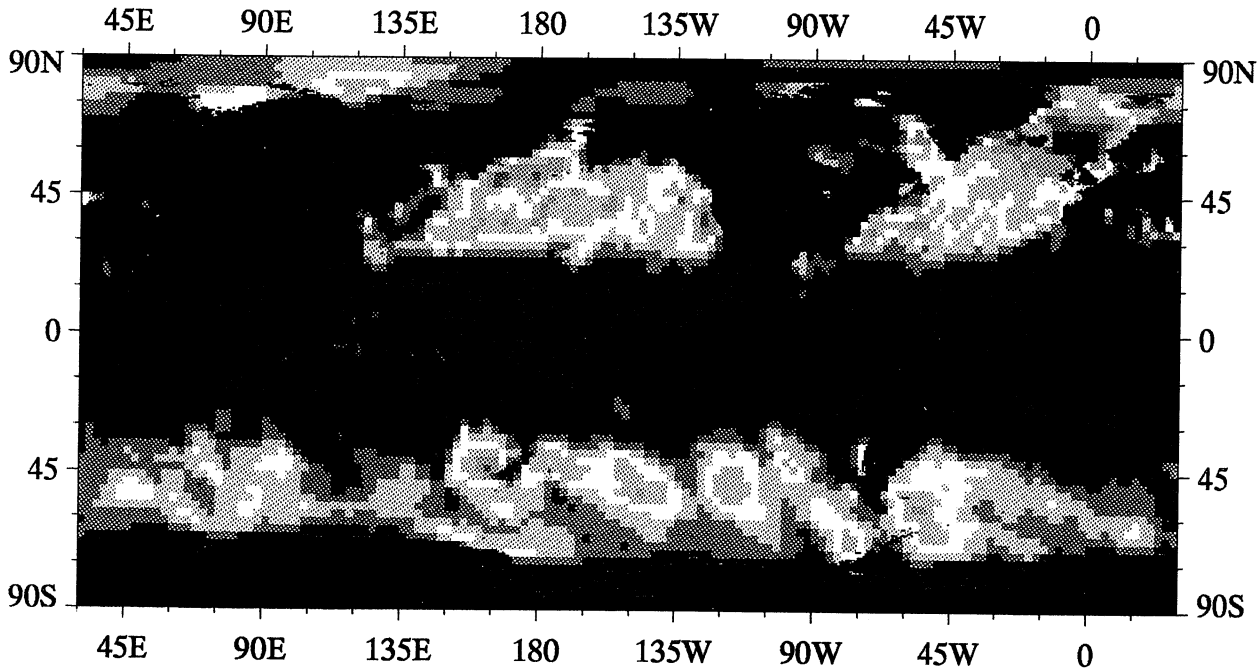

Meridional Wind Speed, March 1987

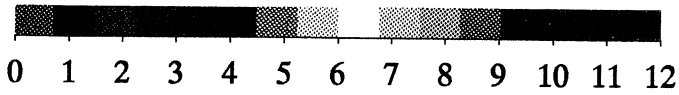

Standard Deviation of ECMWF 10 m Wind Speed, m s^{-1}

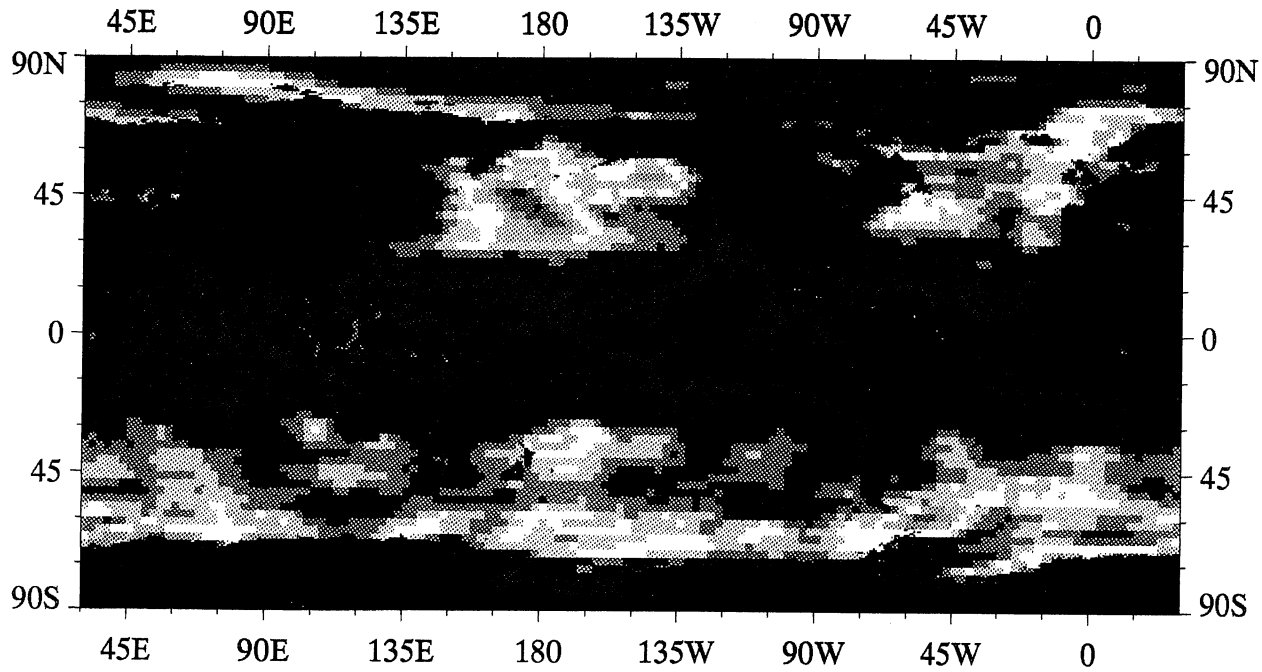

Zonal Wind Speed, April 1987

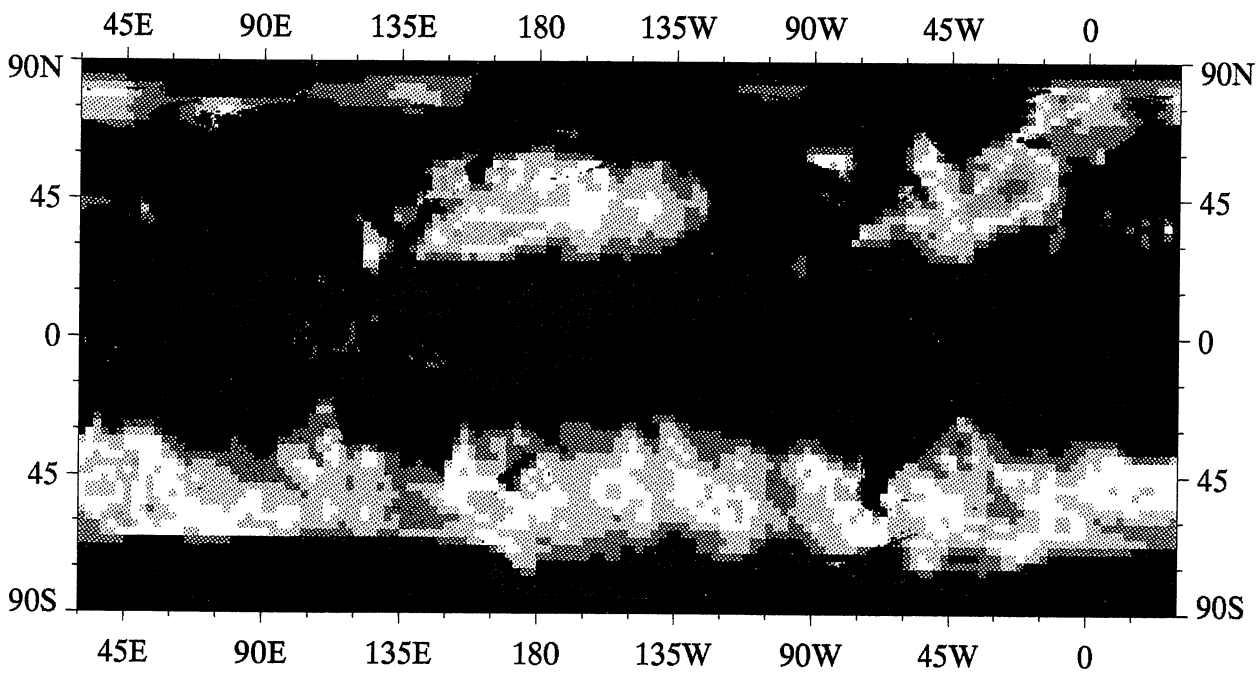

Meridional Wind Speed, April 1987

Standard Deviation of ECMWF 10 m Wind Speed, m s^{-1}

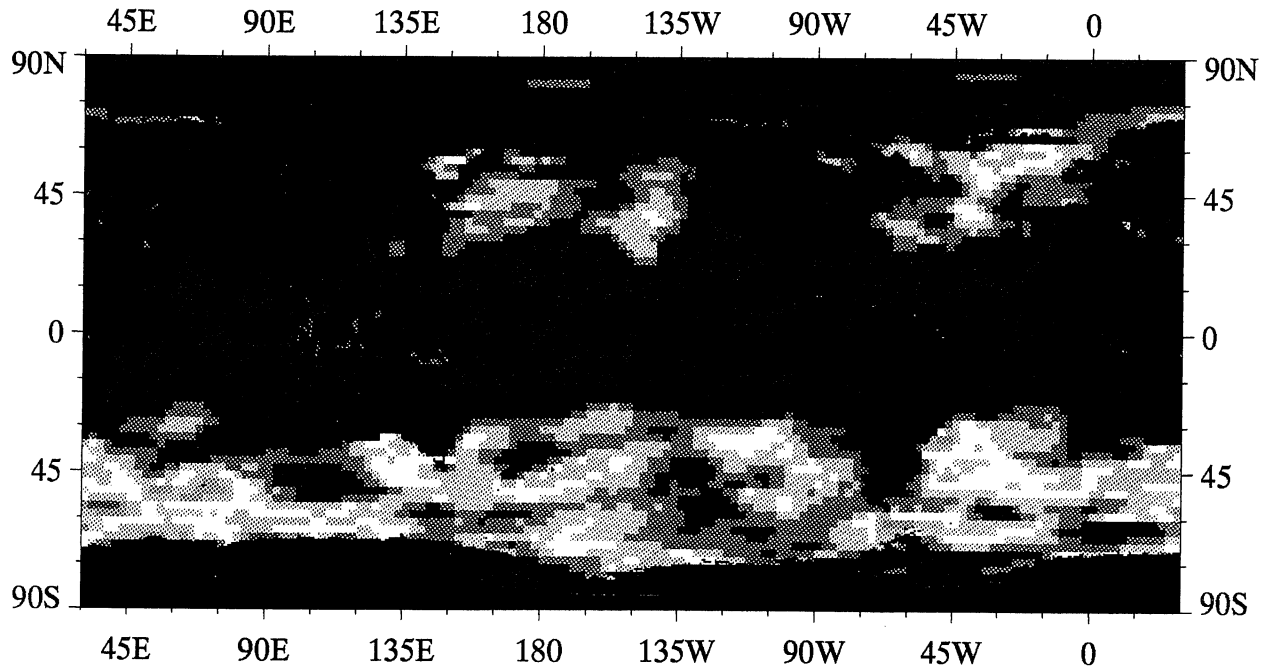

Zonal Wind Speed, May 1987

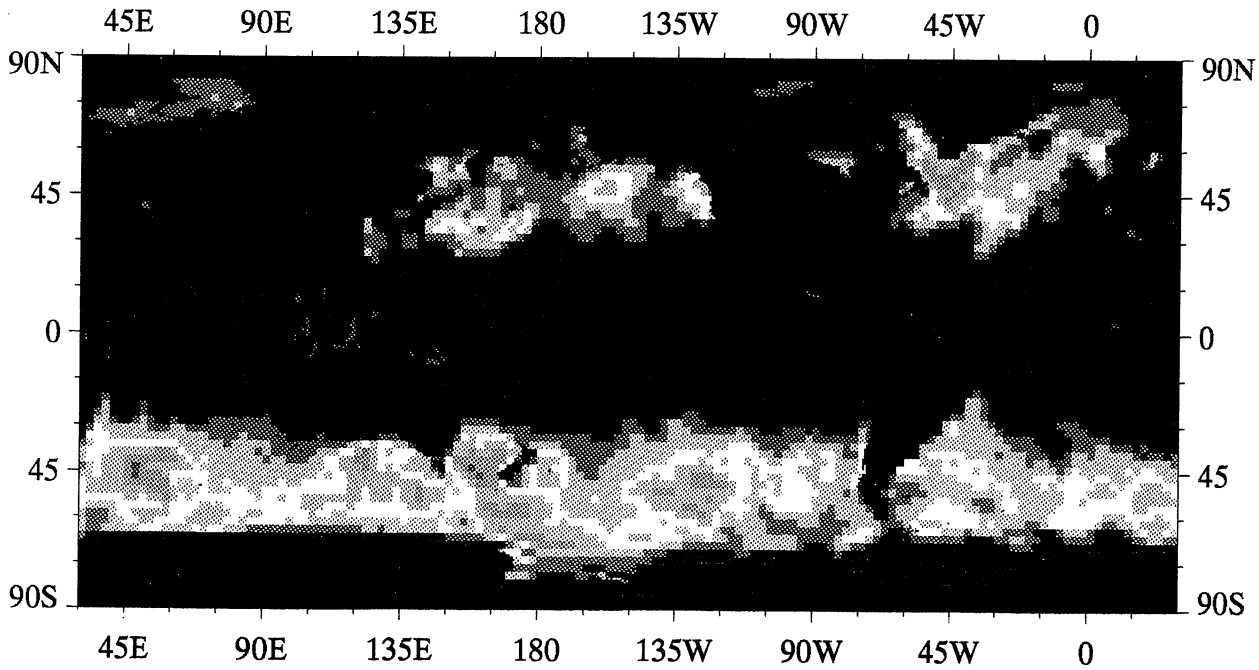

Meridional Wind Speed, May 1987

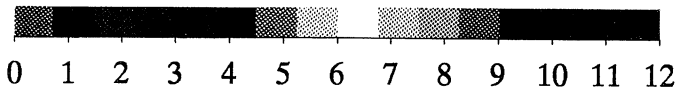

Standard Deviation of ECMWF 10 m Wind Speed, m s^{-1}

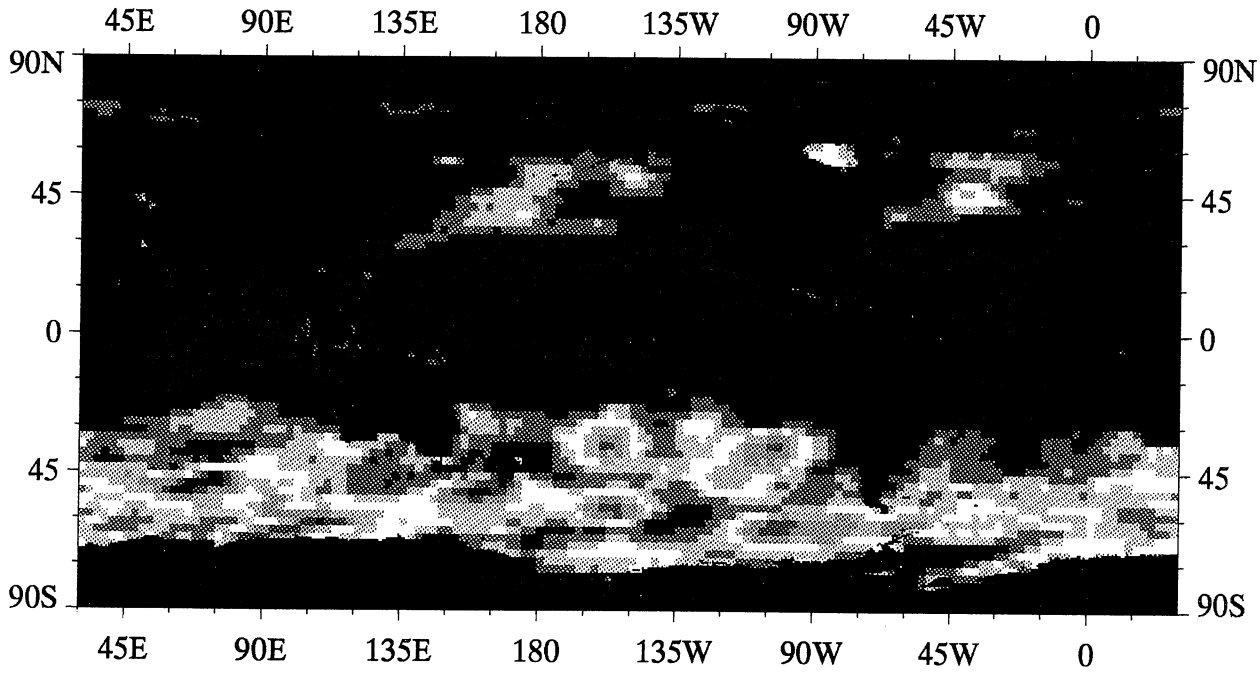

Zonal Wind Speed, June 1987

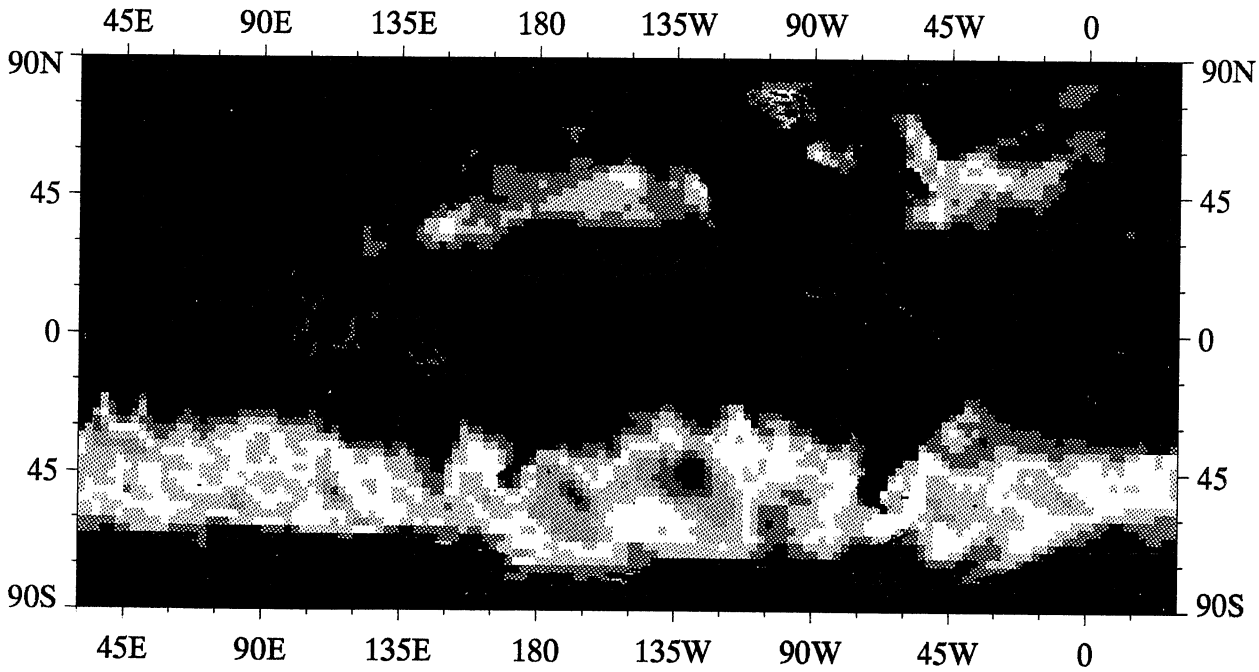

Meridional Wind Speed, June 1987

Standard Deviation of ECMWF 10 m Wind Speed, m s^{-1}

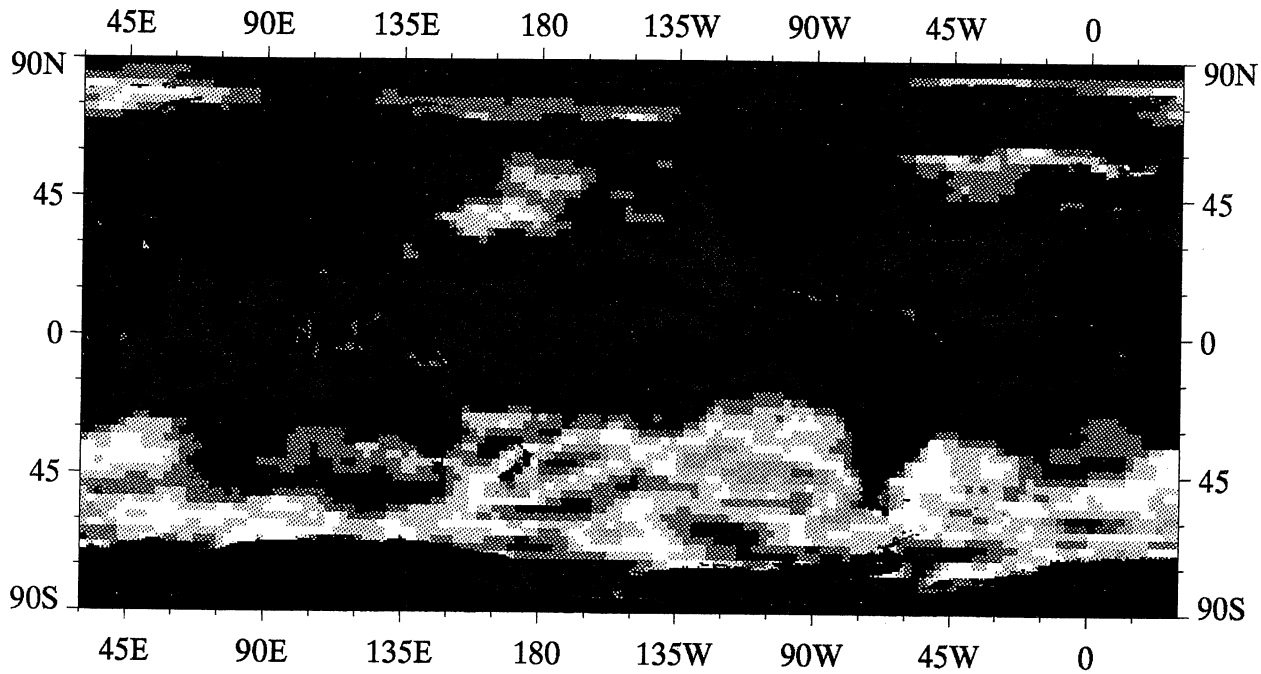

Zonal Wind Speed, July 1987

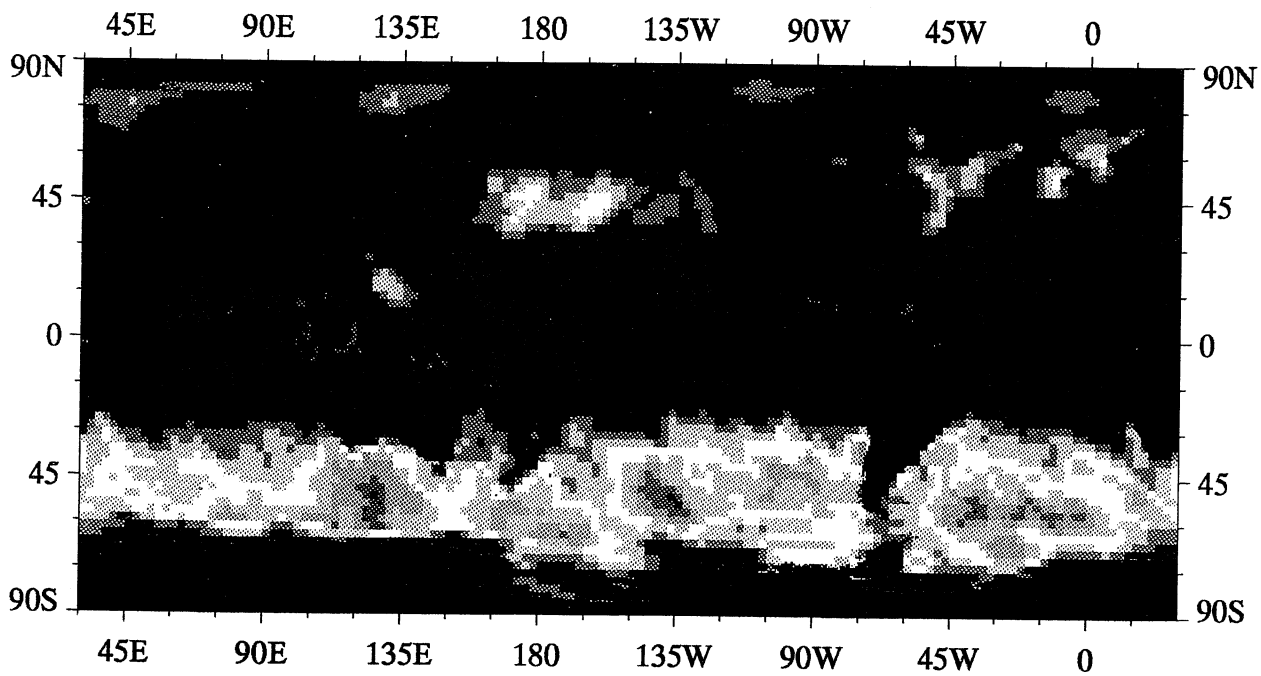

Meridional Wind Speed, July 1987

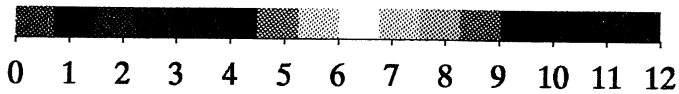

Standard Deviation of ECMWF 10 m Wind Speed, m s^{-1}

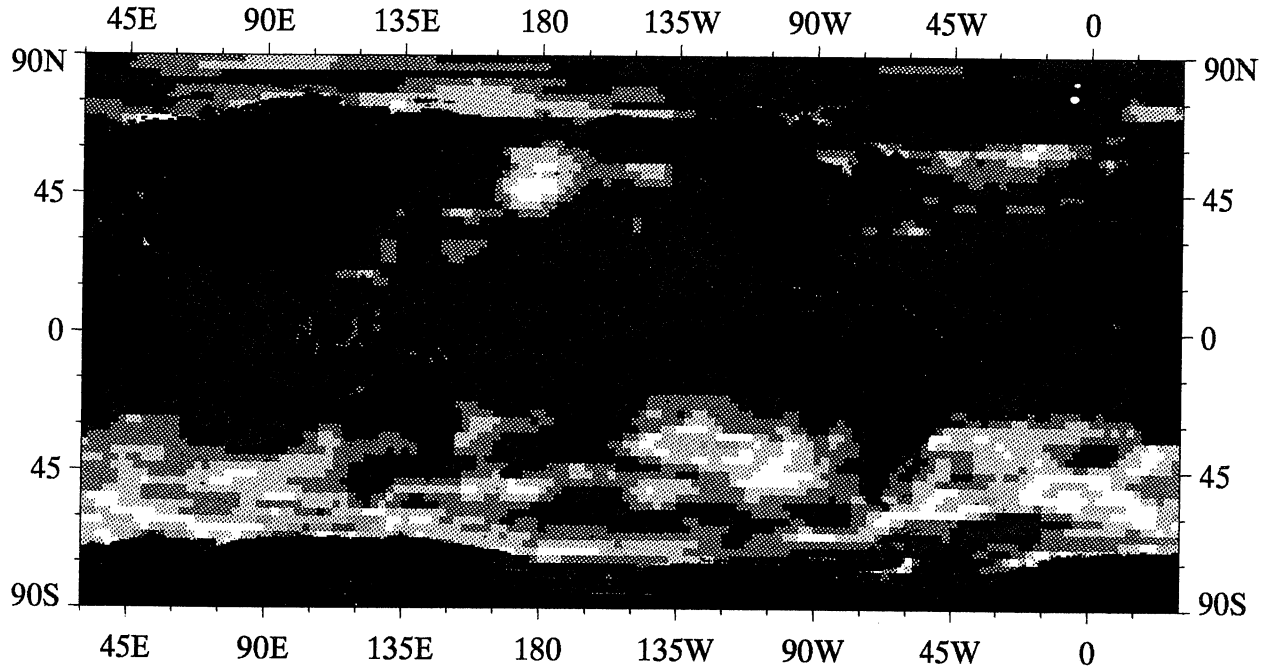

Zonal Wind Speed, August 1987

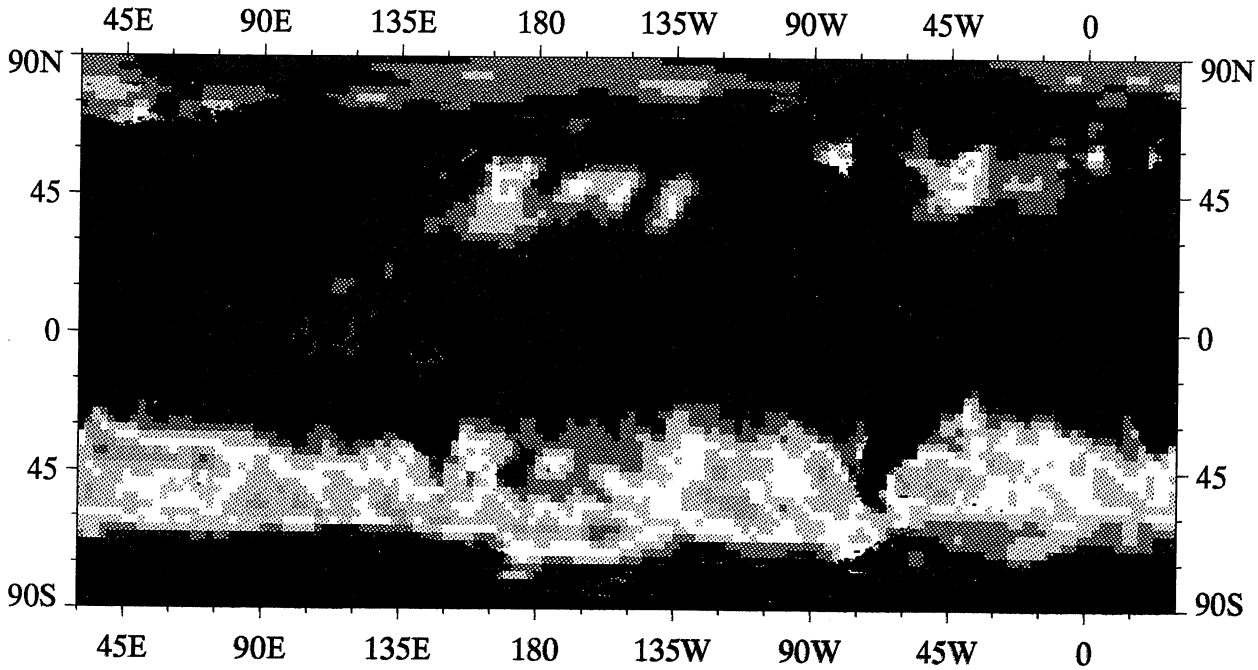

Meridional Wind Speed, August 1987

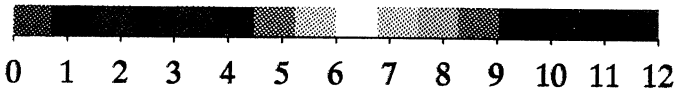

Standard Deviation of ECMWF 10 m Wind Speed, m s^{-1}

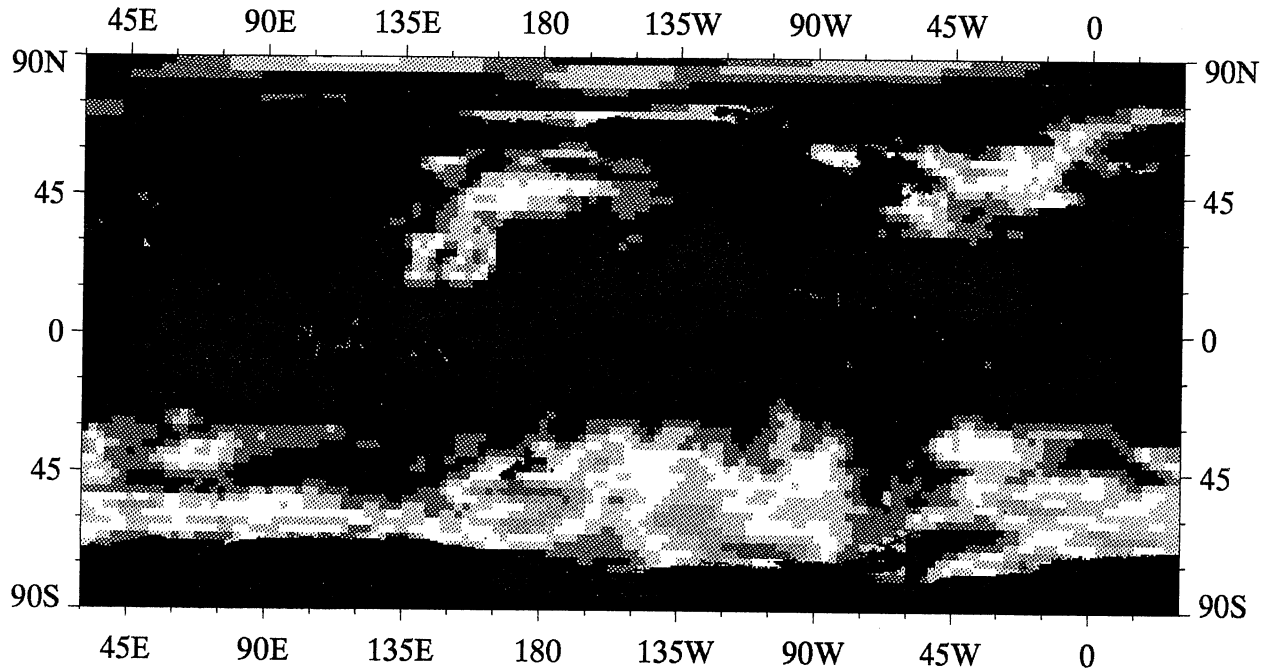

Zonal Wind Speed, September 1987

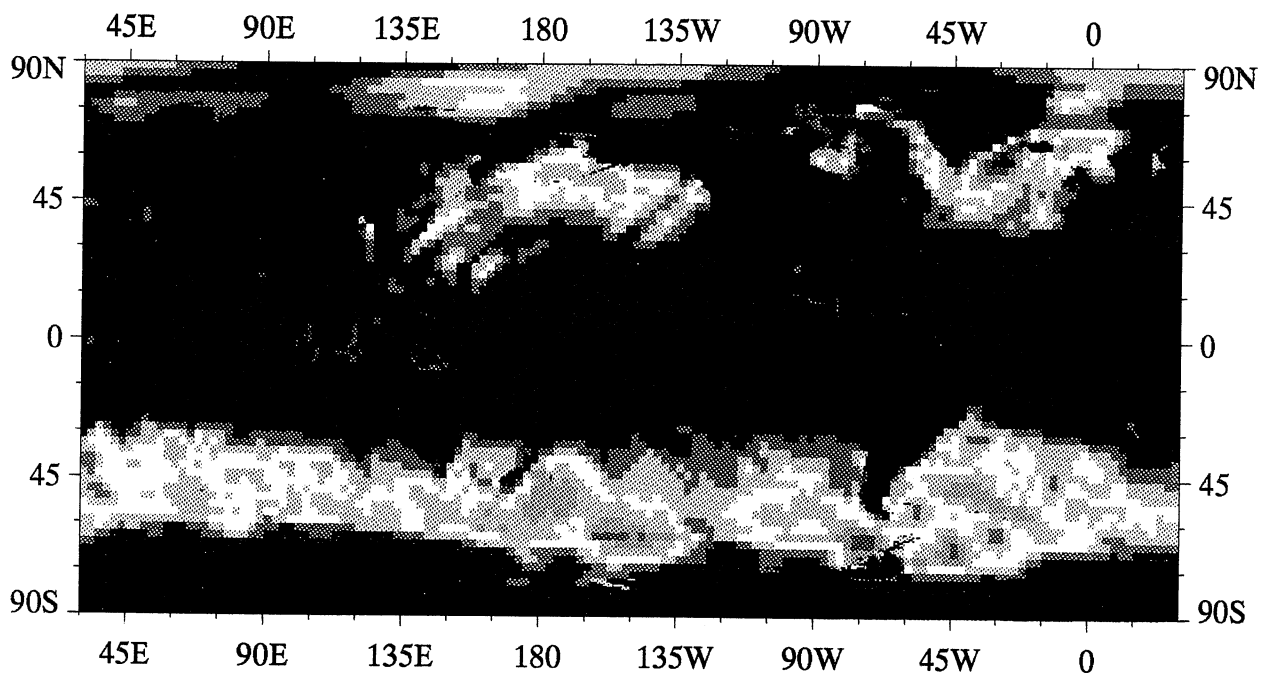

Meridional Wind Speed, September 1987

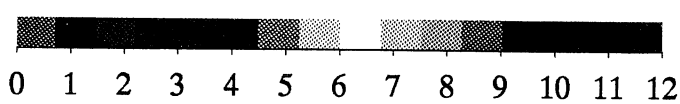

Standard Deviation of ECMWF 10 m Wind Speed, m s^{-1}

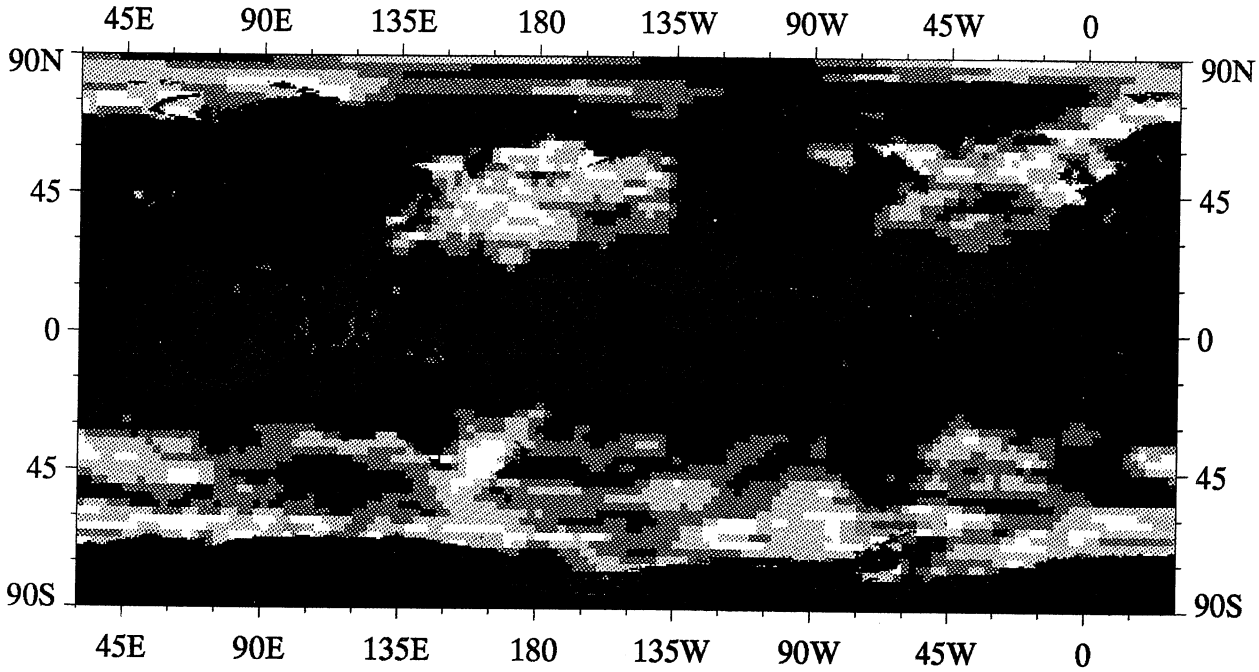

Zonal Wind Speed, October 1987

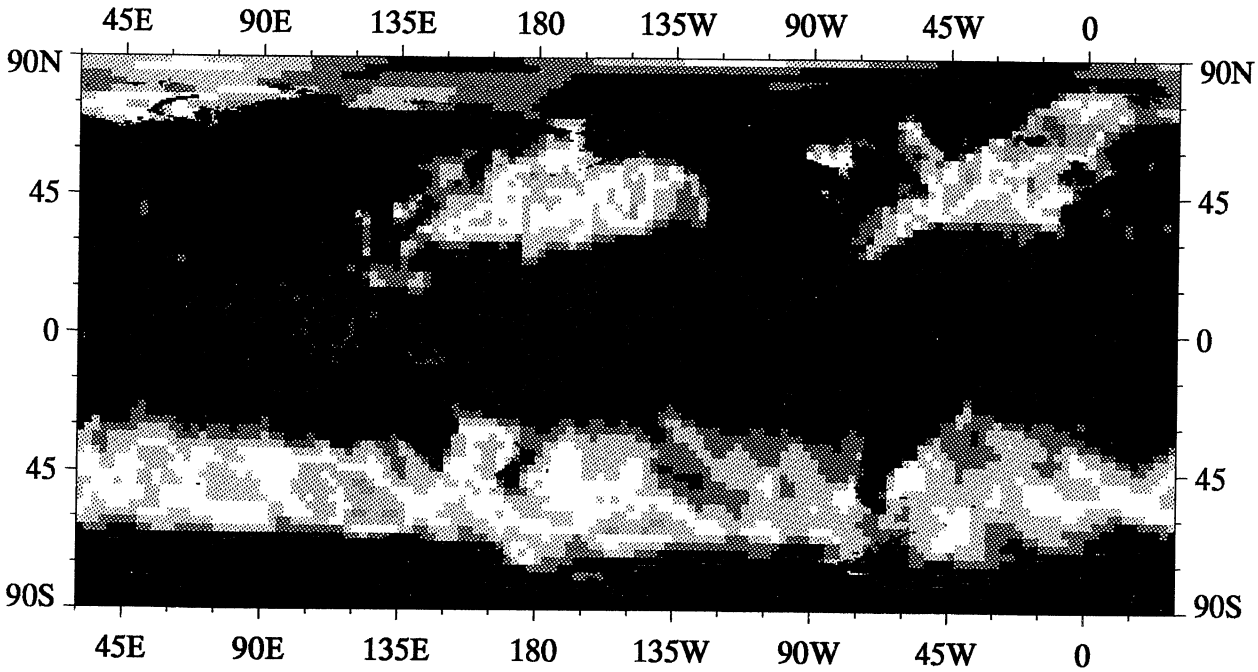

Meridional Wind Speed, October 1987

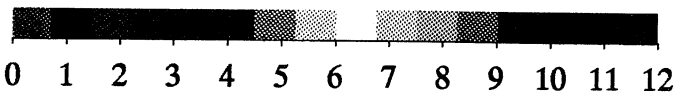

Standard Deviation of ECMWF 10 m Wind Speed, m s^{-1}

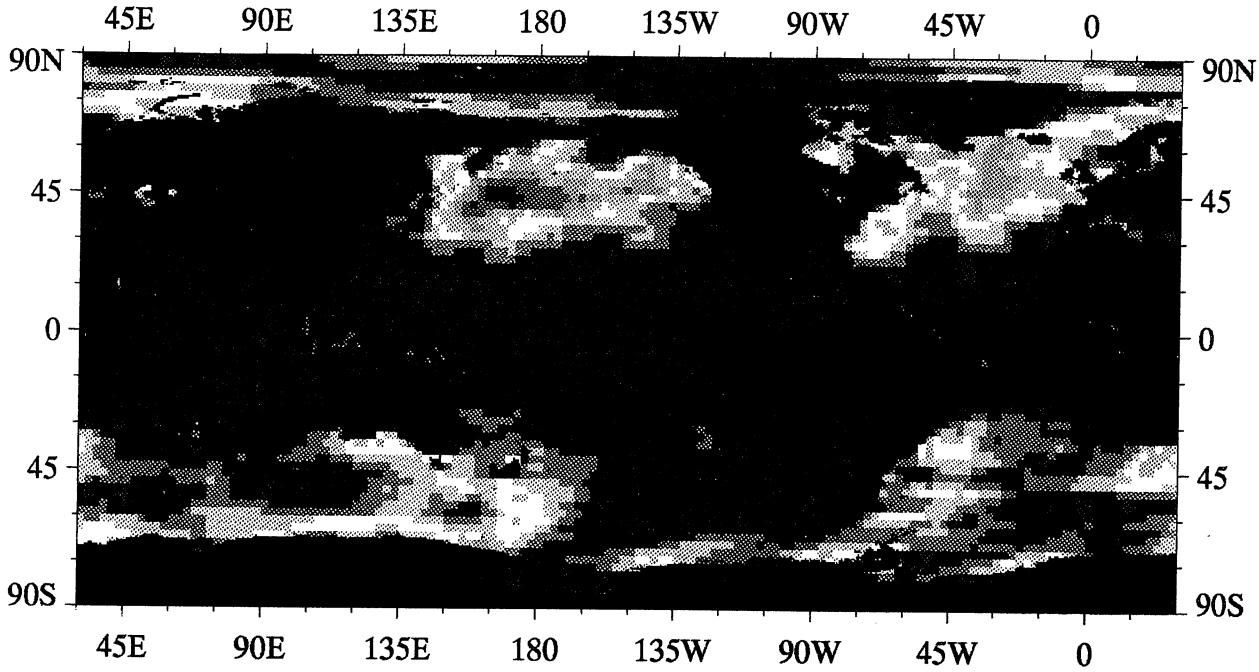

Zonal Wind Speed, November 1987

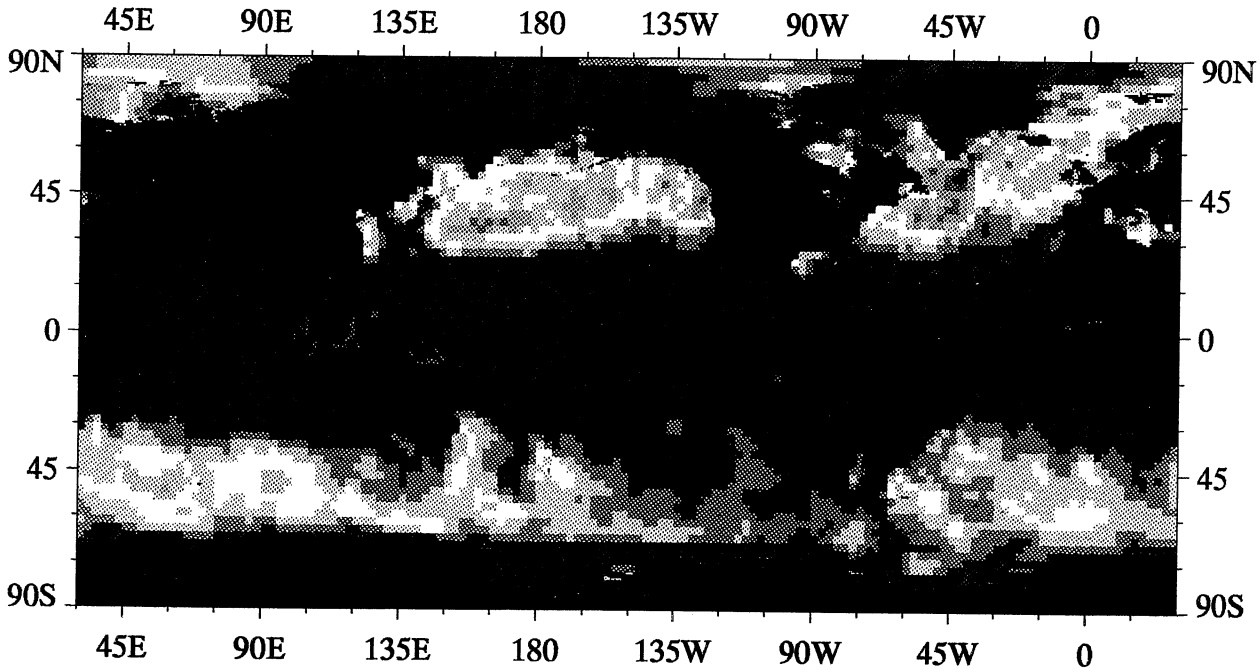

Meridional Wind Speed, November 1987

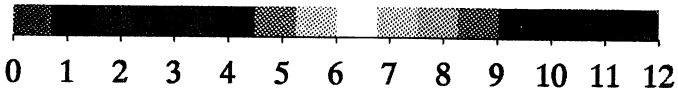

Standard Deviation of ECMWF 10 m Wind Speed, m s^{-1}

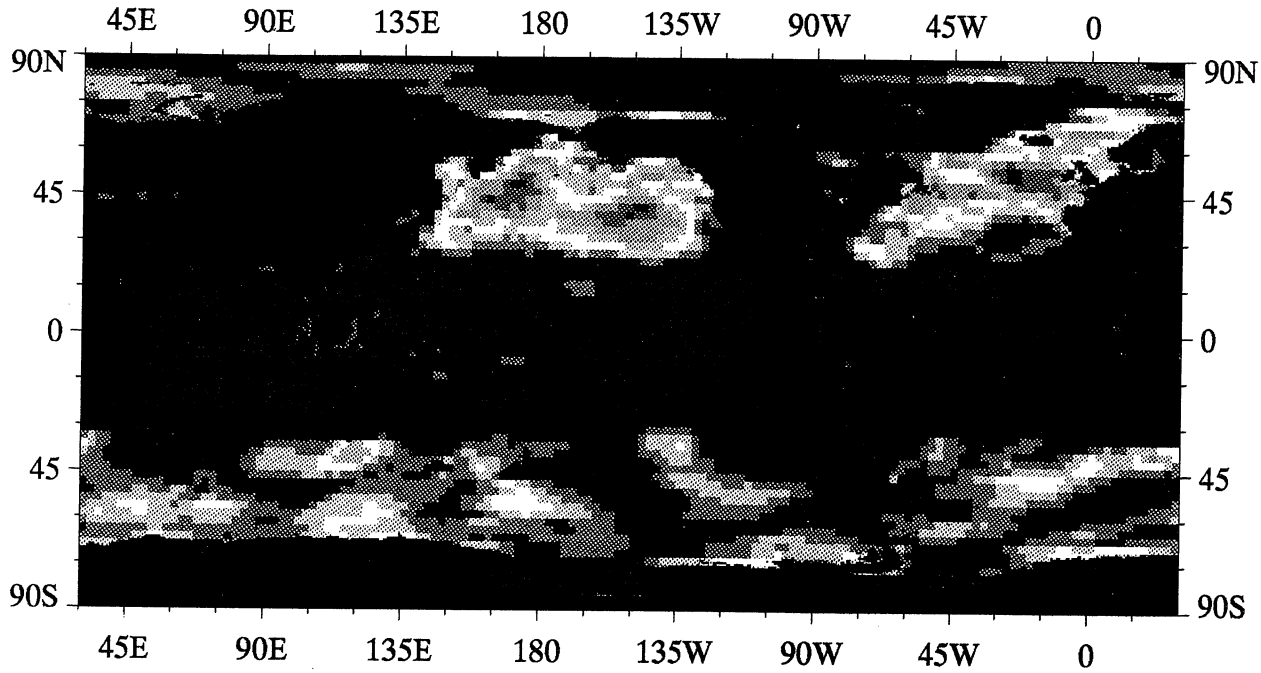

Zonal Wind Speed, December 1987

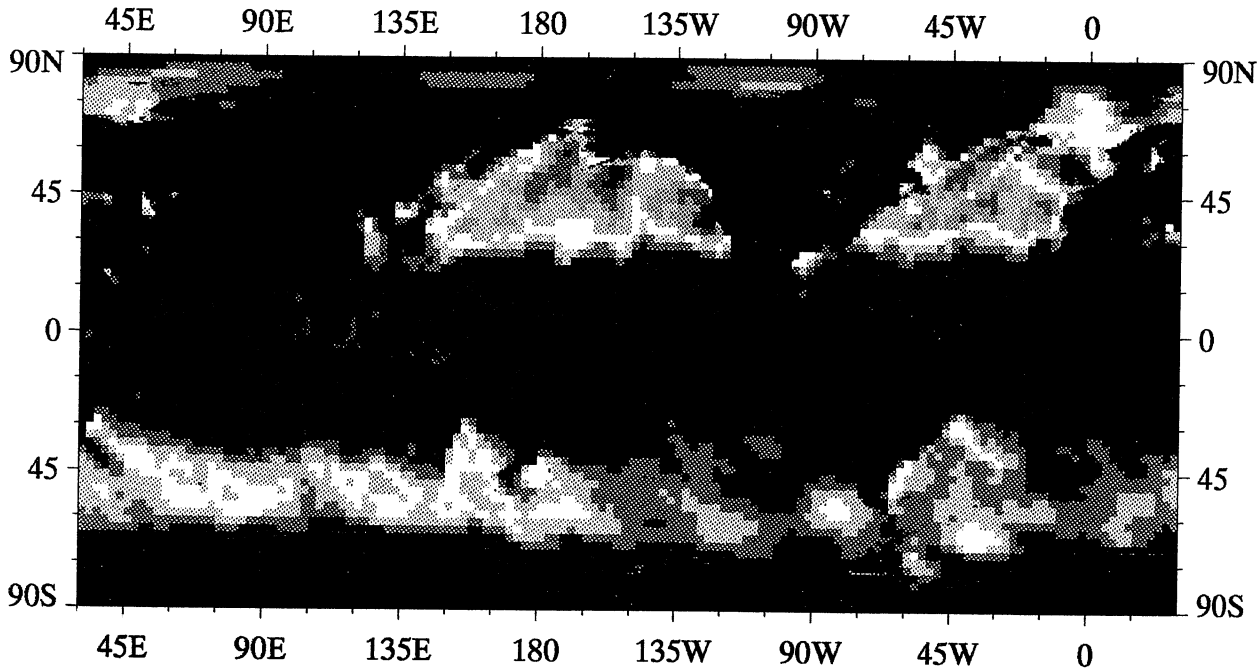

Meridional Wind Speed, December 1987

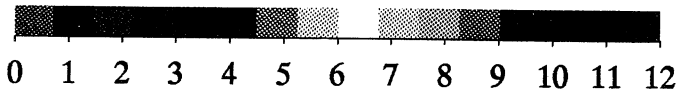

Standard Deviation of ECMWF 10 m Wind Speed, m s^{-1}

A12

Annual Mean ECMWF Surface Wind Speed

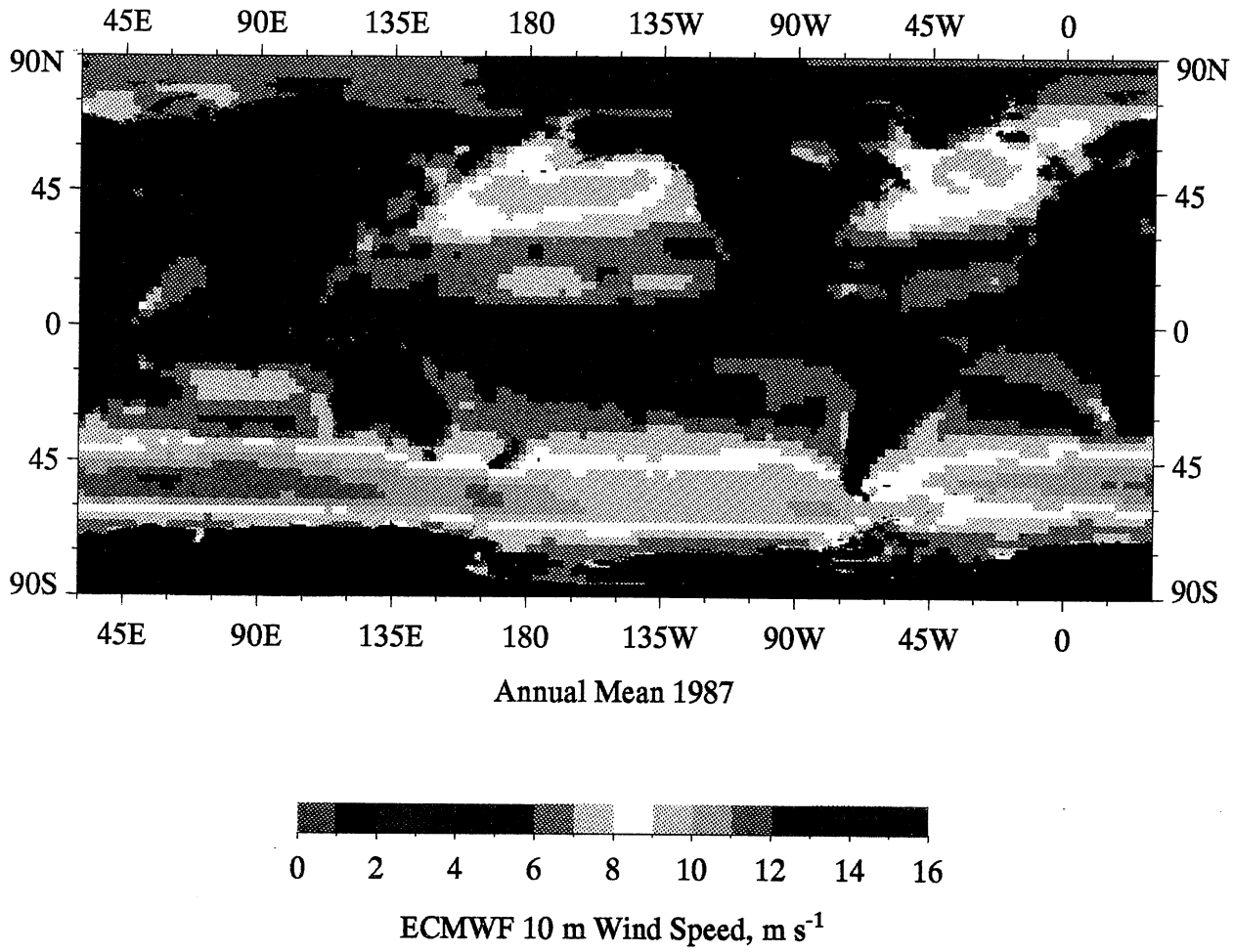
45E
90E
135E
180
135W
90W
45W
0
90N
45
0
45
90S
Annual Mean 1987
0
2
4
6
8
10
12
14
16
ECMWF 10 m Wind Speed, m s-1

A13

Monthly Mean ECMWF Surface Wind Speed

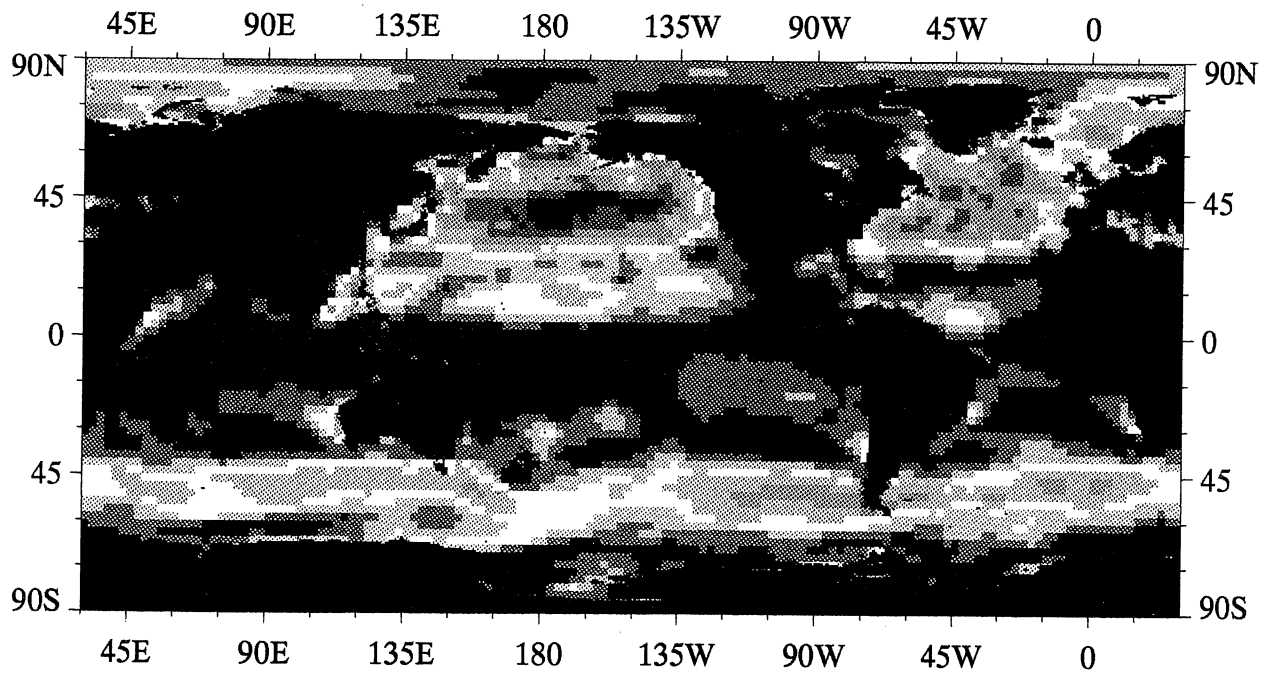

January 1987

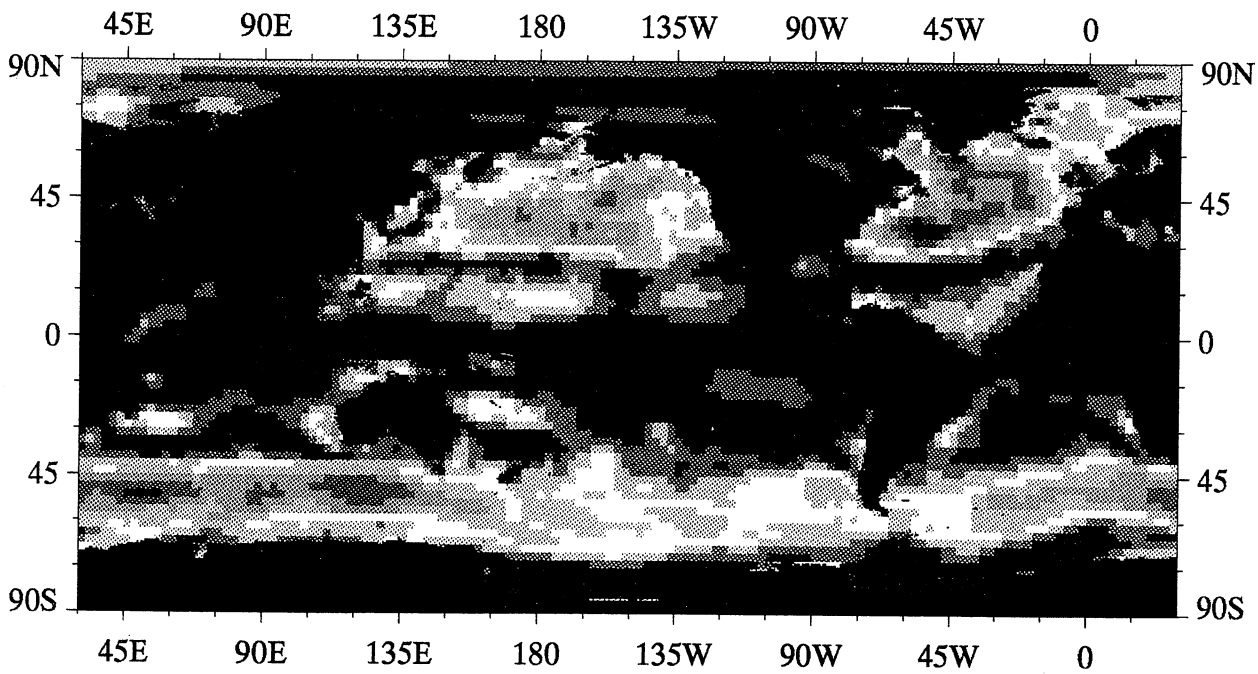

February 1987

ECMWF 10 m Wind Speed, m s^{-1}

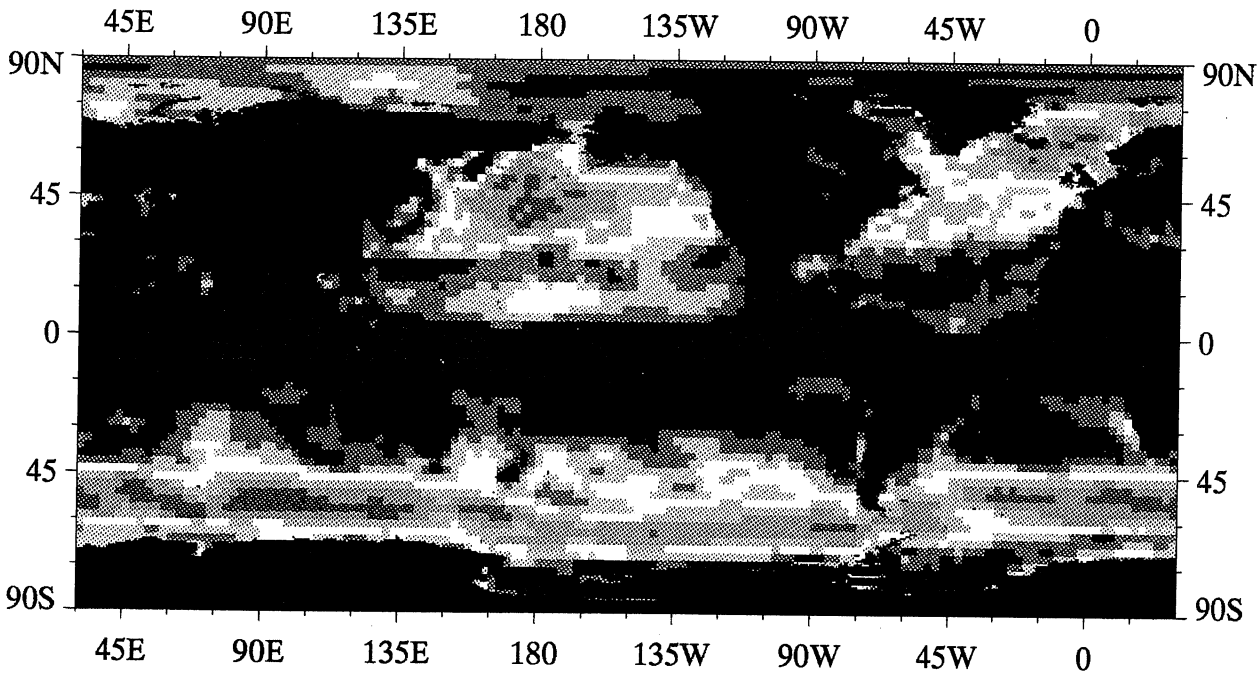

March 1987

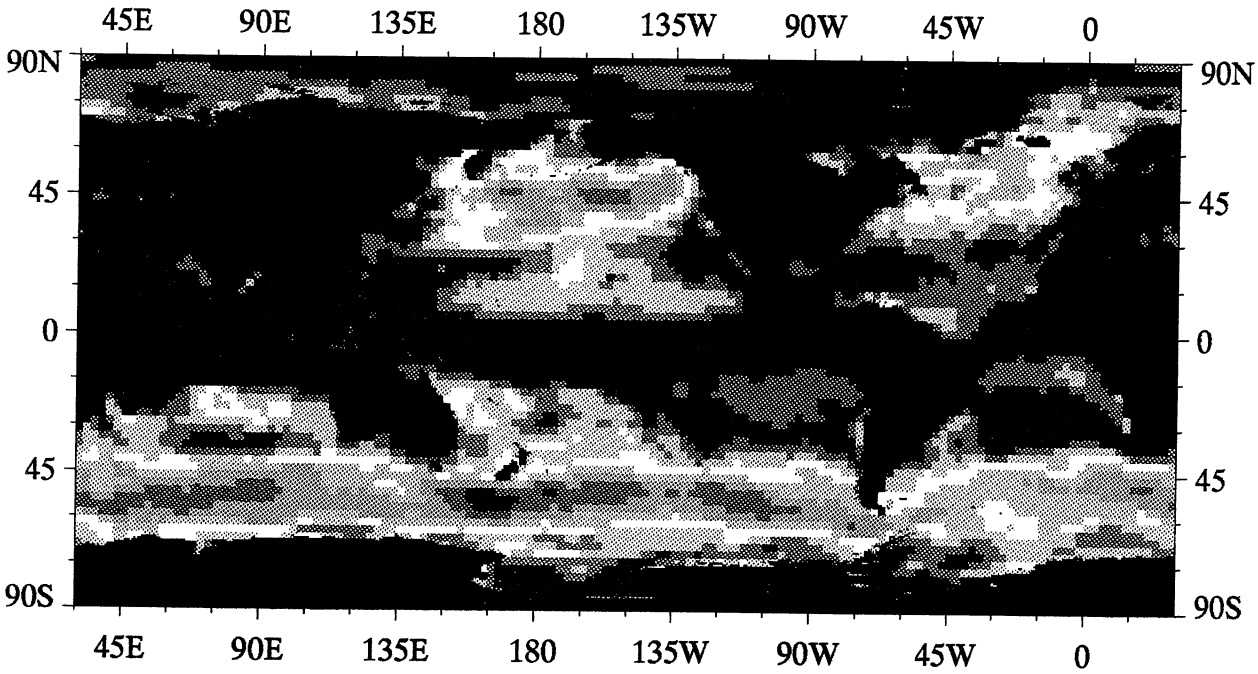

April 1987

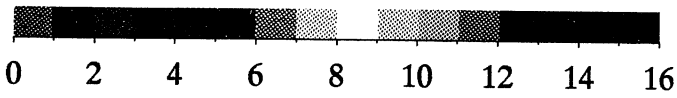

ECMWF 10 m Wind Speed, m s^{-1}

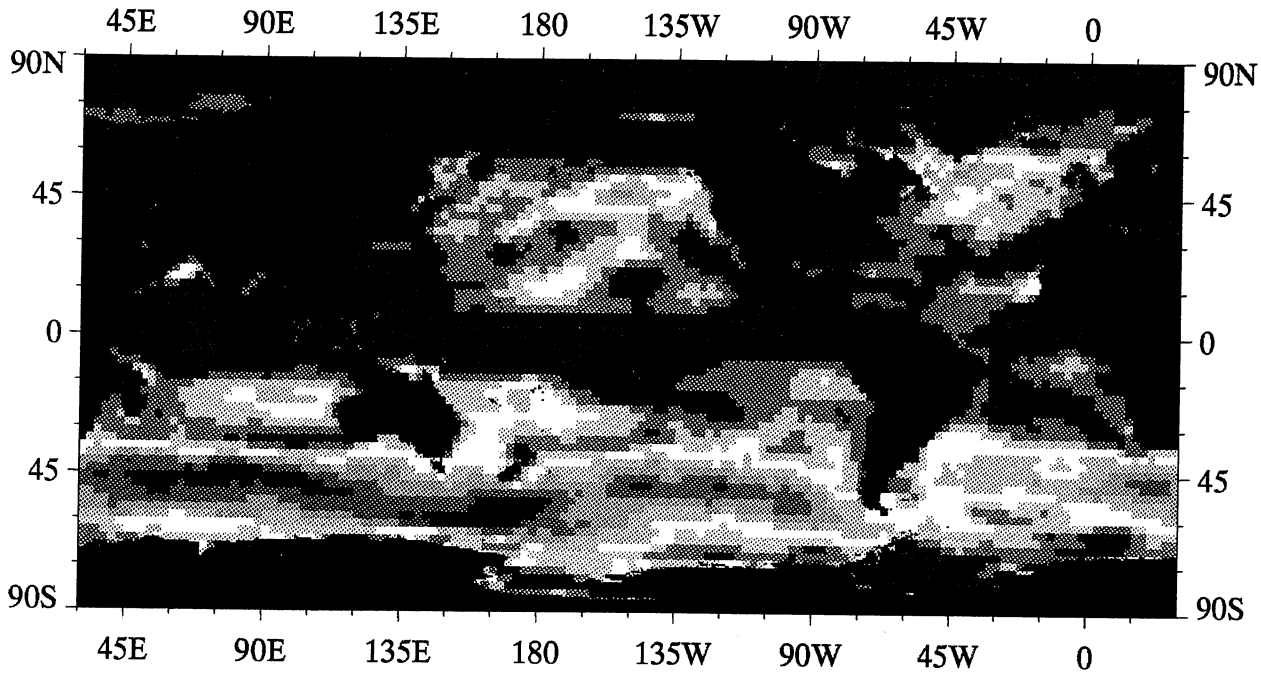

May 1987

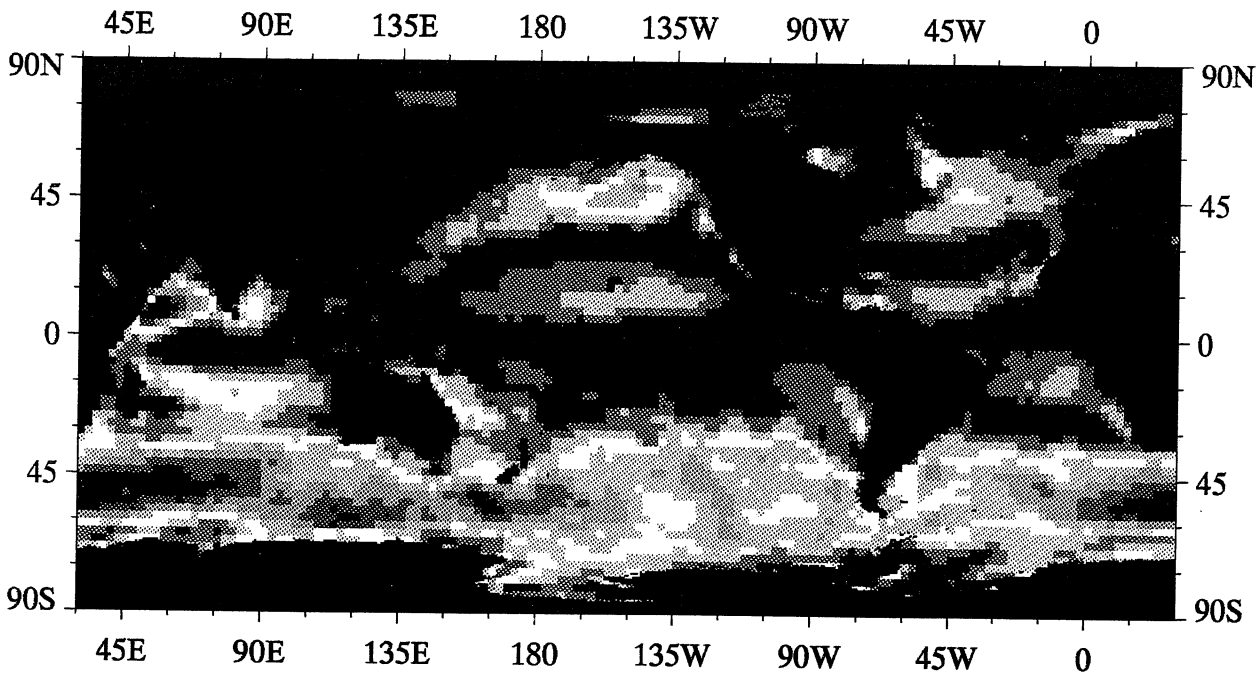

June 1987

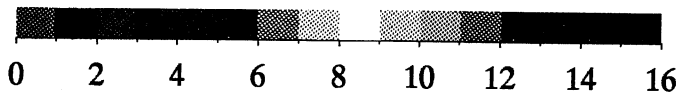

ECMWF 10 m Wind Speed, m s^{-1}

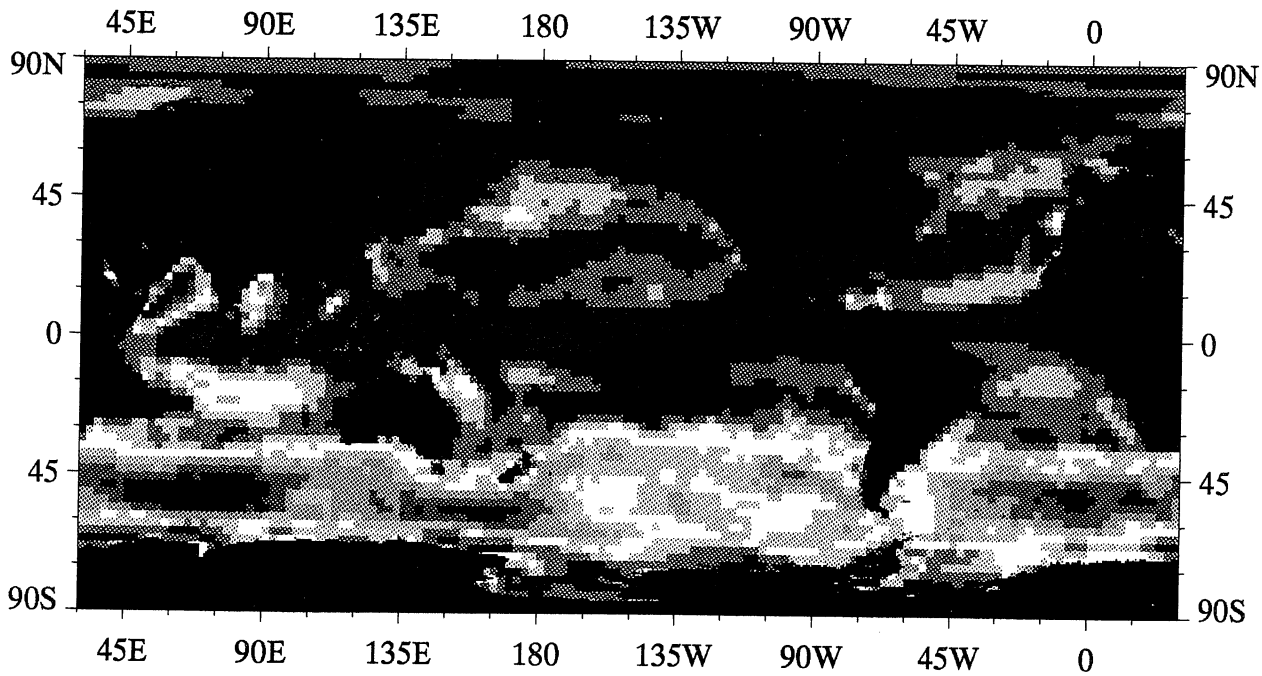

July 1987

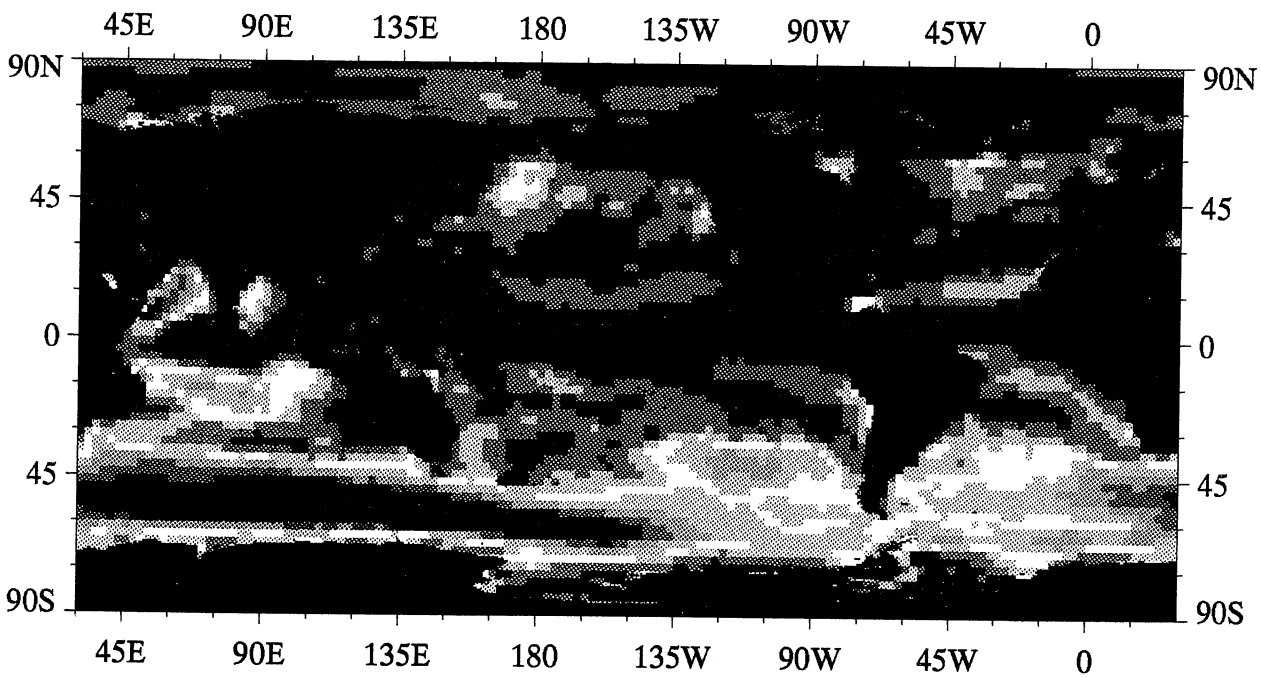

August 1987

ECMWF 10 m Wind Speed, m s^{-1}

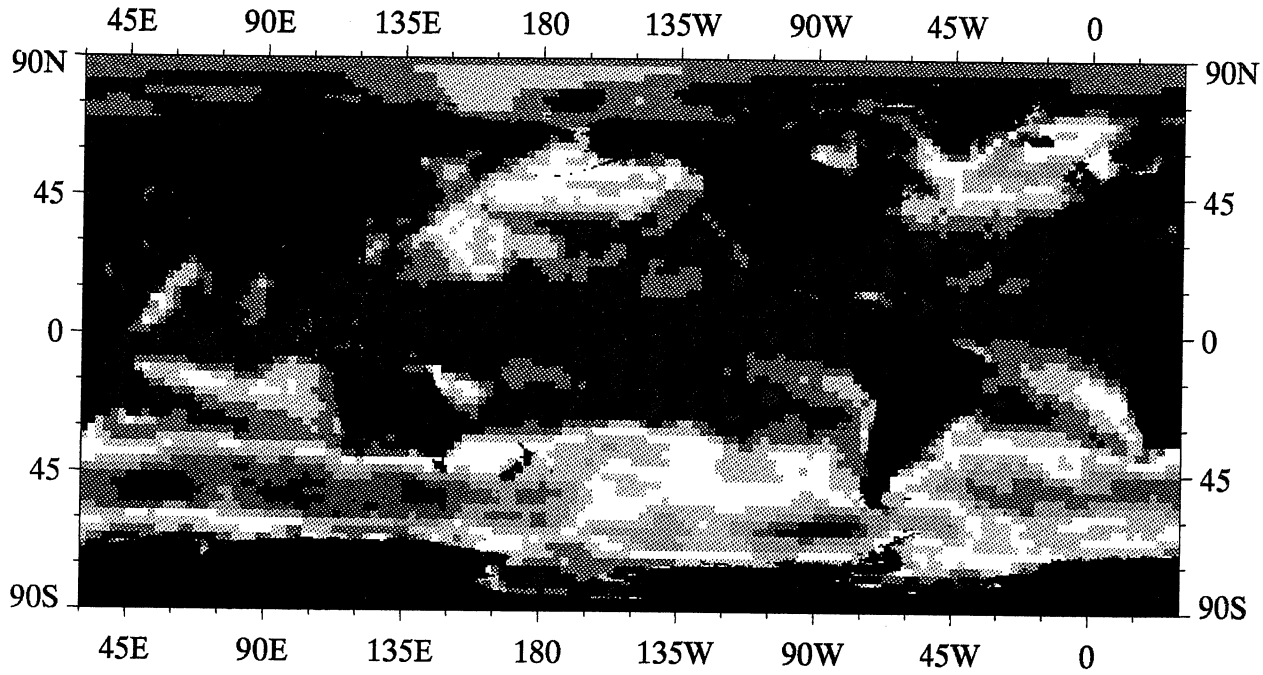

September 1987

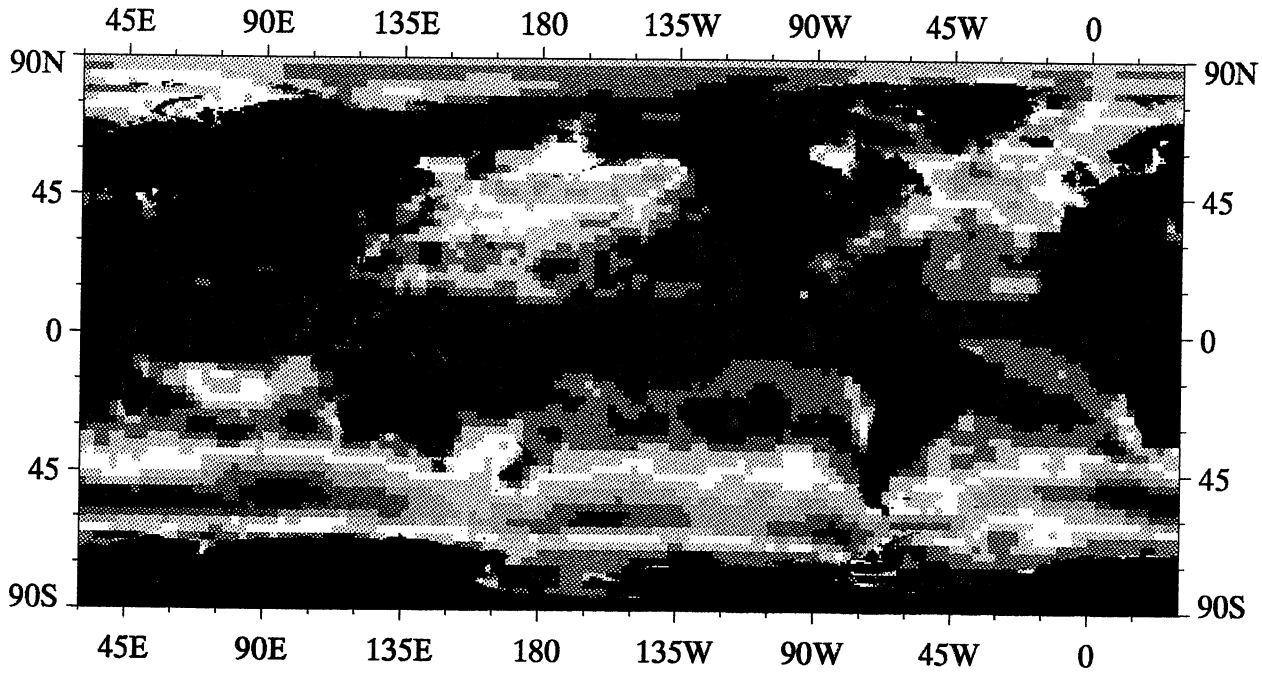

October 1987

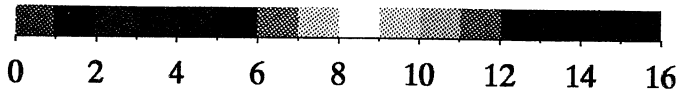

ECMWF 10 m Wind Speed, m s^{-1}

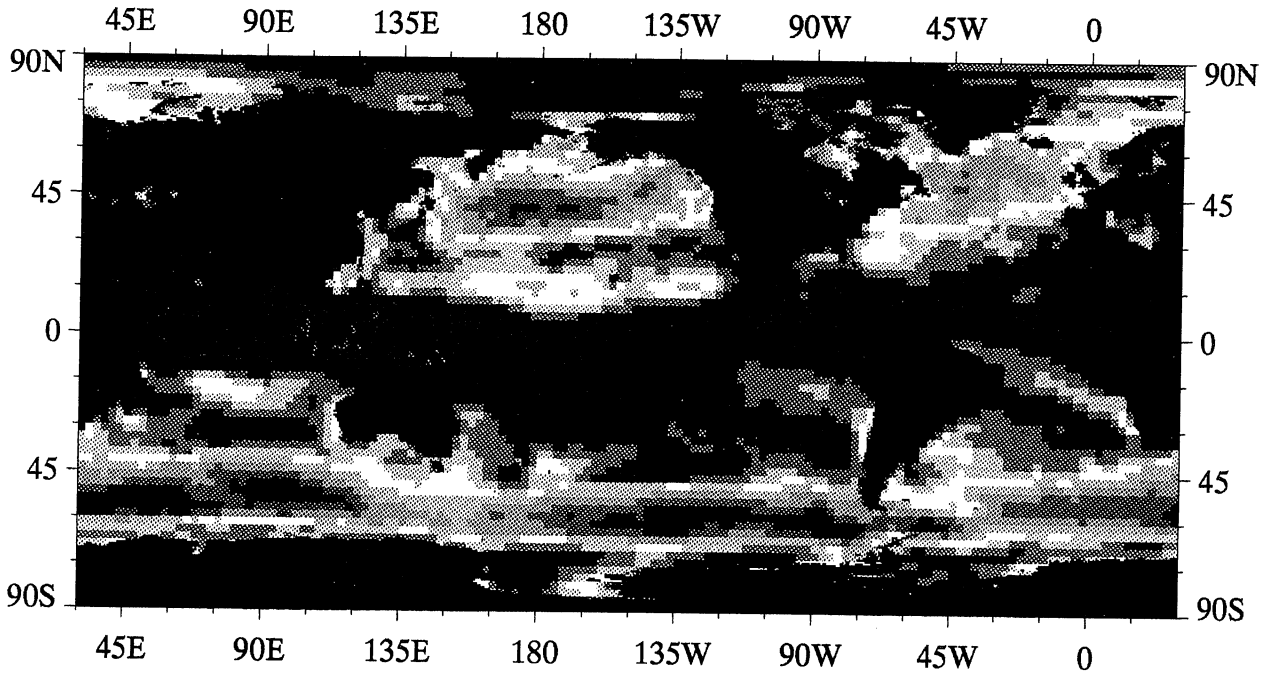

November 1987

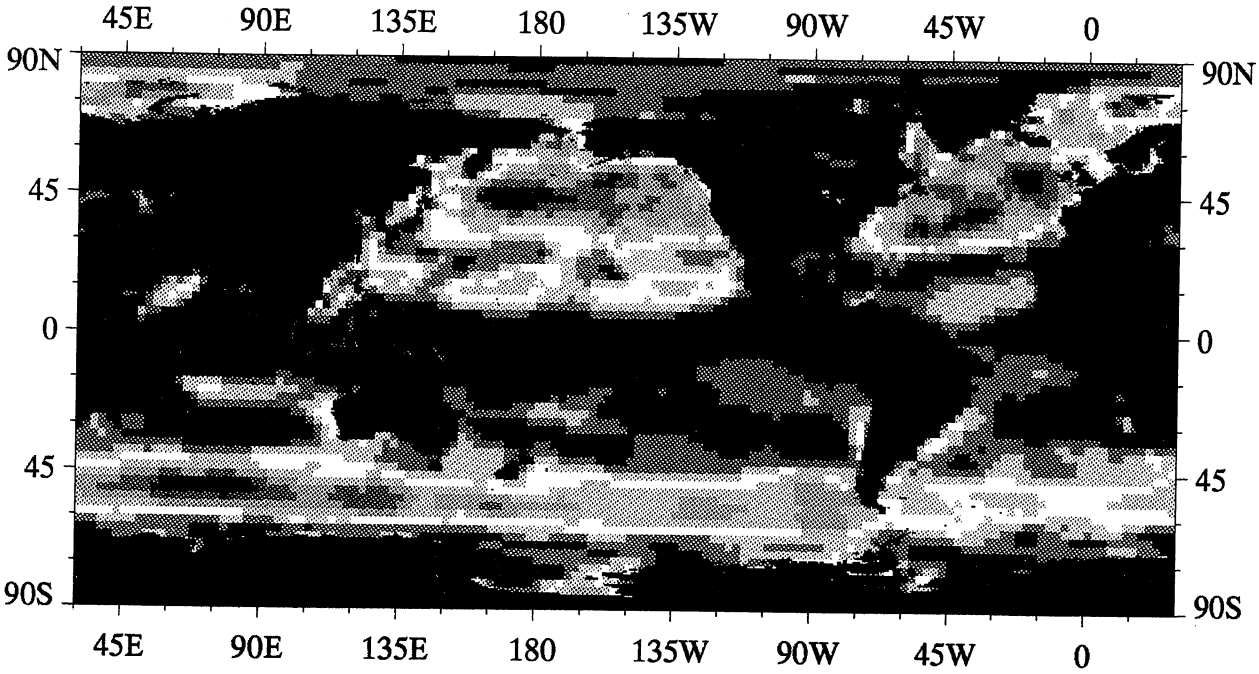

December 1987

ECMWF 10 m Wind Speed, m s^{-1}

A14

Monthly Standard Deviation of ECMWF Surface Wind Speed

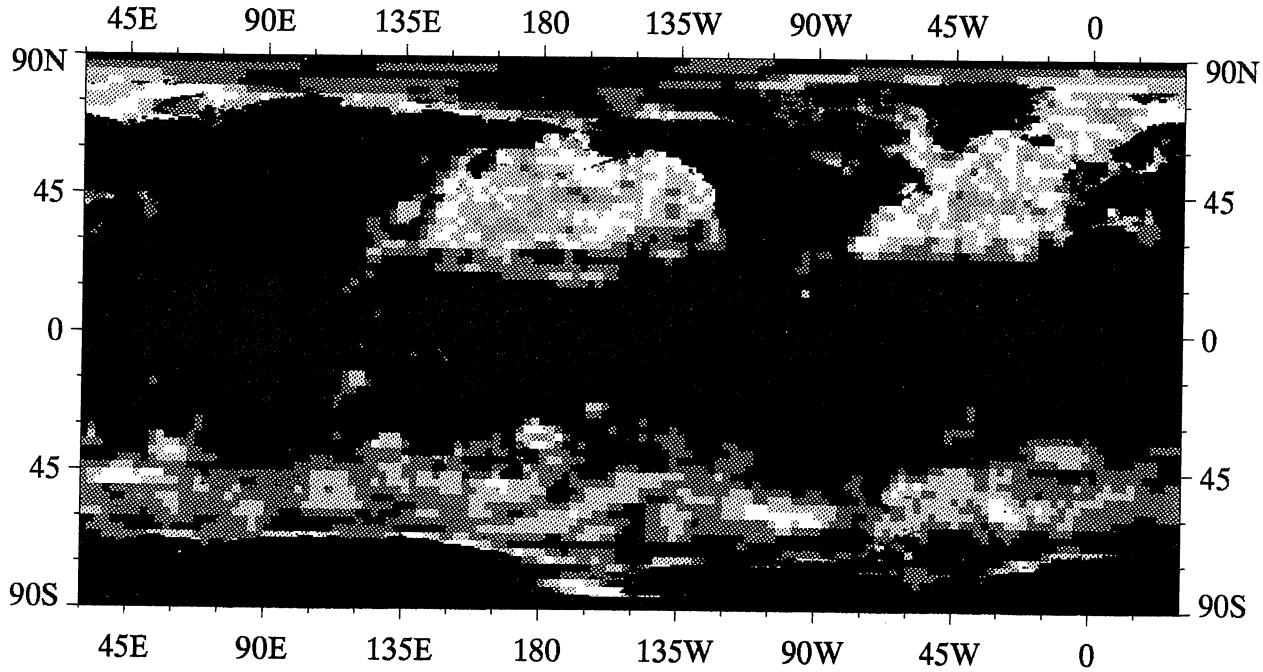

January 1987

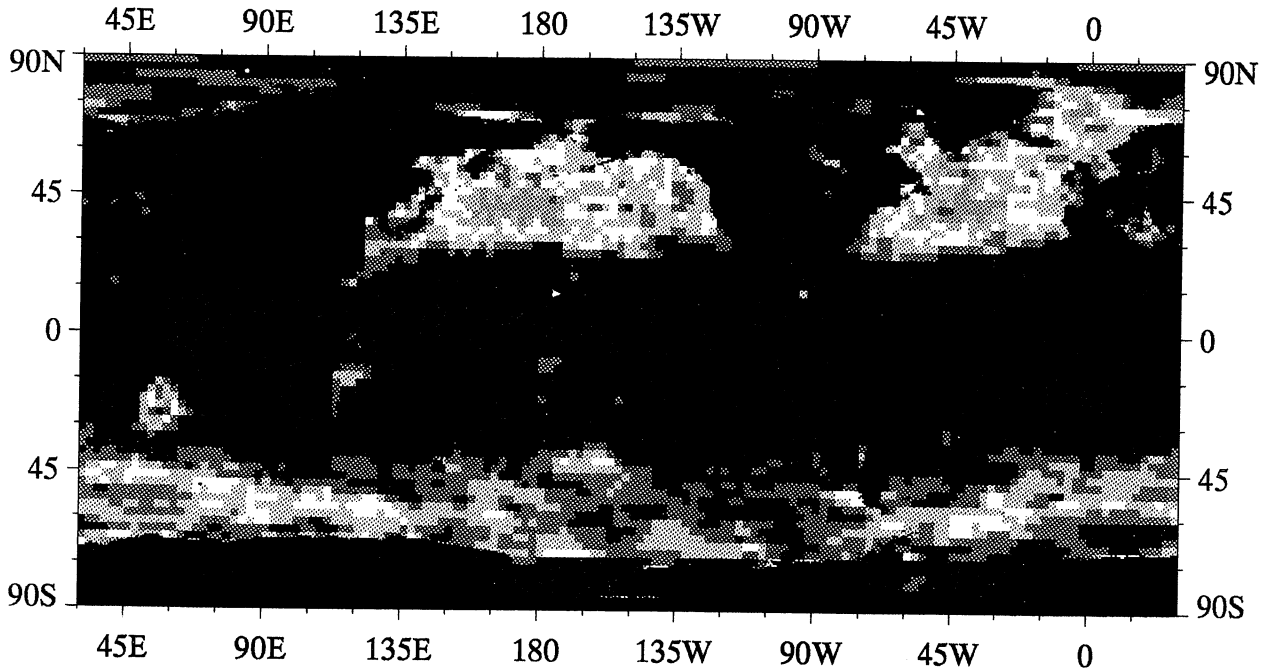

February 1987

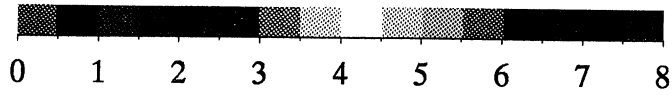

Standard Deviation of ECMWF 10 m Wind Speed, m s^{-1}

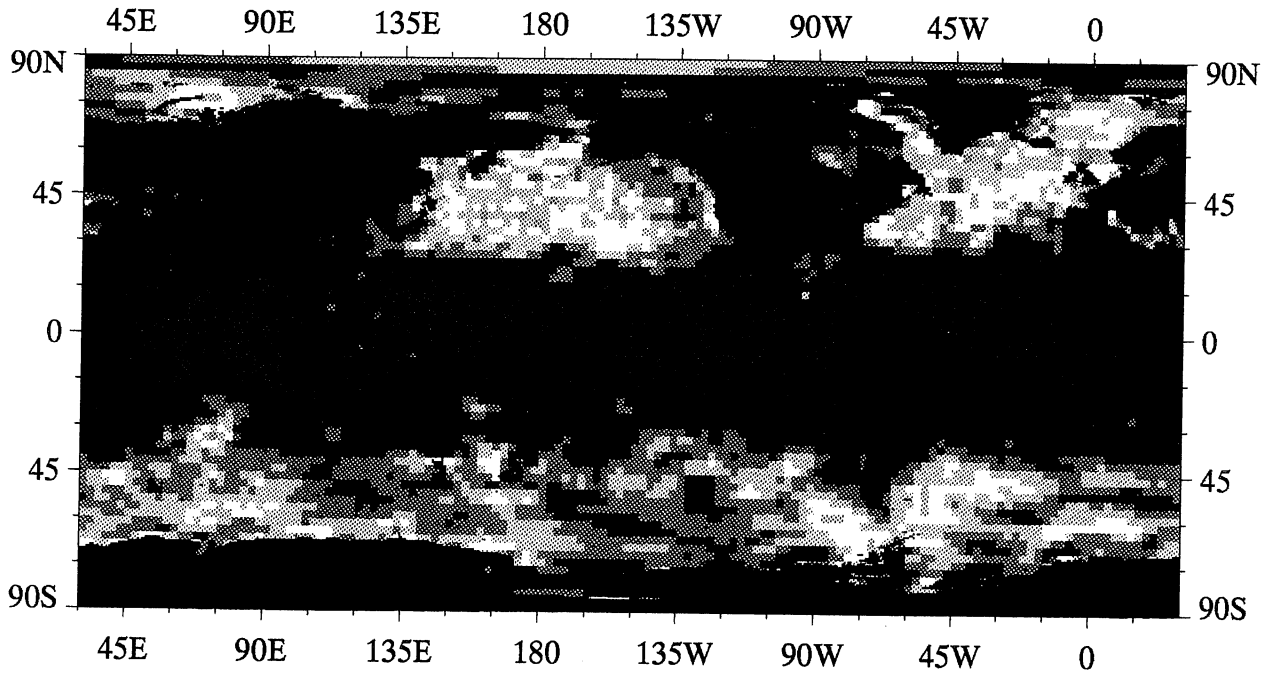

March 1987

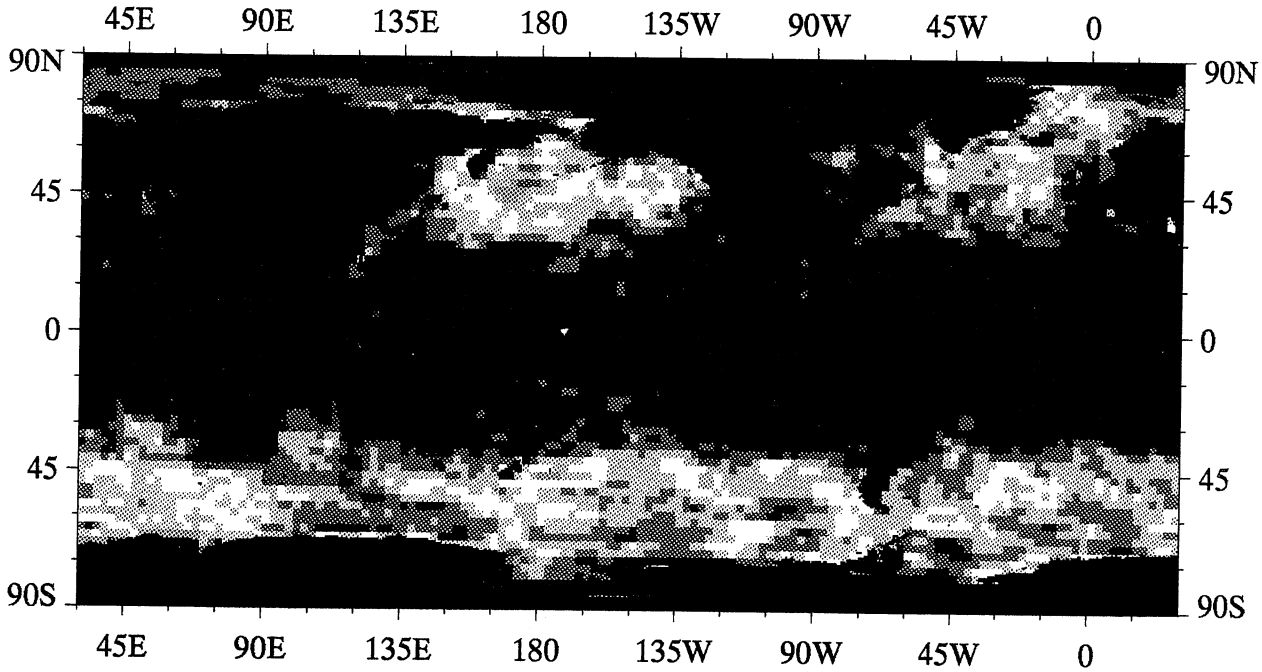

April 1987

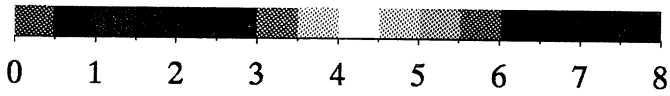

Standard Deviation of ECMWF 10 m Wind Speed, m s^{-1}

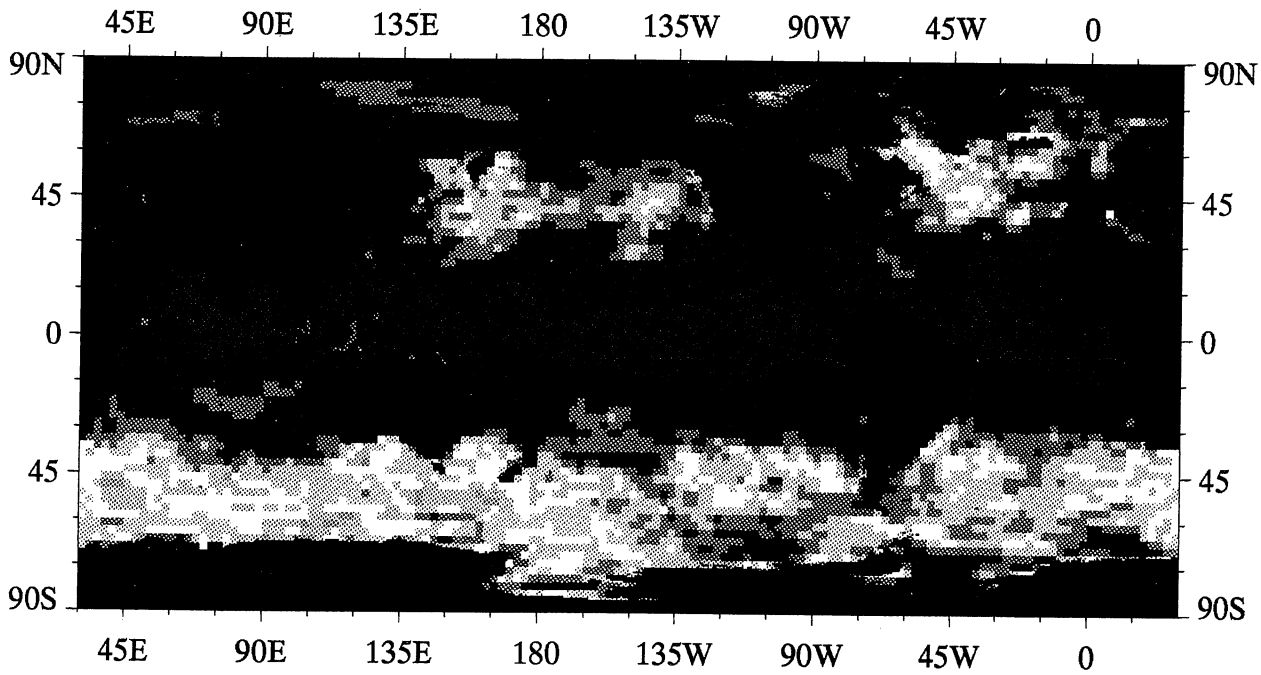

May 1987

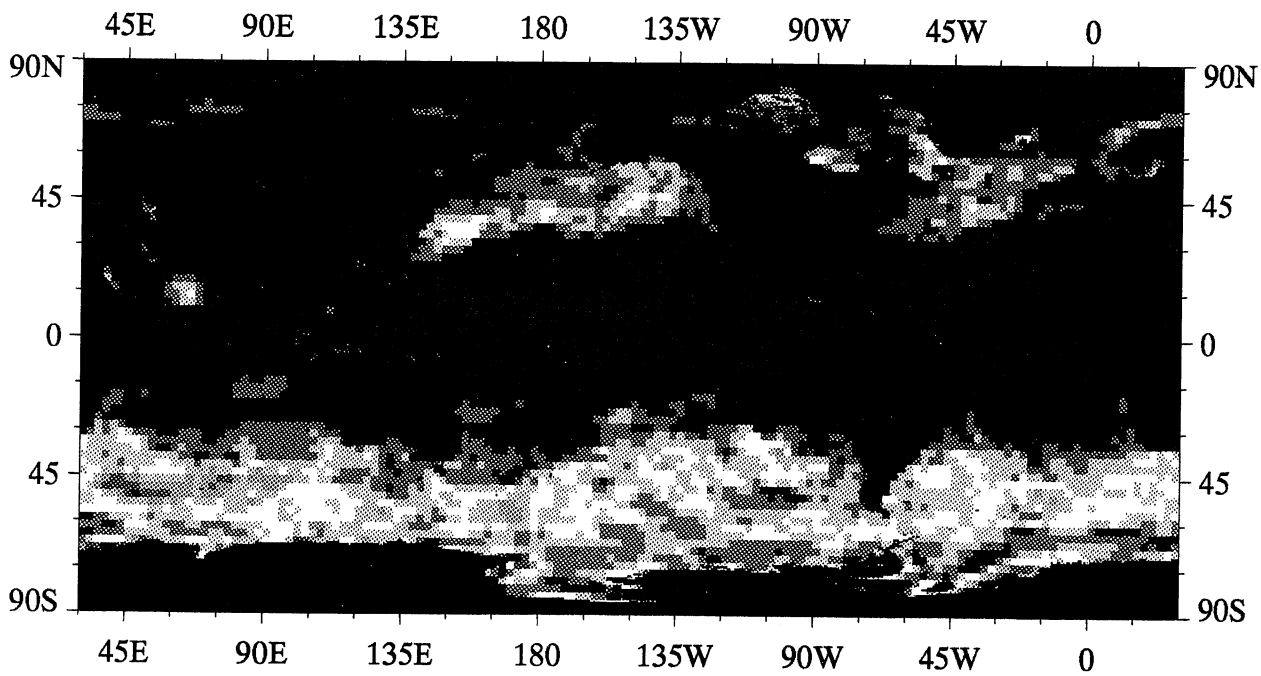

June 1987

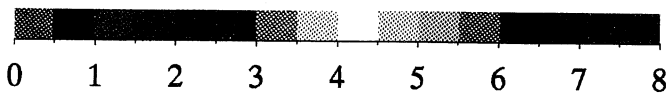

Standard Deviation of ECMWF 10 m Wind Speed, m s^{-1}

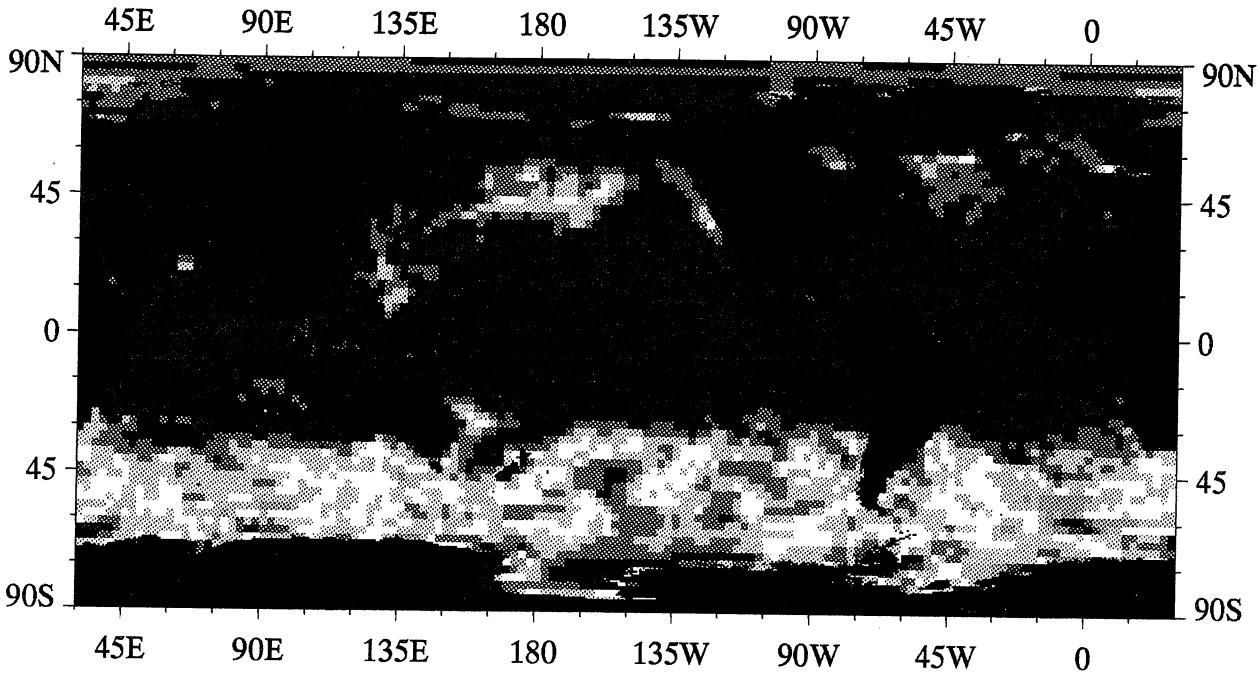

July 1987

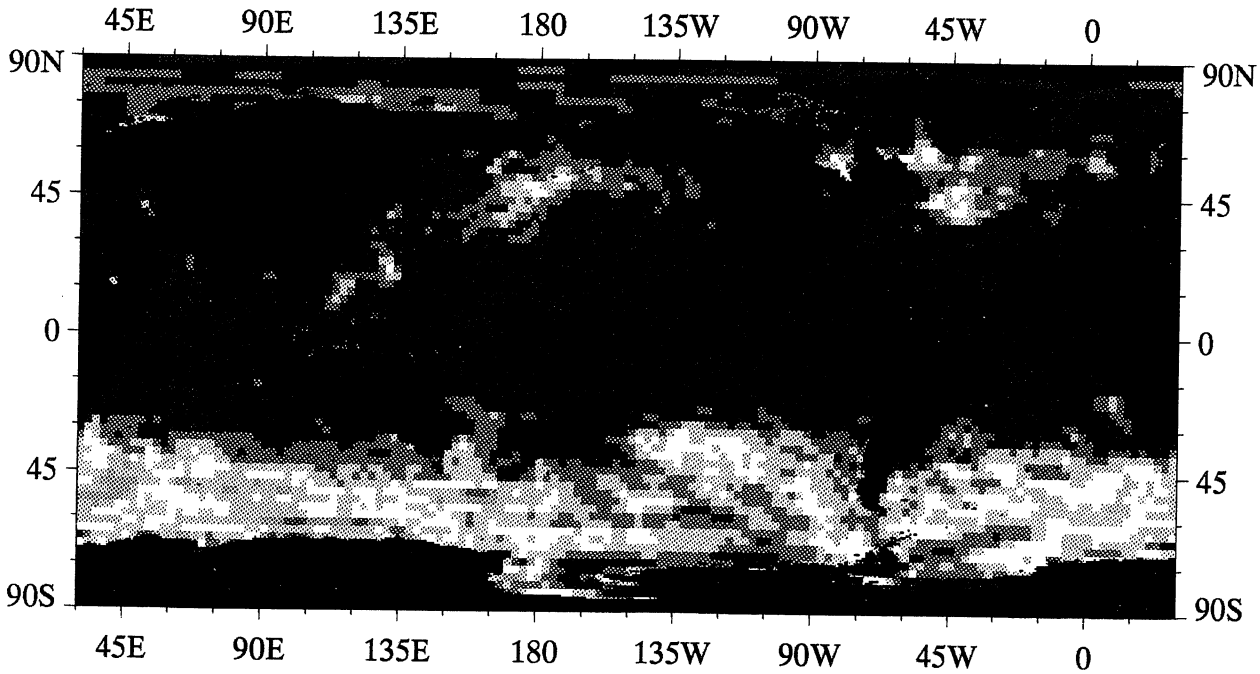

August 1987

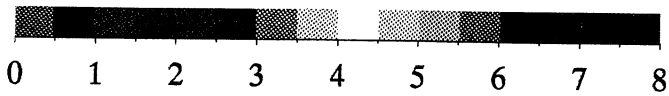

Standard Deviation of ECMWF 10 m Wind Speed, m s^{-1}

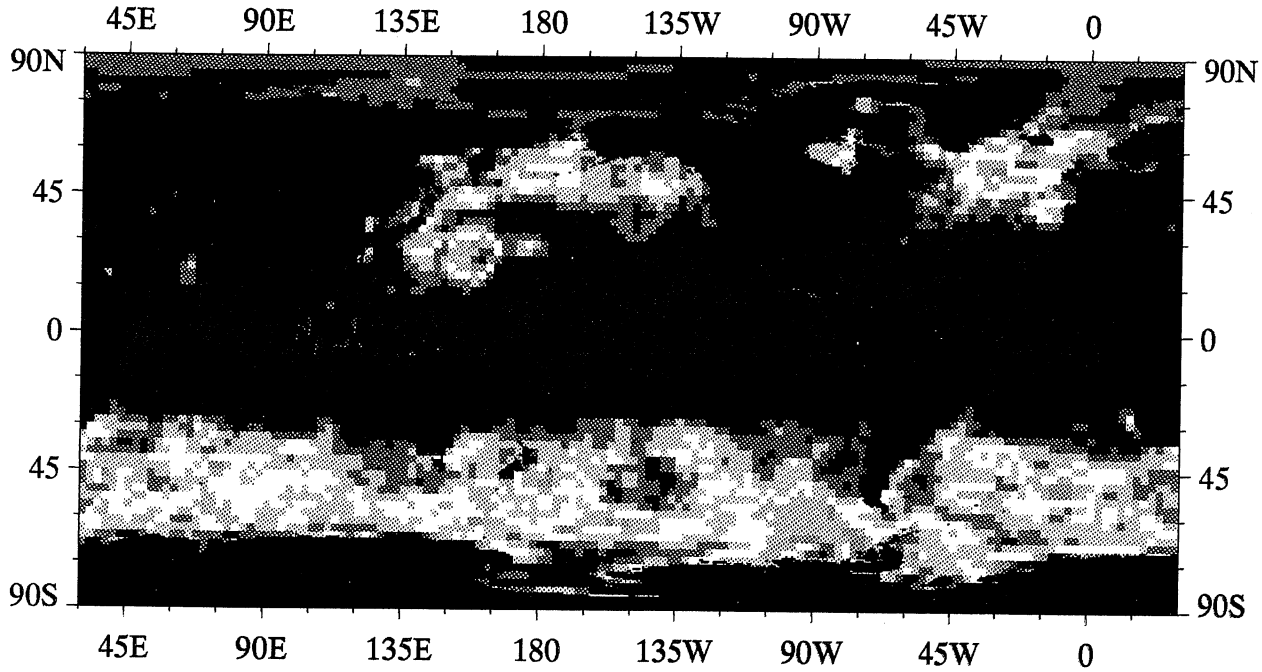

September 1987

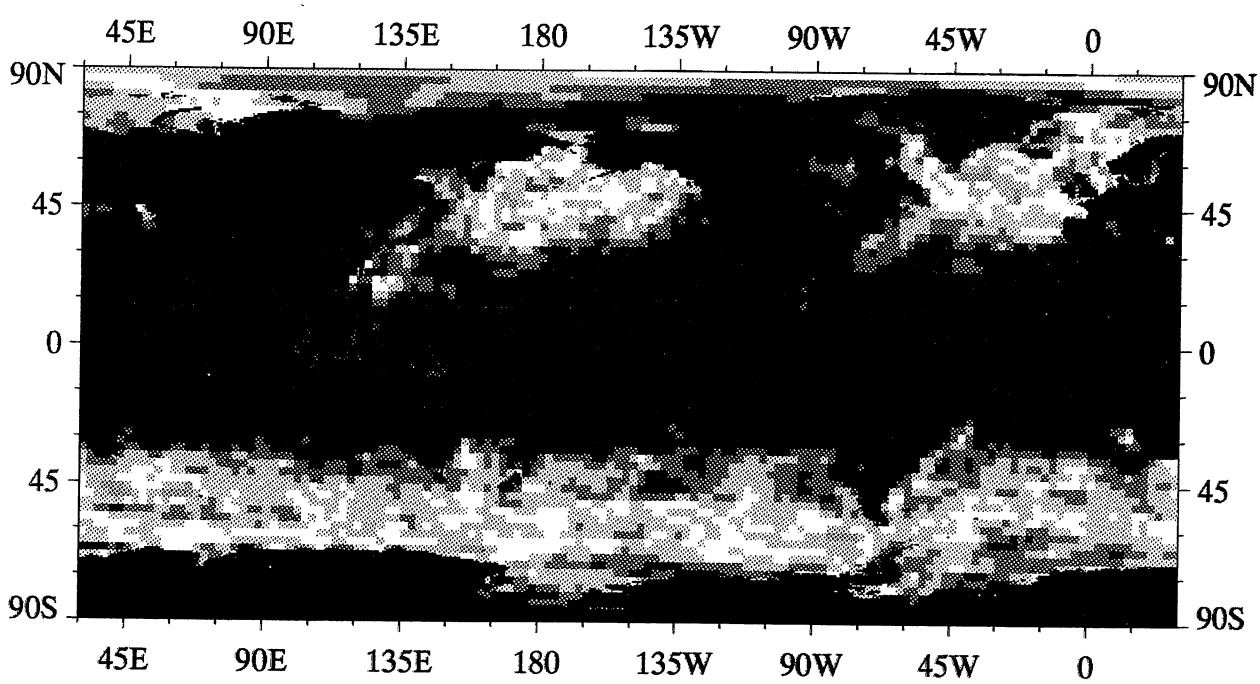

October 1987

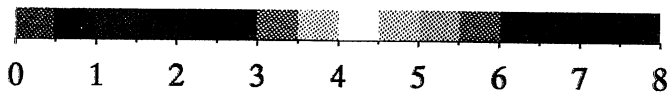

Standard Deviation of ECMWF 10 m Wind Speed, m s^{-1}

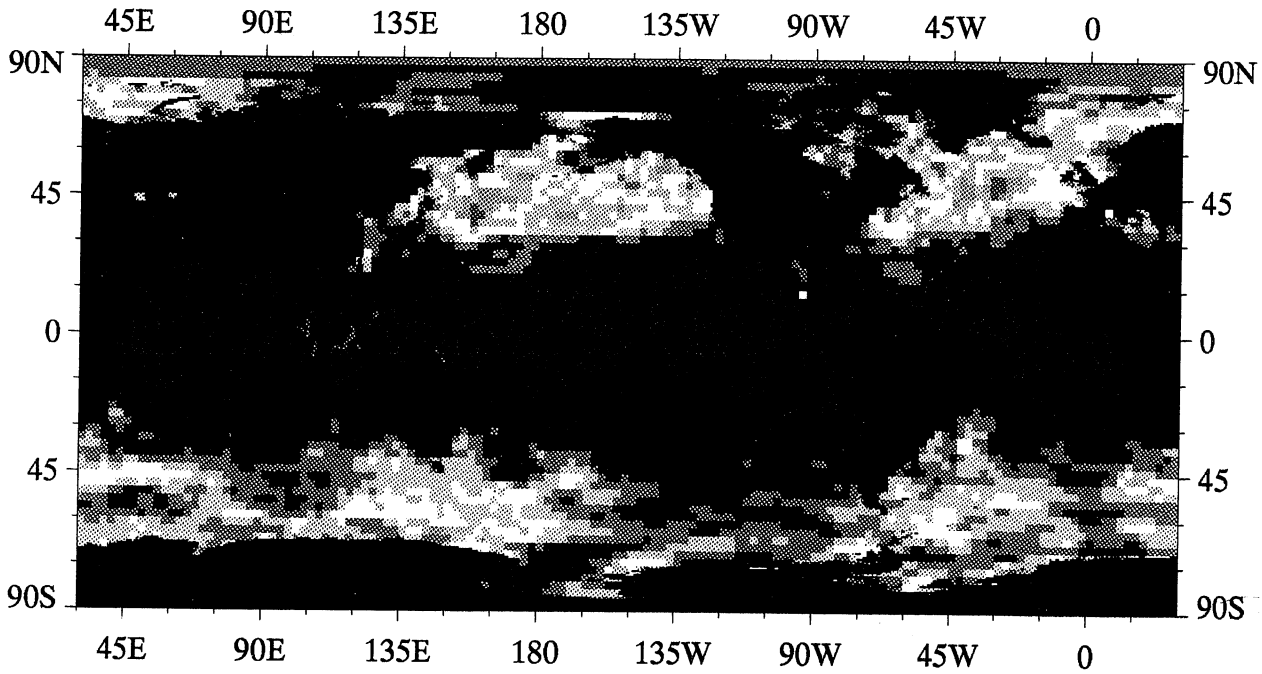

November 1987

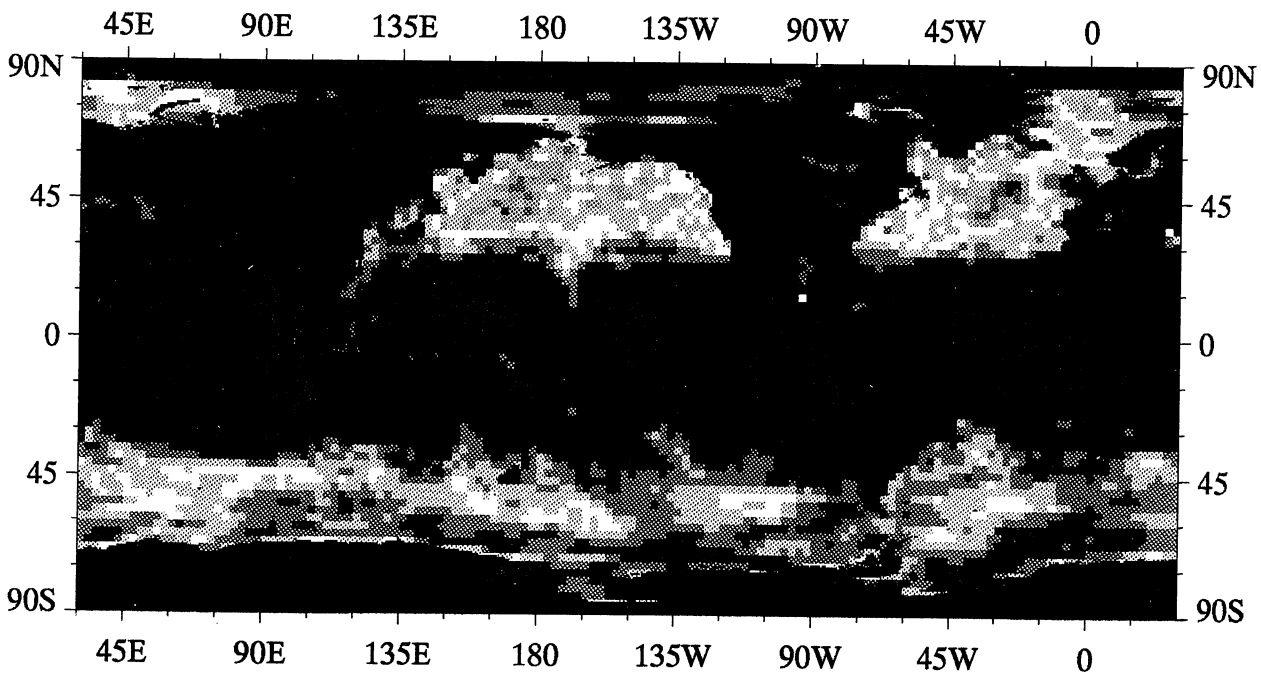

December 1987

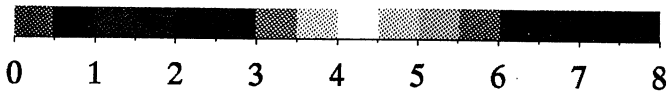

Standard Deviation of ECMWF 10 m Wind Speed, m s^{-1}